UFBA

UNIVERSIDADE FEDERAL DA BAHIA
FACULDADE DE MEDICINA
FUNDAÇÃO OSWALDO CRUZ
INSTITUTO GONÇALO MONIZ

FIOCRUZ

Curso de Pós-Graduação em Patologia

TESE DE DOUTORADO

USO DAS SIRTUÍNAS DO *Trypanosoma cruzi* COMO ALVOS MOLECULARES NO DESENVOLVIMENTO DE FÁRMACOS PARA O TRATAMENTO DA DOENÇA DE CHAGAS

TANIRA MATUTINO BASTOS

Salvador – Bahia
2017

UNIVERSIDADE FEDERAL DA BAHIA
FACULDADE DE MEDICINA
FUNDAÇÃO OSWALDO CRUZ
INSTITUTO GONÇALO MONIZ – FIOCRUZ

Curso de Pós-Graduação em Patologia

USO DAS SIRTUÍNAS DO *Trypanosoma cruzi* COMO ALVOS MOLECULARES NO DESENVOLVIMENTO DE FÁRMACOS PARA O TRATAMENTO DA DOENÇA DE CHAGAS

TANIRA MATUTINO BASTOS

Orientadora: Profª Drª Milena Botelho Pereira Soares

Tese apresentada ao Curso de Pós-Graduação em Patologia Humana para a obtenção do grau de Doutor.

Salvador – Bahia
2017

Ficha Catalográfica elaborada pela Biblioteca do
Instituto Gonçalo Moniz / FIOCRUZ - Salvador - Bahia.

Bastos, Tanira Matutino
B324u Uso das sirtuínas do *Trypanosoma cruzi* como alvos moleculares no desenvolvimento de fármacos para o tratamento da doença de chagas. / Tanira Matutino Bastos. - 2017.
128 f. : il. ; 30 cm.

Orientador: Profª Drª Milena Botelho Pereira Soares, Laboratório de Engenharia Tecidual e Imunofarmacologia.
Tese (Doutorado em Patologia) – Universidade Federal da Bahia. Fundação Oswaldo Cruz, Instituto Gonçalo Moniz, Salvador, 2017.

1. Doença de Chagas. 2. *Trypanosoma cruzi*. 3. Sirtuínas. 4. Fármacos. I. Título.

CDU 616.937

Título da Tese: **"USO DAS SIRTUINAS DO TRIPANOSOMA CRUZI COMO ALVOS MOLECULARES NO DESENVOLVIMENTO DE FÁRMACOS PARA O TRATAMENTO DA DOENÇA DE CHAGAS"**

TANIRA MATUTINO BASTOS

FOLHA DE APROVAÇÃO

Salvador, 21 de setembro de 2017

COMISSÃO EXAMINADORA

Dr. Nilmar Silvio Moretti
Professor Adjunto
UNIFESP

Dra. Patricia Sampaio Tavares Veras
Pesquisadora Titular
IGM/Fiocruz

Dr. Mitermayer Galvão dos Reis
Pesquisador Titular
IGM/Fiocruz

Dr. Geraldo Gileno de Sá Oliveira
Pesquisador
IGM/Fiocruz

Dra. Milena Botelho Pereira Soares
Pesquisadora Titular
IGM/Fiocruz

FONTES DE FINANCIAMENTO

CAPES

CNPq

FAPESB

FAPESP

AGRADECIMENTOS

Após esses 4 anos de doutorado, eu gostaria de agradecer enormemente a todos que fizeram parte dessa trajetória. Nada disso seria possível caminhando sozinha, então obrigada a todos vocês que estiveram comigo e contribuíram para a consolidação desta tese. Inicialmente agradeço à Dra. Milena Botelho Pereira Soares, pela orientação, e confiança, e por ser esse exemplo de pesquisadora em minha vida. Agradeço aos colegas do Centro de Biotecnologia e Terapia Celular e do Laboratório de Engenharia Tecidual e Imunofarmacologia (LETI) do Instituto Gonçalo Moniz/Fiocruz-BA por todos esses anos, desde 2009, antes mesmo do mestrado, pelo convívio diário e por toda e qualquer ajuda, seja em um simples sorriso, em um preparo de meio de cultura ou na execução de um experimento. Agradecimento em especial à Dra. Rejane Carvalho Rughes por toda a dedicação na primeira etapa dos experimentos e nos ensinamentos de biologia molecular. Você foi fundamental no meu aprendizado! Agradecimento mais que especial ao colega Vinícius Pinto Costa Rocha, meu parceiro de laboratório, com quem compartilhei os resultados mais felizes e mais tristes, e quem esteve comigo durante esses 4 anos me ensinando e ajudando com os diferentes experimentos. Obrigada, man! Agradeço do fundo do meu coração pela oportunidade que Dr. Sergio Schenkman e Dr. Nilmar Silvio Moretti me deram de realizar grande parte dos experimentos no Laboratório de Biologia Celular e Molecular de Tripanossomas da Universidade Federal de São Paulo (UNIFESP)-SP, onde fui muito bem recebida por todos os colegas de lá! Muito obrigada mesmo! Aprendi e amadureci profissionalmente muito com vocês! Agradeço também à Lucyvera Imbroinise (Veroca) que com certeza é alguém que guardarei no meu coração para todo o sempre! Uma pessoa que pude compartilhar minhas angústias e felicidades e que sempre esteve disposta a me ouvir e me dar os melhores conselhos profissionais, além de todo o auxílio na área administrativa. Agradeço aos colegas Dr. Diogo Rodrigo de Magalhães Moreira e Cássio Santana Meira, pelas diferentes formas de apoio ao longo desse período. Agradeço aos membros da minha banca de qualificação (Dra. Patrícia Sampaio Tavares Veras, Dr. Mitermayer Galvão dos Reis e Dr. Geraldo Gileno de Sá Oliveira) pelas contribuições que foram realizadas e pelos ensinamentos. Agradeço também ao Dr. Mitermayer pela disponibilidade de utilizar o Laboratório de Patologia e Biologia Molecular (LPBM) do Instituto Gonçalo Moniz/Fiocruz-BA para a realização de experimentos. Agradecer também aos colegas Dra. Carine Machado

Azevedo Cardoso, Dra. Clarissa Xavier Resende Valim, Dra. Luciana Souza de Aragão França e ao Dr. Bruno Diaz Paredes, que apesar de termos feitos diversos experimentos que não entraram na tese, vocês me ajudaram muito ao longo deste período! Agradeço ao Dr. Bruno Solano de Freitas Souza por ser também um exemplo de jovem pesquisador com sinônimo de competência e eficiência. Agradeço a todos, desde o auxílio técnico ao administrativo do CBTC e da Fiocruz, em especial à Roquelina Assis, à Secretaria Acadêmica do PGPAT pelo suporte, aos professores que tive pelos ensinamentos ao longo destes anos, às plataformas de Sequenciamento (Fiocruz/BA) e de proteômica (Fiocruz/RJ) e à biblioteca do Instituto Gonçalo Moniz/Fiocruz-BA.

Mas, por trás de uma pesquisadora, existe uma filha, uma irmã, uma cunhada e uma tia. Minha família é sem dúvidas a grande responsável por toda essa conquista. É quem me dá toda a base para ser quem eu sou, seja profissionalmente ou pessoalmente. São eles quem mais entenderam o quanto eu estava extremamente exausta ou maravilhada com um experimento e outro. Agradeço também aos meus amigos que são pessoas tão especiais na minha vida e que contribuíram com os diferentes momentos de alegria e para que eu mantivesse a mente sã ao longo deste período. Sou muito agradecida! Obrigada a todos vocês!

BASTOS, Tanira Matutino. Uso das sirtuínas do *Trypanosoma cruzi* como alvos moleculares no desenvolvimento de fármacos para o tratamento da doença de chagas. 128 f. il. Tese (Doutorado em Patologia) – Universidade Federal da Bahia. Fundação Oswaldo Cruz, Instituto Gonçalo Moniz, Salvador, 2017.

RESUMO

INTRODUÇÃO: A doença de Chagas, causada pelo protozoário flagelado *Trypanosoma cruzi*, afeta em torno de 6 a 7 milhões de pessoas mundialmente. O benznidazol e o nifurtimox, medicamentos utilizados no tratamento da doença, apresentam eficácia limitada, e estão associados com a presença de efeitos colaterais graves. Portanto, torna-se necessária a identificação de novos alvos farmacológicos para a seleção de moléculas com boa eficácia contra o parasito e baixa toxicidade. Neste contexto, devido ao fato de atuarem em processos celulares vitais, as sirtuínas têm atraído interesse como potenciais alvos farmacológicos para o tratamento de diferentes doenças, incluindo a doença de Chagas. **OBJETIVO:** O objetivo deste estudo foi caracterizar as sirtuínas de *T. cruzi*, TcSir2rp1 e TcSir2rp3, como alvos farmacológicos para a identificação de novas drogas para o tratamento da doença de Chagas. **METODOLOGIA:** As TcSir2rp1 e TcSir2rp3 recombinantes foram produzidas utilizando sistema de expressão em bactérias e purificadas para posterior validação da atividade biológica das enzimas e triagem de 48 moléculas sintéticas e isoladas de produtos naturais. As moléculas que apresentaram atividade inibitória para as enzimas foram investigadas para avaliar o potencial em inibir as formas tripomastigota e amastigota do parasito, além da toxicidade em fibroblastos humanos. Além disso, foi investigada a propriedade antiparasitária *in vivo* de outros compostos que, apesar de não inibirem as sirtuínas do parasito, apresentaram atividade antiparasitária nos ensaios de triagem em sistema de *High Content Screening* padronizado para atividade tripanocida. **RESULTADOS:** As sirtuínas recombinantes produzidas apresentam atividade de lisina desacetilase NAD+ dependente, sendo demonstrado, pela primeira vez, a atividade biológica de TcSir2rp1 em ensaio funcional. Dentre os 48 compostos que foram triados, 10 apresentaram atividade inibitória de sirtuínas do parasito, sendo 3 inibidores de TcSir2rp1 (compostos **14**, **17** e **40**), 5 deles inibidores de TcSir2rp3 (compostos **10**, **12**, **13**, **33** e **35**) e 2 inibidores de ambas as sirtuínas do parasito (compostos **43** e **44**). Foi verificada atividade antiparasitária de todos os compostos selecionados no ensaio de triagem com as enzimas recombinantes. Porém, o ensaio de toxicidade em fibroblasto humano indica que a atividade destes compostos não é seletiva. Dentre os compostos que não inibiram as sirtuínas de *T. cruzi*, mas apresentaram atividade antiparasitária potente e seletiva (compostos **45**, **46**, **47** e **48**), 2 deles foram selecionados para o ensaio de atividade em camundongo (compostos **45** e **48**) e apesar do tratamento *in vivo* causar a redução da parasitemia, os animais vieram ao óbito, com sinais de toxicidade. **CONCLUSÕES:** Este trabalho reforça o uso das sirtuínas do parasito como alvos farmacológicos, com a identificação de diferentes compostos que podem ser otimizados através da química medicinal com o intuito de identificar moléculas mais seletivas e potentes para serem usadas no tratamento da doença de Chagas.

Palavras-chave: Doença de Chagas; *Trypanosoma cruzi*; Sirtuínas; Alvos farmacológicos, Desenvolvimento de fármacos.

BASTOS, Tanira Matutino. Use of sirtuins of *Trypanosoma cruzi* as molecular targets in drug development for the treatment of chagas disease. 128 f. il. Tese (Doutorado em Patologia) – Universidade Federal da Bahia. Fundação Oswaldo Cruz, Instituto Gonçalo Moniz, Salvador, 2017.

ABSTRACT

INTRODUCTION: Chagas disease, caused by protozoa parasite *Trypanosoma cruzi*, affects around 6 to 7 million people worldwide. Nifurtimox and benznidazol, the drugs used in the treatment of the disease, have limited efficacy and have been associated with severe side effects. Thus, there is an urgent need to find new biotargets for the identification of compounds with good efficacy against the parasite and low toxicity. In this context, due to their biological function on vital cellular processes, sirtuins have attracted interest as potential pharmacological targets for the treatment of different diseases, including Chagas disease. **OBJECTIVE:** The objective of this study was to characterize *T. cruzi* sirtuins, TcSir2rp1 and TcSir2rp3, as pharmacological targets for the identification of new drugs for the treatment of Chagas disease. **METHODOLOGY:** For this, recombinant TcSir2rp1 and TcSir2rp3 were produced, using expression system in bactéria, and purified for subsequent validation of biological activity of enzymes and screening of 48 synthetic molecules or isolated from natural products. The molecules that presented inhibitory activity for enzymes were investigated to assess the potential to inhibit the trypomastigote and amastigote forms of the parasite, and the toxicity effect in human fibroblasts. In addition, we also investigated the antiparasitic effects in vivo of other compounds which, although did not inhibit the sirtuin activity, showed anti-*T. cruzi* activity when screened in vitro using the High Content Screening System. **RESULTS**: The recombinant sirtuins produced presented NAD + dependent lysine desacetilase activity, being the first time this is shown for TcSir2rp1 in a functional test. Among the 48 compounds screened, 10 showed inhibitory activity of *T. cruzi* sirtuins, being 3 TcSir2rp1 inhibitors (compounds **14**, **17** and **40**), 5 of them anti-TcSir2rp3 (compounds **10**, **12**, **13**, **33** and **35**) and 2 inhibitors of both sirtuins of the parasite (compounds **43** and **44**). Antiparasitic activity was found in all compounds selected in screening assays with recombinant enzymes. However, the toxicity test in human fibroblasts indicates that the activity of these compounds is not selective. Among the compounds that did not inhibit the sirtuins of *T. cruzi*, but showed potent and selective antiparasitic activity (compounds **45**, **46**, **47** and **48**). Two of them (compounds **45** and **48**) were tested in vivo in *T. cruzi*-infected mice, and although they caused a reduction of parasitemia, mortality was seen associated with signs of drug toxicity. **CONCLUSIONS:** This study reinforces the use of the sirtuins of the parasite as pharmacological targets, with the identification of different compounds that can be optimized through the medicinal chemistry in order to identify more selective and potent molecules to be used in the treatment of Chagas disease.

Keywords: Chagas disease; *Trypanosoma cruzi*; Sirtuins; Pharmacological target; Drug development.

LISTA DE ILUSTRAÇÕES

LISTA DE TABELAS

SUMÁRIO

1 INTRODUÇÃO

1.1 A DOENÇA DE CHAGAS

A doença de Chagas pertence ao grupo das doenças negligenciadas, que são causadas por agentes infecciosos endêmicos, sobretudo nos países em desenvolvimento, nas populações que vivem em condições de pobreza e sem saneamento básico adequado. Segundo dados da Organização Mundial de Saúde, mais de um bilhão de pessoas estão infectadas com um ou mais agentes etiológicos causadores de doenças negligenciadas, o que representa um sexto da população mundial (WORLD HEALTH ORGANIZATION, 2017a).

A doença de Chagas e seu agente causal, o protozoário hemoflagelado *Trypanosoma cruzi*, foram descobertos no Brasil por Carlos Chagas, em 1909 (CHAGAS, 1909). A acuidade científica do pesquisador mineiro permitiu-lhe ainda descrever os reservatórios silvestres do parasito, o desenvolvimento do parasito no vetor e as características clínicas da doença (CHAGAS, 1916). Ele foi o primeiro, e até os dias atuais, permanece como o único cientista na história da medicina a descrever completamente uma doença infecciosa.

O *T. cruzi* é um flagelado da ordem Kinetoplastida, família Trypanosomatidae, caracterizada pela existência de um único flagelo e do cinetoplasto, uma estrutura que contém o DNA mitocondrial (kDNA) (DE SOUZA, 2002). Além do *T. cruzi*, espécies do gênero *Leishmania* e o *Trypanosoma brucei* representam importantes tripanossomatídeos de relevância médica, sendo responsáveis pela leishmaniose e a tripanossomíase africana ou doença do sono, respectivamente.

Os vetores da doença de Chagas, que compreendem mais de 150 espécies de triatomíneos hematófagos principalmente dos gêneros *Triatoma*, *Panstrongylus* e *Rhodnius*, foram capazes de transmitir o parasito, como uma enzoose, causando a doença em mais de cem espécies de mamíferos, sobretudo em espécies silvestres, tais como marsupiais, roedores e primatas por milhões de anos (COURA; VIÑAS, 2010). A chegada dos seres humanos na América e o consequente aumento das atividades agrícolas e da domesticação de animais proporcionaram a transmissão acidental de *T. cruzi* na população humana e a doença de Chagas passou a ser considerada uma antropozoonose (COURA; DIAS, 2009).

Evidências da presença de *Triatoma infestans* em habitações humanas em tempos pré-colombianos, como nas culturas Inca e Chinchorro, e a identificação de DNA de *T. cruzi* em múmias encontradas na região norte do Chile e sul do Peru, com datações de nove mil anos, indicam uma introdução gradual da transmissão domiciliar da doença de Chagas (AUFDERHEIDE et al., 2004). Nos últimos 200-300 anos, como resultado do desmatamento provocado pela expansão da agricultura e agropecuária, além da abertura de vias terrestres de transporte, os insetos silvestres adaptaram-se ao ambiente doméstico na procura de nova fonte alimentar, a exemplo do sangue de animais domésticos e de seres humanos. Deste modo, um novo ciclo de infecção foi estabelecido e a doença de Chagas passou a ser classificada como uma zoonose (ZINGALES, 2011).

1.2 CICLO BIOLÓGICO E MECANISMOS DE TRANSMISSÃO DO *T. cruzi*

Classicamente, a doença de Chagas é transmitida pela via vetorial, ou seja, através das fezes de triatomíneos contendo a forma infectiva tripomastigota metacíclica. O triatomíneo infecta-se através do repasto sanguíneo, alimentando-se do sangue de um mamífero infectado com a forma tripomastigota sanguícola. Dentro do inseto, o parasito diferencia-se em epimastigota e replica-se no intestino do vetor por divisão binária. Antes de ser eliminado nas fezes, a forma epimastigota diferencia-se em tripomastigota metacíclica. Quando o triatomíneo infectado realiza o repasto sanguíneo, ele defeca na pele do hospedeiro vertebrado, eliminando o parasito através das fezes. O parasito penetra no hospedeiro a partir de cortes e abrasões na pele ou através das mucosas (GARCIA; AZAMBUJA, 1991).

O parasito pode infectar macrófagos e uma variedade de outras células nucleadas, com predominância das células do baço, fígado, linfonodos, tecido conjuntivo intersticial, miocárdio ou músculos esqueléticos. A forma amastigota, intracelular e replicativa nos mamíferos, multiplica-se nos tecidos, formando pseudocistos, que se rompem e liberam as tripomastigotas sanguícolas na corrente sanguínea. Alguns parasitos, sob a forma de tripomastigota, recirculam e voltam a infectar outras células ou são ingeridos durante o repasto sanguíneo pelo vetor, reiniciando o ciclo (COURA, 2003) (Figura 1).

Além da via vetorial, a transmissão da doença de Chagas em humanos pode ocorrer pelas vias oral e congênita, por transfusão de sangue e, de forma menos

frequente, por acidentes de laboratório e transplante de órgãos (doador infectado com o parasito) (COURA, 2015). No Brasil, desde o controle da transmissão através do *Triatoma infestans* e por transfusão sanguínea, a via oral representa a principal forma de infecção do *T. cruzi* (COURA, 2006).

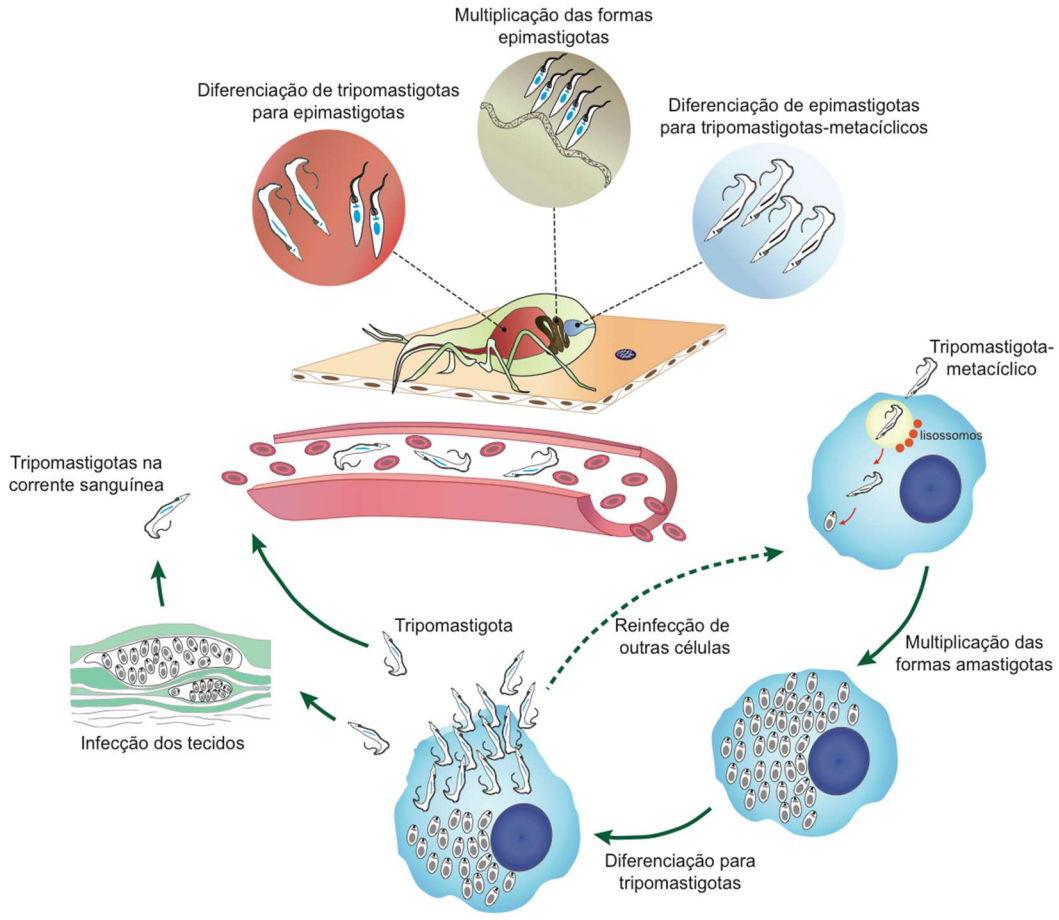

Figura 1 – Ciclo de vida do *T. cruzi*, o agente causal da doença de Chagas.
Fonte: Elaborado pelo colaborador Dr. Nilmar Silvio Moretti.

1.3 EPIDEMIOLOGIA DA DOENÇA DE CHAGAS

A doença de Chagas representa um importante problema de saúde pública no continente americano, acarretando impactos socioeconômicos com ampla distribuição geográfica. A Organização Mundial de Saúde estima que existam entre 6 e 7 milhões de pessoas infectadas com o *T. cruzi* em todo o mundo, principalmente na América Latina, onde a doença de Chagas é considerada endêmica (WORLD HEALTH ORGANIZATION, 2017b).

No Brasil, atualmente, predominam os casos da doença de Chagas crônica decorrentes de infecções, por via vetorial, adquiridas em décadas passadas. Nos

últimos anos, a ocorrência de doença de Chagas aguda tem sido observada principalmente, nos estados da Amazônia Legal, principalmente no Pará, onde o fruto do açaizeiro é uma importante fonte de contaminação por via oral (MONCAYO; SILVEIRA, 2009). No período de 2000 a 2013, foram registrados, no Brasil, 1.570 casos de doença de Chagas aguda, sendo a região norte do país responsável por 91% destes, e o estado do Pará por 75%. Do número total de casos confirmados de doença de Chagas aguda, 68,9% (1081/1.570) foram por transmissão oral, 6,4% por transmissão vetorial (100/1.570), apenas 0,4% (6/1.570) por transmissão vertical, e em 23,7% (372/1.570) dos casos não foi identificada a forma de transmissão (BRASIL, 2015). Casos agudos resultantes da contaminação oral têm sido documentados não só na região amazônica, assim como, em diferentes localidades da América Latina, como na Venezuela, Guiana Francesa e nas regiões nordeste e sul do Brasil (ALARCÓN DE NOYA et al., 2010; DIAS et al., 2008; STEINDEL et al., 2008; ZINGALES et al., 2012).

A doença de Chagas endêmica na América Latina começou como uma doença de populações pobres e rurais. A urbanização da população rural fez com que a doença de Chagas se tornasse um importante problema de saúde pública, introduzindo novos riscos, tais como a possibilidade de transmissão de *T. cruzi* por meio de transfusão sanguínea (COURA; VIÑAS, 2010). No Brasil, em 2010, a Resolução da Diretoria Colegiada – RDC N° 57 passou a determinar a triagem sorológica para a doença de Chagas nas transfusões sanguíneas, que levou a um controle da infecção transmitida através desta via. Apesar de outros países da América Latina também realizarem este controle, o sangue contaminado ainda é um grande problema na Bolívia, onde, em cidades como Santa Cruz de la Sierra e Cochabamba, até a metade de doadores de sangue podem estar infectados com o *T. cruzi* (COURA; VIÑAS, 2010; MONCAYO; SILVEIRA, 2009).

O aumento da migração da população no mundo mudou o cenário da distribuição da doença de Chagas. O movimento populacional dos países endêmicos para os países não endêmicos, além da possibilidade de transmissão da doença de Chagas por transfusão de sangue, transplante de órgãos e via congênita, favoreceram a entrada do *T. cruzi* em diferentes regiões geográficas, incluindo a América do Norte (Estados Unidos e Canadá), oeste do Pacífico (principalmente Japão e Austrália) e Europa (SCHMUNIS, 2007). Estima-se que mais de 300.000 indivíduos estejam infectados com o *T. cruzi* nos Estados Unidos, mais de 5.500 no Canadá, mais de

80.000 na Europa e na região do Pacífico ocidental, mais de 3.000 no Japão e mais de 1.500 na Austrália (RIBEIRO et al., 2012) (Figura 2).

Figura 2 – Distribuição global de indivíduos infectados com *T. cruzi* e sua associação com a transmissão vetorial (dados estimados entre 2006 e 2009).
Adaptado de: RIBEIRO et al., 2012.

A ocorrência da doença de Chagas em países não endêmicos começou a criar novos desafios epidemiológicos, econômicos, sociais e políticos, uma vez que, em decorrência do novo cenário de distribuição da doença de Chagas, existe a necessidade de melhora no sistema de vigilância sanitária nestes países, a incluir triagem sorológica nos bancos de sangue e controle no transplante de órgãos, além da inclusão do diagnóstico diferencial e tratamento específico para a doença de Chagas (CONNERS et al., 2016).

1.4 PATOGENIA DA DOENÇA DE CHAGAS

A infecção chagásica apresenta duas fases bem distintas: fase aguda e fase crônica. A fase aguda é caracterizada pela alta parasitemia e apresenta diferentes manifestações clínicas, sendo elas: assintomática, oligossintomática e sintomática. Na forma sintomática, observa-se a presença de adenomegalia, hepatoesplenomegalia, alteração bipalpebral unilateral (sinal de Romaña), e, em 1%

das infecções, meningoencefalite e miocardite, que corresponde a principal causa de óbito durante esta fase da doença (BERN, 2015).

Após 4 a 8 semanas, a resposta imune mediada por células controla a replicação do parasito, levando à redução da parasitemia e à resolução dos sintomas. Após o período de latência de 10 a 15 anos, no qual os indivíduos permanecem assintomáticos na chamada forma indeterminada, em torno de 20 a 30% dos pacientes evoluem para a forma sintomática da fase crônica, desenvolvendo as formas cardíaca - que inclui a cardiopatia chagásica -, digestiva ou mista (BERN, 2015). A forma cardíaca é caracterizada por miocardite crônica, insuficiência cardíaca e, eventualmente, morte súbita por arritmia cardíaca. Pacientes que evoluem para a forma digestiva da doença de Chagas podem desenvolver megaesôfago e/ou megacólon, ou seja, dilatação exagerada do esôfago ou cólon. A forma mista é caracterizada pela presença da forma cardíaca e digestiva, simultaneamente (COURA, 2003).

Estima-se que, anualmente, 2 a 3% dos indivíduos assintomáticos passam a apresentar as manifestações clínicas da fase crônica da doença. A comunidade científica vem debatendo sobre quais são os principais fatores associados com esta conversão e se isto é o resultado da variabilidade genética do parasito, da imunogenética do hospedeiro humano, de fatores ambientais ou da ação combinada destes elementos (LEWIS et al., 2016; TAFURI, 1987; ZINGALES, 2011). Embora a patogênese da doença não seja completamente compreendida, existe um consenso que a persistência do parasito tem um papel central na evolução para as formas sintomáticas da fase crônica da doença, que é caracterizada pela presença de infiltrado inflamatório de células mononucleares, fibrose e parasitismo (RIBEIRO et al., 2012). Os dados da literatura atualmente sugerem que a persistência do parasito pode levar à inflamação do tecido, causando disfunções vasculares, autoimunidade e disfunção neurogênica, pela destruição de células ganglionares e lesões do sistema de condução, culminando na gravidade da cardiopatia chagásica (MACHADO et al., 2012; MARIN-NETO et al., 2007; RIBEIRO et al., 2012). Tem sido também observado que fatores epigenéticos podem estar envolvidos com a patogênese da doença, como foi demonstrado por LAUGIER et al., 2017, que verificaram alteração dos níveis de expressão de genes envolvidos principalmente com ativação de células T, canais iônicos, e, remodelamento e proteção do miocárdio em pacientes com cardiopatia chagásica. A forma digestiva da doença tem sido associada com a destruição de

plexos mioentéricos de Auerbach (BERMUDEZ et al., 2016). A persistência do parasitismo é de 20-50% nos casos de megaesôfago (ADAD et al., 1991; CÔBO et al., 2012) e a detecção molecular do parasito é de 100% em pacientes com megaesôfago comparado a 60% de detecção positiva em pacientes com doença de Chagas sem megaesôfago (SILVEIRA et al., 2005).

1.5 TRATAMENTOS DISPONÍVEIS

Os medicamentos existentes para o tratamento da doença de Chagas foram introduzidos na clínica na década de 70. O benznidazol, um derivado 2-nitroimidazólico, e o nifurtimox, um derivado 5-nitrofurano, fazem parte de uma mesma família, a dos nitro-heterocíclicos. O mecanismo de ação destes fármacos ainda é pouco esclarecido, mas acredita-se que a ação anti-*T. cruzi* do nifurtimox se deva à redução metabólica do grupo nitro, gerando radicais nitroânion reativos e tóxicos ao parasito (DOCAMPO; STOPPANI, 1979). O principal mecanismo de ação do benznidazol está relacionado com a ligação de intermediários nitroreduzidos a moléculas tióis de baixo peso molecular, assim como de proteínas tióis, levando a uma depleção de tióis endógenos, provocando, assim, o efeito tóxico ao parasito (TROCHINE et al., 2014).

Ambos os medicamentos apresentam boa eficácia quando administrados logo após a infecção, durante a fase aguda da doença, incluindo os casos de transmissão congênita, ou em casos de reativação da infecção. Entretanto, a eficácia de cura do benznidazol e do nifurtimox diminui se administrados em uma fase mais tardia e com baixa parasitemia (WORLD HEALTH ORGANIZATION, 2017b). Com isso, o tratamento da doença de Chagas é considerado limitado durante a fase crônica da infecção (COURA, 2003). Todavia, de acordo com a Organização Mundial da Saúde, existem evidências sugerindo que a persistência do parasitismo é a maior causa de progressão clínica para a cardiopatia chagásica, e que o tratamento com o benznidazol durante a fase assintomática e/ou no início da fase crônica contribua com uma prevenção no desenvolvimento das manifestações clínicas (GARCIA et al., 2005; MARIN-NETO et al., 2008, 2009; MORILLO et al., 2015; RIBEIRO et al., 2012). Por esta razão, a Organização Mundial da Saúde tem recomendado o tratamento para os pacientes não apenas na fase aguda da doença (WORLD HEALTH ORGANIZATION, 2017b).

Apesar do benznidazol e nifurtimox serem eficazes quando administrados na fase inicial da doença, já foram descritas na literatura a existência de cepas resistentes aos medicamentos durante a infecção aguda, que requer longos períodos de tratamento (60 dias para o benznidazol e até 90 dias para nifurtimox). A deficiência no sistema de saúde de muitas comunidades rurais e pobres, em países endêmicos, também contribui para a redução da eficácia do tratamento e o favorecimento de resistência aos medicamentos, em decorrência da infraestrutura limitada e da falta de suporte para oferecer o tratamento completo aos pacientes (CLAYTON, 2010).

O uso do nifurtimox e benznidazol está associado a presença de efeitos colaterais potenciais, incluindo erupções cutâneas, náuseas e insuficiência renal e hepática (CLAYTON, 2010). O nifurtimox tem se mostrado mais tóxico que o benznidazol, induzindo efeitos adversos neurológicos graves, incluindo polineurite, convulsões e eventos psicóticos. Neste contexto, em muitos países, o benznidazol tem sido considerado a terapia de primeira escolha para o tratamento da doença de Chagas. Diferentes estratégias têm sido pensadas com o objetivo de superar a toxicidade associada ao benznidazol, incluindo a redução da administração do medicamento ou um esquema de administração intermitente, seja sozinho ou em combinação com outros fármacos (BERMUDEZ et al., 2016). Em paralelo, a busca pela identificação de novos fármacos para o tratamento da doença de Chagas torna-se fundamental e urgente.

1.6 DESENVOLVIMENTO DE NOVOS FÁRMACOS ANTI-*T. cruzi*

Investigações bioquímicas e fisiológicas comparativas entre o parasito e o hospedeiro representam uma interessante abordagem na busca de novas opções terapêuticas para doenças parasitárias (SMIRLIS; SOARES, 2014; SOEIRO; DE CASTRO, 2011). Estudos têm permitido a identificação de alvos potenciais em *T. cruzi*, que incluem diferentes enzimas como a tripanotiona redutase, as cisteíno-proteases, a gliceraldeído-3-fosfato desidrogenase e as enzimas da síntese de esteróis, como C14α-esterol desmetilase (revisto por SOEIRO; DE CASTRO, 2011).

Além da determinação de alvo(s) específico(s) identificado(s) em vias metabólicas chave para o parasito, outros métodos também estão sendo utilizados na busca de novas quimioterapias. Dentre eles, o reposicionamento de fármacos, ou seja, o uso de fármacos já aprovados no tratamento de outras doenças, uma vez que

já foram submetidos a ensaios clínicos dispendiosos (CLAYTON, 2010) e a terapia combinada (COURA; DIAS, 2009). Ensaios pré-clínicos contra o *T. cruzi* têm identificado diferentes moléculas com potencial para a terapia clínica da doença de Chagas (KEENAN; CHAPLIN, 2015). Dentre os compostos testados nas últimas três décadas, os inibidores da biossíntese de ergosterol têm ganhado destaque. Inibidores da enzima C14α-esterol desmetilase do parasito, posaconazol e ravuconazol, medicamentos já utilizados na clínica como antifúngicos triazólicos, demonstraram atividade anti-*T. cruzi* promissora, e como resultado, o posaconazol e um pró-fármaco do ravuconazol (E1224) foram submetidos a ensaios clínicos de fase II (BUCKNER; URBINA, 2012). Entretanto, os dados demonstraram uma ação não-curativa de ambos os fármacos, com percentual de falha terapêutica superior a 70% (MOLINA et al., 2014; KEENAN; CHAPLIN, 2015).

Diante deste contexto, a identificação de novos alvos terapêuticos torna-se necessária para o desenvolvimento de fármacos com atividade anti-*T. cruzi* para o tratamento da doença de Chagas. Dentre os alvos que têm sido explorados, temos as sirtuínas (KEENAN; CHAPLIN, 2015; WANG et al., 2015; ZHENG, 2013).

1.7 SIRTUÍNAS COMO POTENCIAIS ALVOS FARMACOLÓGICOS NA DOENÇA DE CHAGAS

Os níveis de acetilação de proteínas são regulados através do balanço entre a atividade de duas famílias de enzimas: as lisinas acetiltransferases (KATs) e as lisinas desacetilases (KDACs). As KDACs podem ser divididas em quatro classes, sendo as de classe I, II, e IV classificadas como zinco-dependentes e as de classe III, dependentes de NAD+, sirtuínas ou Sir2 (GREGORETTI; LEE; GOODSON, 2004).

As sirtuínas são enzimas conservadas desde as *Archaea* até eucariontes superiores (BRACHMANN et al., 1995) sendo encontradas em diferentes organelas, dependendo do organismo. Essas enzimas participam de diversos processos celulares, tais como silenciamento gênico, regulação do ciclo celular, mecanismos de reparo de dano no DNA, diferenciação e crescimento parasitário e processos metabólicos (ALSFORD et al., 2007; GARCÍA-SALCEDO et al., 2003; MORETTI et al., 2015; RITAGLIATI et al., 2015; SOARES et al., 2012; VEIGA-SANTOS et al., 2014; VERGNES; GAZANION; GRENTZINGER, 2016).

Tem sido descrito na literatura o papel de sirtuínas na regulação dos níveis de outras modificações pós-traducionais além de desacetilação (NORTH; VERDIN, 2004), tais como atividade ADP-ribosiltransferase (FRYE, 1999), lisina glutarilação (do inglês, *lysine glutarylation*) (TAN et al., 2014), lisina demalonilase (do inglês, *lysine demalonylase*) (DU et al., 2011) e lisina desucciliação (do inglês, *lysine desuccinylation*) (DU et al., 2011; PARK et al., 2013). Entretanto, além da função de lisina desacetilase, apenas a função ADP-ribosiltransferase tem sido também associada a sirtuínas em tripanossomatídeos (ALSFORD et al., 2007; TAVARES et al., 2008).

Enquanto o genoma humano codifica sete sirtuínas, os tripanossomatídeos apresentam um repertório menor destas proteínas. Em *T. brucei* existem três proteínas desta classe, sendo denominadas TbSir2rp (Sir2-*related proteins*) 1, 2 e 3. Duas delas, TbSir2rp2 e rp3, possuem localização mitocondrial, enquanto TbSir2rp1 é uma desacetilase nuclear e também apresenta função ADP-ribosiltransferase envolvida no silenciamento de genes presentes na região telomérica e não é necessária para a viabilidade do parasito (ALSFORD et al., 2007). O gênero *Leishmania* também possui três genes que codificam sirtuínas, sendo a Sir2rp1 localizada no citoplasma, apresenta atividade de desacetilase NAD+ dependente, assim como ADP-ribosiltransferase, sendo essencial para a sobrevivência do parasito, e as demais (Sir2rp2 e Sir2rp3) localizadas na mitocôndria (IVENS et al., 2006; TAVARES et al., 2008; VERGNES; GAZANION; GRENTZINGER, 2016). Por outro lado, o *T. cruzi* apresenta apenas dois genes que codificam para sirtuínas, TcSir2rp1 e TcSir2rp3, localizadas no citoplasma e mitocôndria, respectivamente. Enquanto a TcSir2rp1 parece estar envolvida com o processo da metaciclogênese, a TcSir2rp3 está relacionada com o crescimento parasitário (RITAGLIATI et al., 2015; MORETTI et al., 2015). Não é descrito na literatura o papel das sirtuínas de *T. cruzi* em nenhuma outra modificação pós-traducional, além de lisina desacetilase. As discrepâncias entre os ortólogos Sir2 em tripanossomatídeos é inesperado, considerando que as sirtuínas são enzimas conservadas entre as espécies, porém as predições por modelagem molecular demonstram diferenças no sítios ativos das enzimas das diferentes espécies (KAUR; SHIVANGE; ROY, 2010). Durante a reação de desacetilação, acetil-lisina e NAD+ são convertidos em lisina, nicotinamida e O-acetil-ADP-ribose (TANNER et al., 2000). Portanto, o espectro de funções desta família de enzimas em cada espécie pode ser explicado pela variedade de proteínas modificadas pós-

traducionalmente, além dos diferentes substratos e produtos gerados após reação (ALSFORD et al., 2007).

As sirtuínas são classificadas em cinco diferentes classes (I, II, III, IV e U), a depender da conservação de motivos específicos no domínio central da sequência proteica (FRYE, 2000). Enquanto os genes codificantes para as sete sirtuínas humanas estão distribuídas nas classes I à IV, as sirtuínas do *T. cruzi*, TcSIR2rp1 e TcSIR2rp3, pertencem, respectivamente as classes I e III (SACCONNAY et al., 2013).

Devido ao fato de atuarem em processos celulares vitais, as sirtuínas têm atraído interesse como potenciais alvos farmacológicos para o tratamento de diferentes doenças, tais como o câncer e doenças neurodegenerativas (GERTZ; STEEGBORN, 2016). Além disso, a inibição de sirtuínas em diferentes patógenos, incluindo o *T. brucei* e *Leishmania* spp., tem demonstrado atividade antiparasitária promissora, indicando que essas enzimas podem ser utilizadas como alvos terapêuticos alternativos contra infecção por parasitos (WANG et al., 2015).

Em *T. cruzi*, a base estrutural para a inibição de sirtuínas como alvos farmacológicos tem sido estabelecida através de estudos estruturais e funcionais (KAUR; SHIVANGE; ROY, 2010; MORETTI et al., 2015; RITAGLIATI et al., 2015; SACCONNAY et al., 2013; SOARES et al., 2012). Ensaios *in silico* sugerem que, apesar da similaridade das sequências, os domínios catalíticos de ligação das sirtuínas do parasito TcSir2rp1 e TcSir2rp3, apresentam diferenças estruturais com as enzimas humanas filogeneticamente relacionadas, hSirT1 e hSirT5, respectivamente, permitindo assim a identificação de moléculas seletivas inibitórias de sirtuínas do parasito (KAUR; SHIVANGE; ROY, 2010; SACCONNAY et al., 2013). Estudos *in vitro*, realizados por nosso grupo, sugeriram ser as sirtuínas potenciais alvos terapêuticos em *T. cruzi*, uma vez que a nicotinamida, um inibidor clássico destas enzimas (AVALOS; BEVER; WOLBERGER, 2005), demonstrou atividade inibitória sobre as diferentes formas evolutivas do parasito (SOARES et al., 2012). Recentemente, foi descrito que o uso de diferentes inibidores de sirtuínas interferem na viabilidade e crescimento do parasito, além de reduzir a parasitemia em ensaios realizados em camundongos. Além disso, foi verificada que a superexpressão das sirtuínas foi capaz de proteger os parasitos dos efeitos destes inibidores, reforçando o uso das sirtuínas como potenciais alvos farmacológicos em *T. cruzi* (RITAGLIATI et al., 2015; MORETTI et al., 2015).

Assim, no presente trabalho, propõe-se caracterizar melhor as sirtuínas do *T. cruzi* como alvos terapêuticos, bem como identificar e validar novos inibidores com potencial uso no tratamento da doença de Chagas.

2 JUSTIFICATIVA E HIPÓTESE

As únicas opções de tratamento da doença de Chagas existentes por mais de quarenta anos têm sido os fármacos benznidazol e nifurtimox. Ambos são considerados mais eficazes na fase aguda da doença, com uma taxa de cura em torno de 80%, e menos eficazes em pacientes na fase crônica da doença. Além disso, o benznidazol e o nifurtimox não são considerados medicamentos ideais, uma vez que os seus efeitos colaterais podem ser graves, e já existem relatos de cepas resistentes a estas drogas. Sendo assim, existe uma grande necessidade de novas pesquisas objetivando a identificação de moléculas com atividade antiparasitária para o tratamento da doença de Chagas. Estudos recentes têm permitido a identificação de alvos potenciais em *T. cruzi*¸ incluindo as sirtuínas. Tem sido demonstrando em tripanossomatídeos a importância desta família de proteínas para o parasito, sendo assim, a hipótese deste trabalho é que as sirtuínas podem ser alvos farmacológicos importantes do *T. cruzi* e com isso, o uso de inibidores farmacológicos de desacetilases NAD+ dependentes inviabilizariam a sobrevivência parasitária.

3 OBJETIVOS

3.1 GERAL

- Caracterizar as sirtuínas de *T. cruzi* como alvos farmacológicos para a identificação de novas drogas a serem utilizadas no tratamento da doença de Chagas.

3.2 ESPECÍFICOS

- Clonar, expressar e purificar as proteínas TcSir2rp1 e TcSir2rp3;
- Validar a atividade de desacetilação das proteínas recombinantes TcSir2rp1 e de TcSir2rp3;
- Avaliar o efeito de potenciais inibidores de sirtuínas na atividade de desacetilação *in vitro* de TcSir2rp1 e TcSir2rp3;
- Validar o ensaio de atividade anti-*T. cruzi in vitro* em sistema de *High Content Screening* para testes dos compostos selecionados;
- Avaliar a atividade anti-*T. cruzi* dos inibidores de sirtuínas.

4 MATERIAIS E MÉTODOS

4.1 PARASITOS

Todos os experimentos foram realizados com a cepa Y do *T. cruzi*. Os parasitos na forma epimastigota foram obtidos de amostras criopreservadas e armazenadas no Laboratório de Engenharia Tecidual e Imunofarmacologia (LETI - IGM – FIOCRUZ/BA) por sucessivas passagens *in vitro*. As formas epimastigotas do *T. cruzi* foram cultivadas em meio LIT (“liver infusion tryptose”) suplementado com 10% de soro bovino fetal (Cultilab, Campinas, SP, Brasil), 1% de hemina (Sigma-Aldrich, St. Louis, MO, EUA), 1% de meio R9 e 50 µg/mL de gentamicina (Novafarma, Anápolis, GO, Brasil) e mantidos em estufa a 26ºC.

Já os parasitos na forma tripomastigota sanguícola foram coletados do sangue de animais da linhagem BALB/c infectados por via intraperitoneal sete dias pós-infecção. A manutenção da forma tripomastigota também foi realizada por sucessivas passagens *in vitro*. Os parasitos foram cultivados em meio de cultura DMEM (Gibco/Life Technologies, Grand Island, NE, EUA) suplementado com 10% de soro bovino fetal (Cultilab) e Penicillina-Estreptomicina (100 U/mL) (Gibco/Life Technologies), juntamente com células da linhagem LLC-MK2 (ATCC CCL-7) e mantidos em estufa a 37ºC e 5% de CO_2.

4.2 EXTRAÇÃO DE DNA GENÔMICO DE *T. cruzi*

O DNA genômico foi obtido a partir da forma epimastigota do *T. cruzi*. As células foram lavadas com solução tampão fosfato-salino (PBS) (137 mM NaCl; 10 mM Na_2HPO_4; 1,8 mM KH_2PO_4; 2,7 mM KCl; pH de 7,4), ressuspensas em solução de lise (0,2 M Tris-HCl; pH 8,0; 0,01 M EDTA; 50 mg/mL proteinase K e dodecil sulfato de sódio [SDS] 10%) e incubadas a 37ºC por 16 horas. A purificação do DNA genômico foi feita através de duas extrações com fenol:clorofórmio:álcool isoamílico e duas extrações com clorofórmio. Cada extração foi seguida de centrifugação a 3.500 rpm por 5 minutos, coletando-se a fase aquosa. O DNA foi precipitado pela adição de 2 volumes de etanol 100%, seguido da lavagem com etanol 70%. Por fim, o DNA obtido foi ressuspenso em solução TE (10 mM Tris-HCl; pH 7,4; 1 mM EDTA) com RNAse 10 µg/mL e estocado a 4ºC.

4.3 ELETROFORESE EM GEL DE AGAROSE

Os produtos da reação em cadeia da polimerase (PCR), as mini-preparações de DNA plasmidial e as digestões com enzimas de restrição foram separados pela técnica de eletroforese em gel de agarose 1%, preparado em tampão tris acetato/EDTA (TAE) (40 mM Tris Base; 20 mM ácido acético glacial; 57,1 mM EDTA; pH 8,0) contendo 0,5 µg/mL de brometo de etídio. Após a eletroforese, o DNA foi visualizado sob luz ultravioleta e os géis foram fotodocumentados através do sistema de fotodocumentação Gel Logic 112 (Carestream, Rochester, NY, EUA).

4.4 CLONAGEM DO GENE TcSir2rp1

As etapas de clonagem, expressão e purificação de TcSir2rp1 foram realizadas em São Paulo, em colaboração com o Laboratório de Biologia Celular e Molecular de Tripanossomas - Universidade Federal de São Paulo (UNIFESP), chefiado pelo Dr. Sergio Schenkman.

O gene TcSir2rp1 foi amplificado utilizando-se a reação em cadeia da polimerase (PCR) a partir do DNA genômico do *T. cruzi* sob as seguintes condições: 1x → 94°C x 3 min, 35x → 94°C x 30 s, 60°C x 30 s, 72°C x 60 s, 1x → 72°C x 3 min. Para a PCR, utilizou-se a enzima Taq DNA polimerase recombinante (Thermo Fisher Scientific, Carlsbad, CA, EUA), de acordo com as recomendações do fabricante, utilizando 5 ng de DNA molde, 1,5 mM de cloreto de magnésio, 200 µM de cada dNTP e 0,5 µM de cada oligonucleotídeo e água em quantidade suficiente para um volume final de 50 µl. Os oligonucleotídeos foram desenhados com a inserção das sequências adaptadoras NheI; TcSir2rp1_NheI_F_5'-GCTAGCCATATGAATCAAGATAACGCCAACT-3' e XhoI; TcSir2rp1_XhoI_R_ 5'-CCCTCGAGTTATTTTCGGTCTGT-3'. As regiões sublinhadas representam os sítios de restrição NheI e XhoI, respectivamente.

Os produtos amplificados foram purificados utilizando-se o kit QIAquick Gel Purification (Qiagen, Gaithersburg, MD, EUA), de acordo com instruções do fabricante e clonados no vetor pET-28α. Para a clonagem, tanto o vetor quanto o fragmento amplificado foram submetidos a reação de digestão com as enzimas de restrição NheI e XhoI (New England Biolabs, Ipswich, MA, EUA) utilizando-se as condições especificadas pelo fabricante. Os produtos das digestões foram purificados utilizando

o kit QIAquick Gel Purification (Qiagen) e a reação de ligação foi realizada utilizando-se a enzima T4 DNA ligase (Thermo Fisher Scientific) de acordo com as orientações do fabricante.

4.5 CLONAGEM DO GENE TcSir2rp3

De forma similar, a reação de amplificação foi realizada utilizando-se o par de oligonucleotídeos desenhados com a inserção das sequências adaptadoras BamHI; TcSir2rp3_BamHI_F_5'-ATCAGGATCCATGAGGCCGCGGCGTCAG-3' e NotI; TcSir2rp3_NotI_R_5'-GAATGCGGCCGCCTACACCGCGTCTTGAAG-3' em condições semelhantes às descritas anteriormente. As regiões sublinhadas representam os sítios de restrição BamHI e NotI, respectivamente. O produto amplificado foi purificado utilizando-se o kit Nucleospin Gel and PCR clean-up (Machenerey-Nagel, Dueren, Alemanha). Para a clonagem, tanto o inserto quanto o vetor foram submetidos a uma reação de digestão com as enzimas de restrição BamHI e NotI (New England Biolabs) e após purificação do produto das reações o gene TcSir2rp3 foi clonado no plasmídeo pGEX-6P-1 nos respectivos sítios de restrição. Os produtos das digestões foram purificados utilizando-se o kit "Nucleospin Gel and PCR clean-up" (Machenerey-Nagel) e a reação de ligação foi realizada utilizando-se a enzima T4 DNA ligase (Thermo Fisher Scientific) de acordo com as recomendações fabricante.

4.6 TRANSFORMAÇÃO DE *Escherichia coli* E SELEÇÃO DOS CLONES

Bactérias *E. coli* (TOP10, DH5α ou Stable 3) competentes foram transformadas, por choque térmico, com os plasmídeos recombinantes gerados. Para isso, 1 ng do plasmídeo recombinante foi incubado com as bactérias em gelo durante 30 minutos, 42°C durante 2 minutos, e, em seguida, novamente em gelo durante 2 minutos. As células foram recuperadas em meio Luria-Bertani (LB) líquido e incubadas a 37ºC, sob agitação, por 1 hora. A seleção de transformantes foi feita em placas com meio LB sólido com ágar 1,5% contendo o antibiótico de seleção específico. As placas foram mantidas em estufa a 37ºC de 14-18 horas. Os clones selecionados foram inoculados em 5 mL de meio LB contendo o antibiótico de seleção específico e incubados sob agitação constante a 37ºC por 18 horas. Do volume total da cultura, 1 mL foi utilizado

para armazenamento, congelado em glicerol 25% a -80ºC e 4 mL da cultura submetidos a extração de DNA plasmidial pelo método de lise alcalina (BIRNBOIM; DOLY, 1979).

O DNA plasmidial obtido de diferentes clones foi submetido a reação de digestão com as enzimas de restrição NheI e XhoI, para os clones referentes ao vetor recombinante pET28α_TcSir2rp1, e com as enzimas BamHI e NotI, para os clones referentes ao vetor recombinante pGEX-6P-1_TcSir2rp3 a fim de confirmar os clones com os plasmídeos recombinantes corretos.

Para confirmar a integridade da sequência do gene TcSir2rp3, os DNAs plasmidiais recombinantes de interesse foram utilizados como molde para as reações de sequenciamento de nucleotídeos realizadas pela plataforma de sequenciamento de DNA do Instituto Gonçalo Moniz – Fiocruz/BA. Para a reação de sequenciamento, foi utilizado o método de Sanger (SANGER; NICKLEN; COULSON, 1992), baseado no método da terminação em cadeia e na eletroforese capilar como metodologia para leitura da reação através do sequenciador 3500xl Genetic Analyser (Applied Biosystems, Foster City, CA, EUA). Para cada reação foram utilizados 150 ng de DNA e 4 pmol de cada oligonucleotídeo. Os pares de oligonlucleotídeos utilizados para a reação de sequenciamento foram os mesmos utilizados para a PCR descritos anteriormente. A integridade da sequência do gene TcSir2rp1 também será confirmada a partir da reação de sequenciamento a ser realizada no Instituto Gonçalo Moniz – Fiocruz/BA.

4.7 EXPRESSÃO DA PROTEÍNA HETERÓLOGA TcSir2rp1

Bactérias BL21 (DE3) foram transformadas com o plasmídeo recombinante pET28α_TcSir2rp1. Um dos clones selecionados foi incubado em meio LB contendo o antibiótico de seleção canamicina (50 µg/mL) por 16-20 horas à 37°C sob agitação. Após este período, 10 mL dessa cultura foi expandida para 1.000 mL em meio LB e droga de seleção canamicina (50 µg/mL) e incubado a 37°C até OD_{600} de 0,8-1,0. 1 mM de isopropil-3-D-tiogalactopiranosídeo (IPTG) (Thermo Fisher Scientific) foi adicionado à suspensão bacteriana, que foi mantida sob agitação constante à 37°C durante 2 horas. Após o tempo de indução, a suspensão foi centrifugada por 10 minutos à 4°C a 7.700 x g, e as células foram submetidas à etapa de purificação.

4.8 EXPRESSÃO DA PROTEÍNA HETERÓLOGA TcSir2rp3

Bactérias BL21 (DE3) pRARE 2 foram transformadas com o vetor pGEX-6P-1_TcSir2rp3. Um dos clones selecionados foi incubado em meio LB contendo as drogas de seleção ampicilina (100 µg/mL) e clorafenicol (34 µg/mL) por 16-20 horas à 37°C sob agitação. Após este período, 10 mL dessa cultura foi expandida para 1.000 mL em meio LB com glicose 1%, e as drogas de seleção ampicilina (100 µg/mL) e clorafenicol (34 µg/mL) e foram incubadas a 37°C até OD_{600} de 0,8-1,0. Neste ponto, 0,1 mM de IPTG (Thermo Fisher Scientific) foi adicionado à suspensão bacteriana, que foi mantida sob agitação constante a 20°C durante 16-18 horas. Após o tempo de indução, a suspensão bacteriana foi centrifugada por 10 minutos à 4°C a 7.700 x g, e as células foram submetidas à etapa de purificação.

4.9 PURIFICAÇÃO DA PROTEÍNA HETERÓLOGA TcSir2rp1

As bactérias obtidas após o protocolo de expressão foram ressuspensas em tampão de lise (200 mM NaCl, 5% glicerol, 5 mM 2-mercaptoetanol, and 25 mM HEPES-NaOH [pH 7.5] e inibidores de protease [Sigma-Aldrich]) e lisadas a partir do processo de “French Press” (Thermo Electron Corporation, Beverly, MA, USA) ou por sonicação (Branson, Danbury, CT, EUA). A purificação da proteína foi feita por cromatografia de afinidade em resina contendo níquel, utilizando as colunas Ni-NTA superflow (Qiagen), como recomendado pelo fabricante. A purificação foi realizada utilizando-se a fração solúvel, obtida a partir da centrifugação do lisado celular (3.600 x g por 10 minutos) e coleta do sobrenadante. A fração solúvel foi incubada com a resina previamente equilibrada (200 mM NaCl, 5% Glicerol, 5 mM 2-mercaptoetanol, 25 mM imidazole, 25 mM HEPES-NaOH, pH 7.5) e incubada por 1 hora à 4°C. A resina foi lavada com o tampão de lavagem (200 mM NaCl, 5% glicerol, 5 mM 2-beta-mercaptoetanol, 50 mM imidazole, 25 mM HEPES-NaOH pH 7.5) e as enzimas foram eluídas com o mesmo tampão contendo 250 mM de imidazole. O produto da purificação de TcSir2rp1 foi submetido à análise por eletroforese desnaturante em gel de poliacrilamida (SDS-PAGE) 12%, seguida da coloração com azul de Coomassie (Sigma-Aldrich). As proteínas purificadas foram armazenadas à -80°C. A identidade da proteína heteróloga TcSir2rp1 purificada será confirmada através de análises por

espectrometria de massas MALDI-TOF a serem realizadas pela plataforma de proteômica do Instituto Oswaldo Cruz – Fiocruz/RJ.

4.10 PURIFICAÇÃO DA PROTEÍNA HETERÓLOGA TcSir2rp3

As bactérias obtidas após o protocolo de expressão foram ressuspensas em tampão de lise (2 mM ditiotreitol [DTT], 1 mM fenilmetilsulfonil fluoreto [PMSF], 100 µg/mL lisozima em solução PBS e inibidores de protease [Sigma-Aldrich]), e submetidas ao método de sonicação. Com as amostras em gelo, foram aplicados 10 pulsos de 5 segundos em amplitude 70 intercalados com intervalos de 1 minuto. Então foi adicionado Triton X-100 para atingir uma concentração final de 1% e a suspensão bacteriana foi centrifugada a 4°C, 18.000 g, por 30 minutos. O sobrenadante foi coletado e submetido à purificação por coluna cromatográfica de afinidade de glutationa sepharose (GSTrap™ FF) (GE Healthcare, Little Chalfont, Reino Unido) em cromatógrafo Äkta™ Avant (GE Healthcare). A cauda de glutationa-S-transferase (GST) expressa a partir da construção pGEX-6P-1_TcSir2rp3 foi clivada na coluna cromatográfica utilizando a protease 3C de rinovirus humano (HRV) (GE Healthcare) a 4°C por 1 hora. A proteína heteróloga TcSir2rp3 foi obtida a partir da lavagem da coluna cromatográfica utilizando a solução Tris-HCl 50 mM e foi armazenada à -80°C.

O produto da purificação de TcSir2rp3 foi submetido à análise por SDS-PAGE 12%, seguida da coloração com azul de Coomassie (Sigma-Aldrich). A identidade da proteína heteróloga TcSir2rp3 purificada foi confirmada através de análises por espectrometria de massas MALDI-TOF. As análises foram realizadas na plataforma de proteômica do Instituto Oswaldo Cruz – Fiocruz/RJ.

4.11 MOLÉCULAS INIBIDORAS DE SIRTUÍNAS

Diferentes moléculas, totalizando 48 compostos, separadas em 3 grupos, foram utilizadas para avaliar a capacidade de inibição de TcSir2rp1 e TcSir2rp3. Em colaboração com Prof. Dr. Antonello Mai, do Istituto Pasteur-Fondazione Cenci Bolognetti, Itália, o grupo 1 é composto por 38 já conhecidos inibidores de KDACs humanas (WANG et al., 2015). O grupo 2, em colaboração com o Prof. Dr. Emerson Ferreira Queiroz, da Universidade de Genebra, Suiça, baseado em uma triagem virtual de modelagem molecular (SACCONNAY et al., 2014), é composto por seis

substâncias puras extraídas do líquido da castanha do caju (*Anacardium occidentale*). A partir destes ensaios *in silico* foram identificadas estruturas moleculares que potencialmente interagem com as sirtuínas do *T. cruzi*, incluindo um derivado de ácido anacárdico obtido a partir do CNSL. Assim, foram incluídos neste estudo 2 ácidos anacárdicos, 2 substâncias do tipo cardol e duas moléculas do tipo cardanol. O grupo 3, em colaboração com o Prof. Dr. Sylvian Cretton, da Universidade de Genebra, Suiça, é composto por 4 substâncias puras extraídas da raíz de *Waltheria indica* com atividade antiparasitária descrita (CRETTON et al., 2014, 2015) que foram incluídas neste estudo com o objetivo de investigar se o mecanismo de ação destas estavam associadas com a inibição de sirtuínas.

4.12 ENSAIO DE ATIVIDADE ENZIMÁTICA TcSir2rp1 e TcSir2rp3

A validação da atividade enzimática de TcSir2rp1 e TcSir2rp3 e a triagem das moléculas inibidoras de TcSir2rp3 foram realizadas em São Paulo, em colaboração com o Laboratório de Biologia Celular e Molecular de Tripanossomas – UNIFESP.

Os ensaios de inibição enzimática de TcSir2rp1 e TcSir2rp3 foram realizados a partir do protocolo estabelecido previamente pelo grupo (MORETTI et al., 2015). Em resumo, o substrato para a atividade enzimática consiste de um peptídeo contendo um resíduo de lisina acetilado associado a um grupamento fluorescente e um grupamento apagador (Abz-Gly-Proacetil-Lys-Ser-Gln-EDDnp), sendo Abz, ácido orto-aminobenzoico; e EDDnp, N-[2,4-dinitrofenil]etilenediamina). A reação é dividida em duas etapas, sendo a primeira; a reação de desacetilação do resíduo de lisina acetilado pelas enzimas em estudo, e a segunda; a etapa de tripsinização do peptídeo, que resulta na separação do grupamento fluorescente do seu grupo apagador. Assim, a medida de fluorescência é diretamente proporcional à atividade de desacetilação de cada amostra (Figura 3).

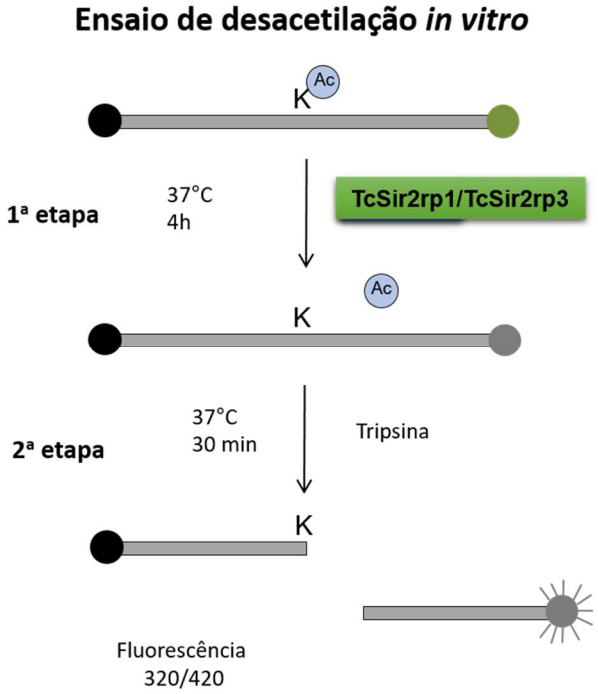

Figura 3 – Esquematização do ensaio de desacetilaçao *in vitro* realizado com as enzimas TcSir2rp1 e TcSir2rp3.
O ensaio foi realizado em duas etapas. Na primeira etapa foi utilizado um peptídeo contendo uma lisina acetilada, incubado na presença das enzimas TcSir2rp1 ou TcSir2rp3. A segunda etapa detecta a fluorescência gerada a partir da clivagem do peptídeo desacetilado utilizando a tripsina após incubação à 37ºC por 30 minutos.
Fonte: Elaborado pelo colaborador Dr. Nilmar Silvio Moretti.

A fim de otimizar os ensaios de inibição enzimática foram realizados diferentes experimentos incluindo como variáveis o tempo de incubação, concentração da enzima e concentração de peptídeo.

As reações foram realizadas em placa escura de 96 poços, incubadas por 4 horas a 37ºC em 50 µL contendo o tampão de atividade de sirtuína (25 mM Tris-HCl pH 8; 137 mM NaCl; 2,7 mM KCl; 1 mM $MgCl_2$), 0,6 mM NAD^+ (Sigma-Aldrich). Para ensaio com a TcSir2rp1 foi adicionado 0,25 µg de proteína recombinante e 100 µM de peptídeo sintético. Para o ensaio com a TcSir2rp3 foi também utilizado 0,25 µg de proteína cSir2rp1 e 500 µM de peptídeo sintético. Após o tempo de reação, uma solução 12 mM de nicotinamida em 100 mM de NaCl e 50 mM Tris-HCl, pH 8, contendo 0,6 mM de tripsina (Sigma-Aldrich) foi adicionada à reação. Após 30 minutos de incubação à 37ºC, fluorescência no comprimento de onda de 420 nm foi detectada utilizando o equipamento SpectraMax M3 (Molecular Devices, Sunnyvale, CA, EUA).

Para a triagem de potenciais inibidores de sirtuínas, os compostos foram pré-incubados com as enzimas TcSir2rp1 e TcSir2rp3 na concentração de 5 µM, durante

30 minutos, a temperatura ambiente, e, em seguida o peptídeo foi adicionado, iniciando assim a reação de desacetilação. Os compostos que apresentaram atividade inibitória acima de 30% foram incubados em diferentes concentrações com a proteína recombinante a fim de obter o valor de IC_{50} (concentração inibitória em 50%), calculado a partir do percentual de redução de atividade enzimática quando comparado ao controle negativo, ou seja, sem tratamento. O cálculo de regressão não linear para a obtenção dos valores de IC_{50} foi efetuado a partir do programa Prism 5.01 GraphPad (GraphPad Software, San Diego, CA, EUA).

4.13 ATIVIDADE ANTI-*T. cruzi IN VITRO*

Os parasitos na forma tripomastigota (2 x 10^6 tripomastigotas/mL) foram incubados em placa de 96 poços, em triplicata, em meio de cultura DMEM (Gibco/Life Technologies suplementado com 10% de soro bovino fetal (Cultilab) e Penicillina-Estreptomicina (100 U/mL) (Gibco/Life Technologies (Gibco) na presença dos compostos em diferentes concentrações. Após 24 horas de incubação, os parasitos viáveis foram contados em câmara de Neubauer.

Foi avaliada também a ação tripanocida dos compostos no ensaio de infecção *in vitro* em sistema de *High Content Screening* (HCS). O ensaio foi inicialmente padronizado utilizando macrófagos do exsudato peritoneal coletados de camundongos da linhagem BALB/c, a partir da indução de inflamação através da injeção de tioglicolato a 3% (Sigma). Após cinco dias da indução, os animais foram submetidos à eutanásia em câmara de gás de dióxido de carbono e, sob condições estéreis, a pele da região abdominal foi retirada para a visualização do peritônio. Foram injetados 10 mL de solução salina na cavidade peritoneal dos animais, e, após uma massagem no abdômen, os macrófagos foram coletados com auxílio de uma seringa. As células foram centrifugadas a 1.500 RPM (363 x g) por 10 minutos, contadas e plaqueadas (5 x 10^4 células/poço) em placas de 96 poços em diferentes condições visando padronizar o ensaio de infecção *in vitro*. Para validar os dados gerados pelo sistema HCS, foi utilizada a droga padrão benznidazol em diferentes concentrações. O protocolo de infecção previamente utilizado pelo laboratório era realizado em lamínulas de 13 mm, em placa de 24 poços, com coloração de hematoxilina e eosina, contados por microscopia óptica (BASTOS et al., 2014). Uma vez padronizado o ensaio de infecção *in vitro* em sistema HCS, e visando a redução

do uso de animais em pesquisa, assim como a melhor compreensão do efeito de moléculas em células humanas, o protocolo foi adaptado para a infecção em fibroblastos humanos (hFIB).

Os hFIB (3 x 10^4 células/mL), isolados de material de descarte de cirurgia plástica (procedimento aprovado pelo comitê de ética do Hospital São Rafael, CAAE: 20032313.6.0000.0048), foram incubados em placa de 96 poços em estufa umidificada à 37ºC e 5% de CO_2 por 24 horas. Após este período, as células foram infectadas com 6 x 10^4 tripomastigotas/poço por dezoito horas. Em seguida, os poços foram lavados e os compostos foram adicionados em diferentes concentrações. Após 72 horas de incubação em estufa a 37ºC e 5% de CO_2, os poços foram lavados com solução salina, fixados com solução paraformaldeído 4% e corados com 4 µM de Draq5 (Biostatus, Reino Unido). A aquisição das imagens foi realizada em microscópio confocal Operetta High-Content Imaging System (Perkin Elmer, Waltham, MA, EUA) como descrito por (ALONSO-PADILLA et al., 2015).

As diferentes concentrações dos compostos foram avaliadas com o objetivo de determinar a concentração que inibe em 50% o crescimento (IC_{50}) ou a viabilidade dos parasitos (EC_{50}). Os valores de IC_{50} e EC_{50} foram determinados com base na porcentagem de inibição do crescimento e viabilidade do parasito do controle negativo, ou seja, sem adição de droga. O cálculo de regressão não linear para a obtenção dos valores de IC_{50} e EC_{50} foi efetuado a partir do programa Prism 5.01 GraphPad (GraphPad Software). O fármaco padrão utilizado como controle positivo foi o benznidazol. A análise estatística do experimento de validação de infecção de macrófagos foi realizada através do programa Prism 5.01 GraphPad (GraphPad Software), utilizando o teste One-Way ANOVA e o pós-teste de Bonferroni, ou o teste t pareado, sendo considerado valores estatisticamente significante aqueles com valores $p < 0,05$.

4.14 AVALIAÇÃO DE CITOTOXICIDADE

A determinação da concentração letal para 50% da população celular (CC_{50}) foi realizada através do ensaio de Alamar Blue® (Invitrogen, Carlsbad, CA, EUA), seguindo as recomendações do fabricante. Os fibroblastos humanos (hFIB) (3 x 10^4 células/mL) foram cultivados em placa de cultura de 96 poços e incubados em estufa umidificada à 37ºC e 5% de CO_2 por 24 horas. Posteriormente, os compostos foram

adicionados em diferentes concentrações e incubador por 72 horas nas mesmas condições de temperatura e umidade. Após este período de incubação, os poços foram lavados com solução salina e, em seguida, foi adicionado o reagente Alamar Blue (Invitrogen) na concentração de 10%. As células foram incubadas por mais 24 horas e, em seguida, foram realizadas as leituras colorimétricas da placa de 96 poços com os comprimentos de onda de 570 e 600 nm. O cálculo para a obtenção do valor de CC_{50} foi efetuado utilizando-se a regressão não linear no programa Prism 5.01 GraphPad (GraphPad Software).

Os ensaios de citotoxicidade e de infecção de hFIB foram realizados a partir de condições semelhantes com o objetivo de avaliar o índice de seletividade (IS) dos compostos, ou seja, para avaliar quão seletivo o composto é ao parasito em relação às células humanas.

$$IS = CC_{50} \div IC_{50} \text{ (amastigota)}$$

4.15 ATIVIDADE ANTI-*T. cruzi IN VIVO*

4.15.1 Infecção e tratamento

Todos os procedimentos realizados foram aprovados pela Comissão de Ética em Uso de Animais (CEUA/FIOCRUZ/IGM), nº.016/2013 (ID Projeto 1296). Camundongos fêmeas da linhagem BALB/c (6 animais por grupo, apresentando entre 18-20 g), foram infectados por via intraperitoneal com 10^4 tripomastigotas sanguícolas por animal. Os camundongos foram tratados, por via oral, por cinco dias consecutivos, a partir do 5º dia de infecção. Os grupos de animais tratados com as drogas em teste receberam a dose de 50 mg/kg/dia. Como controle positivo foi utilizado o benznidazol na dose de 100 mg/kg/dia. Os compostos e o benznidazol foram diluídos em dimetilsulfóxido (DMSO) (Sigma) a 10% em solução salina. O grupo controle foi tratado com veículo (10% de DMSO em salina).

4.15.2 Avaliação da parasitemia e mortalidade

Cerca de 5 µL de sangue foram coletados da cauda dos camundongos infectados e dispostos em lâmina, coberta com lamínula de 22 x 22 mm, obtendo-se

uma camada única e homogênea de hemácias. As lâminas foram levadas diretamente ao microscópio óptico para a realização da contagem de 50 campos microscópicos aleatórios em objetiva de 40x. O número de parasitos encontrados foi dividido pelo número de campos microscópicos observados e multiplicado por um fator de correção de 7. O resultado foi apresentado em gráfico com 10^5 tripomastigotas/mL (método de BRENER, 1962 baseado no de BRENER, Z.; ANDRADE, Z. A.; BARRAL-NETTO, 2000). A parasitemia foi acompanhada nos dias 5, 8, 10 e 12 pós-infecção, enquanto a mortalidade dos animais foi avaliada através de acompanhamento diário por 30 dias.

A análise estatística da parasitemia foi realizada através do programa Prism 5.01 GraphPad (GraphPad Software), utilizando o teste One-Way ANOVA e o pós-teste de Bonferroni, sendo considerado valores estatisticamente significante aqueles com valores $p < 0,05$. Em relação à mortalidade, a curva de sobrevida dos animais foi elaborada utilizando o programa Prism 5.01 GraphPad (GraphPad Software).

5 RESULTADOS

5.1 CLONAGEM, EXPRESSÃO E PURIFICAÇÃO DA PROTEÍNA TcSir2rp1 RECOMBINANTE

5.1.1 Construção pET28α_TcSir2rp1

Com o objetivo de obter a TcSir2rp1 heteróloga, foi realizada a clonagem do gene de interesse no plasmídeo pET28α, nos sítios de restrição NheI e XhoI (Figura 4). Este vetor acrescenta uma cauda de histidina (6xHis) na extremidade N-terminal da proteína recombinante, o que permite a sua rápida purificação por cromatografia de afinidade em resina contendo níquel. Esse plasmídeo contém um gene de resistência à canamicina e é compatível com a expressão de proteínas recombinantes em cepas B de bactérias *E. coli*, como BL21 (DE3), por exemplo. A expressão da sequência de interesse, sob o controle do promotor T7, é induzível por IPTG.

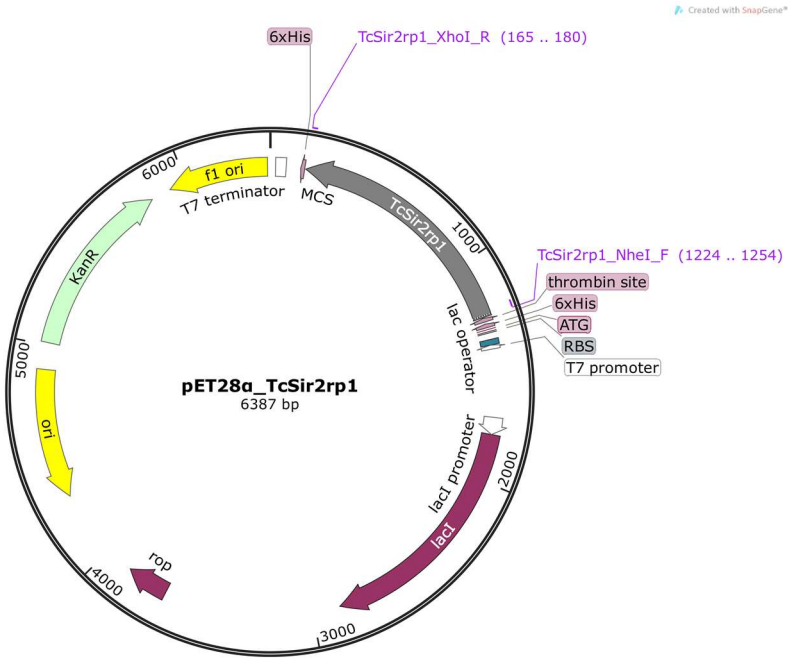

Figura 4 – Mapa do plasmídeo recombinante pET28α_TcSir2rp1.
O inserto foi clonado nos sítios de restrição NheI e XhoI do plasmídeo. A imagem foi gerada a partir do programa SnapGene, versão 3.2.1.

Para a obtenção do plasmídeo recombinante pET28α_TcSir2rp1, inicialmente foi realizada a reação de amplificação do gene TcSir2rp1 a partir do DNA genômico

do *T. cruzi* (cepa Y). O produto da reação de PCR, com tamanho aproximado de 1074 pares de base (pb), corresponde à sequência do gene TcSir2rp1 (Figura 5).

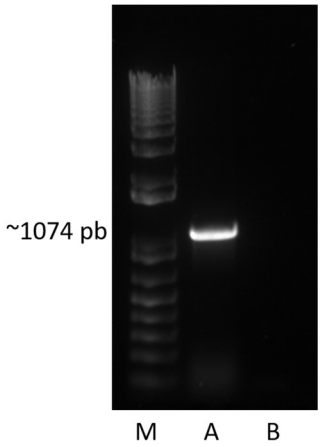

Figura 5 – Análise por eletroforese de gel de agarose 1% da PCR para amplificação do gene TcSir2rp1. A reação foi realizada utilizando o par de iniciador TcSir2rp1_NheI_F_5'-GCTAGCCATATGAATCAAGATAACGCCAACT-3' e TcSir2rp1_XhoI_R_ 5'-CCCTCGAGTTATTTTCGGTCTGT-3'. O produto amplificado apresenta em torno de 1074 pares de base (pb) que corresponde ao fragmento do gene TcSir2rp1. M = marcador de peso molecular 1 Kb Plus DNA; A = amostra amplificada; B = reação controle, com ausência de DNA molde.

O produto da PCR amplificado foi purificado e submetido à ação das enzimas de restrição NheI e XhoI, assim como o plasmídeo pET28α. Após a ligação e transformação, foram selecionados 8 clones para confirmar o sucesso da clonagem, através da reação de digestão utilizando as mesmas enzimas de restrição. Todos os clones selecionados apresentaram o fragmento equivalente a 1074 pb correspondente à sequência do gene TcSir2rp1 (Figura 6).

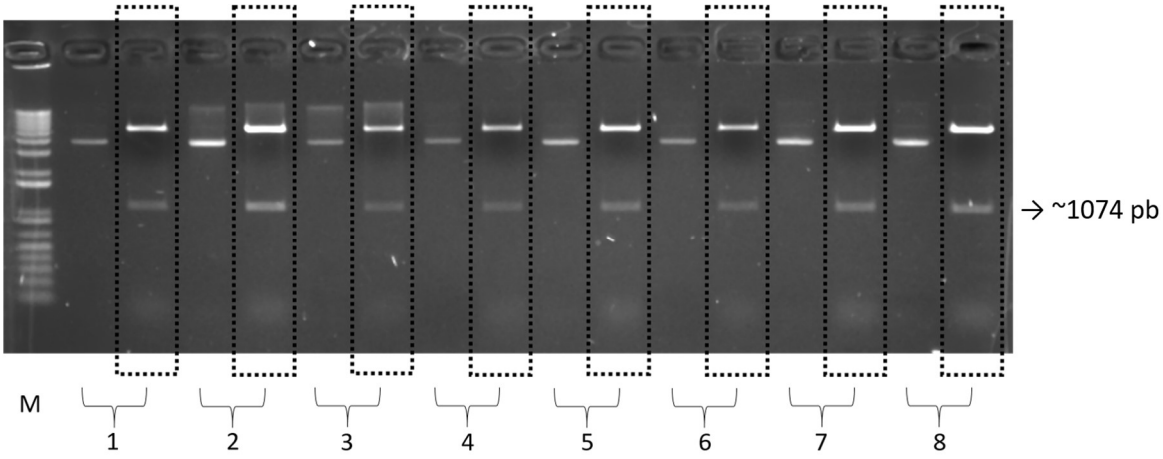

Figura 6 – Análise por eletroforese de gel de agarose 1% da reação de digestão do plasmídeo recombinante pET28α_TcSir2rp1 utilizando as enzimas de restrição NheI e XhoI.
Foram selecionados 8 clones. Em destaque estão as amostras que submetidas à reação com as enzimas de restrição. Para cada clone, como controle interno, estão representadas as amostras sem a digestão enzimática e após a reação. O produto da digestão enzimática apresenta em torno de 1074

pares de base (pb) que corresponde ao fragmento do gene TcSir2rp1. A amostra não digerida apresenta em torno de 6387 pb correspondente ao plasmídeo recombinante. M = marcador de peso molecular 1 Kb Plus DNA; 1 = clone 1, 2 = clone 2; 3 = clone 3; 4 = clone 4, 5 = clone 5, 6 = clone 6; 7 = clone 7; 8 = clone 8.

5.1.2 Expressão da proteína heteróloga TcSir2rp1

A expressão da proteína recombinante TcSir2rp1 foi realizada utilizando o sistema de expressão em bactérias *E. coli* BL21 (DE3). Assim, bactérias *E. coli* BL21 (DE3) foram transformadas com o plasmídeo recombinante clone 2 e posteriormente foram submetidas a indução para a expressão da proteína TcSir2rp1.

Após expressão, a TcSir2rp1 foi purificada por cromatografia de afinidade em resina contendo níquel. O produto da purificação foi visualizado em gel SDS-PAGE 12% onde foi possível verificar a presença da banda no gel equivalentes ao peso molecular aproximado da TcSir2rp1 (40 kDa) (Figura 7).

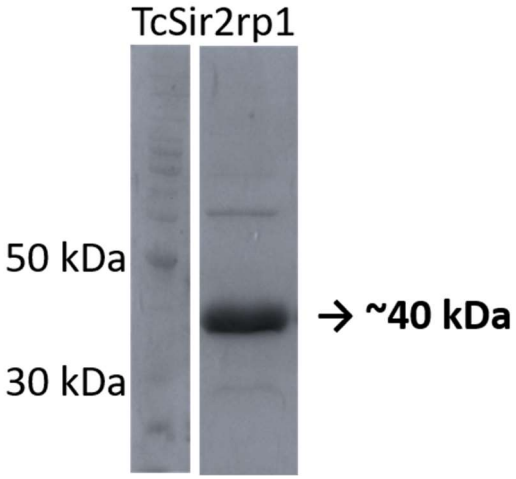

Figura 7- Purificação da proteína heteróloga TcSir2rp1.
A purificação foi realizada por cromatografia de afinidade em resina contendo níquel. A banda que apresenta o peso molecular de ~40 kDa equivale a TcSir2rp1.

5.2 CLONAGEM, EXPRESSÃO E PURIFICAÇÃO DA PROTEÍNA TcSir2rp3 RECOMBINANTE

5.2.1 Construção pGEX-6P-1_TcSir2rp3

Com o objetivo de obter a TcSir2rp3 heteróloga, foi realizada a clonagem do gene de interesse no vetor pGEX-6P-1. Para isso, inicialmente foi realizada a reação de amplificação do gene TcSir2rp3 a partir do DNA genômico do *T. cruzi* cepa Y

(Figura 8). O produto amplificado corresponde à sequência do gene TcSir2rp3 que apresenta 726 pb.

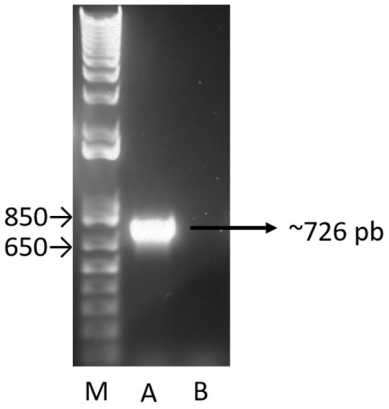

Figura 8 – Análise por eletroforese de gel de agarose 1% da PCR para amplificação do gene TcSir2rp3. A reação foi realizada utilizando o par de iniciador TcSir2rp3_BamHI_F_5'-ATCAGGATCCATGAGGCCGCGGCGTCAG-3' e TcSir2rp3_NotI_R_5'-GAATGCGGCCGCCTACACCGCGTCTTGAAG-3'. O produto amplificado apresenta em torno de 726 pares de base (pb) que corresponde ao fragmento do gene TcSir2rp3. M = marcador de peso molecular 1 Kb Plus DNA; A = amostra amplificada; B = reação controle, com ausência de DNA molde.

O produto amplificado foi então clonado no vetor, gerando a construção pGEX-6P-1_TcSir2rp3 (Figura 9). Os vetores pGEX são plasmídeos para expressão de proteínas fusionadas à cauda GST em bactérias, que favorecem a purificação realizada por cromatografia por afinidade. A sequência de nucleotídeos do vetor pGEX-6P-1 contém o sítio de clivagem protease PreScission que permite a clivagem entre o domínio GST e a proteína recombinante de interesse com uso da protease 3C de rinovírus humano. Desta forma, é possível obter a proteína TcSir2rp3 heteróloga purificada sem a proteína de fusão GST.

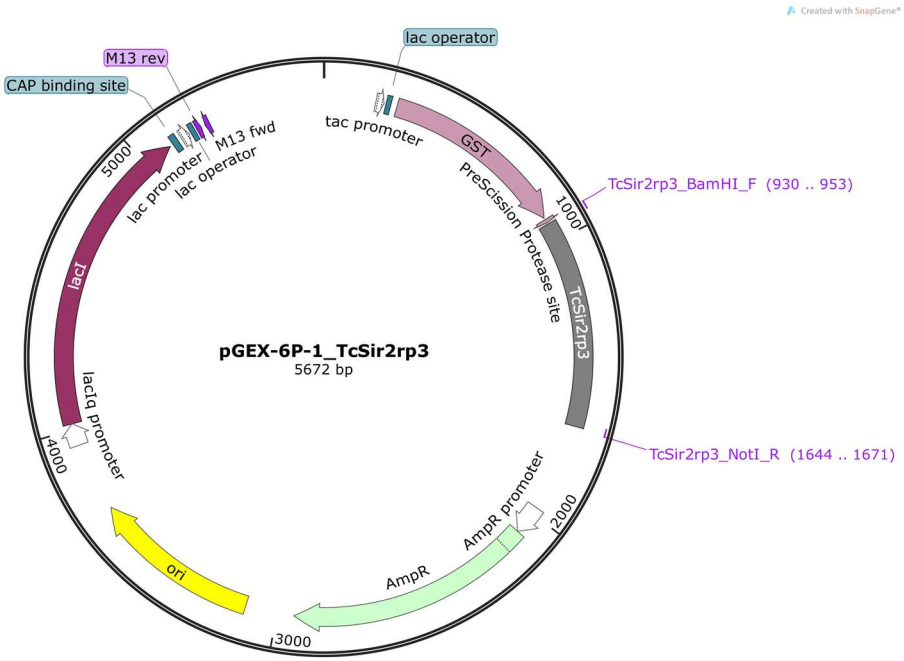

Figura 9 – Mapa do plasmídeo recombinante pGEX-6P-1_TcSir2rp3.
O inserto foi clonado nos sítios de restrição BamHI e NotI do vetor. A imagem foi gerada a partir do programa SnapGene, versão 3.2.1.

O gene TcSir2rp3 foi clonado nos sítios de restrição BamHI e NotI. Para confirmar o sucesso da clonagem, foram selecionados 6 clones de bactérias transformadas com o plasmídeo recombinante, e o DNA plasmidial extraído das bactérias foi submetido à reação de digestão enzimática com as enzimas BamHI e NotI (Figura 10). Dos 6 clones selecionados, 5 deles apresentaram como produto da digestão enzimática um fragmento de tamanho equivalente ao gene TcSir2rp3 (726 pb). Assim, o clone 2 foi excluído da análise e os clones 1, 3, 4, 5 e 6 foram sequenciados.

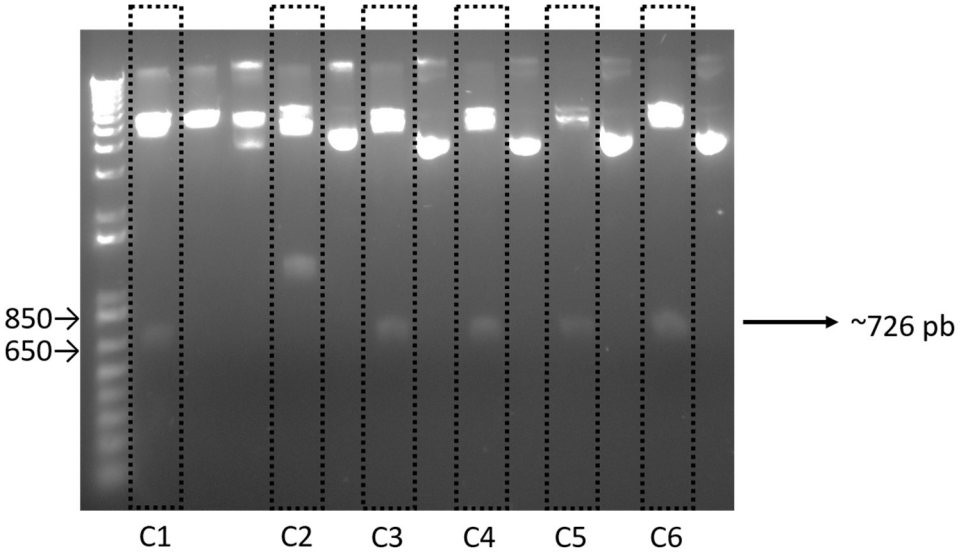

Figura 10 – Produto da reação de digestão do plasmídeo recombinante pGEX-6P-1_TcSir2rp3 utilizando as enzimas de restrição BamHI e NotI.
O produto reação foi visualizado a partir da técnica de eletroforese em gel de agarose 1%. Em destaque, estão as reações utilizando ambas as enzimas nos diferentes clones testados. O produto da digestão enzimática apresenta em torno de 1074 pares de base (pb) que corresponde ao fragmento do gene TcSir2rp3. A amostra não digerida apresenta em torno de 5572 pb correspondente ao plasmídeo recombinante. C1 = clone 1; C2 = clone 2; C3 = clone 3; C4 = clone 4; C5 = clone 5; C6 = clone 6.

A sequência dos 5 clones selecionados foi analisada e foi possível verificar que apenas a sequência do clone 3 apresentava-se sem mutação (Figura 11). Assim, o plasmídeo recombinante pGEX-6P-1_TcSir2rp3 clone 3 foi utilizado para a expressão da proteína heteróloga TcSir2rp3.

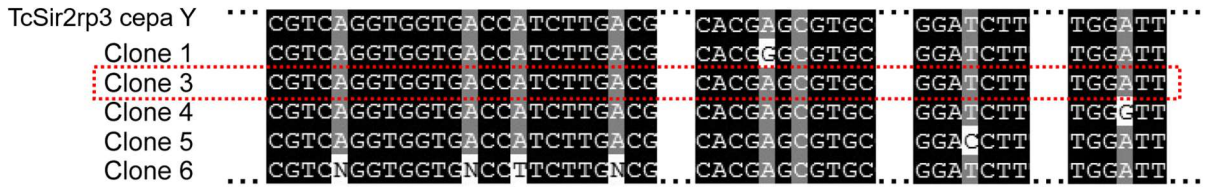

Figura 11 – Análise da sequência de nucleotídeos de clones TcSir2rp3.
As sequências de nucleotídeos foram geradas a partir da técnica de sequenciamento. A sequência referência (TcSir2rp3 cepa Y) foi utilizada para permitir o alinhamento com as demais sequências em análise. A figura representa apenas os sítios do gene com presença de pontos de mutação. Apenas a sequência referente ao clone 3 (em destaque) não apresenta mutação.

5.2.2 Expressão da proteína heteróloga TcSir2rp3

A expressão da proteína recombinante TcSir2rp3 foi realizada utilizando o sistema de expressão em bactérias *E. coli* BL21 (DE3) pRARE 2. Estas bactérias apresentam como particularidade a presença do vetor pRARE, um plasmídeo que permite a expressão de tRNAs raros em bactérias (AGA, AGG, CGA, CGG, GGA,

AUA, CUA, AUG, CCC, ACA, ACC e UAC) e favorece a expressão de proteínas heterólogas de interesse de forma mais eficiente. Assim, bactérias *E. coli* BL21 (DE3) pRARE 2 foram transformadas com o plasmídeo recombinante clone 3 e as bactérias foram submetidas à indução para a expressão da proteína TcSir2rp3.

Após expressão, a TcSir2rp3 fusionada com GST foi purificada por cromatografia de afinidade, seguida da clivagem de GST para a obtenção de TcSir2rp3. O produto da purificação foi visualizado em gel SDS-PAGE 12% onde foi possível verificar a presença da banda no gel equivalente ao peso molecular aproximado da TcSir2rp3 (27 kDa) (Figura 12). A análise por espectrometria de massas, confirmou que a banda visualizada no gel correspondia à TcSir2rp3.

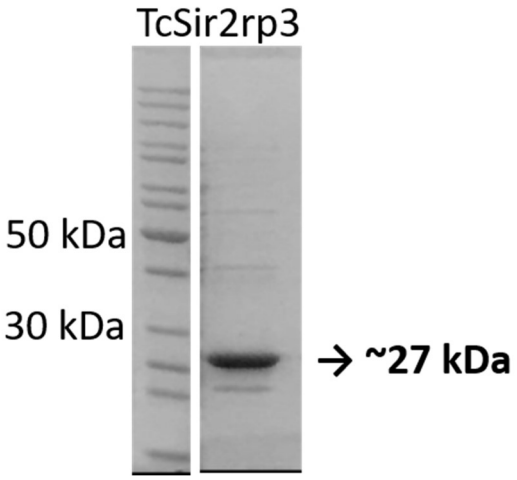

Figura 12 – Purificação da proteína heteróloga TcSir2rp3.
A purificação foi realizada por cromatografia de afinidade para proteínas com cauda de GST, seguida da clivagem de GST a partir da protease 3C de rinovirus humano (HRV) (GE Healthcare) a 4°C por 1 hora. A banda que apresenta o peso molecular de 27 kDa equivale a TcSir2rp3.

5.3 VALIDAÇÃO DA ATIVIDADE DE DESACETILASE DAS TcSir2rp1 e TcSir2rp3 RECOMBINANTES

Após a obtenção das proteínas purificadas foram realizados os ensaios de atividade de desacetilação de resíduo de lisina acetilado, com o objetivo de verificar a atividade funcional das proteínas TcSir2rp1 e TcSir2rp3 recombinantes. Neste ensaio foram realizadas diferentes condições de incubação: 1 – com ausência de NAD+ e presença de tripsina; 2 - com presença de NAD+, mas ausência de tripsina; 3 - com presença de NAD+ e de tripsina (Figura 13). Como esperado, as condições 1 e 2 não apresentam atividade enzimática, enquanto a condição 3 confirma a atividade de desacetilase NAD+ dependente das proteínas TcSir2rp1 e TcSir2rp3.

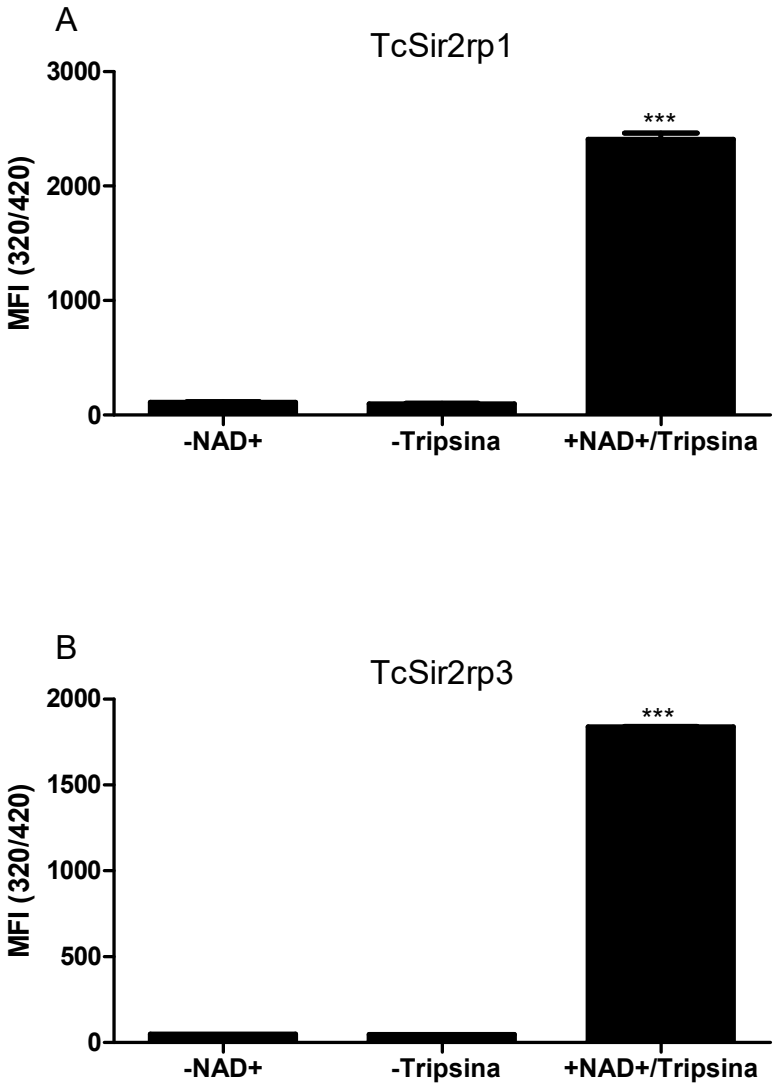

Figura 13 – Avaliação da atividade de desacetilase das proteínas TcSir2rp1 (A) e TcSir2rp3 (B). Foram realizadas diferentes condições de reações com o objetivo de validar a atividade biológica das enzimas. -NAD+ = com ausência de NAD+ e presença de tripsina; -Tripsina = presença de NAD+, mas ausência de tripsina; +NAD+/Tripsina = com presença de NAD+ e de tripsina. *** $p < 0{,}001$.

5.4 EFEITO DE POTENCIAIS INIBIDORES DE SIRTUÍNAS NA ATIVIDADE DE DESACETILAÇÃO DE TcSir2rp1 e TcSir2rp3

Após a validação da atividade enzimática, foi realizada a triagem com os compostos selecionados (grupos 1, 2 e 3) com o objetivo de identificar inibidores de TcSir2rp1 e TcSir2rp3. De um total de 48 compostos testados na concentração de 5 µM, 5 deles apresentaram atividade inibitória para TcSir2rp1 e 7 apresentaram atividade inibitória para TcSir2rp3, sendo que 2 compostos apresentaram atividade inibitória em relação a ambas as sirtuínas (representados pelos números **43** e **44**)

(Figura 14). Destes, os compostos **10**, **12**, **13**, **14**, **17**, **33** e **35**, pertencem ao grupo 1, e são identificados como inibidores de sirtuínas humanas. Os compostos **40**, **43** e **44**, pertencentes ao grupo 2, são substâncias puras extraídas da *Anacardium occidentale*, sendo o composto **40** classificado como cardol e os compostos **43** e **44** como ácido anacárdico. Estes inibidores foram selecionados para serem melhor investigados. Nenhum composto do grupo 3 apresentou atividade inibitória para as sirtuínas de *T. cruzi*, indicando que o mecanismo de ação destes compostos não está associado com a inibição de TcSir2rp1 e TcSir2rp3, mas diante do efeito antiparasitário previamente identificado (CRETTON et al., 2014, 2015) com a cepa Tuluhaen C2C4, decidimos investigar o efeito tripanocida destes compostos na cepa Y. A lista com todas as estruturas químicas avaliadas neste trabalho encontra-se em anexo.

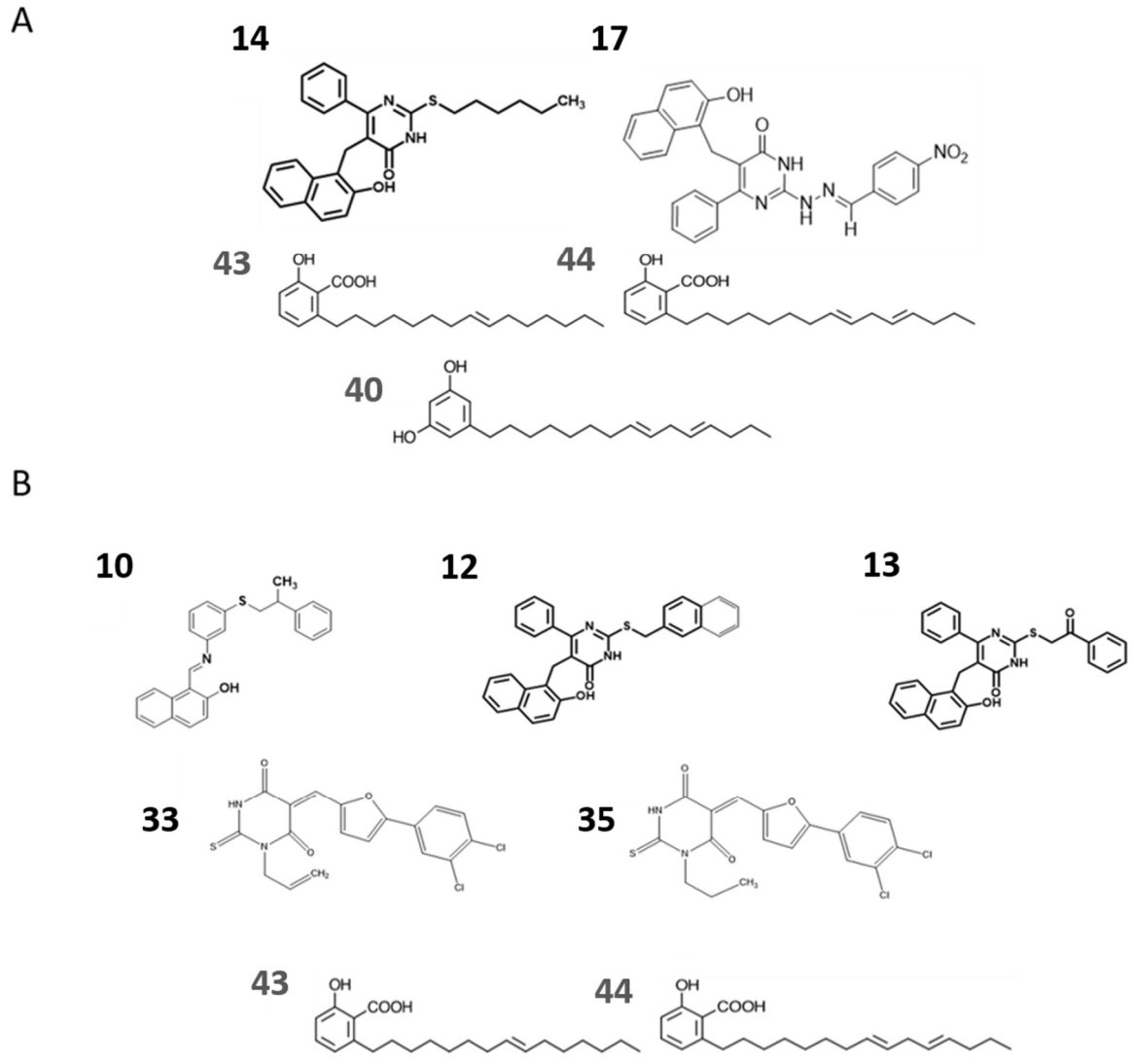

Figura 14 – Estrutura química dos inibidores de TcSir2rp1 (A) e TcSir2rp3 (B) identificados a partir da triagem de atividade de desacetilação com as respectivas enzimas.

Os compostos de grupo 1 estão representados com as numerações **10**, **12**, **13**, **14**, **17**, **33** e **35** (em preto), enquanto os compostos de grupo 2 estão representados pelos números **40**, **43** e **44** (em cinza).

Os dez compostos selecionados na triagem foram então incubados em diferentes concentrações com as proteínas recombinantes TcSir2rp1 ou TcSir2rp3, com o objetivo de calcular o valor de IC_{50}. Em relação aos inibidores de TcSir2rp1, os valores de IC_{50} variaram entre 16,2 e 32,4 μM, sendo que o composto **43** apresentou melhor atividade inibitória da ação de desacetilase da enzima, seguido do composto **44** que apresentou valor de IC_{50} de 23,4 μM. Ambos os compostos são classificados como ácido anacárdico. Em relação aos inibidores de TcSir2rp3, os valores de IC_{50} variaram entre 6,1 e 18,8 μM, sendo que o composto **44** apresentou melhor atividade inibitória, seguido do composto **43** que apresentou valor de IC_{50} de 7,4 μM (Tabela 1).

Tabela 1 – Atividades anti-TcSir2rp1 e TcSir2rp3 dos compostos.

	TcSir2rp1	TcSir2rp3
Compostos	IC_{50} ± SEM (μM)	IC_{50} ± SEM (μM)
10		18,8 ± 3,78
12		14,3 ± 3,50
13		18,5 ± 1,39
14	32,4 ± 5,58	
17	28,8 ± 2,70	
33		16,4 ± 4,74
35		16,3 ± 4,77
40	31,4 ± 2,33	
43	16,2 ± 4,88	7,4 ± 0,65
44	23,4 ± 2,51	6,1 ± 1,16

*SEM – Erro padrão da média
**Valores foram calculados com base em ao menos três experimentos distintos, realizados em triplicata.

5.5 VALIDAÇÃO DO ENSAIO DE INFECÇÃO EM SISTEMA HCS

O ensaio de infecção *in vitro* utilizando o sistema HCS foi inicialmente validado utilizando macrófagos peritoneais coletados de camundongos, já que o protocolo padrão utilizado pelo laboratório foi estabelecido com estas células. A partir dos parâmetros previamente descritos (ALONSO-PADILLA et al., 2015) em linhagem de célula H9c2, foi realizada a identificação de núcleo, citoplasma e a determinação de amastigota com base na intensidade de marcação com o corante Draq5 que tem afinidade ao DNA dupla fita.

Inicialmente foi avaliada a melhor proporção parasito:célula para ser estabelecida como padrão de infecção. A infecção de macrófagos com o parasito na proporção 5:1 (parasito:célula) apresenta uma taxa de infecção reduzida quando comparada com as proporções 10:1 e 20:1. Não foi verificada diferença estatisticamente significativa entre as proporções 10:1 e 20:1, assim mantivemos a proporção 10:1 como padrão (Figura 15).

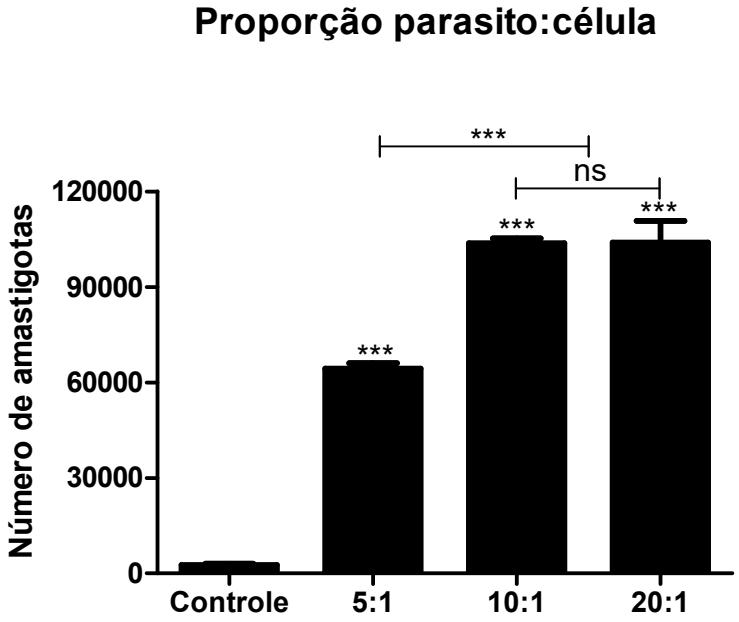

Figura 15 – Padronização de proporção parasito:célula de ensaio de infecção *in vitro* utilizando o sistema HCS.
O ensaio foi padronizado utilizando macrófagos peritoneais isolados de camundongos da linhagem BALB/c. Foram utilizadas 3 diferentes proporções parasito:célula, 5:1, 10:1 e 20:1. O controle representa as células não infectadas utilizadas para estabelecer os parâmetros de determinação de núcleo, citoplasma e amastigotas no Operetta. *** $p < 0,001$.

Em seguida, o ensaio foi validado comparando os valores de IC_{50} de células infectadas e tratadas com a droga de referência benznidazol obtidos no ensaio utilizando sistema HCS e o modelo previamente utilizado pelo grupo, além da análise comparativa com o dado da literatura estabelecido por ALONSO-PADILLA et al., 2015, utilizando esta mesma abordagem. Foi possível verificar uma curva concentração-resposta em relação ao tratamento com benznidazol, com valor de IC_{50} 2,7 ± 0,11 µM (Figura 16). O resultado obtido é próximo ao dado da literatura, que apresenta como valor de IC_{50} 1,43 ± 0,21 µM (ALONSO-PADILLA et al., 2015). Entretanto, o valor foi menor quando comparado com o protocolo previamente realizado pelo grupo que apresentou valor de IC_{50} de 14,0 ± 0,30 µM (BASTOS et al., 2014), que pode ser justificado pelo viés na contagem do número de amastigotas coradas com hematoxlina

e eosina, e pelo número reduzido de células avaliadas (100 macrófagos) comparado ao das 15.300 células analisadas pelo Operetta. A partir das condições estabelecidas em macrófago peritoneal, foi realizada uma adaptação para o ensaio de infecção em células humanas (hFIB).

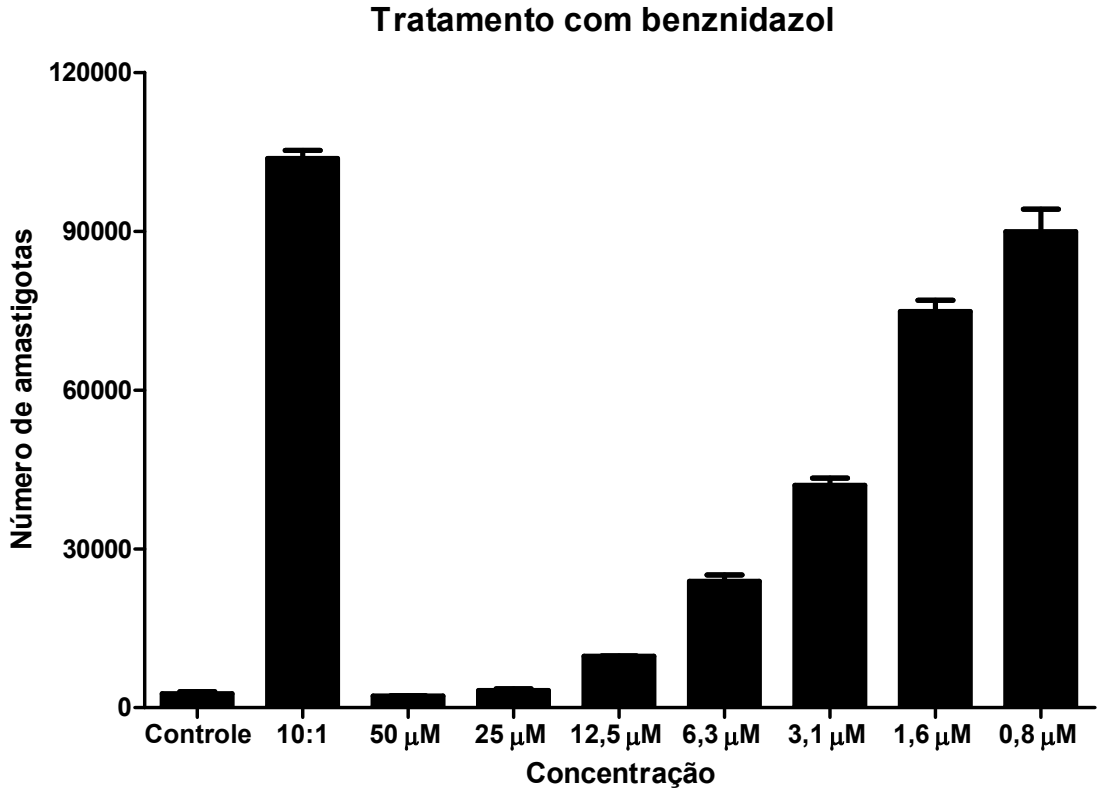

Figura 16 – Curva concentração-resposta de células infectadas e tratadas com benznidazol. Diferentes concentrações do benznidazol (50 – 0,8 μM) foram utilizadas a fim de validar o ensaio de infecção de macrófago utilizando o sistema HCS. Os macrófagos foram plaqueados e infectados com os parasitos com a proporção parasito:célula previamente estabelecida (10:1). O controle representa as células não infectadas utilizadas para estabelecer os parâmetros de determinação de núcleo, citoplasma e amastigotas no Operetta.

5.6 AVALIAÇÃO DA ATIVIDADE ANTIPARASITÁRIA E CITOTÓXICA DOS INIBIDORES DE TcSir2rp1 e TcSir2rp3

Os inibidores selecionados **10**, **12**, **13**, **14**, **17**, **33**, **35**, **40**, **43** e **44** foram então testados frente a diferentes formas do *T. cruzi*. Os inibidores **10**, **12**, **13**, **14**, **17**, **33**, **35** e **40** apresentaram atividade inibitória em relação a forma infectante tripomastigota, já os compostos **43** e **44**, que inibiram ambas as sirtuínas de *T. cruzi* e com valores de IC_{50} mais baixos, não apresentaram atividade antiparasitária para a forma tripomastigota quando testadas na concentração máxima de 50 μM.

Dentre os inibidores de TcSir2rp1 que apresentaram efeito inibitório em relação a tripomastigotas, o composto **17** apresentou menor valor de EC_{50}, indicando uma melhor atividade antiparasitária. Já os compostos **14** e **40** apresentaram valores de EC_{50} de 12,3 μM. O valor de EC_{50} da droga de referência benznidazol é de 11,4 μM, portanto o composto **17** apresentou melhor atividade quando comparado ao controle.

Em relação aos inibidores de TcSir2rp3, os valores de EC_{50} variaram entre 28,1 e 41,6 μM, sendo o composto **33** o mais ativo, porém com atividade antiparasitária inferior quando comparada ao controle.

Essas moléculas foram também avaliadas no ensaio de infecção de fibroblasto e foi avaliado como parâmetro para o cálculo de IC_{50} o percentual de inibição no número de amastigotas comparado ao controle sem tratamento. Em relação aos inibidores de TcSir2rp1, os valores de IC_{50} variaram entre 6,2 e 42,4 μM, sendo o composto **17** também o mais ativo neste ensaio antiparasitário. Os compostos **43** e **44**, que também são inibidores de TcSir2rp3 e não inibiram a forma tripomastigota, inibiram a proliferação de amastigotas intracelular com valores de IC_{50} 42,4 e 41,7 μM, respectivamente. O valor de IC_{50} da droga de referência é de 3,1 μM, portanto, nenhum inibidor de TcSir2rp1 apresentou atividade antiparasitária no ensaio de infecção de hFIB superior ao benznidazol.

Em relação aos inibidores de TcSir2rp3, os valores de IC_{50} variaram entre 21,1 e 42,4 μM, sendo que o composto **33**, também neste ensaio antiparasitário, apresentou melhor atividade inibitória em relação a proliferação de amastigotas. Dentre as moléculas triadas, nenhuma delas apresentou atividade anti-*T. cruzi* com atividade superior à droga de referência.

Os compostos foram também avaliados em relação ao perfil citotóxico para as células humanas (hFIB). Destes, os compostos **13**, **35**, **43** e **44** não apresentaram atividade tóxica quando incubadas na concentração máxima de 100 μM. O composto **17**, inibidor de TcSir2rp1, apresentou maior atividade citotóxica, apresentando um índice de seletividade de 3. Portanto, apesar deste composto apresentar a melhor atividade antiparasitária dentre os inibidores de TcSir2rp1, este apresenta-se como uma molécula tóxica aos fibroblastos humanos. O composto **33**, inibidor de TcSir2rp3 com melhor atividade antiparasitária, apresentou valor de CC_{50} de 86 μM, apresentando um índice de seletividade de 4. O composto **13** (inibidor de TcSir2rp3) apresentou melhor índice de seletividade (>5), porém com valor inferior ao do benznidazol (>32) (Tabela 2).

Tabela 2 – Atividades antiparasitárias e citotóxicas dos inibidores de sirtuínas.

	Tripomastigota	Amastigota	hFIB	IS[d]
Compostos	EC_{50} ± SEM (μM)[a]	IC_{50} ± SEM (μM)[b]	CC_{50} ± SEM (μM)[c]	
10	38,5 ± 6,04	24,1 ± 5,46	86,1 ± 4,79	4
12	41,6 ± 6,17	27,3 ± 3,83	56,9 ± 6,55	2
13	41,1 ± 9,20	21,4 ± 7,37	>100	> 5
14	12,3 ± 0,97	18,8 ± 4,87	36,4 ± 2,05	2
17	5,1 ± 1,59	6,2 ± 3,56	19,6 ± 4,82	3
33	28,1 ± 3,76	21,1 ± 6,23	86,0 ± 6,06	4
35	41,2 ± 8,40	41,8 ± 6,35	>100	> 2
40	12,3 ± 0,25	14,7 ± 3,27	53,7 ± 7,08	4
43	ND	42,4 ± 5,11	>100	> 2
44	ND	41,7 ± 5,53	>100	> 2
Benznidazol	11,4 ± 1,09	3,1 ± 0,87	>100	> 32

[a] Determinado 24 horas após incubação com os compostos.
[b] Fibroblastos humanos (hFIB) infectados foram incubados com os compostos e a atividade foi determinada após 72 horas de tratamento.
[c] A viabilidade de hFIB foi determinada após 72 horas de tratamento.
[d] Índice de seletividade (IS), calculado a partir da razão entre CC_{50} (hFIB) e IC50 (amastigota).
*IC_{50}, concentração inibitória em 50%; EC_{50}, concentração efetiva em 50%; CC_{50}, concentração citotóxica em 50%.
**ND – não determinado em razão da falta de atividade na concentração máxima testada (50 μM para os ensaios antiparasitários e 100 μM para o ensaio de toxicidade de hFIB.
*** SEM – Erro padrão da média.
****Valores foram calculados com base em ao menos três experimentos distintos, realizados em triplicata.

5.7 ATIVIDADES ANTIPARASITÁRIAS E CITOTÓXICAS DOS COMPOSTOS DE GRUPO 3

Os compostos do grupo 3 foram descritos como agentes tripanocidas quando testados contra a cepa Tulahuen C2C4 (CRETTON et al., 2014, 2015). Porém, o mecanismo de ação destes compostos ainda não foi identificado. Com o objetivo de investigar se as sirtuínas seriam alvos farmacológicos envolvidos na ação destes compostos, foram realizados os ensaios de atividade de desacetilase com as enzimas TcSir2rp1 e TcSir2rp3. Entretanto, não foram identificadas atividades inibitórias mesmo quando essas moléculas (**45**-**48**) foram testadas com a concentração máxima de 40 μM.

Conhecendo o efeito anti-*T. cruzi* destes compostos, sendo eles mais potentes que a droga de referência benznidazol, estas moléculas foram testadas para a avaliar a atividade tripanocida frente a cepa Y. Em relação à forma tripomastigota, os valores de EC_{50} variaram entre 3,5 e 13,6 μM, sendo o composto **46** o mais ativo. As

substâncias puras **45**, **46** e **48** mostram-se mais potentes quando comparadas ao controle. Em relação a capacidade de inibir a proliferação de amastigotas, os valores de IC_{50} variaram entre 0,2 e 3,5 µM, sendo os compostos **45** e **48** os mais ativos. Mais uma vez, os compostos **45**, **46** e **48** também se mostraram mais potentes quando comparados ao controle benznidazol.

Os compostos **46**, **47** e **48** não apresentaram atividade citotóxica em hFIB quando testados na concentração máxima de 100 µM. Por outro lado, o composto **45** apresentou valor de CC_{50} de 60,1 µM. Entretanto, diante do potente efeito anti-*T. cruzi* o índice de seletividade deste composto foi de 300. O composto **48** também se destaca em relação ao índice de seletividade, com valor >500 (Tabela 3). Diante deste cenário, os compostos **45** e **48** foram selecionados para a avaliação do efeito tripanocida em camundongos.

Tabela 3 – Atividades antiparasitárias e citotóxicas dos compostos do grupo 3.

	Tripomastigota	Amastigota	hFIB	IS[d]
Compostos	EC_{50} ± SEM (µM)[a]	IC_{50} ± SEM (µM)[b]	CC_{50} ± SEM (µM)[c]	
45	5,1 ± 1,53	0,2 ± 0,15	60,1 ± 6,58	300
46	3,5 ± 1,71	0,8 ± 0,71	>100	>125
47	13,6 ± 2,52	3,5 ± 1,65	>100	>29
48	5,8 ± 0,98	0,2 ± 0,08	>100	>500
Benznidazol	11,4 ± 1,09	3,1 ± 0,87	>100	> 32

[a] Determinado 24 horas após incubação com os compostos.
[b] Fibroblastos humanos (hFIB) infectados foram incubados com os compostos e a atividade foi determinada após 72 horas de tratamento.
[c] A viabilidade de hFIB foi determinada após 72 horas de tratamento.
[d] Índice de seletividade (IS), calculado a partir da razão entre CC_{50} (hFIB) e IC50 (amastigota).
*IC_{50}, concentração inibitória em 50%; EC_{50}, concentração efetiva em 50%; CC_{50}, concentração citotóxica em 50%.
** SEM – Erro padrão da média.
***Valores foram calculados com base em ao menos três experimentos distintos, realizados em triplicata.

Os compostos **45** e **48** foram testados *in vivo* com a dose diária de 50 mg/kg com objetivo de avaliar a potência do efeito tripanocida em modelo animal. Ambos os grupos de camundongos tratados com as drogas em teste apresentaram redução da parasitemia após o tratamento quando comparado ao grupo de animais controle sem tratamento (veículo). Entretanto, a redução da parasitemia foi inferior quando comparada à parasitemia do grupo de animais tratados com benznidazol, que foi capaz de eliminar os parasitos circulantes nos dias 8, 10 e 12 pós-infecção. Durante o pico de parasitemia, dia 10 pós-infecção, os animais tratados com o composto **48**

apresentaram redução no número de parasitos circulantes no sangue de 47,54%, enquanto o composto **45** reduziu em 13,56%. Já no dia 12 pós-infecção houve redução de parasitemia de 48,99% e 28,86% nos animais tratados com os compostos **48** e **45**, respectivamente (Figura 17).

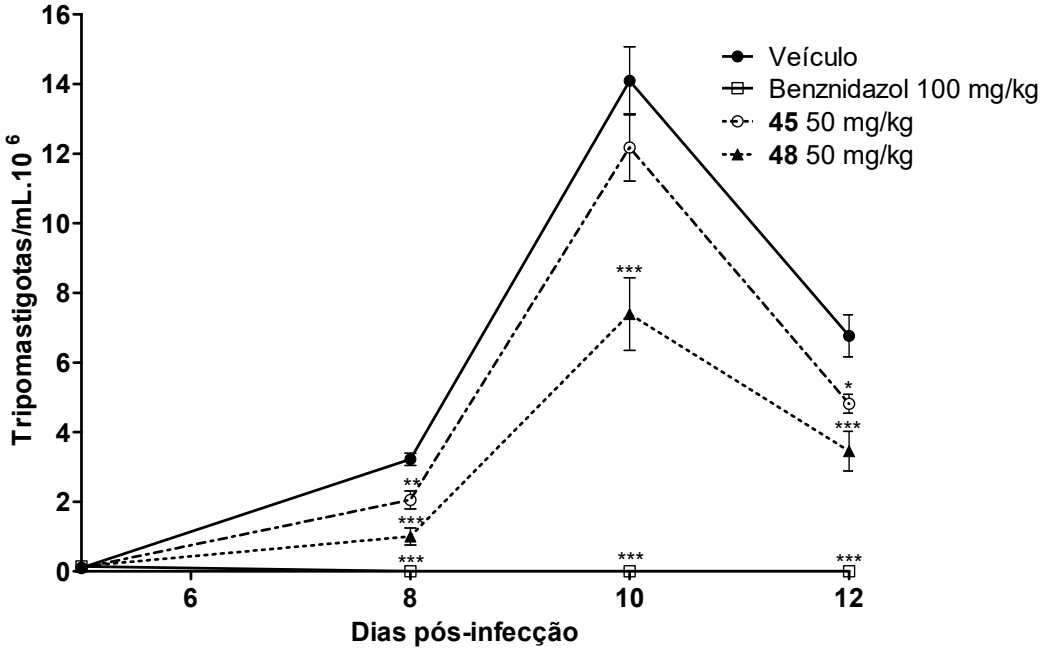

Figura 17 – Parasitemia de animais infectados com *T. cruzi* tratados ou não com os compostos **45** e **48**.
Os camundongos foram tratados por via oral com a dose de 50 mg/kg/dia por 5 dias consecutivos e a parasitemia foi realizada nos dias 5, 8, 10 e 12 pós- infecção. Foi utilizado como controle positivo o fármaco de referência, benznidazol, com a dose de 100 mg/kg/dia, e, como controle negativo, apenas o veículo. Os dados representam a mediana de 6 animais/grupo. * p <0,05. ** p <0,01. *** p < 0,001

Em relação à mortalidade, o tratamento com os compostos **45** e **48** causou óbito dos camundongos que apresentaram sinais de toxicidade, como pelo eriçado e prostração. Os animais tratados com o composto **45** apresentaram um tempo média de vida aproximado de 16 dias, variando entre 16 e 17 dias pós-infecção. Os animais tratados com o composto **48** apresentaram uma maior média de sobrevivência (aproximadamente 17 dias, variando entre 16 e 20 dias) comparada à média de vida dos animais tratados com o composto **45**. Os animais controle, sem tratamento, apresentaram um tempo média de vida de 20 dias, variando entre 16 e 23 dias pós-infecção. Por outro lado, todos os animais tratados com o benznidazol sobreviveram (Figura 18). Assim, a redução da parasitemia dos animais tratados com os compostos **45** e **48** não foi suficiente para a garantia da sobrevivência, e, diante do óbito precoce

dos animais tratados comparados com os animais controle sem tratamento, é possível sugerir um efeito tóxico destes compostos em camundongos, nesta dose utilizada.

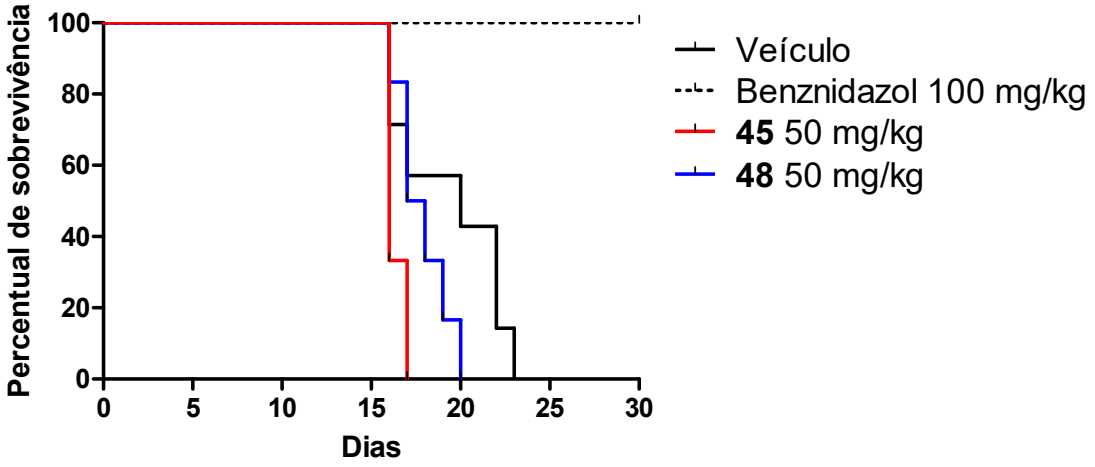

Figura 18 – Curva de sobrevivência dos animais tratados ou não com os compostos **45** e **48**.
A taxa da mortalidade dos grupos foi observada até o dia 30 pós- infecção. Foi utilizado como controle positivo o fármaco de referência, benznidazol, com a dose de 100 mg/kg/dia, e, como controle negativo, apenas o veículo. Os dados representam o % de animais vivos (6 animais/grupo) em cada ponto analisado.

6 DISCUSSÃO

O controle da infecção por *T. cruzi* baseia-se, principalmente, na quimioterapia, restrita ao benznidazol e nifurtimox, drogas que apresentam alta toxicidade, eficácia limitada durante a fase crônica da doença, e que podem induzir o aparecimento de cepas resistentes. Assim, é urgente a identificação de candidatos a fármacos seletivos e com baixa toxicidade. Dentre as diferentes abordagens que têm sido utilizadas nas pesquisas envolvendo desenvolvimento de fármacos em tripanossomatídeos, foi realizada a abordagem baseada nos alvos moleculares TcSir2rp1 e TcSir2rp3, sirtuínas de *T. cruzi*.

O ponto chave para uma abordagem que enfoque uma enzima específica é a identificação e seleção do alvo molecular promissor. Em tripanossomatídeos, o sucesso desta abordagem é limitado, principalmente, pela falta de correlação entre a atividade inibitória da enzima alvo, com a inibição da proliferação do parasito *in vitro* e *in vivo* (FIELD et al., 2017). Entretanto, dentre os inibidores de sirtuínas que foram identificados no ensaio de triagem com as enzimas purificadas, TcSir2rp1 e TcSir2rp3, os compostos exibiram atividade tripanocida contra as formas tripomastigota e amastigota, exceto nos compostos **43** e **44**, que inibiram apenas a proliferação da forma intracelular do parasito, apesar de terem inibido ambas as enzimas, com os menores valores IC_{50}.

Os compostos **43** e **44** são ácidos anacárdicos isolados do extrato diclorometano da *Anacardium occidentale*, conhecida popularmente como cajueiro. Em ensaio de modelagem molecular composto por uma biblioteca de fitocompostos, foram identificados possíveis inibidores de sirtuínas de *T. cruzi*, incluindo um ácido anacárdico extraído do líquido da castanha do caju, que apresentou os melhores resultados *in silico,* inibindo ambas as sirtuínas (SACCONNAY et al., 2014). Os dados encontrados em nosso trabalho validam os dados de predição de modelagem molecular, indicando o potencial de ácidos anacárdicos na inibição de TcSir2rp1 e TcSir2rp3.

Já foram descritas na literatura diferentes propriedades biológicas do líquido da castanha do caju, principalmente associadas à sua constituição fenólica (ácido anacárdico, cardol e cardanol). Estes compartilham uma cadeia lateral de 15 átomos de carbono, e variam em relação ao grau de insaturação (monoeno, dieno e trieno) (OLIVEIRA et al., 2011), o que torna o cajueiro uma importante fonte natural de

compostos fenólicos contendo longas cadeias de carbono na posição meta, que é difícil de se obter a partir da rota sintética (ATTANASI et al., 2006).

O líquido da castanha do caju e o ácido anacárdico apresentam grande potencial terapêutico e são descritos como agentes microbicidas, com propriedades anti-inflamatórias, antitumoral, antioxidante e inseticida contra o *Aedes aegypti* (BALASUBRAMANYAM et al., 2003; KUBO et al., 1993; MAI et al., 2006; MORAIS et al., 2017; OLIVEIRA et al., 2011; WU et al., 2011). Em relação a uma potencial atividade tripanocida, diferentes ácidos anacárdicos foram descritos na literatura como agentes inibitórios da enzima gliceraldeído-3- fosfato desidrogenase de *T. cruzi*, entretanto não foram realizados estudos para avaliar a atvidade anti-parasitária (PEREIRA et al., 2008). Assim, nosso trabalho descreve, pela primeira vez, a atividade anti-*T. cruzi* de ácidos anacárdicos (compostos **43** e **44**), com inibição das sirtuínas do parasito.

Dentre os demais isolados do líquido da castanha do caju (*Anacardium occidentale*) que foram também estudados neste trabalho, 2 são compostos com característica cardol e 2 cardanol. Nenhum dos compostos classificados como cardanol inibiu as sirtuínas de *T. cruzi*, enquanto um dos compostos do tipo cardol (**40**) inibiu a TcSir2rp1. Foi recentemente desmonstrado que mudanças na estrutura de ácidos anacárdicos causam diferenças na polaridade da molécula, que podem contribuir para a diversidade de atividades biológicas (MORAIS et al., 2017). Em relação aos compostos **43** e **44** (monoeno – 15:1, dieno – 15:2), não foram verificadas diferenças de atividade biológicas. No entanto, em relação aos compostos classificados como cardol (dieno – 15:2, trieno – 15:3), diferenças entre as insaturações na cadeia de carbono das moléculas resultaram em variado grau de inibição da enzima TcSir2rp1. O cardol trieno – 15:3 testado neste trabalho não apresentou atividade inibitória contra qualquer das enzimas do parasito, enquanto que o composto cardol **40** (dieno – 15:2) inibiu a sirtuína citoplasmática do parasito, além de inibir a viabilidade das formas tripomastigota e amastigota do parasito. Esta também é a primeira vez que é descrita na literatura a atividade tripanocida desta classe de compostos naturais.

Em relação aos compostos do grupo 1, que envolve os diferentes inibidores de KDACs humanas (WANG et al., 2015), verificamos que 7 dos 38 compostos testados neste trabalho inibiram as sirtuínas de *T. cruzi*. As moléculas **14** e **17** inibiram

TcSir2rp1, enquanto **10**, **12**, **13**, **33** e **35** inibiram TcSir2rp3, e todos os compostos foram capazes de inibir as formas tripomastigota e amastigota do parasito.

É descrito na literatura um estudo semelhante com diferentes inibidores de KDACs humanas testadas contra o *T. brucei* (CARRILLO; GUIGUEMDE; GUY, 2015). Os inibidores selecionados para a triagem em *T. brucei* foram compostos que estavam/estão sendo utilizados em ensaios clínicos oncológicos e foram capazes de inibir a proliferação do parasito *in vitro*. Entretanto, não foi verificada seletividade destes compostos, uma vez que, quando testados em concentrações não tóxicas a células humanas, não houve atividade antiparasitária (CARRILLO; GUIGUEMDE; GUY, 2015). Um outro estudo realizado com inibidores de KDACs, em que 4 inibidores que também apresentam atividade anti-câncer foram testados contra o *T. brucei* e *Plasmodium falciparum*, demonstrou a seletividade do composto em relação ao *Plasmodium*, mas falta de seletividade na atividade inibitória do tripanassomatídeo (ENGEL et al., 2015). Isso confirma que a seletividade de uma droga é um importante parâmetro para ser avaliar quando um grupo de drogas é proposto como agentes antiparasitários (ANDREWS; FISHER; SKINNER-ADAMS, 2014).

Em nosso estudo, os inibidores de KDACs humanas que apresentaram atividade inibitória para as sirtuínas de *T. cruzi* inibiram o parasito em concentrações atóxicas avaliadas em hFIB, entretanto, apresentaram um baixo índice de seletividade, variando entre 2 e >5. A literatura sugere que drogas que apresentem índices de seletividade <50 não devem ser utilizadas em modelo animal ou devem ser reconsideradas (ROMANHA et al., 2010) ou, ao menos, com valores próximos ou maiores que o índice de seletividade do benznidazol (>32) (SIMÕES-SILVA et al., 2016). Dentre os compostos testados em nosso trabalho, tanto os compostos isolados da *Anacardium occidentale* assim como os diferentes inibidores de KDACs humanas não apresentaram índices de seletividade satisfatórios, e desta forma não foram selecionados para o ensaio de atividade anti-*T. cruzi* utilizando modelo animal.

Os compostos alcalóides do tipo quinolina isolados dos extratos diclorometano da raiz de *Waltheria indica* foram triados para avaliar o potencial destes compostos (**45** – **48**) em inibir as sirtuínas de *T. cruzi*, umas vez que já foi descrita a atividade tripanocida destes compostos, mas não foi investigado o seu mecanismo de ação (CRETTON et al., 2014, 2015). Nos estudos publicados, os compostos foram triados contra a cepa Tulahuen do parasito, enquanto que os ensaios aqui demonstrados foram realizados contra a cepa Y de *T. cruzi*. Os dados da literatura demonstram uma

atividade anti-*T. cruzi* com valores de IC_{50} variando entre 0,02 e 1,93 μM (CRETTON et al., 2014, 2015), enquanto os valores IC_{50} encontrados em nosso trabalho variaram entre 0,2 e 3,5 μM. Os compostos que apresentaram melhor atividade tripanocida em nosso trabalho (**45** e **48**) apresentaram valor de IC_{50} de 0,2 μM, enquanto que estes compostos quando testados contra a cepa Tulahuen apresentaram valores de IC_{50} de 1,1 e 0,23 μM, respectivamente (CRETTON et al., 2014, 2015). Em relação ao índice de seletividade destes compostos, em nosso trabalho os valores foram de 300 e >500, respectivamente, enquanto o artigo publicado, que utilizou a linhagem celular L6, apresentou valores 22,7 e 4, respectivamente (CRETTON et al., 2014, 2015). Estas diferenças entre os valores podem ser justificadas pela diferença entre as células utilizadas para a infecção e para o ensaio de citotoxicidade. Enquanto nosso grupo utilizou fibroblasto humanos, o grupo utilizou mioblastos de ratos. Com base no índice de seletividade elevado, principalmente dos compostos **45** e **48**, avaliamos a atividade anti-*T. cruzi* em camundongos. Foi verificada a redução da parasitemia, entretanto os animais tratados com os compostos **45** e **48**, na dose de 50 mg/kg/dia por 5 dias consecutivos vieram a óbito, com sinais de toxicidade ocasionados pelo tratamento. Os efeitos tóxicos dos tratamentos em camundongos não previstos pelo ensaio de citotoxicidade pode ser explicado pela célula utilizada em nossa avaliação da atividade tóxica, e pode ser explicada pelos valores de citotoxicidade e dos respectivos índices de seletividade observados em mioblastos de ratos (CRETTON et al., 2014, 2015).

Uma estratégia que pode ser utilizada visando à redução dos efeitos tóxicos das drogas é o uso da terapia combinada. Atualmente, a combinação de fármacos com diferentes mecanismos de ação tem sido muito utilizada no tratamento de diversas doenças dentre elas a AIDS, tuberculose, hanseníase e a malária, e pode ser também uma alternativa viável para o tratamento da doença de Chagas. A terapia combinada com o benzonidazol e/ou nifurtimox permite a utilização de baixas doses destes medicamentos, diminuindo os efeitos colaterais decorrentes do tratamento. Além disso, a terapia combinada pode não só aumentar a resposta terapêutica como ajudar a evitar o desenvolvimento da resistência quimioterápica pelo parasito, uma vez que podem atuar em diferentes vias metabólicas (COURA; DIAS, 2009).

As sirtuínas são descritas como enzimas com função de desacetilase NAD+ dependente. A atividade desacetilase de TcSir2rp3 foi recentemente demonstrada (MORETTI et al., 2015), entretanto a atividade de TcSir2rp1 ainda não havia sido caracterizada. Nosso trabalho demonstrou a importância da presença de NAD+ para

atividade biológica das enzimas, sendo caracterizado, pela primeira vez, o efeito da ausência e presença de NAD+ na função desacetilase de TcSir2rp1.

Apesar das sirtuínas de *T. cruzi* serem homólogas, existem domínios específicos em cada uma delas que podem contribuir com a especificidade de interação com um fármaco (SACCONNAY et al., 2013). Comparando o perfil inibitório do mesmo conjunto de drogas para ambas as enzimas, pudemos verificar que apenas 2 compostos (**43** e **44**) inibiram TcSir2rp1 e TcSir2rp3. Os demais compostos apresentaram atividade inibitória seletiva para uma das sirtuínas do parasito, com predominância de TcSir2rp3. A comparação entre os valores de IC_{50} de TcSir2rp1 e TcSir2rp3 demonstrou que a enzima mitocondrial foi inibida de forma mais potente, porém, foram os inibidores de TcSir2rp1 que apresentaram uma melhor atividade antiparasitária. Foi observada uma correlação entre a capacidade dos compostos em inibir tanto as enzimas recombinantes quanto o parasito. Assim como foi verificada uma atividade semelhante de inibição da forma tripomastigota e amastigota, com exceção dos compostos **43** e **44** que não inibiram a forma tripomastigota. Esses dados reforçam a ideia que as sirtuínas do parasito são potenciais alvos farmacológicos para o tratamento da doença de Chagas.

Já é descrito na literatura que a superexpressão das enzimas no parasito interferem no crescimento parasitário assim como na metaciclogênese (MORETTI et al., 2015; RITAGLIATI et al., 2015), porém a obtenção de parasitos *knockout* para TcSir2rp1 e TcSir2rp3 é essencial para a validação das sirtuínas como alvos farmacológicos. Em colaboração com o Laboratório de Biologia Celular e Molecular de Tripanossomas – UNIFESP, iniciamos os ensaios para a obtenção de parasitos *knockout* utilizando a técnica de CRISPR/Cas 9 com base no protocolo estabelecido por LANDER et al., 2015, porém não obtivemos sucesso até o momento.

Do ponto de vista de planejamento de fármacos e da química medicinal, torna-se interessante que sejam determinadas as estruturas das enzimas por cristalografia com o objetivo de favorecer uma triagem virtual de produtos naturais ou compostos sintéticos, facilitando assim a identificação, seleção e otimização de moléculas capazes de interagir com alta afinidade e seletividade as sirtuínas do parasito (GUIDO; ANDRICOPULO; OLIVA, 2010). Além da abordagem virtual, o uso de triagens biológicas automatizadas a partir do sistema de HCS contribui com o desenvolvimento de fármacos não só permitindo a identificação de moléculas inibitórias ao parasito,

assim como auxiliando com os estudos de mecanismo de ação dos fármacos e nos ensaios de toxicidade *in vitro* (FRAIETTA; GASPARRI, 2016).

A aquisição do Operetta pelo nosso grupo representou um avanço na pesquisa do nosso estado, que é um dos únicos no país que utiliza um sistema HCS na etapa pré-clínica para o desenvolvimento e identificação de fármacos. A análise de moléculas utilizando uma técnica automatizada favorece uma triagem em larga escala com rapidez e bom rendimento, associados a resultados confiáveis. Já a padronização do ensaio de infecção envolvendo uma célula humana, como hFIB, substituindo o uso de células isoladas de camundongos, representa um refinamento, e permite a substituição de modelos, visando a promoção do uso racional de animais na pesquisa.

Em geral, nas fases iniciais de desenvolvimento de fármacos, são identificadas moléculas de baixa potência e afinidade que devem ser otimizadas em relação às suas propriedades farmacocinéticas e farmacodinâmicas. Desta forma, nosso trabalho permitiu a identificação de diferentes moléculas inibidoras de sirtuínas de *T. cruzi*, que podem ser otimizadas a partir de modificações em suas estruturas, visando uma atividade parasitária mais potente e seletiva.

Como perspectivas futuras, em colaboração com o Laboratório de Biologia Celular e Molecular de Tripanossomas – UNIFESP, daremos continuidade com os ensaios para a obtenção de parasitos *knockout* para as sirtuínas do *T. cruz*i, assim como para a obtenção das estruturas cristalográficas de TcSir2rp1 e TcSir2rp3, visando melhor compreender o papel das enzimas para o parasito, assim como para validar as sirtuínas como alvos farmacológicos para o tratamento da doença de Chagas.

7 CONCLUSÃO

A partir da obtenção das sirtuínas recombinantes do *T. cruzi* e da validação da atividade de desacetilase das enzimas, foi possível identificar diferentes moléculas com perfil inibitório para TcSir2rp1 e TcSir2rp3, que foram também identificadas como agentes antiparasitários, reforçando o uso de sirtuínas como alvos farmacológicos no tratamento da doença de Chagas.

REFERÊNCIAS

ADAD, S. J. et al. Contribuição ao estudo da anatomia patolôgica do megaesôfago chagásico. **Revista do Instituto de Medicina Tropical de Sao Paulo**, v. 33, n. 6, p. 443–450, 1991.

ALARCÓN DE NOYA, B. et al. Large urban outbreak of orally acquired acute Chagas disease at a school in Caracas, Venezuela. **The Journal of Infectious Diseases**, v. 201, n. 9, p. 1308–1315, 2010.

ALONSO-PADILLA, J. et al. Automated High-Content Assay for Compounds Selectively Toxic to *Trypanosoma cruzi* in a Myoblastic Cell Line. **PLoS Neglected Tropical Diseases**, v. 9, n. 1, p. 1–17, 2015.

ALSFORD, S. et al. A sirtuin in the African trypanosome is involved in both DNA repair and telomeric gene silencing but is not required for antigenic variation. **Molecular Microbiology**, v. 63, n. 3, p. 724–736, 2007.

ANDREWS, K. T.; FISHER, G.; SKINNER-ADAMS, T. S. Drug repurposing and human parasitic protozoan diseases. **International Journal for Parasitology: Drugs and Drug Resistance**, v. 4, n. 2, p. 95–111, 2014.

ATTANASI, O. A. et al. Synthesis and reactions of nitro derivatives of hydrogenated cardanol. **Tetrahedron**, v. 62, n. 25, p. 6113–6120, 2006.

AUFDERHEIDE, A. C. et al. A 9,000-year record of Chagas' disease. **Proceedings of the National Academy Sciiences**, v. 101, n. 7, p. 2034–2039, 2004.

AVALOS, J. L.; BEVER, K. M.; WOLBERGER, C. Mechanism of sirtuin nhibition by nicotinamide: Altering the NAD + cosubstrate specificity of a Sir2 enzyme. **Molecular Cell**, v. 17, n. 6, p. 855–868, 2005.

BALASUBRAMANYAM, K. et al. Small molecule modulators of histone acetyltransferase p300. **Journal of Biological Chemistry**, v. 278, n. 21, p. 19134–19140, 2003.

BASTOS, T. M. et al. Nitro/Nitrosyl- Ruthenium complexes are potent and selective anti-*Trypanosoma cruzi* agents causing autophagy and Necrotic parasite death. **Antimicrobial Agents and Chemotherapy**, v. 58, n. 10, p. 6044–6055, 2014.

BERMUDEZ, J. et al. Current drug therapy and pharmaceutical challenges for Chagas disease. **Acta Tropica**, v. 156, p. 1–16, 2016.

BERN, C. Chagas' Disease. **The New England Journal of Medicine**, v. 373, p. 456–466, 2015.

BIRNBOIM, H. C.; DOLY, J. A rapid alkaline extraction procedure for screening recombinant plasmid DNA. **Nucleic Acids Research**, v. 7, n. 6, p. 1513–23, 24 nov. 1979.

BRACHMANN, C. B. et al. The SIR2 gene family, conserved from bacteria to humans, functions in silencing, cell cycle progression, and chromosome stability. **Genes and Development**, v. 9, n. 23, p. 2888–2902, 1995.

BRASIL. MINISTÉRIO DE SAÚDE. **Boletim Epidemiológico - Doença de Chagas aguda no Brasil: série histórica de 2000 a 2013**. Secretaria de Vigilância em Saúde, v. 46, n. 21, p. 1–9, 2015.

BRENER, Z.; ANDRADE, Z. A.; BARRAL-NETTO, M. ***Trypanosoma cruzi* e Doença de Chagas**. Rio de Janeiro: Editora Guanabara Koogan, 2000.

BRENER, Z. Therapeutic activity and criterion of cure on mice experimentally infected with *Trypanosoma cruzi*. **Revista do Instituto de Medicina Tropical de Sao Paulo**, v. 4, p. 389–96, 1962.

BUCKNER, F. S.; URBINA, J. A. Recent developments in sterol 14-demethylase inhibitors for Chagas disease. **International Journal for Parasitology: Drugs and Drug Resistance**, v. 2, p. 236–242, 2012.

CARRILLO, A. K.; GUIGUEMDE, W. A.; GUY, R. K. Evaluation of histone deacetylase inhibitors (HDACi) as therapeutic leads for human African trypanosomiasis (HAT). **Bioorganic and Medicinal Chemistry**, v. 23, n. 16, p. 5151–5155, 2015.

CHAGAS, C. Nova tripanozomiaze humana: estudos sobre a morfolojia e o ciclo evolutivo do *Schizotrypanum cruzi* n. gen., n. sp., ajente etiolojico de nova entidade morbida do homem. **Memórias do Instituto Oswaldo Cruz**, v. 1, n. 2, p. 159–218, ago. 1909.

CHAGAS, C. Tripanosomiase americana - forma aguda da molestia. **Memórias do Instituto Oswaldo Cruz**, v. 8, p. 37–65, 1916.

CLAYTON, J. Chagas disease : pushing through the pipeline. **Nature**, p. 12–15, 2010.

CÔBO, E. D. C. et al. Research on *Trypanosoma cruzi* and analysis of inflammatory infiltrate in esophagus and colon from chronic chagasic patients with and without mega. **Journal of Tropical Medicine**, v. 2012, 2012.

CONNERS, E. E. et al. A global systematic review of Chagas disease prevalence among migrants. **Acta Tropica**, v. 156, p. 68–78, 2016.

COURA, J. R. Tripanosomose, doença de Chagas. **Ciência e Cultura**, v. 55, n. 1, p. 30–33, 2003.

COURA, J. R. Transmission of chagasic infection by oral route in the natural history of Chagas disease. **Revista da Sociedade Brasileira de Medicina Tropical**, v. 39 Suppl 3, p. 113–7, 2006.

COURA, J. R. The main sceneries of chagas disease transmission. The vectors, blood and oral transmissions - A comprehensive review. **Memorias do Instituto Oswaldo Cruz**, v. 110, n. 3, p. 277–282, 2015.

COURA, J. R.; DIAS, J. C. P. Epidemiology, control and surveillance of Chagas disease: 100 years after its discovery. **Memórias do Instituto Oswaldo Cruz**, v. 104, n. i, p. 31–40, 2009.

COURA, J. R.; VIÑAS, P. A. Chagas disease: a new worldwide challenge. **Nature**, v. 465, n. n7301_supp, p. S6–S7, 24 jun. 2010.

CRETTON, S. et al. Antitrypanosomal quinoline alkaloids from the roots of waltheria indica. **Journal of Natural Products**, v. 77, n. 10, p. 2304–2311, 2014.

CRETTON, S. et al. Chemical constituents from Waltheria indica exert in vitro activity against *Trypanosoma brucei* and *T. cruzi*. **Fitoterapia**, v. 105, p. 55–60, 2015.

DE SOUZA, W. Basic cell biology of *Trypanosoma cruzi*. **Current Pharmaceutical Design**, v. 8, n. 4, p. 269–85, 2002.

DIAS, J. P. et al. Acute Chagas disease outbreak associated with oral transmission. **Revista da Sociedade Brasileira de Medicina Tropical**, v. 41, n. 3, p. 296–300, 2008.

DOCAMPO, R.; STOPPANI, A. Generation of Superoxide Anion and Hydrogen Peroxide Induced by Nifurtimox in *Trypanosoma cruzi*. **Archives of Biochemistry and Biophysics**, v. 19, n. 1, p. 317–321, 1979.

DU, J. et al. Sirt5 Is a NAD-Dependent Protein Lysine Demalonylase and Desuccinylase. **Science**, v. 334, n. 6057, p. 806–809, 11 nov. 2011.

ENGEL, J. A. et al. Profiling the anti-protozoal activity of anti-cancer HDAC inhibitors against *Plasmodium* and *Trypanosoma* parasites. **International Journal for Parasitology: Drugs and Drug Resistance**, v. 5, n. 3, p. 117–126, 2015.

FIELD, M. C. et al. Anti-trypanosomatid drug discovery: an ongoing challenge and a continuing need. **Nature Reviews Microbiology**, v. 15, n. 4, p. 217–231, 2017.

FRAIETTA, I.; GASPARRI, F. The development of high-content screening (HCS) technology and its importance to drug discovery. **Expert Opinion on Drug Discovery**, v. 11, n. 5, p. 501–514, 2016.

FRYE, R. A. Characterization of Five Human cDNAs with Homology to the Yeast SIR2 Gene: Sir2-like Proteins (Sirtuins) Metabolize NAD and May Have Protein ADP-Ribosyltransferase Activity. **Biochemical and Biophysical Research Communications**, v. 260, n. 1, p. 273–279, jun. 1999.

FRYE, R. A. Phylogenetic Classification of Prokaryotic and Eukaryotic Sir2-like Proteins. **Biochemical and Biophysical Research Communications**, v. 273, n. 2, p. 793–798, 2000.

GARCÍA-SALCEDO, J. A. et al. A chromosomal SIR2 homologue with both histone NAD-dependent ADP-ribosyltransferase and deacetylase activities is involved in DNA repair in *Trypanosoma brucei*. **EMBO Journal**, v. 22, n. 21, p. 5851–5862, 2003.

GARCIA, E. S.; AZAMBUJA, P. Development and interactions of *Trypanosoma cruzi* within the insect vector. **Parasitology Today**, v. 7, n. 9, p. 240–244, 1991.

GARCIA, S. et al. Treatment with Benznidazole during the Chronic Phase of Experimental Chagas' Disease Decreases Cardiac Alterations Treatment with Benznidazole during the Chronic Phase of Experimental Chagas' Disease Decreases Cardiac Alterations. **Antimicrobial Agents and Chemotherapy**, v. 49, n. 4, p. 1521–1528, 2005.

GERTZ, M.; STEEGBORN, C. Using mitochondrial sirtuins as drug targets: disease implications and available compounds. **Cellular and Molecular Life Sciences**, p. 1–26, 2016.

GREGORETTI, I. V.; LEE, Y. M.; GOODSON, H. V. Molecular evolution of the histone deacetylase family: Functional implications of phylogenetic analysis. **Journal of Molecular Biology**, v. 338, n. 1, p. 17–31, 2004.

GUIDO, R. V. C.; ANDRICOPULO, A. D.; OLIVA, G. Planejamento de fármacos, biotecnologia e química medicinal: aplicações em doenças infecciosas. **Estudos Avançados**, v. 24, n. 70, p. 81–98, 2010.

IVENS, A. C. et al. The genome of the kinetoplastid parasite, *Leishmania major*. **Science**, v. 309, n. 5733, p. 436–442, 2006.

KAUR, S.; SHIVANGE, A. V.; ROY, N. Structural analysis of trypanosomal sirtuin: an insight for selective drug design. **Molecular Diversity**, v. 14, n. 1, p. 169–178, fev. 2010.

KEENAN, M.; CHAPLIN, J. H. A new era for chagas disease drug discovery? **Progress in Medicinal Chemistry**, v. 54, p. 185–230, 2015.

KUBO, I. et al. Structure-antibacterial activity relationships of anacardic acids. **Journal of Agricultural and Food Chemistry**, v. 41, n. 6, p. 1016–1019, jun. 1993.

LANDER, N. et al. CRISPR/Cas9-Induced Disruption of Paraflagellar Rod Protein 1 and 2 Genes in *Trypanosoma cruz*i Reveals Their Role in Flagellar Attachment. **mBio**, v. 6, n. 4, p. e01012-15, 1 set. 2015.

LAUGIER, L. et al. Whole genome Cardiac DNA methylation fingerprint and gene expression analysis provide new insights in the pathogenesis of Chronic Chagas disease Cardiomyopathy. **Clinical Infectious Diseases**, p. 1–32, 30 maio 2017.

LEWIS, M. D. et al. Host and parasite genetics shape a link between *Trypanosoma cruzi* infection dynamics and chronic cardiomyopathy. **Cellular Microbiology**, v. 44, p. 1429–1443, 2016.

MACHADO, F. S. et al. Pathogenesis of Chagas disease: time to move on. **Frontiers in Bioscience**, v. 4, p. 1743–58, 2012.

MAI, A. et al. Small-molecule inhibitors of histone acetyltransferase activity:

Identification and biological properties. **Journal of Medicinal Chemistry**, v. 49, n. 23, p. 6897–6907, 2006.

MARIN-NETO, J. A. et al. Pathogenesis of chronic Chagas heart disease. **Circulation**, v. 115, n. 9, p. 1109–1123, 2007.

MARIN-NETO, J. A. et al. Rationale and design of a randomized placebo-controlled trial assessing the effects of etiologic treatment in Chagas' cardiomyopathy: The BENznidazole Evaluation For Interrupting Trypanosomiasis (BENEFIT). **American Heart Journal**, v. 156, n. 1, p. 37–43, jul. 2008.

MARIN-NETO, J. A. et al. The BENEFIT trial: testing the hypothesis that trypanocidal therapy is beneficial for patients with chronic Chagas heart disease. **Memórias do Instituto Oswaldo Cruz**, v. 104, n. suppl 1, p. 319–324, jul. 2009.

MOLINA, I. et al. Randomized trial of posaconazole and benznidazole for chronic Chagas' disease. **The New England Journal of Medicine**, v. 370, p. 1899–908, 2014.

MONCAYO, Á.´; SILVEIRA, A. C. Current epidemiological trends for Chagas disease in Latin America and future challenges in epidemiology, surveillance and health policy. **Memorias do Instituto Oswaldo Cruz**, v. 104, n. SUPPL. 1, p. 17–30, 2009.

MORAIS, S. M. et al. Anacardic acid constituents from cashew nut shell liquid: NMR characterization and the effect of unsaturation on its biological activities. **Pharmaceuticals**, v. 10, n. 1, p. 1–10, 2017.

MORETTI, N. S. et al. Characterization of *Trypanosoma cruzi* Sirtuins as Possible Drug Targets for Chagas Disease. **Antimicrobial Agents and Chemotherapy**, v. 59, n. 8, p. 4669–4679, 2015.

MORILLO, C. A. et al. Randomized Trial of Benznidazole for Chronic Chagas' Cardiomyopathy. **New England Journal of Medicine**, v. 373, n. 14, p. 1295–1306, 2015.

NORTH, B. J.; VERDIN, E. Protein family review Sirtuins: Sir2-related NAD-dependent protein deacetylases. **Genome Biology**, p. 1–12, 2004.

OLIVEIRA, M. S. C. et al. Antioxidant, larvicidal and antiacetylcholinesterase activities of cashew nut shell liquid constituents. **Acta Tropica**, v. 117, n. 3, p. 165–170, mar. 2011.

PARK, J. et al. SIRT5-Mediated Lysine Desuccinylation Impacts Diverse Metabolic Pathways. **Molecular Cell**, v. 50, n. 6, p. 919–930, 2013.

PEREIRA, J. M. et al. Anacardic acid derivatives as inhibitors of glyceraldehyde-3-phosphate dehydrogenase from *Trypanosoma cruzi*. **Bioorganic & Medicinal Chemistry**, v. 16, n. 19, p. 8889–8895, 2008.

RIBEIRO, A. L. et al. Diagnosis and management of Chagas disease and cardiomyopathy. **Nature Reviews Cardiology**, v. 9, n. 10, p. 576–589, 2012.

RITAGLIATI, C. et al. Overexpression of Cytoplasmic TcSIR2RP1 and Mitochondrial TcSIR2RP3 Impacts on Trypanosoma cruzi Growth and Cell Invasion. **PLoS Neglected Tropical Diseases**, v. 9, n. 4, p. 1–22, 2015.

ROMANHA, A. J. et al. In vitro and in vivo experimental models for drug screening and development for Chagas disease. **Memórias do Instituto Oswaldo Cruz**, v. 105, n. 2, p. 233–238, 2010.

SACCONNAY, L. et al. Structural insights of SIR2rp3 proteins as promising biotargets to fight against Chagas disease and leishmaniasis. **Molecular bioSystems,** v. 9, n. 9, p. 2171–2392, 2013.

SACCONNAY, L. et al. Computational Studies on Sirtuins from *Trypanosoma cruzi*: Structures, Conformations and Interactions with Phytochemicals. **PLoS Neglected Tropical Diseases**, v. 8, n. 2, 2014.

SANGER, F.; NICKLEN, S.; COULSON, A. R. DNA sequencing with chain-terminating inhibitors. 1977. **Biotechnology**, v. 24, p. 104–8, 1992.

SCHMUNIS, G. A. The globalization of Chagas disease. **ISBT Science Series**, v. 2, n. 1, p. 6–11, 2007.

SILVEIRA, A B. M. et al. Comparative study of the presence of *Trypanosoma cruzi* kDNA, inflammation and denervation in chagasic patients with and without megaesophagus. **Parasitology**, v. 131, n. Pt 5, p. 627–34, 2005.

SIMÕES-SILVA, M. R. et al. Phenotypic screening in vitro of novel aromatic amidines against *Trypanosoma cruzi*. **Antimicrobial Agents and Chemotherapy**, v. 60, n. 8, p. 4701–4707, 2016.

SMIRLIS, D.; SOARES, M. B. P. Selection of Molecular Targets for Drug Development Against Trypanosomatids. In: ANDRÉ L.S. et al. (Ed.). **Subcellular Biochemistry**. Dordrecht: Springer, 2014. p. 43–76.

SOARES, M. B. P. et al. Anti-*Trypanosoma cruzi* activity of nicotinamide. **Acta Tropica**, v. 122, n. 2, p. 224–229, 2012.

SOEIRO, M. D. N. C.; DE CASTRO, S. L. Screening of Potential anti-*Trypanosoma cruzi* Candidates: In Vitro and In Vivo Studies. **The open medicinal chemistry journal**, v. 5, p. 21–30, 2011.

STEINDEL, M. et al. Characterization of *Trypanosoma cruzi* isolated from humans, vectors, and animal reservoirs following an outbreak of acute human Chagas disease in Santa Catarina State, Brazil. **Diagnostic Microbiology and Infectious Disease**, v. 60, n. 1, p. 25–32, jan. 2008.

TAFURI, W. L. Patogenia da doença de Chagas. **Revista do Instituto de Medicina Tropical de Sao Paulo**, v. 29, n. 4, p. 194–199, 1987.

TAN, M. et al. Lysine glutarylation is a protein posttranslational modification regulated by SIRT5. **Cell Metabolism**, v. 19, n. 4, p. 605–617, 2014.

TANNER, K. G. et al. Silent information regulator 2 family of NAD- dependent histone/protein deacetylases generates a unique product, 1-O-acetyl-ADP-ribose. **Proceedings of the National Academy of Sciences**, v. 97, n. 26, p. 14178–14182, 19 dez. 2000.

TAVARES, J. et al. The *Leishmania infantum* cytosolic SIR2-related protein 1 (LiSIR2RP1) is an NAD + -dependent deacetylase and ADP-ribosyltransferase. **Biochemical Journal**, v. 415, n. 3, p. 377–386, 1 nov. 2008.

TROCHINE, A. et al. Benznidazole Biotransformation and Multiple Targets in *Trypanosoma cruzi* Revealed by Metabolomics. **PLoS Neglected Tropical Diseases**, v. 8, n. 5, 2014.

VEIGA-SANTOS, P. et al. Inhibition of NAD+-dependent histone deacetylases (sirtuins) causes growth arrest and activates both apoptosis and autophagy in the pathogenic protozoan *Trypanosoma cruzi*. **Parasitology**, v. 141, n. 6, p. 814–825, 2014.

VERGNES, B.; GAZANION, E.; GRENTZINGER, T. Functional divergence of SIR2 orthologs between trypanosomatid parasites. **Molecular and Biochemical Parasitology**, n. July, 2016.

WANG, Q. et al. Targeting Lysine Deacetylases (KDACs) in Parasites. **PLoS Neglected Tropical Diseases**, v. 9, n. 9, 2015.

WORLD HEALTH ORGANIZATION. **Neglected tropical diseases**. Disponível em: <http://www.who.int/neglected_diseases/diseases/en/>. Acesso em: 21 jul. 2017a.

WORLD HEALTH ORGANIZATION. **Chagas disease (American trypanosomiasis)**. Disponível em: <http://www.who.int/mediacentre/factsheets/fs340/en>. Acesso em: 29 maio. 2017b.

WU, Y. et al. Anacardic Acid (6-Pentadecylsalicylic Acid) Inhibits Tumor Angiogenesis by Targeting Src / FAK / Rho GTPases Signaling Pathway. **The Journal of Pharmacology and Experimental Therapeutics**, v. 339, n. 2, p. 403–411, 2011.

ZHENG, W. Sirtuins as emerging anti-parasitic targets. **European Journal of Medicinal Chemistry**, v. 59, p. 132–140, 2013.

ZINGALES, B. *Trypanosoma cruzi*: um parasita, dois parasitas ou vários parasitas da doença de chagas? **Revista da Biologia**, v. 6b, p. 44–48, 2011.

ZINGALES, B. et al. The revised *Trypanosoma cruzi* subspecific nomenclature: Rationale, epidemiological relevance and research applications. **Infection, Genetics and Evolution**, v. 12, n. 2, p. 240–253, 2012.

ANEXOS

Compostos	Estrutura Química
1	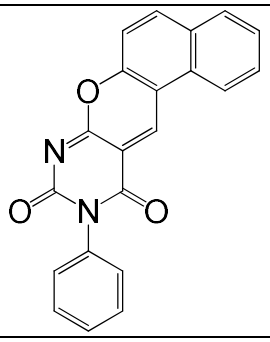
2 -	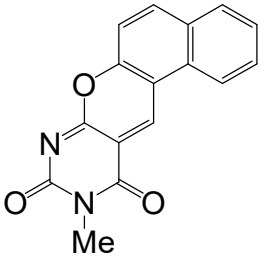
3	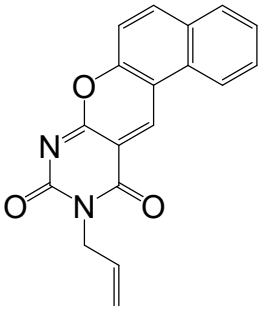
4	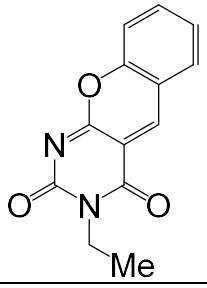
5	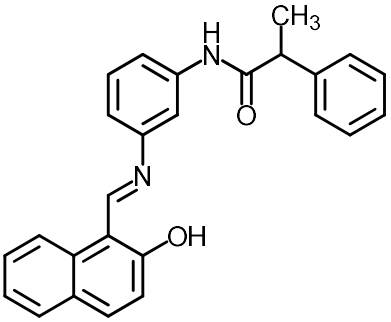

6	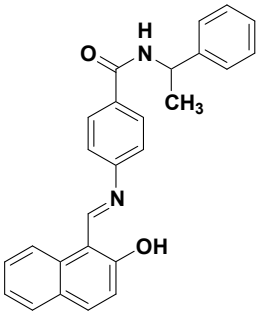
7	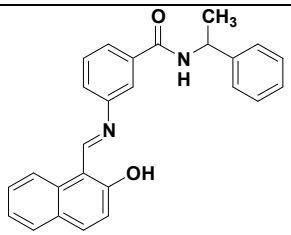
8	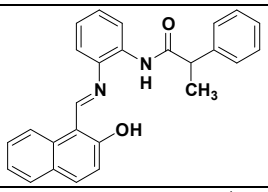
9	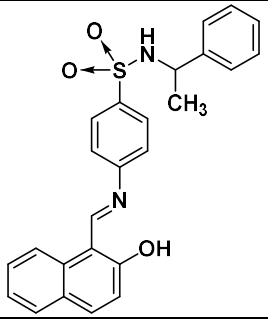
10	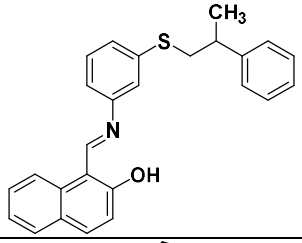
11	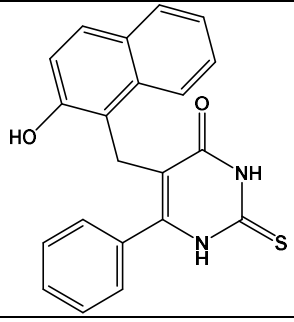

12	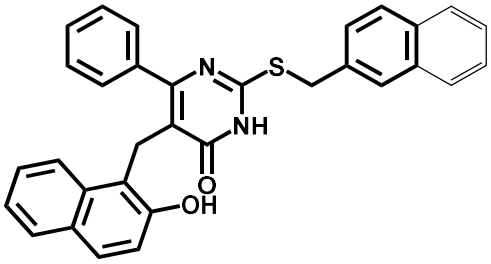
13	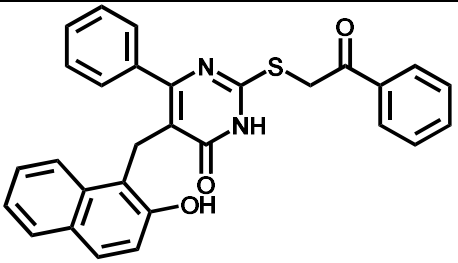
14	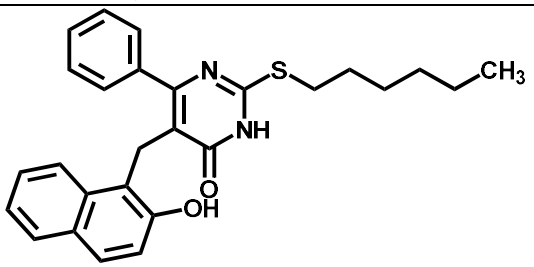
15	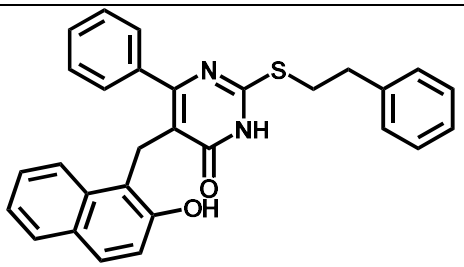
16	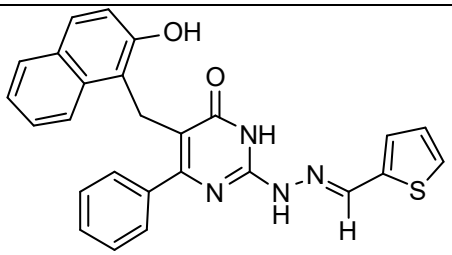
17	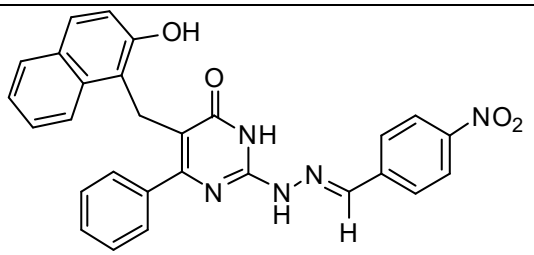
18	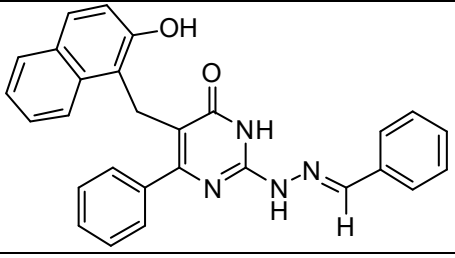

19	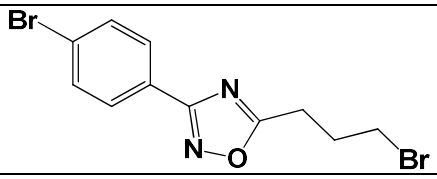
20	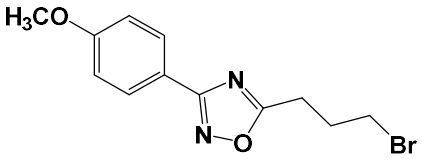
21	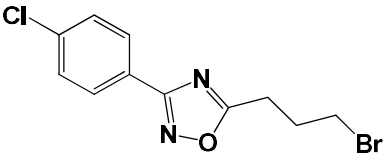
22	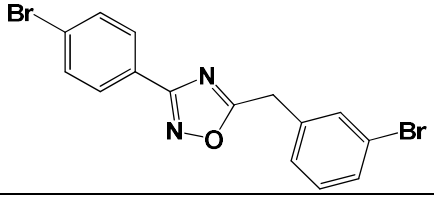
23	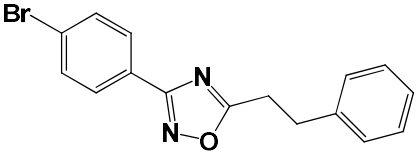
24	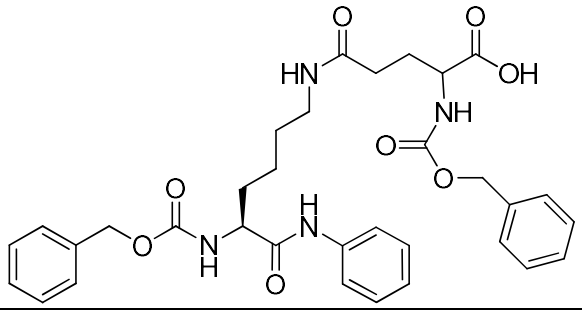
25	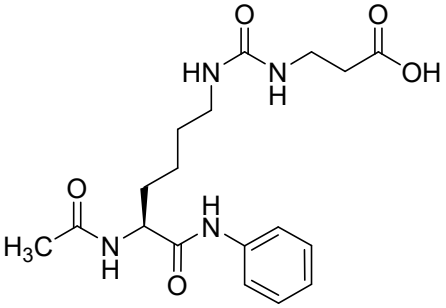

26	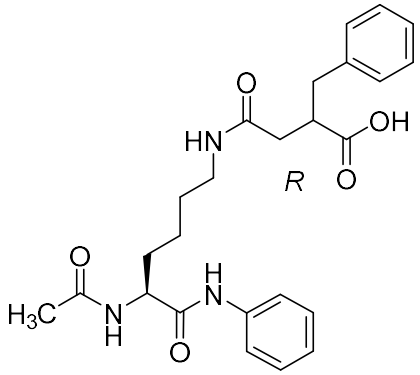
27	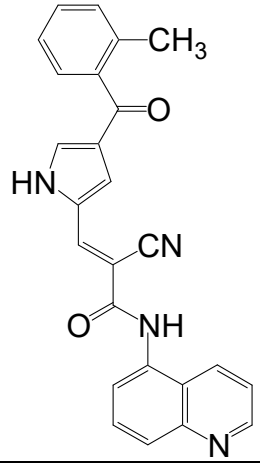
28	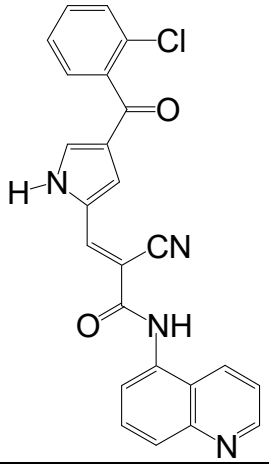
29	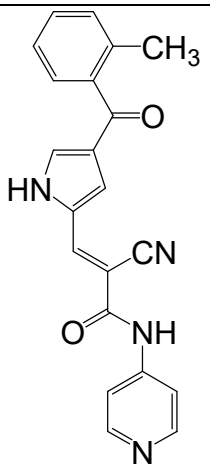

30	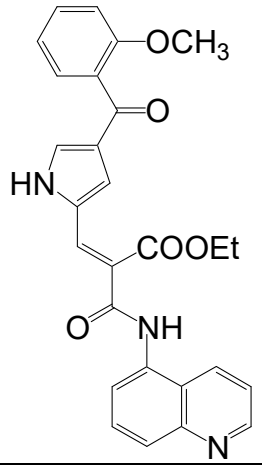
31	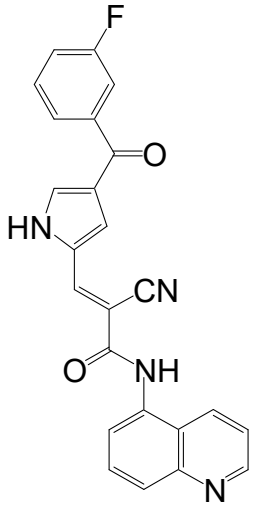
32	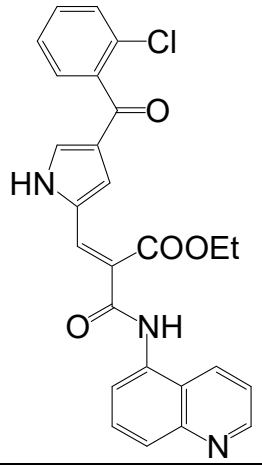
33	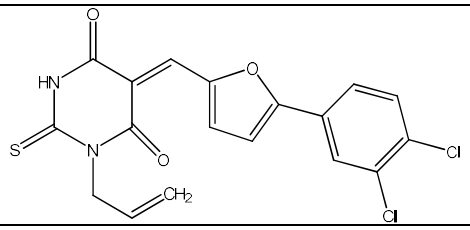

34	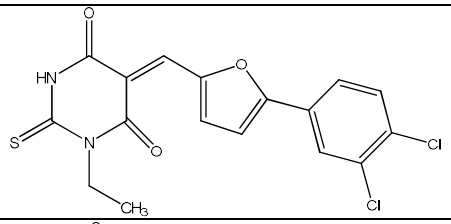
35	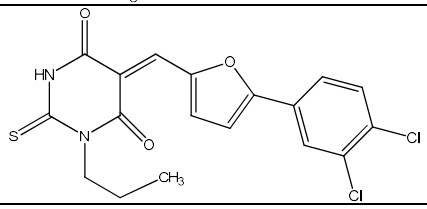
36	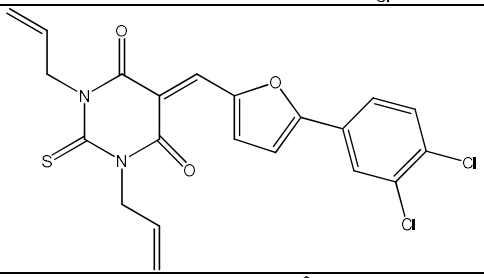
37	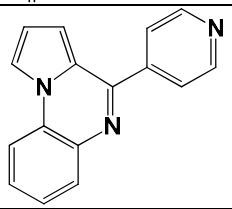
38	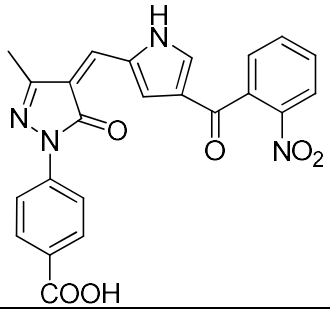
39	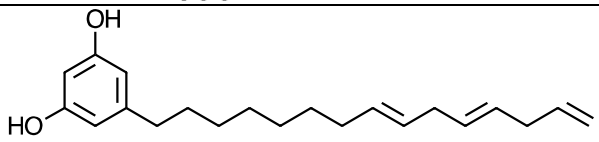
40	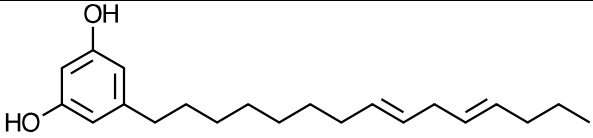
41	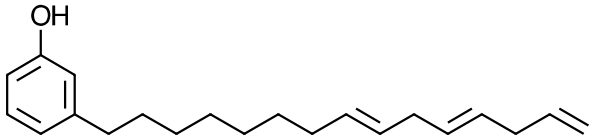
42	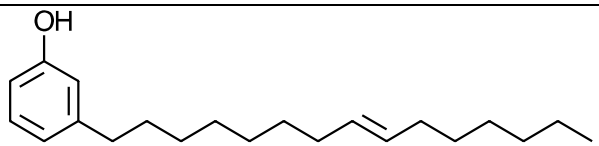

43	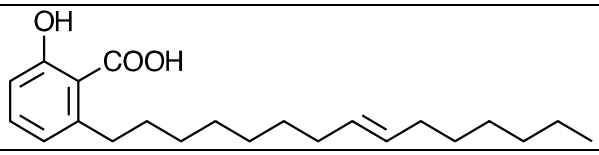
44	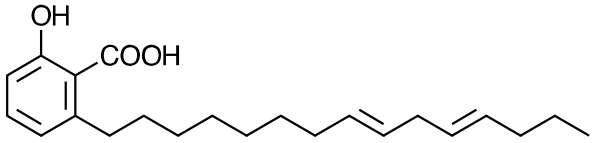
45	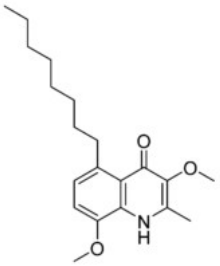
46	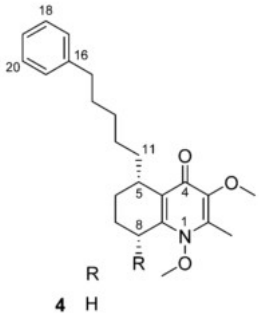
47	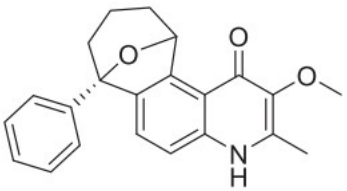
48	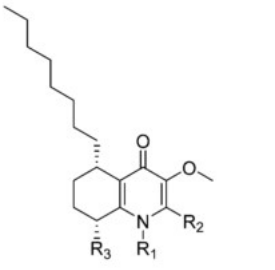

AAC Journals.ASM.org

Nitro/Nitrosyl-Ruthenium Complexes Are Potent and Selective Anti-*Trypanosoma cruzi* Agents Causing Autophagy and Necrotic Parasite Death

Tanira M. Bastos,[a] Marília I. F. Barbosa,[b] Monize M. da Silva,[b] José W. da C. Júnior,[b] Cássio S. Meira,[a] Elisalva T. Guimaraes,[a,c] Javier Ellena,[d] Diogo R. M. Moreira,[a,e] Alzir A. Batista,[b] Milena B. P. Soares[a,e]

FIOCRUZ, Centro de Pesquisas Gonçalo Moniz, Salvador, Bahia, Brazil[a]; UFSCAR, Departamento de Química, São Carlos, São Paulo, Brazil[b]; UNEB, Departamento de Ciências da Vida, Salvador, Bahia, Brazil[c]; USP, Instituto de Física de São Carlos, São Carlos, São Paulo, Brazil[d]; Centro de Biotecnologia e Terapia Celular, Hospital São Rafael, Salvador, Bahia, Brazil[e]

***cis*-[RuCl(NO$_2$)(dppb)(5,5′-mebipy)] (complex 1), *cis*-[Ru(NO$_2$)$_2$(dppb)(5,5′-mebipy)] (complex 2), *ct*-[RuCl(NO)(dppb)(5,5′-mebipy)](PF$_6$)$_2$ (complex 3), and *cc*-[RuCl(NO)(dppb)(5,5′-mebipy)](PF$_6$)$_2$ (complex 4), where 5,5′-mebipy is 5,5′-dimethyl-2,2′-bipyridine and dppb is 1,4-*bis*(diphenylphosphino)butane, were synthesized and characterized. The structure of complex 2 was determined by X-ray crystallography. These complexes exhibited a higher anti-*Trypanosoma cruzi* activity than benznidazole, the current antiparasitic drug. Complex 3 was the most potent, displaying a 50% effective concentration (EC$_{50}$) of 2.1 ± 0.6 μM against trypomastigotes and a 50% inhibitory concentration (IC$_{50}$) of 1.3 ± 0.2 μM against amastigotes, while it displayed a 50% cytotoxic concentration (CC$_{50}$) of 51.4 ± 0.2 μM in macrophages. It was observed that the nitrosyl complex 3, but not its analog lacking the nitrosyl group, releases nitric oxide into parasite cells. This release has a diminished effect on the trypanosomal protease cruzain but induces substantial parasite autophagy, which is followed by a series of irreversible morphological impairments to the parasites and finally results in cell death by necrosis. In infected mice, orally administered complex 3 (five times at a dose of 75 μmol/kg of body weight) reduced blood parasitemia and increased the survival rate of the mice. Combination index analysis of complex 3 indicated that its *in vitro* activity against trypomastigotes is synergic with benznidazole. In addition, drug combination enhanced efficacy in infected mice, suggesting that ruthenium-nitrosyl complexes are potential constituents for drug combinations.**

Chagas disease, caused by the protozoan parasite *Trypanosoma cruzi*, affects approximately 10 million people worldwide, with a high prevalence in Latin America (1). The main drugs used against this disease are benznidazole and nifurtimox (2), both of which are effective in curing the disease when administered during the acute phase but are less effective in patients that have progressed to the chronic phase (3). Furthermore, these drugs are not considered ideal, due to severe side effects, and drug resistance to *T. cruzi* strains has been reported (4). Thus, research aimed at identifying molecules with anti-*T. cruzi* activity is urgently need for the treatment of Chagas disease.

In recent years, a variety of anti-*T. cruzi* drug targets have been identified, including the enzymes lanosterol 14α-demethylase, *trans*-sialidase, trypanothione reductase, and cysteine protease (5). *T. cruzi* contains a cysteine protease homologous to cathepsin L in mammalian cells, called cruzipain or cruzain, which is responsible primarily for the proteolytic activity involved in all stages of the parasite's life cycle (6, 7). Cruzain is important for parasite survival, cell growth, and differentiation (8, 9). Furthermore, this enzyme plays an important role in the process of parasite internalization in mammalian cells and in the intracellular replication of *T. cruzi* (7, 9).

Nitric oxide (NO) is a well-known endogenous trypanocidal molecule which contributes to host control of acute infection (10, 11). NO inactivates cruzain by *S*-nitrosylation of the binding site (12), but *T. cruzi* uses trypanothione reductase to convert NO into a harmless species (13). Therefore, it has been hypothesized that NO donor drugs may be useful against *T. cruzi* infection by producing exogenous NO (14). Organic NO donor molecules have been investigated as anti-*T. cruzi* agents, but compounds with *in vivo* efficacy have not been identified (15). In recent years, ruthenium-nitrosyl complexes have been evaluated as anti-*T. cruzi* agents, demonstrating potent and selective antiparasitic activity, including in *T. cruzi*-infected mice (16–19). In addition, this class of complexes exhibited inhibitory activity against the *T. cruzi* glyceraldehyde 3-phosphate dehydrogenase, suggesting that ruthenium-nitrosyl complexes may have pleiotropic effects (19). From the point of view of medicinal chemistry, ruthenium complexes have been explored as an alternative to platinum complexes in the context of anticancer and anti-infective chemotherapy (20–22). More specifically, ruthenium complexes are described as outstanding bioactive agents because of the phosphine ligands, which provide great stability for these compounds (23–26). Nevertheless, only a few ruthenium complexes containing these ligands have been fully examined against *T. cruzi* (19).

Therefore, in this study we evaluated the *in vitro* and *in vivo* anti-*T. cruzi* activity of four new ruthenium complexes: *cis*-[RuCl

Received 11 March 2014 Returned for modification 16 April 2014
Accepted 18 July 2014
Published ahead of print 4 August 2014
Address correspondence to Milena B. P. Soares, milenabpsoares@gmail.com.
Supplemental material for this article may be found at http://dx.doi.org/10.1128/AAC.02765-14.

doi:10.1128/AAC.02765-14

(NO_2)(dppb)(5,5′-mebipy)] (complex 1), *cis*-[Ru$(NO_2)_2$(dppb)(5,5′-mebipy)] (complex 2), *ct*-[RuCl(NO)(dppb)(5,5′-mebipy)]$(PF_6)_2$ (complex 3), and *cc*-[RuCl(NO)(dppb)(5,5′-mebipy)]$(PF_6)_2$ (complex 4). All the synthesized compounds are mononuclear complexes and contain 5,5′-dimethyl-2,2′-bipyridine (5,5′-mebipy) and 1,4-*bis*(diphenylphosphino)butane (dppb) ligands. To ascertain the importance of the nitrosyl group in antiparasitic activity, the synthesized complexes contained a nitrosyl group in two different positions (*cis* and *trans*), and two complexes contained a nitro group in the place of nitrosyl. Also, a complex lacking the nitro/nitrosyl groups, *cis*-[RuCl_2(dppb)(bipy)] (complex 5), was prepared and tested. By testing complexes 1 to 5 *in vitro*, a potent anti-*T. cruzi* activity was observed in the nitro/nitrosyl complexes (1 to 4), which was higher than that observed for benznidazole. In contrast, complex 5 did not show antiparasitic activity. Complex 3, the most potent compound, exhibited strong trypanocidal activity, through the release of NO, which subsequently induced the formation of vacuoles typical of the autophagy process. Moreover, complex 3 decreased blood parasitemia in *T. cruzi*-infected mice, strengthening the hypothesis that ruthenium complexes are promising drugs for Chagas disease therapy.

MATERIALS AND METHODS

Synthesis and drug dilution. Synthesis, structural characterization, and X-ray analysis of complexes 1 to 5 are described in the supplemental material. All complexes as well as the reference drugs were dissolved in dimethyl sulfoxide (DMSO) (Sigma-Aldrich, St. Louis, MO, USA) and then diluted in cell culture medium. The final concentration of DMSO was less than 1% in all *in vitro* experiments.

Animals. Female BALB/c mice (18 to 20 g) were maintained in sterilized cages under a controlled environment, receiving a rodent balanced diet and water *ad libitum* at Centro de Pesquisas Gonçalo Moniz (Fundação Oswaldo Cruz, Bahia, Brazil). All experiments were carried out in accordance with the recommendations of Ethical Issues Guidelines and were approved by the local Animal Ethics Committee (protocol number 002/2011).

Parasites. All experiments were performed with the Y strain of *T. cruzi*. The epimastigote form was maintained in axenic medium at 28°C, with weekly transfers into liver infusion tryptose (LIT) medium supplemented with 10% fetal bovine serum (FBS; Cultilab, Campinas, Brazil), 1% hemin (Sigma-Aldrich), 1% R9 medium (Sigma-Aldrich), and 50 μg/ml of gentamicin (Novafarma, Anápolis, Brazil). For *in vitro* assays, the metacyclic trypomastigote form of *T. cruzi* was obtained from the supernatant of infected LLC-MK2 cells and maintained in RPMI 1640 medium (Sigma-Aldrich) supplemented with 10% FBS (Cultilab, Campinas, Brazil) and 50 μg/ml of gentamicin (Novafarma, Anápolis, Brazil) at 37°C with 5% CO_2. For *in vivo* assays, bloodstream trypomastigotes were obtained from infected BALB/c mice at the peak of parasitemia.

Activity against epimastigotes. The effect of the treatment on epimastigotes proliferation was observed 5 days after incubation with the complexes at six concentrations. Epimastigote forms were resuspended at 5×10^6 cells/ml in supplemented LIT medium. The number of viable parasites was counted in a hemocytometer, and complex activity was expressed as 50% inhibitory concentration (IC_{50}), in comparison to untreated parasites. Each drug concentration was carried out in triplicate, and three independent experiments were performed. The reference drug, benznidazole (Lafepe, Pernambuco, Brazil), was used as the positive control.

Activity against trypomastigotes. Trypomastigotes were cultured in 96-well plates (2×10^6 cells/ml) in enriched RPMI 1640 medium, in the presence or absence of the complexes at different concentrations for 24 h. Viable parasites were counted in a hemocytometer, and complex activity was expressed as 50% effective concentration (EC_{50}), in comparison to untreated parasites. Each drug concentration was carried out in triplicate, and three independent experiments were performed. The reference drug, benznidazole, was used as the positive control. For *in vitro* drug combinations, doubling dilutions of each drug (ruthenium complex 3 and benznidazole) used alone or in fixed combinations were incubated with 2×10^6 cells/ml trypomastigotes for 24 h. The analysis of the combined effects was performed by calculating the median effect principle using CompuSyn software.

Host cell toxicity. Five days after 3% sodium thioglycolate injection (Sigma-Aldrich), macrophages were obtained by washing with saline solution in the peritoneal cavity of BALB/c mice. Macrophages in RPMI 1640 medium supplemented with 10% FBS were seeded on 96-well plates at 5×10^5 cells/ml and treated with the complexes for 6 h or 24 h of incubation time. Following this, cells were washed with phosphate-buffered saline (PBS) twice, and cell viability was determined by alamarBlue assay (Invitrogen, Carlsbad, CA, USA) according to the manufacturer's instructions. Colorimetric readings were performed after 10 h at 570 and 600 nm. Fifty-percent cytotoxic concentration (CC_{50}) values were calculated using data points gathered from three independent experiments.

***In vitro T. cruzi* infection assay.** Peritoneal macrophages stimulated with 3% sodium thioglycolate (Sigma-Aldrich) were transferred to 24-well plates at 2×10^5 cells/well in supplemented RPMI 1640 medium and maintained overnight at 37°C with 5% CO_2. The cultures were washed with saline solution and infected with trypomastigotes (10 parasites:1 host cell). Following 2 h of incubation, the noninternalized parasites were removed by washing with saline solution, and fresh medium, with or without drugs (25, 10, 5, and 1.0 μM), was added to the cultures and incubated for 6 h. Afterward, the culture was washed with saline, and drug-free medium was added and incubated for 4 days. Cells were fixed in absolute ethanol, stained with hematoxylin and eosin, and analyzed in an optical microscope (Olympus, Tokyo, Japan). The percentage of infected macrophages and the percentage of intracellular parasites per 100 macrophages were determined and compared to the negative control. The IC_{50} of proliferation inhibition of amastigotes was calculated using the number of parasites/100 cells. The reference drug, benznidazole, was used as the positive control. Each drug concentration was carried out in triplicate, and three independent experiments were performed.

Cruzain inhibition. Recombinant cruzain was activated in acetate buffer (0.1 M; pH 5.5) containing 5.5 mM dithiothreitol (DTT) (Invitrogen), and the protein concentration was adjusted to a final concentration of 0.1 μM. Protein was incubated in phosphate buffer containing 0.01% Triton 100 and transferred to a 96-well plate. Following complex addition, the plate was incubated for 10 min at 35°C. A solution containing the Z-FR-AMC (Sigma-Aldrich) protease substrate was then added, incubated for 10 min, and read using the EnVision multilabel reader (PerkinElmer, Connecticut, USA). The percentage of cruzain inhibition was calculated by using the following equation: $100 - (A1/A \times 100)$, where A1 represents the cruzain relative fluorescence units (RFU) in the presence of the test inhibitor and A refers to the control RFU (cruzain and substrate only). IC_{50}s of cruzain activity inhibition were also calculated. (2*S*,3*S*)-*trans*-Epoxysuccinyl-L-leucylamido-3-methylbutane (E-64c) (Sigma-Aldrich) was used as the reference cruzain inhibitor. Each drug concentration was carried out in triplicate, and two independent experiments were performed.

Nitric oxide production. Peritoneal macrophages stimulated with 3% sodium thioglycolate (10^6 cells/well) were incubated in a 24-well plate and infected with trypomastigotes (10^6 parasites/well) for 2 h. This experiment was also performed using J774 macrophages at 10^6 cells/well, which were incubated in a 24-well plate and infected with trypomastigotes (2×10^5 parasites/well) for 3 h. Cells were washed with saline solution and treated with complex 3 or 5 at a concentration of 10 μM for 24 h. For the positive control, cells were stimulated with 5.0 ng/ml of gamma interferon (IFN-γ; R&D Systems, Minneapolis, MN, USA) and 500 ng/ml of lipopolysaccharide (LPS; Sigma-Aldrich). Nitrite levels were determined 24 h after incubation using the Griess method (27).

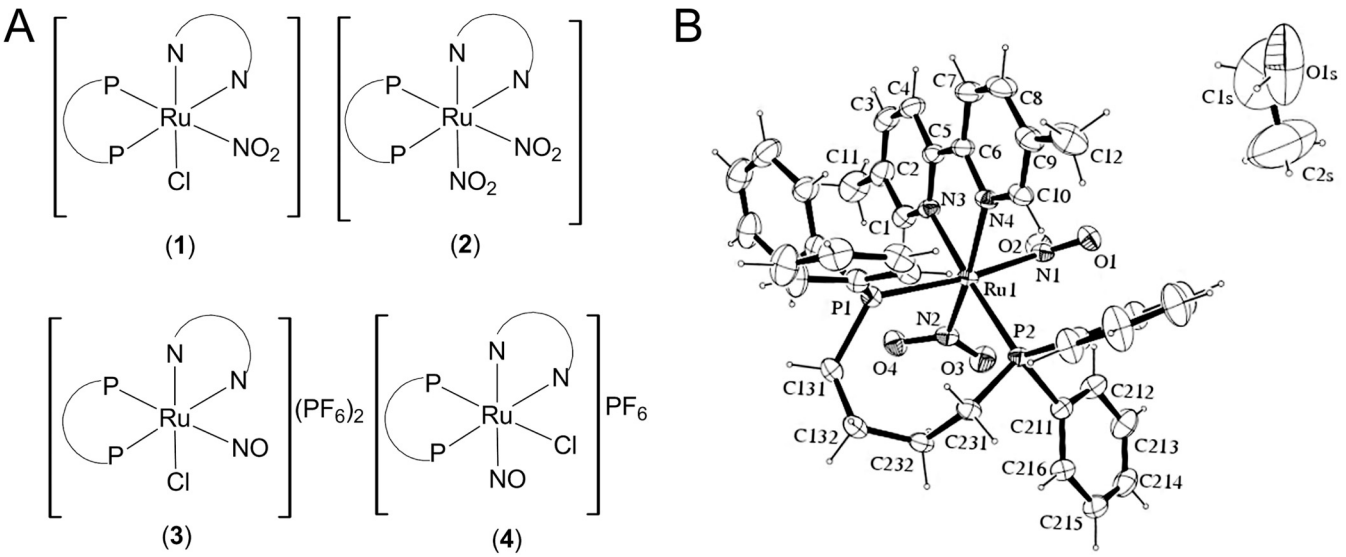

FIG 1 Ruthenium complexes 1 to 4. (A) Representation of the complexes: *cis*-[RuCl(NO_2)(dppb)(5,5-mebipy)] (1), *cis*-[Ru(NO_2)$_2$(dppb)(5,5-mebipy)] (2), *ct*-[RuCl(NO)(dppb)(5,5-mebipy)](PF_6)$_2$ (3), *cc*-[RuCl(NO)(dppb)(5,5-mebipy)](PF_6)$_2$ (4). N-N is 5,5′-dimethyl-2,2′-bipyridine (5,5′-mebipy), and P-P is 1,4-*bis*(diphenylphosphino)butane (dppb). (B) ORTEP-3 view of complex 2 and the atom numbering scheme. Ellipsoids are drawn at the 30% probability level.

Transmission and scanning electron microscopy analysis. Trypomastigotes (10^7 cells/ml) were treated with 2.1 μM complex 3 and incubated for 24 h at 37°C with 5% CO_2. Infected macrophages were treated with 2.1 μM complex 3 and incubated for 6 h. After incubation, parasites were fixed for 1 h at room temperature with 2% formaldehyde and 2.5% glutaraldehyde (Electron Microscopy Sciences, Hatfield, PA, USA) in sodium cacodylate buffer (0.1 M, pH 7.2). Fixed parasites were then washed 4 times with sodium cacodylate buffer (0.1 M, pH 7.2) and postfixed with a 1% solution of osmium tetroxide (Sigma-Aldrich). The cells were dehydrated in an ascending acetone series (30, 50, 70, 90, and 100%) and embedded in PolyBed resin (PolyScience Family, Warrington, PA, USA). Ultrathin sections were prepared on a Leica UC7 ultramicrotome and collected on 300-mesh copper grids, contrasted with uranyl acetate and lead citrate. Images were captured in a JEOL TEM-1230 transmission electron microscope. Alternatively, trypomastigotes were dried by using the critical-point method with CO_2, mounted on aluminum stubs, coated with a 20-nm-thick gold layer, and examined under a JEOL JSM-6390LV scanning electron microscope.

Monodansylcadaverine labeling. Trypomastigotes (10^7 cells/ml) were treated with complex 3 at a concentration of 2.1 μM. After incubation for 24 h, 0.05 mM monodansylcadaverine (MDC; Sigma-Aldrich) was added and incubated for 15 min in the absence of light. For the positive control, cells were treated with 0.1 mg/ml of rapamycin (Sigma-Aldrich). The autophagy inhibitor wortmannin (Sigma-Aldrich) was used at 0.5 μM and added simultaneously with complex 3 to the cell culture. The parasites were washed twice with PBS and analyzed in an FV1000 confocal microscope (Olympus).

LC3B immunolocalization. Infected macrophages (as described above) were treated with complex 3 at a concentration of 2.1 μM. Following 6 h of incubation, cells were washed in PBS and fixed with 4% paraformaldehyde (Electron Microscopy Sciences) for 20 min, permeabilized with 0.2% Triton X-100 (Sigma-Aldrich) in PBS for 15 min at room temperature, and blocked with background blocker (Diagnostic BioSystem, Pleasanton, CA, USA). Cells were incubated overnight with rabbit polyclonal antibody against LC3B (Invitrogen) (1/100 dilution) diluted in 1% PBS-bovine serum albumin (BSA), rinsed, and incubated for 1 h at room temperature with Alexa Fluor 568-conjugated goat anti-rabbit IgG (Molecular Probes, Carlsbad, CA, USA) diluted to 1:400. Subsequently, cells were washed in PBS and mounting medium with 4′,6-diamidino-2-phenylindole (DAPI) (Vector Laboratories, Burlingame, CA, USA). Cells were analyzed by confocal microscopy (FV1000; Olympus).

Flow cytometry analysis. Trypomastigotes (10^7 cells/ml) were resuspended in supplemented RPMI 1640 medium and treated with complex 3 (2.1 or 5 μM) for 36 h at 37°C with 5% CO_2. Parasites were labeled with propidium iodide (PI) and annexin V using the annexin V-fluorescein isothiocyanate (FITC) apoptosis detection kit (Sigma-Aldrich) according to the manufacturer's instructions. The experiment was performed using a BD FACSCalibur flow cytometer (San Jose, CA, USA) by acquiring 10,000 events, and data were analyzed by BD CellQuest software (San Jose, CA, USA).

***In vivo* anti-*T. cruzi* activity.** Female BALB/c mice (18 to 20 g) were infected by intraperitoneal injection of 10^4 bloodstream trypomastigotes of the *T. cruzi* Y strain in a 100-μl solution per mouse. Only mice with positive blood parasitemia were included in the experiment. Each drug was solubilized in DMSO-saline (10:90 [vol/vol]) prior to administration. Mice were randomly divided into groups ($n = 6$ mice per group). Treatment was initiated within 5 days postinfection and given once per day orally by gavage for five consecutive days. Complex 3 doses were administered at 25 (26.6 mg/kg of body weight) or 75 μmol/kg (80 mg/kg), and benznidazole was given at 384 μmol/kg (100 mg/kg). According to recommendations (28, 29), the following parameters were evaluated: (i) microscopic parasitemia analysis at 5, 8, 10, and 12 days postinfection and (ii) animal survival 30 days postinfection. The percentage of parasitemia reduction was calculated as follows: [(average vehicle group − average treated group)/average vehicle group] × 100%. Two independent experiments were carried.

***In vivo* drug combinations.** The same *in vivo* protocol described above was performed. The four groups included were (i) vehicle DMSO-saline (10:90 [vol/vol]), (ii) complex 3 alone at 75 μmol/kg (80 mg/kg), (iii) benznidazole alone at 38 μmol/kg (10 mg/kg), and (iv) simultaneous treatment with complex 3 at 75 μmol/kg and benznidazole at 38 μmol/kg. Two independent experiments were performed.

Statistical analyses. Nonlinear regression analysis was used to calculate CC_{50}, EC_{50}, and IC_{50} values. The selectivity index (SI) was defined as the ratio of CC_{50} (macrophages) to IC_{50} (amastigote form). One-way analysis of variance (ANOVA) and Bonferroni multiple comparison tests were used to determine the statistical significance of group comparisons in the *in vitro* infection assay, and two-way ANOVA with Bonferroni

multiple comparison tests was used in the *in vivo* assay (parasitemia). Results were considered statistically significant when *P* values were <0.05. Analyses were performed using GraphPad Prism version 5.01 (Graph Pad Software, San Diego, CA, USA) and OriginPro version 8.5 (OriginLab, Northampton, MA, USA) (cruzain IC_{50}s only). Animal survival rates were analyzed with GraphPad Prism 1.5 (GraphPad Software). Combined drug analysis was calculated by using CompuSyn (ComboSyn, Inc., Paramus, NJ, USA).

RESULTS

Compound characterization. Figure 1A shows the structures of ruthenium complexes investigated here. Complex 1 is the prototype compound, since it was used as the basis for synthesis of all other compounds. The differences among the complexes are based on the presence or absence of the nitro/nitrosyl group or chlorine. Complex 1 has a nitro group and a chlorine ligand; complex 2 was formed by replacing the chlorine by a nitro group. Complexes 3 and 4 are nitrosyl species. The difference between complexes 3 and 4 is the NO position; in complex 3, the NO is *cis* to chlorine and *trans* to phosphorus atoms, whereas in complex 4, NO is *cis* to chlorine and *cis* to phosphorus atoms.

All complexes were subjected to chemical and spectroscopic analysis. The elemental composition (C, H, and N) of the complexes corresponded closely to the calculated values. The $^{31}P\{^1H\}$ nuclear magnetic resonance (NMR) spectra of complexes 1 to 4 exhibited a pair of doublets that indicated the magnetic inequivalence of the phosphorus atoms present in the dppb (30). The observed doublets showed chemical shifts different from those of the starting material *cis*-[$RuCl_2$(dppb)(5,5′-mebipy)], suggesting that the presence of the nitro or nitrosyl groups coordinated to the metal shifted the electron density of the phosphorus atoms from the dppb.

In the infrared (IR) spectrum of *cis*-[$RuCl(NO_2)$(dppb)(5,5′-mebipy)] (complex 1), there were strong bands at 1,349 cm^{-1} and 1,298 cm^{-1}, which can be assigned to $\nu_{as}NO_2$ and ν_sNO_2, respectively. For *cis*-[$Ru(NO_2)_2$(dppb)(5,5′-mebipy)] (complex 2), these bands were at 1,360 cm^{-1} and 1,310 cm^{-1} for $\nu_{as}NO_2$ and at 1,294 cm^{-1} and 1,269 cm^{-1} for ν_sNO_2. The presence of four bands for this complex indicates that nitro groups are nonequivalent, one being *trans* to the nitrogen of 5,5′-mebipy, while the other is *trans* to the phosphorus of dppb. The nitrosyl complexes *ct*-[RuCl(NO)(dppb)(5,5-mebipy)]$(PF_6)_2$ (complex 3) and *cc*-[RuCl(NO)(dppb)(5,5-mebipy)]$(PF_6)_2$ (complex 4) exhibited strong bands at 1,891 cm^{-1} and at 1,895 cm^{-1}, respectively, which were assigned to the NO^+ stretching (31). Nitro group can be bound to metal through either nitrogen or oxygen, which may produce geometric isomers (32). Complex 1 exhibits its ρ_wNO_2 band at 572 cm^{-1}, while complex 2 has two bands, at 566 and 610 cm^{-1}, suggesting that in both complexes the nitro group is bound to the ruthenium through the nitrogen atom (32, 33). In addition to IR, the electronic absorption spectra for all complexes were characterized by an intense high-energy band centered at about 300 nm, which can be assigned to an intraligand π–π^* transition. Also, these complexes exhibited low-energy bands in the range of 316 to 488 nm, which can be assigned to a metal-to-ligand charge transfer (MLCT) transition, Ru ($d\pi$) to ligand (π^*).

The crystal structure of complex 2 was solved by X-ray crystallography (Table 1), and its ORTEP view was prepared with ORTEP-3 for Windows (Fig. 1B). Selected bond lengths (Å) and angles (°) in the complex are listed in Table S1 in the supplemental material. Complex 2 exhibits a distorted octahedral geometry, and it crystallized in a triclinic system, space group *P*-1, with the metal center coordinated to two bidentate ligands and two NO_2 groups. The nitro groups are *cis*-positioned relative to each other and coordinated through the nitrogen atoms, as suggested by the IR data. From the data in Table S1, it can be seen that the Ru-$N_{(NO2)}$ [Ru-$N_{(NO2)}$ *trans* P] bond length is about 0.5 Å longer than the bond Rui-N(2) [Ru-$N_{(NO2)}$ *trans* $N_{(bipy)}$], which is consistent with the stronger *trans* effect of the phosphorus atoms, relative to the *trans* effect of the nitrogen atoms. Also, this difference explains the two bands for νNO_2 observed in the infrared spectrum of complex 2.

TABLE 1 Crystal data and structure refinement of complex 2

Characteristic	Value
Empirical formula	$[RuC_{42}H_{46}N_4O_5P_2]\cdot CH_3CH_2OH$
Formula wt	849.84
Temp (K)	293(2)
Wavelength (Å)	0.71073
Crystal system	Triclinic
Space group	*P*-1
Unit cell dimensions	
a (Å)	10.2261(7)
b (Å)	12.2153(5)
c (Å)	17.4217(10)
α (°)	74.904(2)
β (°)	74.660(3)
γ (°)	76.827(3)
Vol ($Å^3$)	1996.5(2)
Z	2
Density (calculated) (mg/m^3)	1.414
Absorption coefficient (mm^{-1})	0.522
F(000)	880
Crystal size (mm^3)	0.30 by 0.26 by 0.10
Theta range for data collection (°)	3.13 to 26.41
Index ranges	$-11 \leq h \leq 12$, $-15 \leq k \leq 15$, $-21 \leq l \leq 21$
No. of reflections collected	15,073
No. of independent reflections	8,129 [R(int) = 0.0217]
% completeness to theta = 25.00°	99.0
Absorption correction	Gaussian
Max and min transmission	0.950 and 0.847
Refinement method	Full-matrix least-squares on F^2
Computing	COLLECT, HKL Denzo and Scalepack, SHELXL-97, SHELXS-97[a]
Data/restraints/parameters	8,129/2/491
Goodness of fit on F^2	1.056
Final R index [$I > 2\sigma(I)$]	R1 = 0.0378, wR2 = 0.1010
R index (all data)	R1 = 0.0442, wR2 = 0.1045
Largest diff peak and hole (e $Å^{-3}$)	0.611 and −0.640

[a] Data collection, data processing, structure solution, and structure refinement, respectively.

Anti-*T. cruzi* activity and host cell cytotoxicity. Anti-*T. cruzi* activity was determined in epimastigotes and trypomastigotes of the Y strain, and results were expressed as IC_{50} and EC_{50}, respectively. Cell toxicity in BALB/c mice macrophages was performed under identical drug incubation times for antiparasitic assay in trypomastigotes (i.e., 24-h drug exposure) and expressed as CC_{50}. Benznidazole was used as the reference drug in these assays, and results are reported in Table 2. Benznidazole exhibited an IC_{50} of 10.7 ± 1.6 μM in epimastigote proliferation. Similarly, it was observed that ruthenium complexes 2, 3, and 4 greatly inhibited

TABLE 2 Antiparasitic activity, host cell cytotoxicity, and cruzain inhibition of ruthenium complexes 1 to 5[e]

Compound	*T. cruzi* Y strain			
	Epimastigote $IC_{50} \pm SEM$ (μM)[a]	Trypomastigote $EC_{50} \pm SEM$ (μM)[b]	Macrophage $CC_{50} \pm SEM$ (μM)[c]	Cruzain $IC_{50} \pm SD$ (μM)[d]
Complex 1	>100	8.4 ± 1.1	>100	30.2 ± 7.3
Complex 2	16.6 ± 0.6	2.9 ± 0.2	50.5 ± 0.1	>100
Complex 3	5.7 ± 0.6	2.1 ± 0.6	28.5 ± 2.0	14.4 ± 6.6
Complex 4	26.7 ± 2.0	5.9 ± 1.0	25.4 ± 0.1	0.4 ± 0.1
Complex 5	ND	>100	>100	59.8 ± 4.6
Bdz	10.7 ± 1.6	11.4 ± 1.0	>100	
E-64c				1.0 ± 0.8 nM

[a] Determined 5 days after incubation with complexes.
[b] Determined 24 h after incubation with complexes.
[c] Cell viability of BALB/c mouse macrophages determined 24 h after treatment.
[d] Cruzain activity was determined 10 min after incubation.
[e] Values were calculated using concentrations in triplicate, and two independent experiments were performed. IC_{50}, inhibitory concentration at 50%; EC_{50}, effective concentration at 50%; CC_{50}, cytotoxic concentration at 50%; ND, not determined owing to lack of activity; Bdz, benznidazole; E-64c, standard cruzain inhibitor.

epimastigotes. In contrast, complex 1 did not inhibit epimastigote proliferation. Complexes 1 to 4 decreased trypomastigote viability, with EC_{50}s lower than that of benznidazole. Complex 5, which lacks a nitro/nitrosyl group, did not exhibit antitrypomastigote activity, while complex 3 was the most active compound among them, with an EC_{50} of 2.1 ± 0.6 μM. Complexes 1 and 5 did not demonstrate cytotoxicity in macrophages following the drug exposure, and complex 2 displayed relatively low cytotoxicity. Complexes 3 and 4 had CC_{50} values of 28.5 ± 2.0 and 25.4 ± 0.1 μM, respectively.

Evaluation of cruzain inhibition. Due to the previous findings that ruthenium complexes inhibit cruzain, inhibitory activity was measured here for all five complexes in an assay based on competition with Z-Phe-Arg 7-amido-4-methylcoumarin hydrochloride (Z-FR-AMC). (2*S*,3*S*)-*trans*-Epoxysuccinyl-L-leucylamido-3-methylbutane (E-64c), which is a high-affinity cruzain inhibitor, was used as the reference inhibitor and displayed an IC_{50} of 1.0 ± 0.8 nM. As demonstrated in Table 2, complex 2 did not inhibit cruzain, while complexes 1 and 5 presented weak potency, with IC_{50}s as high as 30 μM. Complexes 3 and 4 showed stronger potency against cruzain, with IC_{50}s of 14.4 ± 6.6 and 0.4 ± 0.1 μM, respectively. Although complex 4 was the most potent ruthenium complex, it had lower potency than E-64c.

***In vitro* infection.** After observing that ruthenium complexes inhibit the extracellular parasite, we investigated their activity against the intracellular parasite. It was observed that all the nitro/nitrosyl complexes at 10 μM caused a statistically significant reduction in the percentage of *T. cruzi*-infected macrophages compared to untreated infected cells (Fig. 2A). Complex 3 was the most potent of the four compounds tested in reducing the *in vitro* infection. Additionally, all the complexes decreased the mean number of intracellular parasites (Fig. 2B) as well as the parasite burden (Fig. 2C). Amastigote IC_{50} was calculated by analyzing the percentage of infected cells (Table 3). Ruthenium complex 3 greatly inhibited this percentage, displaying an IC_{50} of 1.3 ± 0.2 μM, while benznidazole displayed an IC_{50} of 14.0 ± 0.3 μM. Cytotoxicity of ruthenium complexes incubated for 6 h in macrophages demonstrated that neither benznidazole nor complex 1 are cytotoxic at the tested concentrations (CC_{50}s of >100 μM). Complex 2 exhibited a low cytotoxicity (CC_{50} = 93.1 ± 7.7 μM), and complexes 3 and 4 were approximately 2-fold more cytotoxic than

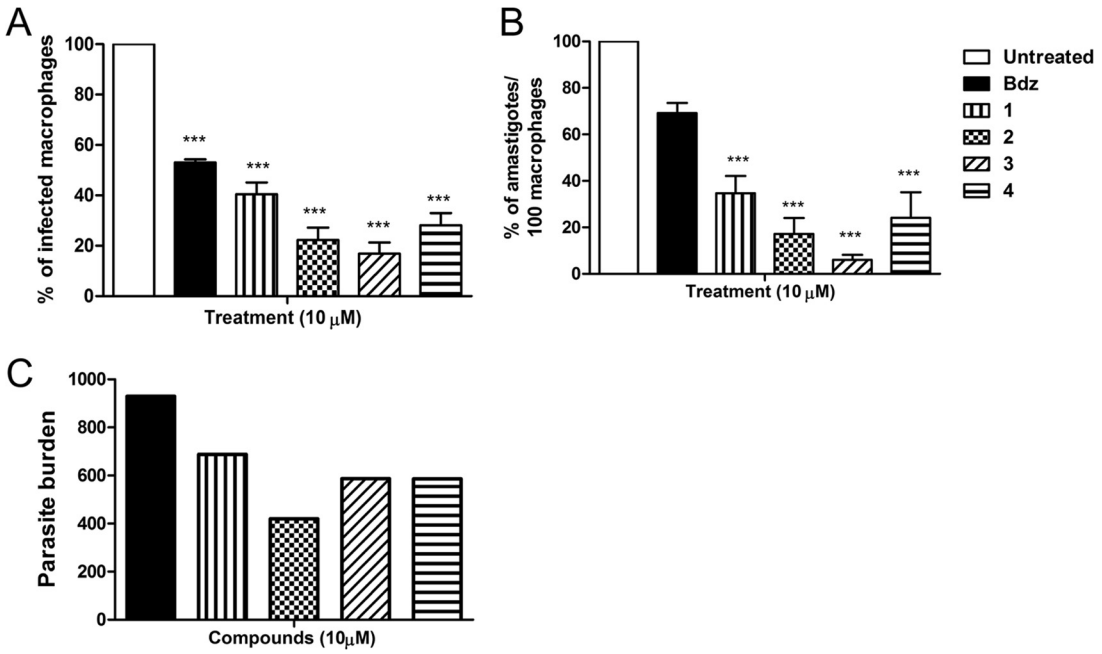

FIG 2 Ruthenium complexes reduce the *in vitro* infection. (A) Percentage of infection in comparison to untreated infected cells; (B) percentage of amastigotes/100 macrophages in comparison to untreated controls; (C) parasite burden, calculated as the percentage of infected cells × the mean number of amastigotes. Infected macrophages were treated for 6 h and then incubated for 4 days. Three independent experiments were performed. Error bars represent the standard errors of the means. ***, $P < 0.0001$ compared to untreated controls.

TABLE 3 Antiparasitic activity in intracellular parasite, host cell cytotoxicity, and selectivity index of ruthenium complexes 1 to 5[d]

Compound	Amastigote IC_{50} ± SEM (μM)[a]	Macrophage CC_{50} ± SEM (μM)[b]	SI[c]
Complex 1	4.2 ± 1.6	>100	>24
Complex 2	2.6 ± 0.7	93.1 ± 7.7	36
Complex 3	1.3 ± 0.2	51.4 ± 0.2	40
Complex 4	2.7 ± 0.6	38.3 ± 2.3	14
Complex 5	ND	>100	ND
Bdz	14.0 ± 0.3	>100	>7

[a] Cells were exposed to complexes for 6 h, and activity was determined 4 days after incubation with complexes.
[b] Cell viability of BALB/c mouse macrophages determined 6 h after treatment.
[c] SI is selectivity index, calculated by the ratio of CC_{50} (macrophages) to IC_{50} (amastigotes).
[d] IC_{50} and CC_{50} values were calculated using concentrations in triplicate, and two independent experiments were performed. IC_{50}, inhibitory concentration at 50%; CC_{50}, cytotoxic concentration at 50%; ND, not determined owing to lack of activity; Bdz, benznidazole.

nitro complex 2. The selectivity index (SI) of the ruthenium complexes was calculated, and it was observed that, among the complexes tested, complex 3 showed the highest SI.

NO level in infected cells. Complex 3 was the most potent and selective antiparasitic ruthenium complex. To investigate whether complex 3 is an NO donor drug, NO levels in infected macrophages were inferred by determining nitrite content. In this assay, infected cells were incubated for 24 h with drugs, and the nitrite content was estimated by the Griess method. As shown in Fig. 3A, untreated infected BALB/c macrophages produced low levels of NO, whereas stimulus with IFN-γ and LPS induced a significant production of NO. In comparison to untreated infected cells, treatment with 10 μM complex 3 presented a significantly elevation in NO ($P < 0.001$). In contrast, treatment with complex 5 did not result in significant production of NO. No measurable NO concentration was observed in a cell-free experiment containing only complex 3 plus culture medium (data not shown). The same conditions were used in infected J774 cell lines, and similar results were observed (Fig. 3B).

Electron microscopy analysis. Trypomastigotes were treated with complex 3 and analyzed by scanning electron microscopy (SEM). In comparison with untreated parasites (Fig. 4A), treatment resulted in parasite shrinkage and caused cell membrane discontinuity and fragmentation (Fig. 4B). Morphological changes following complex 3 treatment were observed in 76% of the parasite cells. Among these cells, 74% showed cell shrinkage, 21% displayed membrane discontinuity, and 21% had membrane fragmentation (data not shown). Next, transmission electron microscopy (TEM) experiments were performed in trypomastigotes and intracellular amastigotes. In comparison with untreated trypomastigotes (Fig. 4C), parasites in the presence of complex 3 exhibited swollen mitochondria (Fig. 4D) and loss of the nuclear membrane (Fig. 4E). In most of the treated trypomastigotes, the presence of atypical cytoplasmic vacuoles and the formation of myelin-like structures (Fig. 4F) were observed. The presence of these atypical cytoplasmic vacuoles was also observed in intracellular amastigotes following treatment with the ruthenium complex (Fig. 4H).

Autophagy markers. The observations by transmission micrographs that ruthenium complex induces the formation of atypical cytoplasmic vacuoles led us to investigate whether the mechanism of action involves autophagy. Trypomastigotes were treated with the complex 3 and then incubated with monodansylcadaverine (MDC) to label the autophagic cytosolic vacuoles. In this experiment, untreated parasites were not stained with MDC (Fig. 5A), while parasites treated with rapamycin, a standard autophagy inducer, were stained (Fig. 5B). Parasites treated with complex 3 were positively stained with MDC (Fig. 5C). In order to distinguish between autophagic and lysosomal vacuoles, an additional experiment was carried out using the autophagy inhibitor wortmannin. MDC staining during complex 3 treatment was blocked in the presence of 0.5 μM wortmannin (data not shown). The presence of microtubule-associated protein 1b light chain 3 (LC3B) was detected in untreated and treated *T. cruzi*-infected macrophages by incubating with anti-LC3B polyclonal antibody. In this controlled experiment, nuclei were stained with 4′,6-diamidino-2-phenylindole (DAPI), and cells were analyzed by immunofluorescence under a confocal microscope. Untreated infected macrophages did not demonstrate LC3B labeling (Fig. 5A). In contrast, infected macrophages treated with 0.1 mg/ml rapamycin displayed intracellular parasites labeled for LC3B (Fig. 5B). Similarly, infected macrophages treated with ruthenium complex 3 at 2.1 μM displayed intracellular parasites labeled for LC3B (Fig. 5C).

Parasite cell death. After observing that ruthenium complexes induce autophagy, we wanted to know the consequence of au-

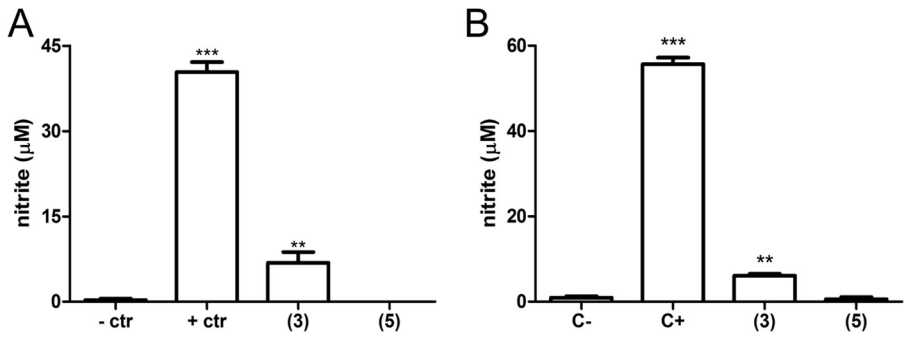

FIG 3 Ruthenium complex 3 increases NO in infected macrophages. Nitrite levels in infected macrophages determined 24 h after treatment. BALB/c peritoneal (A) and J774 (B) macrophages were infected with trypomastigotes and treated with 10 μM of complexes 3 and 5. A positive-control culture (+ctr) was stimulated with IFN-γ and LPS. The negative-control culture (−ctr) received no treatment or stimulus. Nitrite contents in the supernatant were estimated by the Griess nitrite test 24 h later. Values represent the means ± SEM from three independent experiments. ***, $P < 0.0001$ compared to negative control; **, $P < 0.001$ compared to −ctr.

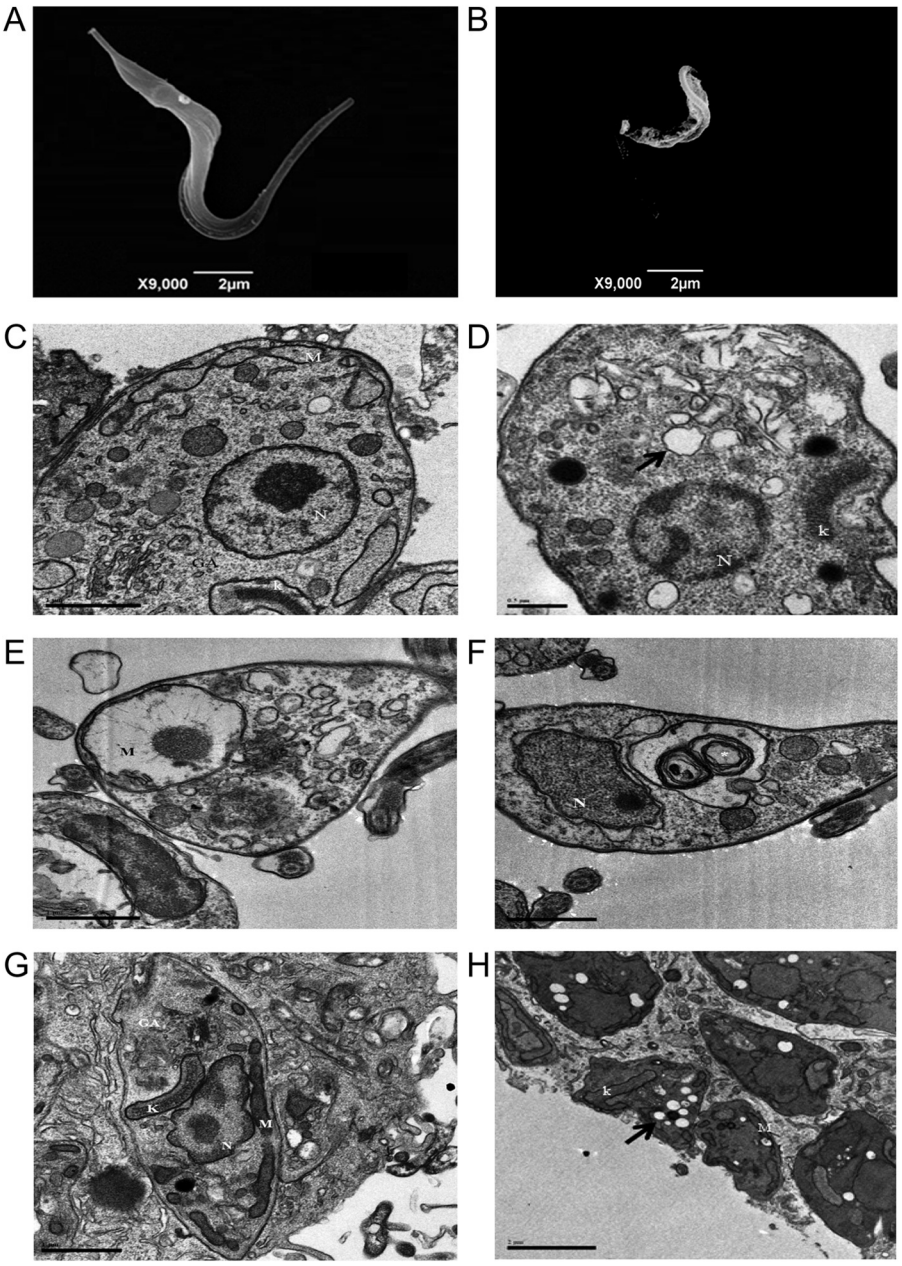

FIG 4 Ruthenium complex 3 causes irreversible morphological impairments to the parasite. Scanning electron micrograph in panel A shows untreated trypomastigote, and panel B shows treated parasite. Transmission electron micrographs in panels C to F are trypomastigotes and in panels G and H are infected macrophages. Panel C shows untreated trypomastigotes, panels D to F are treated parasites. Arrow in panel D indicates cytoplasmic vacuoles; arrow in panel E indicates mitochondrial swelling; arrow and asterisk in panel F indicate nuclear membrane disruption and myelin-like figures, respectively. Panel G shows untreated infected cells, while panel H shows treated infected cells. Arrow in panel H indicates cytoplasmic vacuoles. Complex 3 was added at 2.1 μM and incubated for 24 h in trypomastigotes and 6 h in infected macrophages. GA, Golgi apparatus; K, kinetoplast; N, nucleus; M, mitochondria.

tophagy to the parasite cells. To this end, trypomastigotes were incubated with two different concentrations (2.5 and 5.0 μM) of complex 3 for 36 h at 37°C and then double labeled with annexin V-fluorescein isothiocyanate (FITC) and propidium iodide (PI). Individual cell data were acquired and analyzed by flow cytometry. In comparison to untreated parasites (Fig. 6A), a concentration-related increase in the percentage of stained parasites was observed after complex 3 treatment (Fig. 6B and C). Parasites treated with complex 3 at 5.0 μM showed 34.6% positively stained cells, of which 26.1% were necrotic (PI stain alone), 5.6% were late apoptotic (PI-annexin V), and 2.9% were early apoptotic (annexin staining alone). As shown in Fig. 6D, this ruthenium complex significantly increased the proportion of necrotic *T. cruzi* cells in a concentration-dependent manner.

***In vivo* efficacy study.** Complex 3 was tested in *T. cruzi*-infected mice during the acute phase. Control groups, receiving either benznidazole or vehicle, were included in this experiment. In this assay, 10^4 Y strain trypomastigotes in a 100-μl solution were

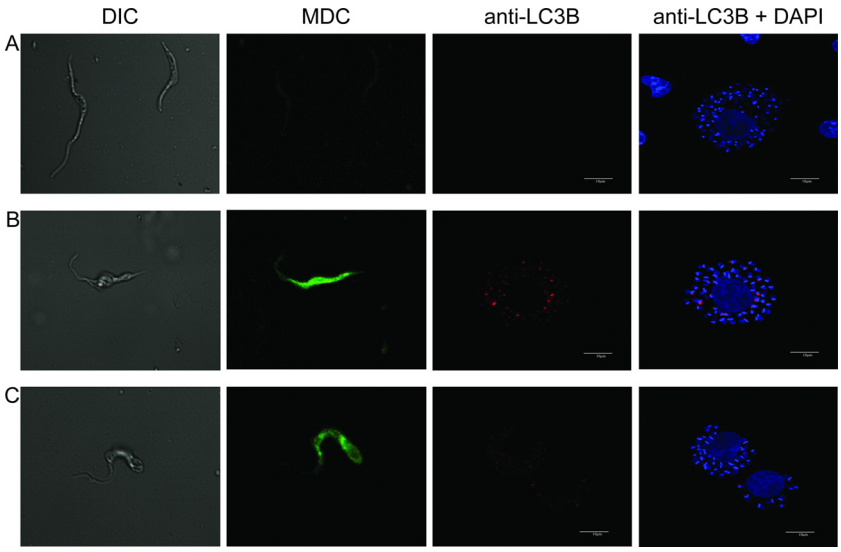

FIG 5 Ruthenium complex 3 induces parasite autophagy. Panel A shows untreated parasites, panel B shows treatment with 0.1 mg/ml rapamycin, and panel C is treatment with 2.1 μM ruthenium complex 3. Axenic trypomastigotes were incubated for 24 h and stained with MDC, and infected macrophages were incubated for 6 h and then stained with anti-LC3B antibody and DAPI. Images were captured using a confocal microscope with a 60× oil-immersion objective at ×3 zoom. DIC, differential interference contrast.

intraperitoneally inoculated in female BALB/c mice (n = 6/group). Treatments were given orally by gavage. Blood parasitemia and survival rates were analyzed. Complex 3 at 25 and 75 μmol/kg was able to decrease the blood parasitemia peak by 25% ($P < 0.001$) and 46% ($P < 0.001$), respectively (Fig. 7A), in comparison to the blood parasitemia in the untreated group. On day 12 postinfection, no parasites were detected by microscopic examination in benznidazole group blood samples, indicating negative parasitemia. But the same was not observed for infected mice receiving 75 μmol/kg of complex 3. Mice mortality rates were monitored up to 30 days postinfection. Complex 3 at 75 μmol/kg significantly decreased mortality compared to that of the untreated group (log rank, $P < 0.01$). The group treated with benznidazole had 100% survival, while the group treated with the highest dose of complex 3 showed a survival rate of 50% (Fig. 7B).

Drug combination. Considering that complex 3 and benznidazole exhibit different mechanism of antiparasitic actions, the possibility of drug combination was studied. Complex 3 and benznidazole alone or in fixed combinations were evaluated against trypomastigote cell cultures, and results were analyzed by CompuSyn software and listed in Table 4. In comparison to individual drug incubation, the combination of complex 3 and benznidazole reduced both EC_{50} and EC_{90} values. Combination index (CI) calculations were used as cutoffs and revealed that this combination has synergistic effects against trypomastigotes. It was observed that drug combinations at the EC_{50}s reduced the percentage of viable trypomastigotes (Fig. 7C) but did not reduce the percentage of viable macrophages (Fig. 7D). Of note, macrophage cytotoxicity was observed when drug combinations were evaluated in concentrations equal or higher than the EC_{90} values.

Based on the *in vitro* synergism, we evaluated the efficacy of ruthenium complex 3 in combination with a suboptimal dose of benznidazole. Complex 3 at 75 μmol/kg (80 mg/kg) and benznidazole at 38 μmol/kg (10 mg/kg) were administered individually or in combination using the *in vivo* protocol described above. Benznidazole at this suboptimal dose reduced blood parasitemia compared to that of the untreated group but did not eliminate circulating parasites. The group receiving the drug combination presented lower parasitemia than the untreated group and groups receiving each individual drug (Fig. 7E). When monitored for up to 30 days postinfection, the group treated with drug combination had 100% survival, while the groups treated with each drug alone showed a survival rate of 60% (Fig. 7F).

DISCUSSION

Identification of new pharmaceuticals is vital for Chagas disease treatment. In order to reach this objective, investigations cannot be limited to small organic molecules but should also include metallic compounds. In fact, coordination complexes and organometallics are recognized as notable anti-*T. cruzi* agents. For instance, the coordination of trypanocidal molecules with metals increases anti-*T. cruzi* activity in comparison with the metal-free molecules. This enhanced activity can be explained by the gain in lipophilicity. This strategy has been performed to enhance the potency of ketoconazole, clotrimazole, benznidazole, risedronate, and quinolones (34–39). Alternatively, metal complexes which are composed of ligands with unique chemical properties (redox and electrochemical behavior based on ligand reductions) exhibit anti-*T. cruzi* properties, possibly due to parasite membrane accumulation, in addition to effects on DNA and enzymes (40–43).

Here, the *in vitro* screening of anti-*T. cruzi* activity demonstrated that both nitro and nitrosyl ruthenium complexes are toxic for trypomastigotes and inhibited epimastigote proliferation at noncytotoxic concentrations in host cells. In contrast, the ruthenium complex lacking nitro and nitrosyl groups did not display anti-*T. cruzi* activity. Regarding structure-activity relationships, the complex containing two nitro groups was more potent than the complex containing only one. However, the nitrosyl complexes showed greater activity than nitro complexes. This suggests that a nitrosyl group contributes more to antiparasitic activity

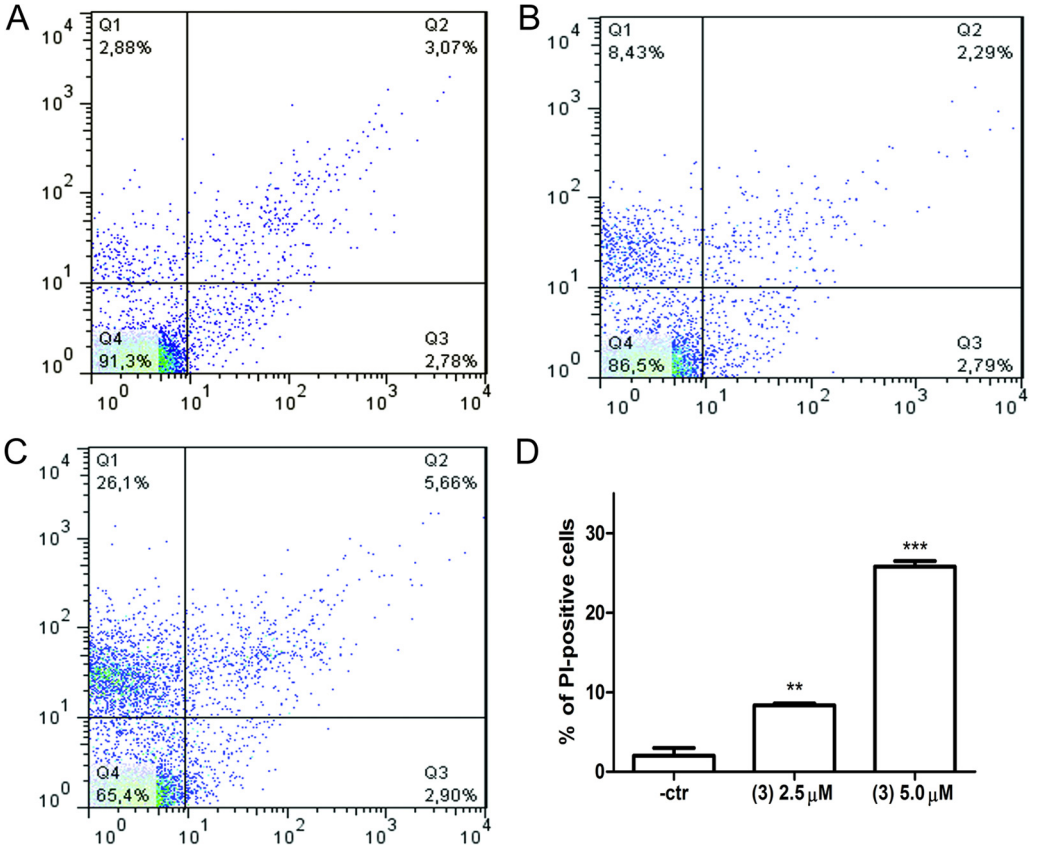

FIG 6 Ruthenium-based treatment causes parasite death by inducing necrosis. Trypomastigotes were treated with complex 3 for 36 h. Parasites were examined by flow cytometry with annexin V and PI staining. Cells plotted in each quadrant represent the following: lower left, double negative; upper left, PI single positive; lower right, annexin V single positive; upper right, PI and annexin V double positive. (A) Untreated; (B) complex 3 at 2.5 μM; (C) complex 3 at 5.0 μM; (D) percentage of PI-positive cells. Values are means ± SD from triplicate tests. −ctr, negative control. **, $P < 0.05$ compared to negative control (ANOVA); ***, $P < 0.0001$ compared to negative control (ANOVA).

than a nitro group. For cruzain, nitro complexes exhibited weak or no inhibitory activity, while nitrosyl complexes exhibited greater inhibitory activity. The nitrosyl complex 4 was only twice less potent as an antiparasitic than its isomer, complex 3, but it presented much higher potency against cruzain than complex 3. These observations indicate that the environment surrounding the metal is important for biological activity.

After determining that these ruthenium complexes inhibit extracellular *T. cruzi*, we examined their activity in infected macrophages. The complexes were able to reduce the number of infected cells more efficiently than benznidazole, and they clearly arrested parasite growth and differentiation inside the host cells. Given the potency of complex 3 against amastigotes, we investigated its mechanism of action in parasites. We observed that nitrosyl complex 3 increased the NO levels in infected macrophages, while the complex lacking the nitrosyl group did not. The antiparasitic activity of ruthenium complex 3 is likely due to its NO-releasing ability or alternatively by indirectly inducing NO production. According to the literature, NO release leads to the inactivation of the protease cruzain in parasite cells. However, complex 3 did not present potency as strong as the powerful cruzain inhibitor E-64c. Therefore, we believe that while complex 3 is an NO donor drug, this property is not related to its ability to inhibit cruzain. Further evidence regarding the mechanism of action of complex 3 was found by analyzing the parasite ultrastructure and morphology. Two main effects were observed in the treated parasites: first, cell membrane discontinuity and fragmentation and, to a lesser extent, nuclear membrane alterations; second, the appearance of atypical cytoplasmic vacuoles, as well as the formation of myelin-like figures.

Lack of cell membrane integrity is very often associated with necrotic parasite death (44). In fact, parasites treated with complex 3 exhibited a cell death pattern via necrosis rather than apoptosis. Our results are consistent with previous findings demonstrating that ruthenium bipyridyl complexes are prone to accumulate in the cell membrane (22). The presence of cytoplasmic vacuoles and myelin-like figures suggested that ruthenium complexes induce parasite autophagy. By assaying MDC staining and LC3B immunolocalization (45, 46), it was observed that trypomastigotes were stained with MDC after ruthenium complex treatment, and this process was blocked by the presence of the autophagy inhibitor wortmannin. Similar to the literature (47, 48), here, ruthenium complex treatment resulted in the accumulation of LC3B in intracellular amastigotes. The findings observed here support the overall idea that nitrosyl-ruthenium complexes release NO, which triggers cellular events, including parasite autophagy. As a result, a number of irreversible morphological im-

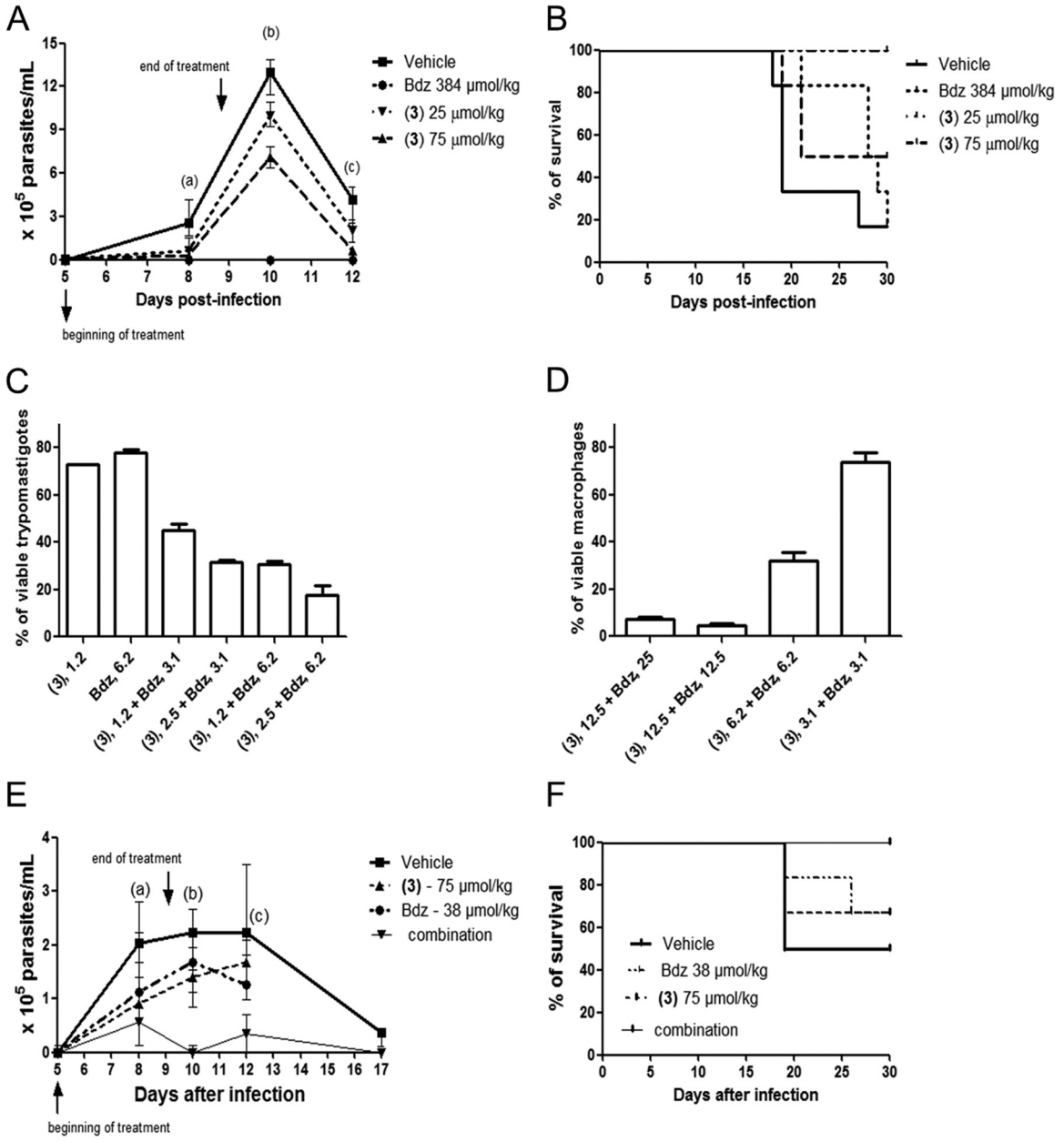

FIG 7 Ruthenium complex 3 reduces acute infection, and this is enhanced under drug combination with benznidazole. Parasitemia (A) and survival (B) of *T. cruzi*-infected mice ($n = 6$/group) orally treated once per day for 5 consecutive days with 25 μmol/kg (26.6 mg/kg) or 75 μmol/kg (80 mg/kg) of complex 3. Benznidazole (Bdz) was given at 384 μmol/kg (100 mg/kg). (A) Sets a, b, c, vehicle versus Bdz ($P < 0.001$), vehicle versus complex 3 at 25 μmol/kg ($P < 0.001$), vehicle versus complex 3 at 75 μmol/kg ($P < 0.001$), respectively. (B) Log rank analysis, vehicle versus complex 3 at 75 μmol/kg ($P < 0.01$), vehicle versus Bdz ($P < 0.001$). Percentage of viable trypomastigotes (C) and macrophages (D). Drug concentration is indicated on the *x* axis in μM, and cell viability was recorded 24 h after incubation. (E) Parasitemia and survival of infected mice ($n = 6$/group) orally treated once per day with a drug combination of complex 3 and benznidazole. (a) Vehicle versus complex 3 ($P < 0.001$), vehicle versus Bdz ($P < 0.01$), vehicle versus drug combination ($P < 0.001$); (b) vehicle versus complex 3 ($P < 0.05$), vehicle versus drug combination ($P < 0.001$); (c) vehicle versus complex 3 ($P < 0.05$), vehicle versus Bdz ($P < 0.001$), vehicle versus drug combination ($P < 0.001$). (F) Log rank analyses revealed curves are not significantly different.

pairments occur to the parasite cells, finally leading to cell death by necrosis.

Due to the strong antiparasitic activity of complex 3, it was evaluated in mice during the acute phase of Chagas disease. Complex 3 had a dose-dependent effect and presented an optimal efficacy when given orally at 75 μmol/kg. This reduced the blood parasitemia and increased mice survival; however, it did not eliminate parasites present in the bloodstream, while the benznidazole regime did. Given the substantial dedication to identifying optimal drug combinations for the treatment of Chagas disease (49, 50), a combination of ruthenium complex 3 and benznidazole would offer a potential therapy to reduce the benznidazole dosage required to cure infection. This is supported by the fact that combination would target *T. cruzi* at two different modes of action:

TABLE 4 Concentration reduction and combination indexes in trypomastigotes treated with ruthenium complex 3 and benznidazole[a]

Compound	EC_{50} ±SD (μM)		CRI at EC_{50}	EC_{90} ±SD (μM)		CRI at EC_{90}	CI at:	
	Alone	Combination		Alone	Combination		EC_{50}	EC_{90}
Complex 3	2.1 ± 0.6	0.8 ± 0.02	2.7 ± 0.2	4.9 ± 0.1	1.7 ± 0.02	2.6 ± 0.2	0.65 ± 0.03	0.56 ± 0.09
Bdz	11.4 ± 1.0	4.1 ± 0.1	3.5 ± 0.1	25.8 ± 0.8	8.7 ± 0.1	4 ± 0.8		

[a] EC_{50} and EC_{90} values were calculated using concentrations in duplicate, and two independent experiments were performed. Cutoff: CI value of 0.3 to 0.7, synergism; 0.7 to 0.85, moderate synergism; 0.85 to 0.9, slight synergism; 0.9 to 1.1, additivity; >1.1, antagonism. CRI, concentration reduction index; CI, combination index; Bdz, benznidazole.

NO release and autophagy induction mediated by complex 3 and nitroreductase inhibition and oxidative stress induction mediated by benznidazole (51, 52). *In vitro*, combinations of complex 3 and benznidazole were synergic in killing trypomastigotes. In infected mice, combination of ruthenium complex with a suboptimal dose of benznidazole exhibited enhanced efficacy in terms of reducing infection and increasing survival compared to each drug used alone. Overall, these findings indicate that ruthenium complexes are a class of suitable constituents for drug combination.

Conclusions. We investigated the NO donor drug strategy by synthesizing new ruthenium complexes that feature nitro or nitrosyl groups. These complexes exhibited a broad spectrum of activities (vector-borne stage, bloodstream form, intracellular stage) against *T. cruzi*. This activity is abolished once nitro and nitrosyl groups are removed from the complex, indicating these groups are structural determinants for activity. By examining the underlying mechanism of action of these complexes, it was observed that they release NO, causing autophagy, which is followed by a series of irreversible morphological impairments to the parasites, culminating in necrotic cell death. More striking, ruthenium-nitrosyl complex 3 was efficient in reducing blood parasitemia in acutely infected mice and presented synergic effects when in combination with benznidazole.

ACKNOWLEDGMENTS

This research was funded by CNPq, FAPESB, and FAPESP. A.A.B., J.E., and M.B.P.S. are recipients of a CNPq fellowship. T.M.B received a CAPES scholarship; C.S.M. and D.R.M.M. are receiving FAPESB scholarships.

We are thankful to Carine Azevedo for assistance with confocal microscopy, Adriano Alcantara for providing cruzain, and Marcos Vannier dos Santos for providing MDC and rapamycin. We are thankful to the electron microscopy unit of CPqGM.

We declare no competing financial interests.

T.M.B. designed and performed most experimental studies and analyses; M.I.F.B., J.W.D.C.J., and M.M.D.S. synthesized and validated the complexes; J.E. assisted with X-ray crystallography; C.S.M. assisted with the transmission electron microscopy analyses and cell culture; E.T.G. assisted with flow cytometry; D.R.M.M. provided guidance and assisted with experimental design and assisted with manuscript preparation; A.A.B. and M.B.P.S. initiated the project and provided guidance for experimental design, interpretation of data, and preparation of the manuscript. All authors have read and approved the final manuscript.

REFERENCES

1. **Schofield CJ, Jannin J, Salvatella R.** 2006. The future of Chagas disease control. Trends Parasitol. **12:**583–588. http://dx.doi.org/10.1016/j.pt.2006.09.011.
2. **Rodrigues Coura J.** 2013. Chagas disease: control, elimination and eradication. Is it possible? Mem. Inst. Oswaldo Cruz **108:**962–967. http://dx.doi.org/10.1590/0074-0276130565.
3. **Pinazo MJ, Muñoz J, Posada E, López-Chejade P, Gállego M, Ayala E, del Cacho E, Soy D, Gascon J.** 2010. Tolerance of benznidazole in treatment of Chagas' disease in adults. Antimicrob. Agents Chemother. **54:**4896–4899. http://dx.doi.org/10.1128/AAC.00537-10.
4. **Urbina JA.** 2010. Specific chemotherapy of Chagas disease: relevance, current limitations and new approaches. Acta Trop. **115:**55–68. http://dx.doi.org/10.1016/j.actatropica.2009.10.023.
5. **Moreira DRM, Leite ACL, dos Santos RR, Soares MBP.** 2009. Approaches for the development of new anti-*Trypanosoma cruzi* agents. Curr. Drug Targets **10:**212–231. http://dx.doi.org/10.2174/138945009787581140.
6. **Scharfstein J, Schechter M, Senna M, Peralta JM, Mendonça-Previato L, Miles MA.** 1986. *Trypanosoma cruzi*: characterization and isolation of a 57/51,000 m.w. surface glycoprotein (GP57/51) expressed by epimastigotes and bloodstream trypomastigotes. J. Immunol. **137:**1336–1341.
7. **Souto-Padrón T, Campetella OE, Cazzulo JJ, de Souza W.** 1990. Cysteine proteinase in *Trypanosoma cruzi*: immunocytochemical localization and involvement in parasite-host cell interaction. J. Cell Sci. **96:**485–490.
8. **McKerrow JH, Caffrey C, Kelly B, Loke P, Sajid M.** 2006. Proteases in parasitic diseases. Annu. Rev. Pathol. **1:**497–536. http://dx.doi.org/10.1146/annurev.pathol.1.110304.100151.
9. **Doyle PS, Zhou YM, Hsieh I, Greenbaum DC, McKerrow JH, Engel JC.** 2011. The *Trypanosoma cruzi* protease cruzain mediates immune evasion. PLoS Pathog. **7:**e1002139. http://dx.doi.org/10.1371/journal.ppat.1002139.
10. **Gazzinelli RT, Oswald IP, Hieny S, James SL, Sher A.** 1992. The microbicidal activity of interferon-gamma-treated macrophages against *Trypanosoma cruzi* involves an L-arginine-dependent, nitrogen oxide-mediated mechanism inhibitable by interleukin-10 and transforming growth factor-beta. Eur. J. Immunol. **22:**2501–2506. http://dx.doi.org/10.1002/eji.1830221006.
11. **Vespa GN, Cunha FQ, Silva JS.** 1994. Nitric oxide is involved in control of *Trypanosoma cruzi*-induced parasitemia and directly kills the parasite *in vitro*. Infect. Immun. **62:**5177–5182.
12. **Venturini G, Salvati L, Muolo M, Colasanti M, Gradoni L, Ascenzi P.** 2000. Nitric oxide inhibits cruzipain, the major papain-like cysteine proteinase from *Trypanosoma cruzi*. Biochem. Biophys. Res. Commun. **270:**437–441. http://dx.doi.org/10.1006/bbrc.2000.2447.
13. **Bocedi A, Dawood KF, Fabrini R, Federici G, Gradoni L, Pedersen JZ, Ricci G.** 2010. Trypanothione efficiently intercepts nitric oxide as a harmless iron complex in trypanosomatid parasites. FASEB J. **24:**1035–1042. http://dx.doi.org/10.1096/fj.09-146407.
14. **Tfouni E, Truzzi DR, Tavares A, Gomes AJ, Figueiredo LE, Franco DW.** 2012. Biological activity of ruthenium nitrosyl complexes. Nitric Oxide **26:**38–53. http://dx.doi.org/10.1016/j.niox.2011.11.005.
15. **Ascenzi P, Bocedi A, Gentile M, Visca P, Gradoni L.** 2004. Inactivation of parasite cysteine proteinases by the NO-donor 4-(phenylsulfonyl)-3-((2-(dimethylamino)ethyl)thio)-furoxan oxalate. Biochim. Biophys. Acta **1703:**69–77. http://dx.doi.org/10.1016/j.bbapap.2004.09.027.
16. **Silva JJ, Osakabe AL, Pavanelli WR, Silva JS, Franco DW.** 2007. *In vitro* and *in vivo* antiproliferative and trypanocidal activities of ruthenium NO donors. Br. J. Pharmacol. **152:**112–121. http://dx.doi.org/10.1038/sj.bjp.0707363.
17. **Silva JJ, Pavanelli WR, Pereira JC, Silva JS, Franco DW.** 2009. Experimental chemotherapy against *Trypanosoma cruzi* infection using ruthenium nitric oxide donors. Antimicrob. Agents Chemother. **53:**4414–4421. http://dx.doi.org/10.1128/AAC.00104-09.
18. **Guedes PM, Oliveira FS, Gutierrez FR, da Silva GK, Rodrigues GJ, Bendhack LM, Franco DW, Do Valle Matta MA, Zamboni DS, da Silva RS, Silva JS.** 2010. Nitric oxide donor *trans*-[RuCl([15]aneN)NO] as a possible therapeutic approach for Chagas' disease. Br. J. Pharmacol. **160:**270–282. http://dx.doi.org/10.1111/j.1476-5381.2009.00576.x.
19. **Silva JJ, Guedes PM, Zottis A, Balliano TL, Nascimento Silva FO, França Lopes LG, Ellena J, Oliva G, Andricopulo AD, Franco DW, Silva JS.** 2010. Novel ruthenium complexes as potential drugs for Chagas's disease: enzyme inhibition and *in vitro*/*in vivo* trypanocidal activity. Br. J. Pharmacol. **160:**260–269. http://dx.doi.org/10.1111/j.1476-5381.2009.00524.x.

20. **Levina A, Mitra A, Lay PA.** 2009. Recent developments in ruthenium anticancer drugs. Metallomics **1:**458–470. http://dx.doi.org/10.1039/b904071d http://dx.doi.org/10.1039/b904071d.
21. **Bergano A, Sava G.** 2011. Ruthenium anticancer compounds: myths and realities of the emerging metal-based drugs. Dalton Trans. **40:**7817–7823. http://dx.doi.org/10.1039/c0dt01816c.
22. **Zava O, Zakeeruddin SM, Danelon C, Vogel H, Grätzel M, Dyson PJ.** 2009. A cytotoxic ruthenium tris(bipyridyl) complex that accumulates at plasma membranes. ChemBioChem **10:**1796–1800. http://dx.doi.org/10.1002/cbic.200900013.
23. **Groessl M, Zava O, Dyson PJ.** 2011. Cellular uptake and subcellular distribution of ruthenium-based metallodrugs under clinical investigation versus cisplatin. Metallomics **3:**591–599. http://dx.doi.org/10.1039/c0mt00101e.
24. **Heinrich TA, Von Poelhsitz G, Reis RI, Castellano EE, Neves A, Lanznaster M, Machado SP, Batista AA, Costa-Neto CM.** 2011. A new nitrosyl ruthenium complex: synthesis, chemical characterization, *in vitro* and *in vivo* antitumor activities and probable mechanism of action. Eur. J. Med. Chem. **46:**3616–3622. http://dx.doi.org/10.1016/j.ejmech.2011.04.064.
25. **Pavan FR, Poelhsitz GV, Barbosa MI, Leite SR, Batista AA, Ellena J, Sato LS, Franzblau SG, Moreno V, Gambino D, Leite CQ.** 2011. Ruthenium(II) phosphine/diimine/picolinate complexes: inorganic compounds as agents against tuberculosis. Eur. J. Med. Chem. **46:**5099–50107. http://dx.doi.org/10.1016/j.ejmech.2011.08.023.
26. **Santos ER, Mondelli MA, Pozzi LV, Corrêa RS, Salistre-de-Araújo SS, Pavan FR, Leite CQF, Ellena J, Malta VRS, Machado SP, Batista AA.** 2013. New ruthenium(II)/phosphines/diimines complexes: promising antitumor (human breast cancer) and *Mycobacterium tuberculosis* fighting agents. Polyhedron **51:**292–297. http://dx.doi.org/10.1016/j.poly.2013.01.004.
27. **Green LC, Wagner DA, Glogowski J, Skipper PL, Wishnok JS, Tannenbaum SR.** 1982. Analysis of nitrate, nitrite, and [^{15}N]nitrate in biological fluids. Anal. Biochem. **126:**131–138.
28. **Brener Z.** 1962. Therapeutic activity and criterion of cure on mice experimentally infected with *Trypanosoma cruzi*. Rev. Inst. Med. Trop. Sao Paulo **4:**386–396.
29. **Romanha AJ, Castro SL, Soeiro MN, Lannes-Vieira J, Ribeiro I, Talvani A, Bourdin B, Blum B, Olivieri B, Zani C, Spadafora C, Chiari E, Chatelain E, Chaves G, Calzada JE, Bustamante JM, Freitas-Junior LH, Romero LI, Bahia MT, Lotrowska M, Soares MBP, Andrade SG, Armstrong T, Degrave W, Andrade ZA.** 2010. *In vitro* and *in vivo* experimental models for drug screening and development for Chagas disease. Mem. Inst. Oswaldo Cruz **105:**233–238. http://dx.doi.org/10.1590/S0074-02762010000200022.
30. **Barbosa MIF, Corrêa RS, Oliveira KM, Rodrigues C, Ellena J, Nascimento OR, Rocha VPC, Nonato FR, Macedo TS, Barbosa-Filho JM, Soares MBP, Batista AA.** 2014. Antiparasitic activities of novel ruthenium/lapachol complexes. J. Inorg. Biochem. **136:**33–39. http://dx.doi.org/10.1016/j.jinorgbio.2014.03.009.
31. **Richter-Addo GB, Legzdins P.** 1992. Metal nitrosyls, p 383. Oxford University Press, New York, NY.
32. **Godwin JB, Meyer TJ.** 1971. Nitrosyl-nitrite, interconversion in ruthenium complexes. Inorg. Chem. **10:**2150–2153. http://dx.doi.org/10.1021/ic50104a012.
33. **Nakamoto K.** 1997. Infrared and Raman spectra of inorganic and coordination compounds, p 384, 5th ed, part B. Wiley-Interscience, New York, NY.
34. **Navarro M, Cisneros-Fajardo EJ, Lehmann T, Sánchez-Delgado RA, Atencio R, Silva P, Lira R, Urbina JA.** 2001. Toward a novel metal-based chemotherapy against tropical diseases. 6. Synthesis and characterization of new copper(II) and gold(I) clotrimazole and ketoconazole complexes and evaluation of their activity against *Trypanosoma cruzi*. Inorg. Chem. **40:**6879–6884. http://dx.doi.org/10.1021/ic0103087.
35. **Nogueira Silva JJ, Pavanelli WR, Gutierrez FR, Alves Lima FC, Ferreira da Silva AB, Santana Silva J, Wagner Franco D.** 2007. Complexation of the anti-*Trypanosoma cruzi* drug benznidazole improves solubility and efficacy. J. Med. Chem. **51:**4104–4114. http://dx.doi.org/10.1021/jm701306r.
36. **Demoro B, Caruso F, Rossi M, Benítez D, Gonzalez M, Cerecetto H, Parajón-Costa B, Castiglioni J, Galizzi M, Docampo R, Otero L, Gambino D.** 2010. Risedronate metal complexes potentially active against Chagas disease. J. Inorg. Biochem. **104:**1252–1258. http://dx.doi.org/10.1016/j.jinorgbio.2010.08.004.
37. **Reis DC, Pinto MC, Souza-Fagundes EM, Rocha LF, Pereira VR, Melo CM, Beraldo H.** 2011. Investigation on the pharmacological profile of antimony(III) complexes with hydroxyquinoline derivatives: antitrypanosomal activity and cytotoxicity against human leukemia cell lines. Biometals **24:**595–601. http://dx.doi.org/10.1007/s10534-011-9407-8.
38. **Martínez A, Carreon T, Iniguez E, Anzellotti A, Sánchez A, Tyan M, Sattler A, Herrera L, Maldonado RA, Sánchez-Delgado RA.** 2012. Searching for new chemotherapies for tropical diseases: ruthenium-clotrimazole complexes display high *in vitro* activity against *Leishmania major* and *Trypanosoma cruzi* and low toxicity toward normal mammalian cells. J. Med. Chem. **55:**3867–3877. http://dx.doi.org/10.1021/jm300070h.
39. **Iniguez E, Sánchez A, Vasquez MA, Martínez A, Olivas J, Sattler A, Sánchez-Delgado RA, Maldonado RA.** 2013. Metal-drug synergy: new ruthenium(II) complexes of ketoconazole are highly active against *Leishmania major* and *Trypanosoma cruzi* and nontoxic to human or murine normal cells. J. Biol. Inorg. Chem. **18:**779–790. http://dx.doi.org/10.1007/s00775-013-1024-2.
40. **Lowe G, Droz AS, Vilaivan T, Weaver GW, Tweedale L, Pratt JM, Rock P, Yardley V, Croft SL.** 1999. Cytotoxicity of (2,2′:6′,2′-terpyridine)platinum(II) complexes to *Leishmania donovani*, *Trypanosoma cruzi*, and *Trypanosoma brucei*. J. Med. Chem. **42:**999–1006. http://dx.doi.org/10.1021/jm981074c.
41. **Vieites M, Smircich P, Parajón-Costa B, Rodríguez J, Galaz V, Olea-Azar C, Otero L, Aguirre G, Cerecetto H, González M, Gómez-Barrio A, Garat B, Gambino D.** 2008. Potent *in vitro* anti-*Trypanosoma cruzi* activity of pyridine-2-thiol *N*-oxide metal complexes having an inhibitory effect on parasite-specific fumarate reductase. J. Biol. Inorg. Chem. **13:**723–735. http://dx.doi.org/10.1007/s00775-008-0358-7.
42. **Donnici CL, Araujo MH, Oliveira HS, Moreira DRM, Pereira VRA, Souza MA, De-Castro MCAB, Leite ACL.** 2009. Ruthenium complexes endowed with potent anti-*Trypanosoma cruzi* activity: synthesis, biological characterization and structure–activity relationships. Bioorg. Med. Chem. **17:**5038–5043. http://dx.doi.org/10.1016/j.bmc.2009.05.071.
43. **Benítez J, Becco L, Correia I, Leal SM, Guiset H, Pessoa JC, Lorenzo J, Tanco S, Escobar P, Moreno V, Garat B, Gambino D.** 2011. Vanadium polypyridyl compounds as potential antiparasitic and antitumoral agents: new achievements. J. Inorg. Biochem. **105:**303–312. http://dx.doi.org/10.1016/j.jinorgbio.2010.11.001.
44. **Vannier-Santos MA, de Castro SL.** 2009. Electron microscopy in antiparasitic chemotherapy: a (close) view to a kill. Curr. Drug Targets **10:**246–260. http://dx.doi.org/10.2174/138945009787581168.
45. **Jimenez V, Paredes R, Sosa MA, Galanti N.** 2008. Natural programmed cell death in *T. cruzi* epimastigotes maintained in axenic cultures. J. Cell. Biochem. **105:**688–698. http://dx.doi.org/10.1002/jcb.21864.
46. **Veiga-Santos P, Barrias ES, Santos JF, de Barros-Moreira TL, de Carvalho TM, Urbina JA, de Souza W.** 2012. Effects of amiodarone and posaconazole on the growth and ultrastructure of *Trypanosoma cruzi*. Int. J. Antimicrob. Agents **40:**61–71. http://dx.doi.org/10.1016/j.ijantimicag.2012.03.009.
47. **Tan C, Lai S, Wu S, Hu S, Zhou L, Chen Y, Wang M, Zhu Y, Lian W, Peng W, Ji L, Xu A.** 2010. Nuclear permeable ruthenium(II) β-carboline complexes induce autophagy to antagonize mitochondrial-mediated apoptosis. J. Med. Chem. **53:**7613–7624. http://dx.doi.org/10.1021/jm1009296.
48. **Castonguay A, Doucet C, Juhas M, Maysinger D.** 2012. New ruthenium(II)-letrozole complexes as anticancer therapeutics. J. Med. Chem. **55:**8799–8806. http://dx.doi.org/10.1021/jm301103y.
49. **Cencig S, Coltel N, Truyens C, Carlier Y.** 2012. Evaluation of benznidazole treatment combined with nifurtimox, posaconazole or AmBisome in mice infected with *Trypanosoma cruzi* strains. Int. J. Antimicrob. Agents **40:**527–532. http://dx.doi.org/10.1016/j.ijantimicag.2012.08.002.
50. **Bustamante JM, Craft JM, Crowe BD, Ketchie SA, Tarleton RL.** 2014. New, combined, and reduced dosing treatment protocols cure *Trypanosoma cruzi* infection in mice. J. Infect. Dis. **209:**150–162. http://dx.doi.org/10.1093/infdis/jit420.
51. **Hall BS, Wilkinson SR.** 2012. Activation of benznidazole by trypanosomal type I nitroreductases results in glyoxal formation. Antimicrob. Agents Chemother. **56:**115–123. http://dx.doi.org/10.1128/AAC.05135-11.
52. **Rajão MA, Furtado C, Alves CL, Passos-Silva DG, de Moura MB, Schamber-Reis BL, Kunrath-Lima M, Zuma AA, Vieira-da-Rocha JP, Borio Ferreira Garcia J, Mendes IC, Junho Pena SD, Macedo AM, Franco GR, de Souza-Pinto NC, de Medeiros MH, Cruz AK, Machado Motta MC, Ribeiro Teixeira SM, Machado CR.** 2014. Unveiling benznidazole's mechanism of action through overexpression of DNA repair proteins in *Trypanosoma cruzi*. Environ. Mol. Mutagen. **55:**309–321. http://dx.doi.org/10.1002/em.21839.

European Journal of Medicinal Chemistry 101 (2015) 818–835

Contents lists available at ScienceDirect

European Journal of Medicinal Chemistry

journal homepage: http://www.elsevier.com/locate/ejmech

Research paper

Synthesis and structure–activity relationship study of a new series of antiparasitic aryloxyl thiosemicarbazones inhibiting *Trypanosoma cruzi* cruzain

José Wanderlan Pontes Espíndola [a], Marcos Veríssimo de Oliveira Cardoso [a], Gevanio Bezerra de Oliveira Filho [a], Dayane Albuquerque Oliveira e Silva [a], Diogo Rodrigo Magalhaes Moreira [b], Tanira Matutino Bastos [b], Carlos Alberto de Simone [c], Milena Botelho Pereira Soares [b, e], Filipe Silva Villela [d], Rafaela Salgado Ferreira [d], Maria Carolina Accioly Brelaz de Castro [f], Valéria Rego Alves Pereira [f], Silvane Maria Fonseca Murta [g], Policarpo Ademar Sales Junior [g], Alvaro José Romanha [g], Ana Cristina Lima Leite [a, *]

[a] Departamento de Ciências Farmacêuticas, Centro de Ciências da Saúde, Universidade Federal de Pernambuco, 50740-520, Recife, PE, Brazil
[b] Centro de Pesquisas Gonçalo Moniz, Fundação Oswaldo Cruz, 40296-750, Salvador, BA, Brazil
[c] Departamento de Física e Informática, Instituto de Física, Universidade de São Paulo, 13560-970, São Carlos, SP, Brazil
[d] Departamento de Bioquímica e Imunologia, Universidade Federal de Minas Gerais, 31270-901, Belo Horizonte, MG, Brazil
[e] Centro de Biotecnologia e Terapia Celular, Hospital São Rafael, 41253-190, Salvador, BA, Brazil
[f] Centro de Pesquisas Aggeu Magalhães, Fundação Oswaldo Cruz, 50670-420, Recife, PE, Brazil
[g] Laboratório de Parasitologia Celular e Molecular, Centro de Pesquisas René Rachou, Fundação Oswaldo Cruz, 30.190-002, Belo Horizonte, MG, Brazil

ARTICLE INFO

Article history:
Received 30 April 2015
Received in revised form
25 June 2015
Accepted 26 June 2015
Available online 3 July 2015

Keywords:
Chagas disease
Trypanosoma cruzi
Conformationally constrained analogs
Thiosemicarbazone
Cruzain
Necrosis

ABSTRACT

The discovery of new antiparasitic compounds against *Trypanosoma cruzi*, the etiological agent of Chagas disease, is necessary. Novel aryloxy/aryl thiosemicarbazone-based conformationally constrained analogs of thiosemicarbazones (**1**) and (**2**) were developed as potential inhibitors of the *T. cruzi* protease cruzain, using a rigidification strategy of the iminic bond of (**1**) and (**2**). A structure–activity relationship analysis was performed in substituents attached in both aryl and aryloxy rings. This study indicated that apolar substituents or halogen atom substitution at the aryl position improved cruzain inhibition and antiparasitic activity in comparison to unsubstituted thiosemicarbazone. Two of these compounds displayed potent inhibitory antiparasitic activity by inhibiting cruzain and consequently were able to reduce the parasite burden in infected cells and cause parasite cell death through necrosis. In conclusion, we demonstrated that conformational restriction is a valuable strategy in the development of antiparasitic thiosemicarbazones.

1. Introduction

Chagas disease, caused by *Trypanosoma cruzi*, represents a serious and alarming health problem [1]. It affects approximately 5–10% of the population of Latin America, but even after more than 100 years since its discovery, the specific treatment of *T. cruzi* remains uncertain [2,3]. Benznidazole, the drug of choice for the treatment of Chagas disease, is able to eliminate the parasite during the acute phase; however, it is poorly effective during the chronic phase, even after long-term administration, and it causes a high dropout rate during treatment due to side effects [4,5]. Human vaccination against *T. cruzi* infection is not available; thus, other therapies aiming to control infection or reduce clinical symptoms are being investigated [6–8].

Knowledge of molecular targets related to various parasite processes has significantly contributed to this investigation. Key enzymes, such as cysteine proteases, are among the preferred targets for the development of new drugs. The structural and

* Corresponding author.
E-mail address: acllb2003@yahoo.com (A.C.L. Leite).

http://dx.doi.org/10.1016/j.ejmech.2015.06.048
0223-5234/

functional biochemistry of cruzain, however, is by far the most studied of the proteases in *T. cruzi* infections [9]. Cruzain belongs to the family of cysteine proteases (papain-like enzymes known as clan CA) and is closely related to cathepsins L and S, which are also associated with other pathologies in humans [10]. This enzyme is involved in the invasion, differentiation and proliferation of parasites in host cells [11], and it is a useful molecular target for the rational design of anti-trypanosomal agents [12].

Regarding the identification of cruzain inhibitors, most of the efforts have been conducted through the investigation of peptides and peptide-like compounds, such as ureas [10,13], hydrazones [14–17], triazoles [18,19] and thiosemicarbazones [20–22]. Thiosemicarbazones were originally developed as potential inhibitors of cathepsin-L, one of the principal proteases involved in cancer cells [20]. However, based on the homology and similar biochemical properties between cathepsin-L and cruzain, thiosemicarbazones were investigated as a potential class of cruzain inhibitors. Later on, aryl thiosemicarbazones were found to be a class of anti-*T. cruzi* compounds that inhibit cruzain activity [21,22].

The general binding mode for aryl thiosemicarbazones with cruzain involves covalent binding of a thioamide group to a Cys25 amino acid, as well as the location of the aryl group within a deep hydrophobic pocket [22,23]. Based on this model, a number of molecular modifications have been investigated, including bis-thiosemicarbazones, heterocyclic-derived thiosemicarbazones, thiosemicarbazones containing bioreductive groups and metallic complexes [24–29].

Recently, our group evaluated the anti-*T. cruzi* activity of a series of aryl thiosemicarbazones obtained by a homologation strategy. This led to the identification of new potent anti-*T. cruzi* agents, such as compounds (**1**) and (**2**) (Fig. 1), which significantly inhibited the proliferation of epimastigotes (IC_{50} = 71.5 and 2.2 μM, respectively) and demonstrated toxicity to trypomastigotes (CC_{50} = 1.4 and 2.2 μM, respectively) but was not cytotoxic against spleen cells. In addition, these compounds induced *T. cruzi* cell death by an apoptotic process; however, they did not exhibit inhibitory activity for cruzain [30].

In parallel to thiosemicarbazones, our group observed that thiazolidinone **18** inhibits cruzain activity but not its homologous proteins in mammalian cells (cathepsin L) [31]. However, it was several times less potent than KB2, a high-efficient cruzain inhibitor [19]. A comparison of cruzain docking between thiazolidinone **18** and KB2 has revealed that the major difference is that KB2 assumes a T-shaped conformation. Therefore, thiazolidinones presenting a T-shape conformation displayed enhanced activity than thiazolidinone (**18**) family. Thus, our findings were suggestive that cruzain inhibitors displaying a conformation resembling a T-shape presented in KB2 compound warrant activity (Fig. 2).

Based on this, we sought that disrupting planarity and symmetry in aryl thiosemicarbazones (**1**) and (**2**) would lead to T-shape conformational compounds and potentially increase cruzain and antiparasitic activity. Among the chemical modifications to achieve this [32–34], we consider attaching an aryl group in the imine group which could change dihedral angles and twist the position of aryl rings, producing new conformationally constrained compounds (Fig. 3).

New aryl thiosemicarbazones (**8a–l**, **9a–t**) were synthesized and evaluated as anti-*T. cruzi* agents as well as cruzain inhibitors. First, compound **8a** was prepared, which contains a phenyl ring without a substituent attached to the iminic carbon, for the purpose of comparison with substituted derivatives **8b–h**. Thereafter, substituents attached to the phenyl ring were examined, such as alkyl, alkoxy, halogen atoms and phenyl rings, generating biphenyl and naphthyl groups. In addition, we investigated a wide range of substituents bonded to the phenoxyl ring (**9a–t**) to assess its functions in terms of electronic and steric contributions to anti-*T. cruzi* activity. We prepared 4-substituted phenyl derivatives, followed by the preparation of derivatives with one substituent in *meta*- or *ortho*-positions in the phenyl ring. Derivatives containing two substituents attached to the phenyl ring were synthesized, as well as the replacement of a phenyl by a naphthyl ring. Finally, aryl thiosemicarbazones were synthesized containing methyl or phenyl groups in *N*4 (**8i–l**). Evaluation of the anti-*T. cruzi* and cruzain activity for these compounds (**8a–l**, **9a–t**) led to the identification of important structure–activity relationships.

2. Results and discussion

2.1. Synthesis

Obtaining aryl thiosemicarbazones (**8a–l**, **9a–t**), as shown in Scheme 1, was performed in two steps from different phenols and halo-substituted acetophenones, both purchased commercially. Initially, various 1-phenoxy-2-acetophenones (**5a–h**; **6a–t**) were obtained from the O-alkylation of various phenols (**3a–t**) with 2-halo-acetophenones (**4a–h**) in a basic medium and temperature environment, similar to a protocol previously described [29]. After 3–4 h of reaction, 1-phenoxy-2-acetophenones compounds were obtained with yields varying from 77 to 95%. These intermediate compounds (**5a–h**; **6a–t**) were then reacted with some thiosemicarbazides (**7a–c**) and catalytic HCl in an ultrasound bath at room temperature [35]. After 2.5–3 h, thiosemicarbazones (**8a–l**, **9a–t**) precipitated in the reaction mixture and were collected by simple filtration. All thiosemicarbazones were recrystallized and obtained at an acceptable purity (>95%) in yields ranging from 69 to 90%. The structures were determined by ^{1}H and ^{13}C NMR, DEPT and IR.

In the ^{1}H NMR spectra of most compounds, it was possible to observe the presence of signals correspondent to the existence of isomers or rotamers. However, two signals for the methylene hydrogens had a chemical shift difference of approximately 0.3 ppm; in the case of rotamers, generally, two signals almost overlapped. These observations were thus suggestive of the formation of a mixture of stereoisomers (*Z*) and (*E*).

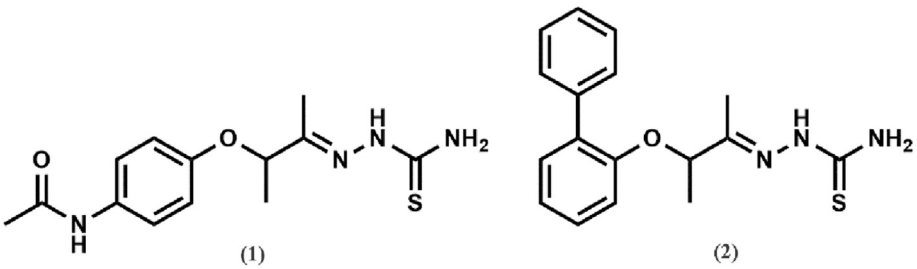

Fig. 1. Structure of thiosemicarbazones (**1**) and (**2**) previously identified as anti-*T. cruzi* agents [30].

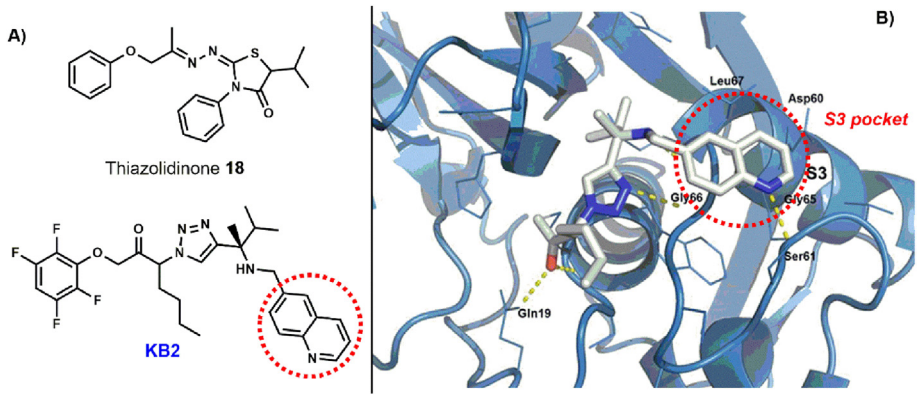

Fig. 2. A) Chemical structures of the thiazolidinone **18** and KB2 compound. B) Crystal structure of cruzain in complex with KB2 compound (PDB 3IUT), highlighting the quinoline ring located in the subsite S3 [19,31].

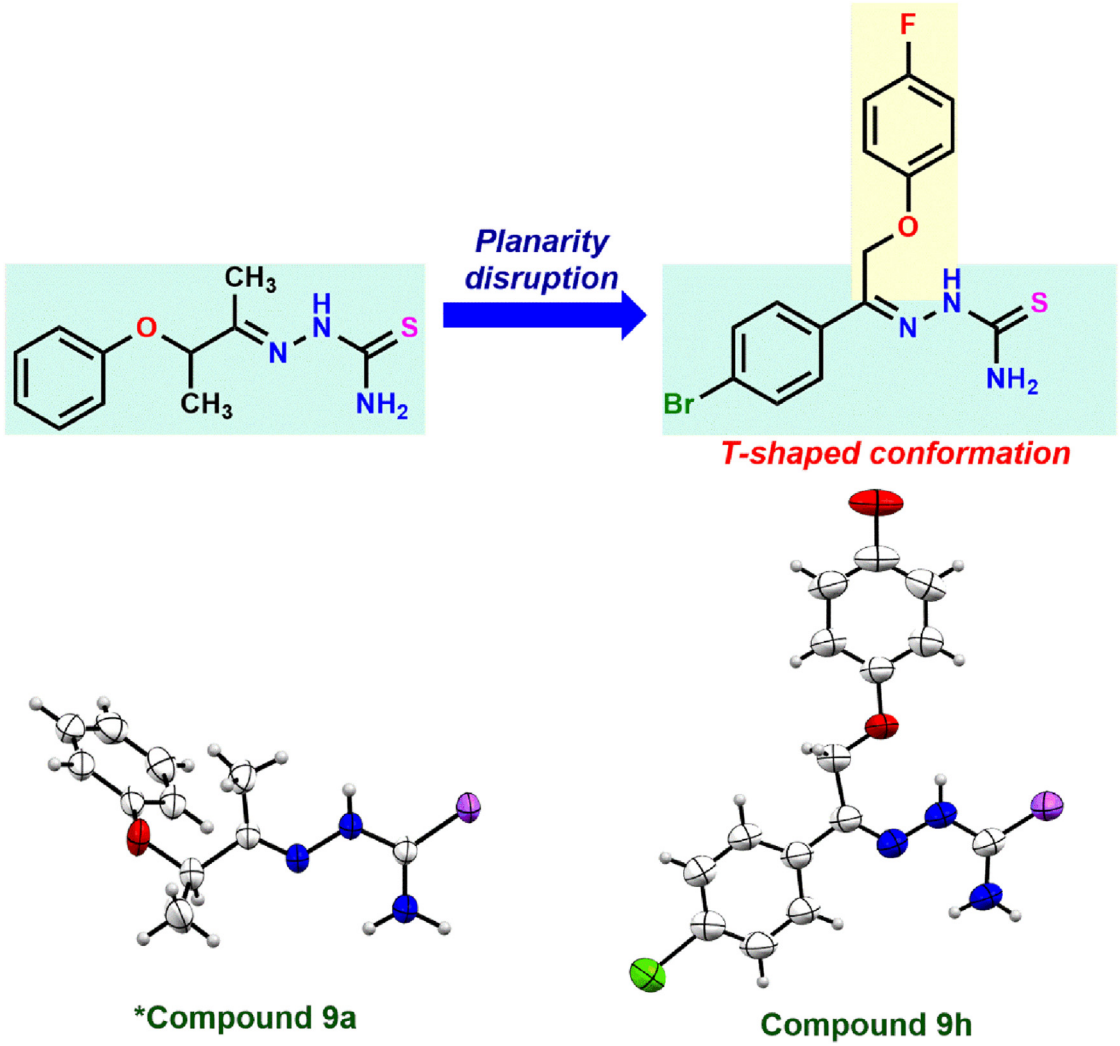

Fig. 3. Difference of molecular planarity between a thiosemicarbazone previously investigated (compound **9a** [30], left) and one proposed here (compound **9h**, right). ORTEP-3 diagram of the compounds **9h** and **9a**. Displacement ellipsoids are drawn at 50% probability level.

Next, we aimed to define the configuration of the major isomer by crystallographic analysis. A single crystal suitable for X-ray analysis was collected from thiosemicarbazones **8e** and **9h**. As shown in the ORTEP-3 representation of thiosemicarbazones **8e** and **9h** (Fig. 4), the *N*2 and sulfur atoms are on the same side, characterizing a *Z* configuration for the C1=N2 bond. These compounds showed ^{1}H NMR chemical shifts similar to thiosemicarbazones (**8a**–**l**, **9a**–**t**); therefore, it is fair to suggest that the major isomer for these thiosemicarbazones has a *Z* configuration about this bond.

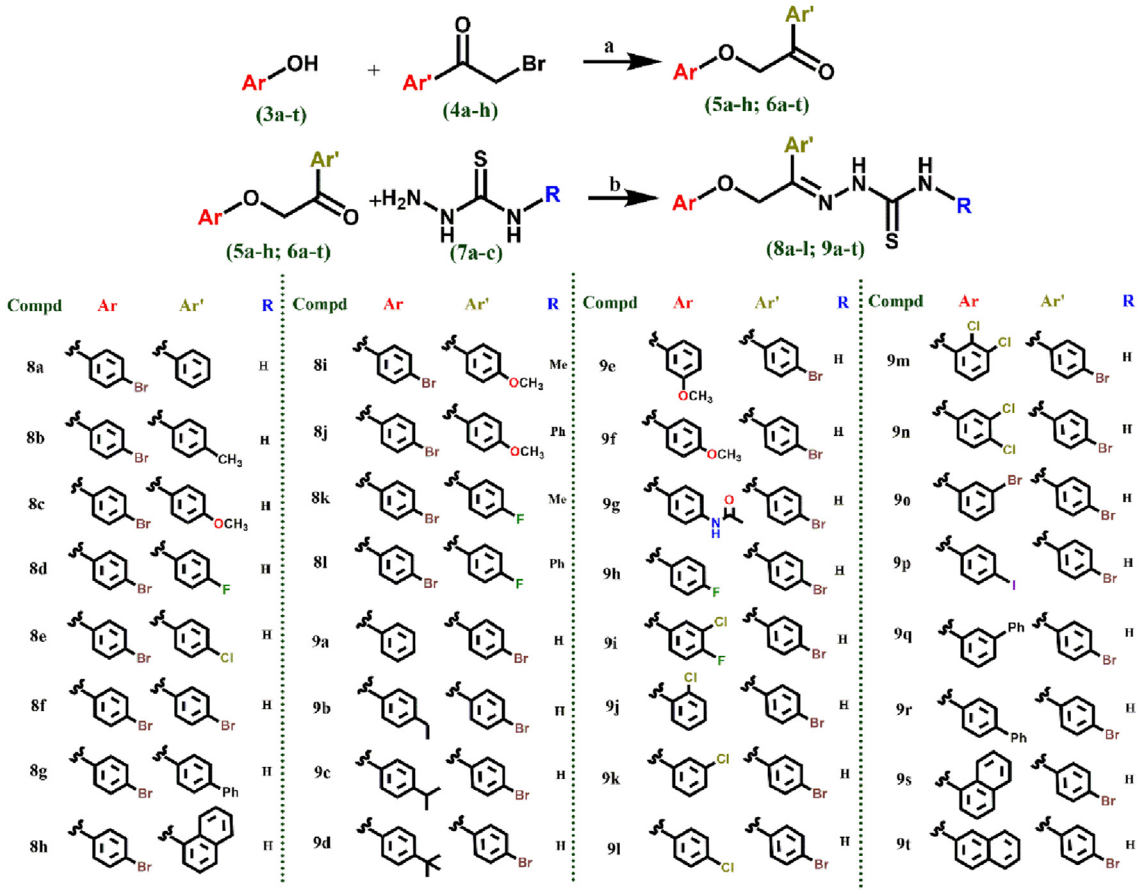

Scheme 1. Synthesis of aryl thiosemicarbazones (**8a**–**l**, **9a**–**t**). Reagents and conditions: (a) K_2CO_3, KI, acetone, r.t., 3–4 h, yields from 77 to 95%. (b) HCl, EtOH, ultrasound bath for 2,5-3 h, yields from 69 to 90%. Ph = Phenyl, Ar = Aromatic ring.

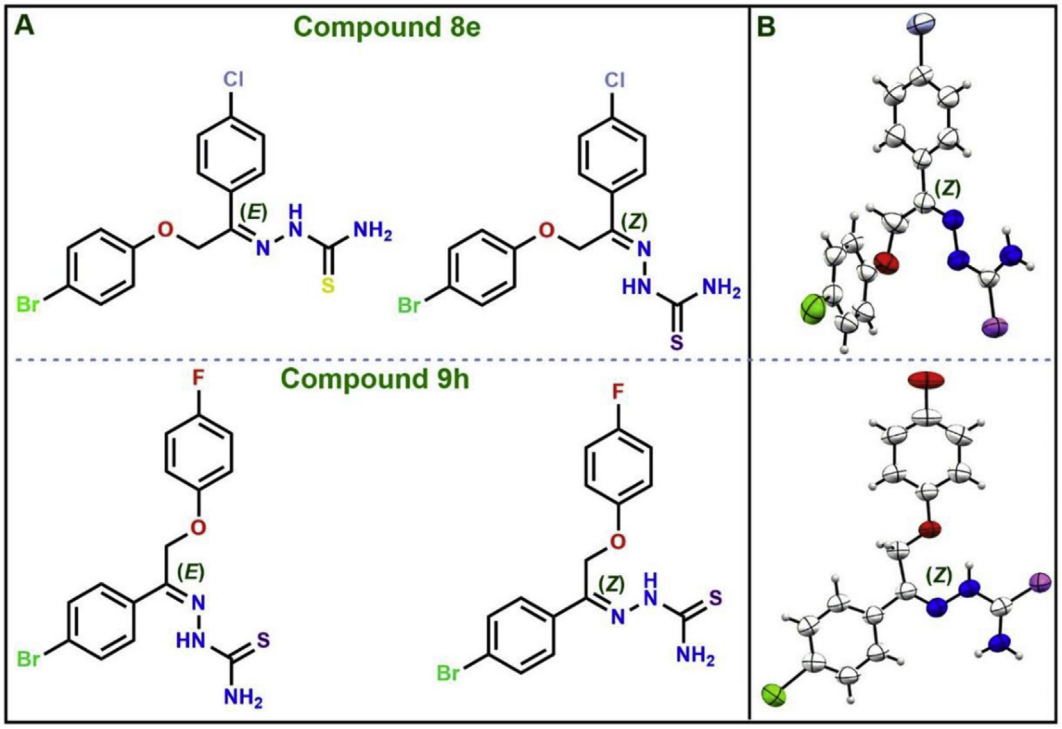

Fig. 4. A) Structures of the possible stereoisomers and B) ORTEP-3 representation for the crystal structure of a thiosemicarbazone previously investigated **8e** and **9h**, respectively.

In contrast, in previous works developed by our group [30,31] aryl-thiosemicarbazones were obtained that exhibited *E* configuration for this bond. The main structural feature that differentiates the thiosemicarbazones (**8a**–**l**, **9a**–**t**) from those previously obtained [30,31] is the presence of a phenyl group at C1. It appears that this reversal in the configuration around that bond is related to the presence of this group (Fig. 5).

The ratio of the stereoisomers *Z*/*E* was estimated by considering the relative intensity of the signals of the methylene protons in ^{1}H NMR spectra and varied according to the compound (Supplementary material). In the spectrum of compound **9c**, for example, only one signal was detected, suggesting that it was obtained in the form of a single stereoisomer (*Z*) or that the ratio of the minor isomer (*E*) was so small that was not detected during analysis. In relation to the compounds **8i**, **8l**, **9a**, **9n** and **9p**, the relative proportion of stereoisomers (*Z*:*E*) was: **8i** (89.2:10.8), **8l** (91.5:8.5), **9a** (93.5:6:5), **9n** (96.5:3:5), **9p** (95.2:4.8), respectively.

2.2. Antiparasitic activity against extracellular forms and cytotoxicity against host cells

First, compounds **8a**–**l** and **9a**–**t** were evaluated against epimastigotes and trypomastigotes of *T. cruzi*. The antiparasitic activity was determined by counting the parasite number in a Neubauer chamber and calculating the concentration of the test compound resulting in 50% inhibition (IC_{50}, epimastigotes) or 50% cytotoxicity (CC_{50}, trypomastigotes). Cytotoxicity in host cells was determined in mouse splenocytes, measured by the incorporation of [^{3}H]-thymidine, and results were expressed as the highest non-cytotoxic concentration (HNC). Benznidazole and nifurtimox were used as reference antiparasitic drugs and exhibited CC_{50} values of 6.2 and 2.7 μM against trypomastigotes, respectively. As a standard, compounds with CC_{50} values ≤6.2 μM against trypomastigotes were considered potent anti-*T. cruzi* compounds. The results are reported in Table 1.

We first analyzed the antiparasitic activity against the trypomastigote form. In analyzing the activity of aryl thiosemicarbazones **8a**–**h**, in which the structural variations were made in the *para*-position of the phenyl ring from the 2-haloacetophenone (**Ar′**), it was observed that, in general, substitutions in the phenyl ring did not favor trypanocidal activity. The compound **8a** (CC_{50} = 2.4 μM), which has no substitution in the phenyl ring, was one of the most potent compounds in the (**8a**–**h**) series, showing higher activity than reference drugs BDZ and NFX (CC_{50} = 6.2 and 2.7 μM, respectively).

Comparing the activity of the substituted aryl-thiosemicarbazones (**8b**–**h**) with BDZ, all compounds exhibited a greater toxicity against trypomastigotes than this reference drug, with the exception of the compound **8h** (CC_{50} = 14.7 μM). The attachment of electron donors groups, such as methyl (**8b**, CC_{50} = 3.1 μM) and methoxy (**8c**, CC_{50} = 5.0 μM), to the phenyl ring at the *para*-position decreased the antiparasitic activity. Substitutions in the *para*-position of the phenyl ring by the halogen atoms -F (**8d**, CC_{50} = 3.6 μM), -Cl (**8e**, CC_{50} = 5.3 μM) and -Br (**8f**, CC_{50} = 3.9 μM) also resulted in less active compounds than the unsubstituted derivative (**8a**). In addition, there was no correlation between the size of the halogen atomic radius and the antiparasitic activity. On the other hand, the attachment of a second phenyl ring at the *para*-position led to a slight increase in activity against trypomastigotes, as can be observed for compound **8g** (CC_{50} = 2.1 μM). These data showed similarity to those obtained in the study by Moreira et al., in which the 4-thiazolinone containing a phenyl at position 4 of the phenyl ring derived from 2-haloacetophenones are among the two most active against the parasite [36]. Interestingly, compound **8h** (CC_{50} = 14.7 μM), which contains a bulky and hydrophobic α-naphthyl group like the biphenyl of compound **8g**, showed the lowest activity among the thiosemicarbazones **8a**–**h**.

By evaluating the trypanocidal activity of thiosemicarbazones **8i**–**l**, it can be noted that the substitution at position *N*4 reduced the toxicity against this evolutionary form in most cases. For example, directly comparing the activity of compounds **8k** (*N*4–Me, CC_{50} = 7.4 μM) and **8l** (*N*4–Ph, CC_{50} = 15.6 μM) to the unsubstituted analog (**8d**, CC_{50} = 3.6 μM), a large reduction of activity is noted after this substitution.

Regarding the toxicity against trypomastigotes of aryl-thiosemicarbazones **9a**–**t**, in which the structural variations occur in the phenoxy ring (**Ar**), they all exhibited higher or similar activity in relation to reference drug benznidazole, with the exception of compounds **9q** (CC_{50} = 28.3 μM) and **9r** (CC_{50} = 12.3 μM). In addition, the functionalization of the phenoxy ring was generally beneficial to the activity against trypomastigote forms, as the compound **9a** (CC_{50} = 6.6 μM), an unsubstituted derivative, was less active than substituted compounds (except compounds **9q** and **9r**).

In comparison to **9a**, anti-*T. cruzi* activity was enhanced when an alkyl group was attached to the *para*-position of the phenoxy ring. Thiosemicarbazone **9b** (CC_{50} = 1.8 μM), with an ethyl group, was about three times more potent. Compounds **9c** (CC_{50} = 2.9 μM) and **9d** (CC_{50} = 2.2 μM), which have branched alkyl groups, also demonstrated increased antiparasitic activity, although with slightly less intensity than the linear alkyl chain analog (**9b**). The attachment of methoxy groups to the phenyl ring also generated more active compounds, as can be observed for thiosemicarbazones **9e** (CC_{50} = 1.2 μM) and **9f** (CC_{50} = 3.7 μM),

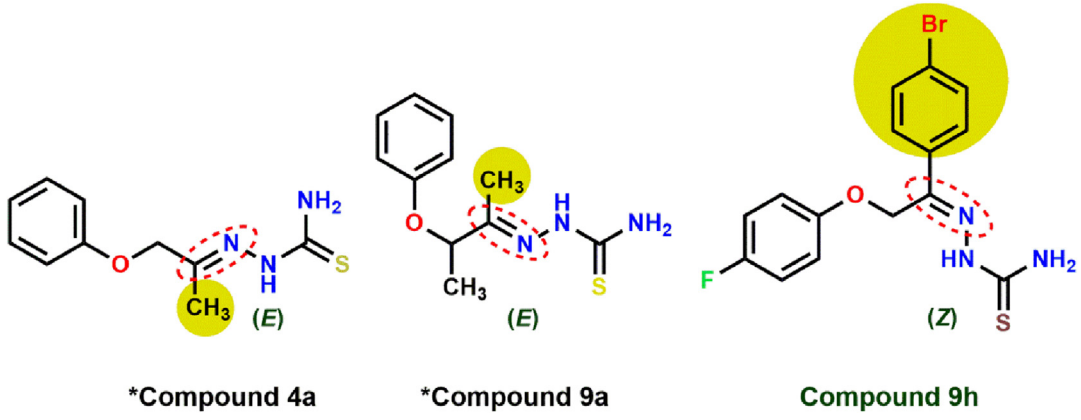

Fig. 5. Influence of bulk substituent (C1) in the molecular configuration. *Thiosemicarbazones previously investigated, compound **4a** [36] and compound **9a** [30].

Table 1
Anti-*T. cruzi* activity against epimastigote and trypomastigote forms and cytotoxicity against splenocytes.

Compound	Ar′/Ar	R	*T. cruzi*		Cytotoxicity HNC [μM][c]
			Epimastigotes IC_{50} [μM][a]	Trypomastigotes CC_{50} [μM][b]	
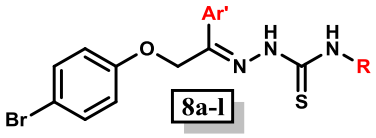					
8a	Ph	H	14.5	2.4	68.6
8b	4-CH_3 Ph	H	3.7	3.1	13.2
8c	4-OCH_3 Ph	H	3.1	5.0	2.5
8d	4-F Ph	H	3.8	3.6	2.6
8e	4-Cl Ph	H	3.6	5.3	12.5
8f	4-Br Ph	H	11.9	3.9	22.6
8g	4-Ph Ph	H	3.9	2.1	2.3
8h	α-Naphthyl	H	7.5	14.7	2.4
8i	4-OCH_3 Ph	Me	4.5	3.6	NT
8j	4-OCH_3 Ph	Ph	10.2	ND	NT
8k	4-F Ph	Me	15.7	7.4	NT
8l	4-F Ph	Ph	ND	15.6	NT
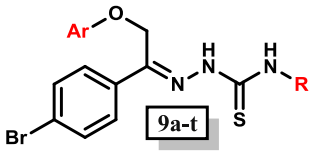					
9a	Ph	H	3.0	6.6	137.3
9b	4-CH_2CH_3 Ph	H	2.1	1.8	2.6
9c	4-$CH(CH_3)_2$ Ph	H	3.8	2.9	>246.0
9d	4-$C(CH_3)_3$ Ph	H	5.2	2.2	2.4
9e	3-OCH_3 Ph	H	3.7	1.2	2.5
9f	4-OCH_3 Ph	H	1.8	3.7	<2.5
9g	4-$NHCOCH_3$ Ph	H	15.6	3.5	2.4
9h	4-F Ph	H	1.8	3.1	2.6
9i	3-Cl, 4-F Ph	H	3.4	1.7	2.4
9j	2-Cl Ph	H	3.5	6.0	<2.5
9k	3-Cl Ph	H	2.2	1.6	2.5
9l	4-Cl Ph	H	4.6	5.7	<2.5
9m	2,3-*di*Cl Ph	H	4.4	5.7	23.1
9n	3,4-*di*Cl Ph	H	1.8	3.0	<2.3
9o	3-Br Ph	H	3.9	6.2	2.7
9p	4-I Ph	H	2.9	2.1	2.1
9q	3-Ph Ph	H	4.4	28.3	2.3

(*continued on next page*)

Table 1 (*continued*)

Compound	Ar′/Ar	R	*T. cruzi*		Cytotoxicity HNC [μM][c]
			Epimastigotes IC_{50} [μM][a]	Trypomastigotes CC_{50} [μM][b]	
9r	4-Ph Ph	H	4.1	12.3	22.7
9s	α-Naphthyl	H	3.0	3.4	2.4
9t	β-Naphthyl	H	5.3	5.0	2.4
BDZ	–	–	48.8	6.2	96.1
NFX	–	–	5.7	2.7	3.5

HNC = highest non-cytotoxic concentration; ND = not determined; NT = not tested; BDZ = benznidazole; NFX = nifurtimox.
[a] Determined 5 days after incubation with compounds, using Dm28c epimastigotes.
[b] Determined 24 h after incubation with compounds, using Y strain trypomastigotes. IC_{50} = inhibitory concentration for 50%. CC_{50} = cytotoxic concentration for 50%. CC_{50} and IC_{50} values were calculated using concentrations in triplicate and experiment was repeated, only values with a standard deviation <10% mean were considered.
[c] Cell viability of BALB/c mouse splenocytes determined 24 h after treatment.

substituted at the *meta*- and *para*-positions, respectively. However, the compound 3-methoxy substituted (**9e**) was the most potent of all of the thiosemicarbazones assessed in this study, approximately five times more active than BDZ. Binding of an acetamide group in the *para*-position of the phenoxy ring (**9g**, $CC_{50} = 3.5$ μM) increased activity compared with **9a**. However, this increase was not as significant as what was observed in previous work from our group, in which the derivative containing such a substituent was among the most active [30].

We also evaluated the antiparasitic activity against trypomastigotes by thiosemicarbazones containing different halogens attached to the phenoxy ring. All derivatives containing halogens were more active than the unsubstituted thiosemicarbazone **9a**, revealing the importance of this structural modification for antiparasitic activity. By comparing the activity of compounds **9p** ($CC_{50} = 2.1$ μM), **8f** ($CC_{50} = 3.9$ μM) and **9l** ($CC_{50} = 5.7$ μM), which show the atoms -I, -Br and -Cl at position 4 of the phenoxy ring, respectively, a potential increase of antiparasitic activity was observed according to the increase of the atomic radius of bound halogen. This trend was also observed in a previous study by our group [30]. We also analyzed the effect of binding chlorine atoms in different positions of the phenoxy ring, *ortho*- (**9j**, $CC_{50} = 6.0$ μM), *meta*- (**9k**, $CC_{50} = 1.6$ μM) and *para*- (**9l**, $CC_{50} = 5.7$ μM). The *meta*-substitution generated the most active chlorine derivative and one of the most active compounds in this study. Moreover, *di*-substitutions were also evaluated in the phenoxy ring by halogen atoms, giving rise to compounds **9i** (3-Cl,4-F–Ph), **9m** (2,3-*di*Cl–Ph) and **9n** (3,4-*di*Cl–Ph). These compounds were more active in relation to compound **9a**, especially thiosemicarbazone **9i**, one of the most trypanocidal of the series with a $CC_{50} = 1.7$ μM, higher than even the reference drug.

The anti-trypanosomal activity for compounds **9p**, **8f** and **9l** increased with the atomic radius of their halogen atoms, suggesting the steric effect is important for activity. Based on this, we evaluated thiosemicarbazones **9q** and **9r**, which possess a second phenyl ring attached to the phenoxy ring in the positions 3 and 4, respectively. Compounds **9s** and **9t**, fitted with a naphthyl ring attached to the imine carbon in α and β positions, respectively, were also obtained. The thiosemicarbazones containing biphenyl **9q** ($CC_{50} = 28.3$ μM) and **9r** ($CC_{50} = 12.3$ μM) were inactive, whereas the compounds containing the naphthyl group **9s** ($CC_{50} = 3.4$ μM) and **9t** ($CC_{50} = 5.0$ μM) only maintained the antiparasitic activity, with the replacement in the position α most favorable. As observed, not only the steric and hydrophobic effects of the substituents in the phenoxy ring are responsible for the potentiation of trypanocidal activity.

Once the toxic activity of all compounds (**8a**–**l**, **9a**–**t**) for the *T. cruzi* trypomastigotes had been determined, we investigated the antiproliferative effect for *T. cruzi* epimastigotes. BDZ, one of the reference drugs used in the experiments, exhibited an IC_{50} of 48.8 μM while NFX presented an IC_{50} of 5.7 μM on this parasite form. All thiosemicarbazones evaluated in this study were more active than the reference drug BDZ.

Regarding the cytotoxicity to splenocytes, most aryl thiosemicarbazones evaluated in this study (**8a**–**l**, **9a**–**t**) caused higher toxicity than the reference drug benznidazole, with the exception of compound **9a**, which was non-toxic at concentrations up to 137.3 μM, and compound **9c**, which was non-toxic to the highest concentration tested (246.0 μM). Taking into account the selectivity, the aryl thiosemicarbazone **9c** stood out among all compounds evaluated, displaying excellent trypanocidal activity for both parasite forms of *T. cruzi* and lower toxicity to splenocytes than the reference drugs. In addition, Lipinski et al. present four criteria that are important to study the pharmacokinetics and drug development. A molecule that agrees with three criteria, would present a good pharmacokinetic and became a drug candidate [37]. It is interesting to note that the calculated values in Table 2 show that thiosemicarbazone **9c** as well as the unsubstituted derivative (**9a**) meet the criteria of Lipinski. On the other hand, structurally-simple thiosemicarbazones present limited aqueous solubility.

2.3. Anti-*T. cruzi* activity against amastigote and trypomastigote forms infecting a vertebrate cell

Due to the good activity shown against epimastigote and trypomastigote forms of *T. cruzi*, the compounds were also assayed *in vitro* against the *T. cruzi* amastigote form, which represents the intracellular form of the parasite. For this, we used a tissue cell culture system that allows evaluating the activity against both amastigote and trypomastigote forms simultaneously because the lengthy time of the assay (seven days) allows compounds to act on trypomastigotes released starting from four days post-infection. This method is considered the *in vitro* method of choice in screening drugs for activity against *T. cruzi* because it mimics the lifecycle of the parasite [38,39].

Results were expressed as the percent of inhibition of parasite growth after treatment with each compound. A cell viability test was performed to evaluate the cytotoxicity of the compounds against the murine fibroblast L-929 cell line [39,40]. The concentrations that caused 50% inhibition of the parasite growth (IC_{50}) were evaluated for the more potent compounds (those presenting more than 70% inhibition in the initial screening at 100 μM) (Table 3).

Table 2
Lipinski criteria for thiosemicarbazones **9a** and **9c**.

Compound	MW (g/mol)	C log *P*	H bond donors	H bond acceptors	Criteria met
Rule	<500	<5	<5	<10	3 at least
9a	364.26	3.57	3	5	All
9c	406.34	4.81	3	5	All

Most of the compounds exhibited activity against these parasite forms of *T. cruzi*, with 12 compounds (**8a**–**b**, **8f**–**h**, **9a**–**b**, **9e**–**f**, **9i**, **9n**, **9p**) showing an $IC_{50} \leq 10$ μM. Furthermore, thiosemicarbazones **8g**, **8h** and **9a** (IC_{50} = 3.3, 4.8 and 5.4 μM, respectively) showed trypanocidal activity comparable to the benznidazole.

Analyzing the activity of thiosemicarbazones **8a**–**h**, it was observed that, relative to compound **8a** (IC_{50} = 10.2 μM), the presence of a methyl group in position 4 of the phenyl ring (**8b**) slightly improved activity. Thiosemicarbazone **8c**, which also contains an electron donor group (OCH_3) at the same position, was less active (IC_{50} = 11.9 μM). The halogen substitution in the phenyl ring (4-F, **8d**; 4-Cl; **8e**; 4-Br, **8f**) generally did not contribute to the activity against intracellular and trypomastigote forms, except for thiosemicarbazone **8f** (IC_{50} = 8.1 μM) a bromine derivative. Compound **8g** (IC_{50} = 3.3 μM), which has a phenyl ring at the same position, was the more active compound tested, suggesting that the presence of bulky and hydrophobic substituents, as bromine and phenyl, may be associated with improved activity. In addition,

Table 3
Anti-*T. cruzi* activity against amastigote and trypomastigote forms infecting a vertebrate cell and inhibitory activity against cruzain.

Compound	Ar′/Ar	R	*T. cruzi* IC_{50} [μM]	Fibroblast CC_{50} [μM]	SI[a]	Cruzain inhibition [%][b]
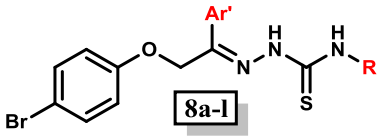						
8a	Ph	H	10.2	<27.5	<2.7	67.6 ± 6.8
8b	4-CH_3 Ph	H	7.9	13.2	1.7	70.9 ± 2.6
8c	4-OCH_3 Ph	H	11.9	<25.4	<2.1	38.7 ± 7.9
8d	4-F Ph	H	10.7	<26.2	<2.5	53.1 ± 5.0
8e	4-Cl Ph	H	14.8	25.1	1.7	67.5 ± 6.2
8f	4-Br Ph	H	<8.1	22.6	>2.8	11.8 ± 13.2
8g	4-Ph Ph	H	3.3	22.7	6.9	88.9 ± 2.6 (0.6 ± 1.5)
8h	α-Naphthyl	H	4.8	12.1	2.5	73.6 ± 8.3
8i	4-OCH_3 Ph	Me	ND	ND	–	29.8 ± 9.0
8j	4-OCH_3 Ph	Ph	ND	ND	–	42.8 ± 16.6
8k	4-F Ph	Me	ND	ND	–	30.0 ± 5.4
8l	4-F Ph	Ph	ND	ND	–	35.0 ± 5.7
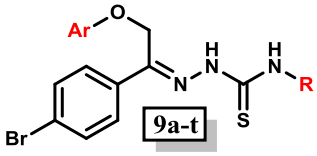						
9a	Ph	H	5.4	54.9	10.2	61.8 ± 9.1
9b	4-CH_2CH_3 Ph	H	6.4	<25.5	<4.0	75.1 ± 5.8
9c	4-$CH(CH_3)_2$ Ph	H	12.3	24.6	2.0	49.7 ± 6.4
9d	4-$C(CH_3)_3$ Ph	H	15.2	23.8	1.6	85.3 ± 5.1
9e	3-OCH_3 Ph	H	9.9	50.7	5.1	62.8 ± 4.7
9f	4-OCH_3 Ph	H	8.9	101.5	11.4	75.8 ± 1.1
9g	4-$NHCOCH_3$ Ph	H	43.2	94.9	2.2	80.7 ± 3.5
9h	4-F Ph	H	15.7	52.3	3.3	84.0 ± 1.3 (0.4 ± 2.1)
9i	3-Cl, 4-F Ph	H	9.0	48.0	5.3	93.7 ± 5.8 (0.07 ± 1.2)
9j	2-Cl Ph	H	13.5	25.1	1.9	58.9 ± 6.3
9k	3-Cl Ph	H	25.1	<50.2	<2.0	51.8 ± 6.3
9l	4-Cl Ph	H	11.2	<25.1	<2.2	76.3 ± 2.4
9m	2,3-*di*Cl Ph	H	10.8	23.1	2.8	81.8 ± 6.6
9n	3,4-*di*Cl Ph	H	8.3	23.1	2.8	99.1 ± 1.5 (0.008 ± 1.6)
9o	3-Br Ph	H	149.4	>180.5	>1.2	81.3 ± 1.4
9p	4-I Ph	H	8.6	<20.4	2.4	63.3 ± 10.2
9q	3-Ph Ph	H	>181.7	ND	–	65.4 ± 17.3
9r	4-Ph Ph	H	76.6	90.8	1.2	63.7 ± 23.1
9s	α-Naphthyl	H	48.3	<96.5	<2.0	ND
9t	β-Naphthyl	H	13.5	>193.1	>14.3	72.1 ± 9.2
BDZ	–		3.8	2381	625	–

BDZ = benznidazole. ND = not determined.
[a] Selectivity index (SI) is the ratio of murine fibroblast viability (CC_{50}) to the IC_{50} on *T. cruzi*.
[b] Compounds were tested at 50 μM and the percent inhibition of catalytic activity was determined; values in parenthesis are IC_{50} values [μM] and represent the mean ± SD of three measurements.

thiosemicarbazone **8h** (IC_{50} = 4.8 μM), also containing a bulky and hydrophobic grouping (naphthyl), is among the most active of the series, suggesting the steric nature of these groups positively influences activity against these forms of the parasite.

Considering the anti-*T. cruzi* activity of thiosemicarbazones **9a**–**t** against these parasite forms, it is noted that substitutions in the phenoxy ring (**Ar**) gave less active compounds compared with the unsubstituted derivative **9a** (IC_{50} = 5.4 μM). However, some structure–activity relationships were identified in this series. Comparing the activity of compounds **9b**, **9c** and **9d** (IC_{50} = 6.4, 12.3 and 15.2 μM, respectively), a reduction in the trypanocidal activity was observed with increased branching of the alkyl chain attached to position 4 in the phenoxy ring. A potentiation of the trypanocidal activity was observed with an increased halogen atomic radius linked to the same ring position by the order: **9h** (4-F, IC_{50} = 15.7 μM) < **9l** (4-Cl, IC_{50} = 11.2 μM) < **8f** (4-Br, IC_{50} = 8.1 μM) ~ **9p** (4-I, IC_{50} = 8.6 μM) (Fig. 6).

Furthermore, the presence of a halogen at position 4 of the ring contributed more significantly to the activity than position 3, as is seen in the comparison of compounds **9l** (4-Cl, IC_{50} = 11.2 μM), and **8f** (4-Br, IC_{50} = 8.1 μM) with compounds **9k** (3-Cl, IC_{50} = 25.1 μM) and **9o** (3-Br, IC_{50} = 149.4 μM), respectively.

The cytotoxicity of the active compounds on uninfected fibroblasts was established *in vitro* to evaluate the selectivity of their antiparasitic effects. The selectivity index (SI) was calculated as the ratio of the CC_{50} value in uninfected cells (cytotoxicity) to the IC_{50} in parasite cells (Table 3). Although most of the compounds exhibited low selectivity, thiosemicarbazones **9a**, **9f** and **9t** showed moderate selectivity (SI > 10), suggesting that these compounds could be prototypes for new trypanocidal drugs.

2.4. Cruzain inhibition activity

To investigate a possible mechanism of action, compounds were tested against the enzyme cruzain of the *T. cruzi*. The inhibition of cruzain enzymatic activity by all compounds was measured using a competition based assay with the substrate Z-Phe-Arg-aminomethylcoumarin (Z-FR-AMC) [41]. All compounds were screened at 50 μM, and only compounds having an inhibition value of >70% were chosen to determine IC_{50} values. However, the IC_{50} values of many compounds exhibiting an inhibition percentage above this value (70%) could not be established due to their low solubility, which made it impossible to achieve cruzain inhibition high enough (>85%) for a good curve determination. Therefore, in some cases, the discussion was performed in terms of the percentage of cruzain inhibition (Table 3).

Analyzing the potential for inhibition of thiosemicarbazones **8a**–**h**, it was observed that the substitution of methoxy group and the halogens -F, -Cl and -Br held in position 4 of the phenyl ring **Ar′** of compound **8a** did not favor inhibitory activity. On the other hand, the compounds **8b** (4-CH_3), **8g** and **8h** showed good inhibition percentages (70.9, 88.9 and 73.6%, respectively), and **8g** showed an IC_{50} of 0.6 ± 1.5 μM. A common feature of the latter two compounds is the presence of bulky and hydrophobic groups, biphenyl (**8g**) and naphthyl (**8h**), attached to C1; previous docking models demonstrated interaction with the subsite S3 enzyme [31].

The **8i**–**l** thiosemicarbazone showed little activity against cruzain, suggesting that replacements at *N*4, either methyl or phenyl grouping, are not conducive to enzyme inhibition. These results confirm data obtained in the study conducted by Du et al. [20] in which it was observed that the binding of various alkyl and aryl radicals in this position generated inactive compounds.

By observing the inhibitory potential of aryl thiosemicarbazones **9a**–**t**, in which the structural variations were made in phenoxy ring **Ar**, it is noted that several of them (**9b**, **9d**, **9f**–**i**, **9l**–**o**, **9t**) had percentages of inhibition greater than 70%. Relative to compound **9a**, substitutions at position 4 of the phenyl ring by alkyl substituents ethyl (**9b**) and *tert*-butyl (**9d**) had increased activity, while thiosemicarbazone **9c** (4-*i*-propyl) was less active. The addition of methoxy substituents at positions 3 and 4 of the phenoxy ring (**9e** and **9f**, respectively) slightly favor enzyme inhibition, so that the compound substituted at position 4 (**9f**) was more active. The work carried out by Du et al. [20] and Siles et al. [22] explained that the presence of halogens in the phenyl ring of some aryl thiosemicarbazones contributes to the inhibition of cruzain. In fact, thiosemicarbazones containing halogens (F, Cl, Br, and I) in the phenyl ring (**8f**, **9h**–**p**) generally showed good percentages of inhibition. These values generally decreased according to the size of the atomic radius of the halogen attached to the phenyl ring at position 4, as can be observed in compounds **9h** (4-F) > **9l** (4-Cl) > **8f** (4-Br) to 84.0 (IC_{50} = 0.4 ± 2.1 μM), 73.6 and 11.8%, respectively. Furthermore, the phenyl ring disubstituted by these halogens increased the inhibition percentage, as demonstrated by thiosemicarbazones **9i** (3-Cl, 4-F) **9m** (2,3-*di*Cl) and **9n** (3,4-*di*Cl), with inhibition percentages of 93.7, 81.8 and 99.1%, respectively. On the other hand, compounds **9i** and **9n** are the most potent compounds of the present study and exhibited IC_{50} values of 0.07 ± 1.2 and 0.008 ± 1.6 μM, respectively. Corroborating with this work, Du et al. demonstrated that the aryl-thiosemicarbazone containing chlorine at the 3 and 4 positions in the phenyl ring was the most active among the tested derivatives [20]. The other thiosemicarbazone that stood out in the studies conducted by the authors and Siles et al. was that which contained a bromine atom at position 3 of the phenyl ring. Similarly, compound **9o**, which contains the same substitution in the phenoxy ring, exhibited an inhibition percentage of 81.3% [20,22].

Considering all evaluated aryl thiosemicarbazones (**8a**–**l**, **9a**–**t**), compounds **8g**, **9d**, **9g**–**i**, and **9m**–**o** inhibited over 80% of *T. cruzi* cruzain activity in the screening at 50 μM. However, the IC_{50} was determined only for compounds **8g**, **9h**–**i** and **9n**. Moreover,

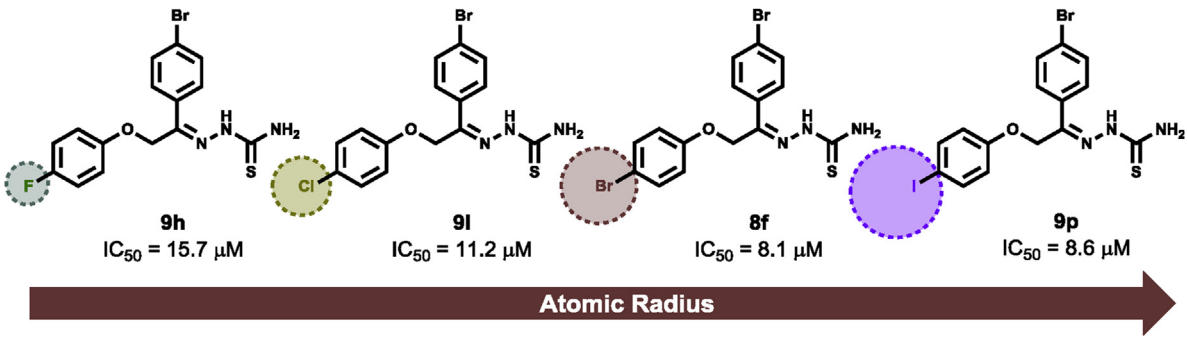

Fig. 6. Relationship of atomic radius and antiparasitic activity.

thiosemicarbazones **9i** and **9n** are noteworthy because they present an IC_{50} of 0.07 ± 1.2 and 0.008 ± 1.6 μM, respectively, comparable to the most potent cruzain inhibitors described in the literature, such as compound K11777 (IC_{50} = 0.004 μM) [42].

Thiosemicarbazones **9i** and **9n** have not been the most active *in vitro* against the parasite, although the thiosemicarbazone **9i** (IC_{50} = 1.7 μM) is among the three most active front trypomastigote form. This may be related to the fact that the *in vitro* test front cruzain was done directly in the isolated enzyme, avoiding the effect of the parasite biological barriers, such as permeability cell. Moreover, it is probably that our compounds act by other mechanisms of action, since some of them exhibited modest cruzain inhibition percentage and good *in vitro* activity against the parasite.

The fact is that the strategy of disruption of the planarity mentioned above (Fig. 3) [30], providing a T-shaped conformation by inserting aryl groups at *C*1 appears to have been effective. Directly comparing the percentage of cruzain inhibition by compound (**1**) with compound **9g**, it is observed that compound (**1**) did not inhibit the enzyme even at a concentration of 100 μM. Thiosemicarbazone **9g**, containing a T-shaped conformation, inhibited the enzyme with a percentage of approximately 80.7% using a concentration of 50 μM, half of the former. In addition to compounds (**1**) and (**2**), none of the thiosemicarbazones evaluated in a previous study [30] demonstrated activity against cruzain.

2.5. Flow cytometry analysis

After confirming that these thiosemicarbazones were able to kill *T. cruzi* parasites, our next step was to understand how they lead to cell death. Therefore, we treated Y strain trypomastigotes with 0.5 μM (average IC_{50} values) or 5.0 (10× IC_{50} values) of each thiosemicarbazone and incubated them for 24 h. Cells were then stained with propidium iodide (PI) and examined by flow cytometry. As shown in Table 4, the positive control (Triton X) led to 67% of cells positively stained for PI. When compared with untreated cells, most of the parasite cells treated with thiosemicarbazones positively stained for PI. Thiosemicarbazone **9c** was the most potent among them, exhibiting concentration-dependent activity (Fig. 7). Moreover, compound **9c** at 5.0 μM was more efficient in inducing parasite cell death than benznidazole at its optimal concentration (25 μM). Therefore, we suggest that thiosemicarbazone-based treatment causes parasite cell death through necrosis.

3. Conclusions

Using a simple and fast method, 32 aryl thiosemicarbazones were synthesized. The trypanocidal activity of these compounds was evaluated for three life stages of the parasite. Most of the compounds exhibited superior activity over the reference drug BDZ against epimastigote and trypomastigote forms of *T. cruzi*. Compounds **9a** and **9c** showed broad and selective antiparasitic activity against *T. cruzi*. Compound **9c** was most selective against the extracellular forms of the parasite and showed non-toxicity on mouse splenocytes at the highest concentration tested. Among all compounds tested, 14 inhibited cruzain at rates higher than 70%, demonstrating that changes in the molecular conformational and planarity in thiosemicarbazones increases the affinity to the cruzain binding site. Thiosemicarbazones **9i** and **9n** were shown to be potent inhibitors, comparable to the compound K11777, a highly potent cruzain inhibitor.

Table 4
Analysis of trypomastigotes positive only for PI.

Compound	Concentration (μM)	% PI-positively stained cells[a]
Triton X-100 (10 μL)	–	67.8
Benznidazole	5.0	4.2
Benznidazole	25	56.4
9c	0.5	2.3
9c	5.0	42.2
9i	0.5	2.7
9i	5.0	34
9n	0.5	2.3
9n	5.0	44.9

[a] Values were taken from two different readings of at least 10,000 events 24 h after incubation with Y strain trypomastigotes.

4. Experimental section

4.1. General

Most the chemicals were purchased from Sigma–Aldrich (St. Louis, MO, USA), Merck (Berlin, Germany) or Alfa-Aesar (Ward Hill, MA, USA). Reactions in ultrasound bath were performed in a Unique EM-804 TGR instrument, with a frequency of 40 kHz and a nominal power of 180 W, and without external heating. Precoated aluminum sheets (silica gel 60 F254, Merck) were used for thinlayer chromatography (TLC) and spots were visualized under UV light. Elemental analysis was performed with a Carlo Erba instrument model E-1110. IR spectra in KBr pellets were acquired at Bruker FT-IR spectrophotometer. ^{1}H and ^{13}C NMR were recorded on a UnityPlus 400 MHz and Bruker AMX-300 MHz spectrometer, using DMSO-d_6 as a solvent and trimethylsilane (TMS) as the internal standard. Splitting patterns were defined as; s, singlet; d, doublet; dd, double doublet; t, triplet; q, quartet; m, multiplet. Chemical shift values were given in ppm. DEPT was employed to confirm the carbon assignment.

4.2. Synthesis of 1-phenoxy-2-acetophenones (*5a–h; 6a–t*). Example for 2-(4-bromophenoxy)-1-(4-methoxyphenyl)ethan-1-one (*5c*)

In a round bottom flask with a capacity of 100 mL, were added 13.2 mmol (2.3 g) of 4-bromophenol, 35 mL of acetone, 13.2 mmol (1.8 g) of powdered K_2CO_3 and KI in catalytic amount. The mixture was kept under magnetic stirring at room temperature. After 30 min, 8.8 mmol (2.0 g) of 2-bromo-1-(4-methoxyphenyl)ethan-1-one are added in portions. The reaction was kept under magnetic stirring at room temperature for 3.0 h. After completion of the reaction, the reaction mixture was filtered, so that the supernatant was evaporated under reduced pressure and the precipitate (K_2CO_3) discarded. After evaporation, a solid was obtained, which was resuspended using diethyl ether and then filtered. The crystal obtained was transferred to a desiccator and placed under vacuum SiO_2. The resulting product was used in the next step without further purification.

4.3. Synthesis of thiosemicarbazones (*8a–l, 9a–t*). Example for 2-(4-bromophenoxy)-1-(4-methoxyphenyl)ethan-1-one thiosemicarbazone (*8c*)

In a round bottom flask for 100 mL, 8.1 mmol (2.6 g) of 1-phenoxy-2-acetophenone **5c** were dissolved in 30 mL EtOH, following by the addition of four drops HCl. The flask was placed in an ultrasound bath (40 kHz, 180 W) and under sonication, 10.5 mmol (1.0 g) of thiosemicarbazide **7a** were added in portions to the reaction. After 2.5 h, the mixture was cooled at 0 °C and the precipitate was filtered in a Büchner funnel with a sintered disc filter, washed with cold water, ethanol and then dried over SiO_2. After drying, the product was recrystallized from toluene.

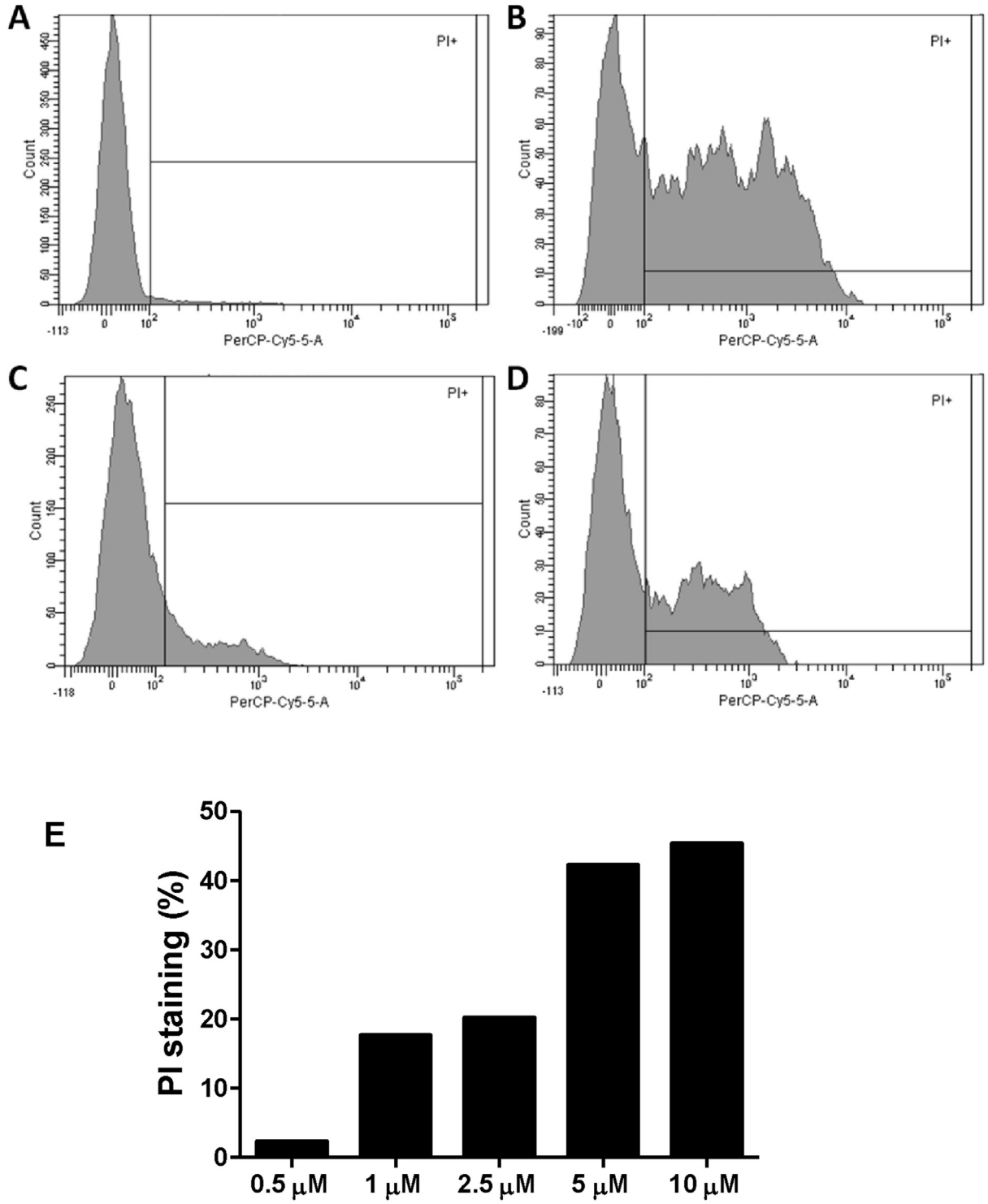

Fig. 7. Thiosemicarbazone **9c** treatment causes parasite death through necrosis. Y strain trypomastigotes were treated with compound **9c** for 24 h. Parasites were examined by flow cytometry with PI staining. Panel (A): Untreated; (B): Positive control (Triton X-100); (C): Thiosemicarbazone **9c** at 1.0 μM; (D): Thiosemicarbazone **9c** at 5.0 μM. E) Thiosemicarbazone **9c** induces necrosis in a concentration-response manner. The percentage of cells in each left quadrants represent the unstained; P5 quadrants represent PI. Two independent experiments were performed, each compound concentration was tested in duplicate.

*4.3.1. 2-(4-Bromophenoxy)-1-phenylethan-1-one thiosemicarbazone (**8a**)*

Recrystallization in toluene afforded beige crystals, yield = 88%. M.p. (°C): 144–146. IR (KBr): 3423 and 3314 (NH_2), 3235 (N–H), 1599 (C=N) cm^{-1}. ^1H NMR (300 MHz, DMSO-d_6): δ 5.32 (s, 2H, CH_2), 6.96 (dd, 2H, J = 9.30, 2.10 Hz, Ar–H), 7.38–7.41 (m, 3H, Ar–H), 7.49 (dd, 2H, J = 9.30, 2.10 Hz, Ar–H), 7.90–7.92 (m, 2H, Ar–H), 8.09 (s broad, 1H, NH_2), 8.48 (s broad, 1H, NH_2), 10.83 (s broad, 1H, NH). ^{13}C NMR (75.5 MHz, DMSO-d_6): δ 61.3 (CH_2), 112.7 (Cq Ar), 117.1 (CH Ar), 127.0 (CH Ar), 128.2 (CH Ar), 129.2 (CH Ar), 132.1 (CH Ar), 135.6 (Cq Ar), 143.7(C=N), 157.0 (C–O, Ar), 179.2 (C=S). Anal. Calcd. For $C_{15}H_{14}BrN_3OS$: C, 49.46; H, 3.87; N, 11.54. Found:

C, 49.88; H, 3.86; N, 11.97.

4.3.2. 2-(4-Bromophenoxy)-1-(p-tolyl)ethan-1-one thiosemicarbazone (**8b**)

Recrystallization in toluene afforded yellow crystals, yield = 73%. M.p. (°C): 138. IR (KBr): 3417 and 3322 (NH_2), 3239 (N–H), 1601 (C=N) cm^{-1}. ^1H NMR (300 MHz, DMSO-d_6): δ 5.29 (s, 2H, CH_2), 6.94 (dd, 2H, J = 6.90, 2.40 Hz, Ar–H), 7.19 (d, 2H, J = 8.10 Hz, Ar–H), 7.48 (dd, 2H, J = 6.90, 2.40 Hz, Ar–H), 7.80 (d, 2H, J = 8.10 Hz, Ar–H), 8.05 (s broad, 1H, NH_2), 8.45 (s broad, 1H, NH_2), 10.76 (s broad, 1H, NH). ^{13}C NMR (75.5 MHz, DMSO-d_6): δ 20.8 (CH_3), 61.3 (CH_2), 112.7 (Cq Ar), 117.1 (CH Ar), 126.9 (CH Ar), 128.9 (CH Ar), 132.1 (CH Ar), 132.8 (Cq Ar), 138.9 (Cq Ar), 143.8 (C=N), 156.9 (C–O, Ar), 179.0 (C=S). Anal. Calcd. For $C_{16}H_{16}BrN_3OS$: C, 50.80; H, 4.26; N, 11.11. Found: C, 50.40; H, 4.25; N, 11.55.

4.3.3. 2-(4-Bromophenoxy)-1-(4-methoxyphenyl)ethan-1-one thiosemicarbazone (**8c**)

Recrystallization in toluene afforded colorless crystals, yield = 76%. M.p. (°C): 109–110. IR (KBr): 3414 and 3334 (NH_2), 3247 (N–H), 1600 (C=N) cm^{-1}. ^1H NMR (300 MHz, DMSO-d_6): δ 5.29 (s, 2H, CH_2), 6.93 (dd, 2H, J = 8.70, 1.20 Hz, Ar–H), 6.95 (dd, 2H, J = 9.00, 1.50 Hz, Ar–H), 7.49 (dd, 2H, J = 9.00, 1.50 Hz, Ar–H), 7.88 (dd, 2H, J = 8.70, 1.20 Hz, Ar–H), 8.04 (s broad, 1H, NH_2), 8.41 (s broad, 1H, NH_2), 10.71 (s broad, 1H, NH). ^{13}C NMR (75.5 MHz, DMSO-d_6): δ 55.2 (CH_3), 61.3 (CH_2), 112.7 (Cq Ar), 113.6 (CH Ar), 117.2 (CH Ar), 127.9 (Cq Ar), 128.6 (CH Ar), 132.1 (CH Ar), 143.7 (C=N), 156.9 (C–O, Ar), 160.2 (C Ar–OCH_3), 178.9 (C=S). Anal. Calcd. For $C_{16}H_{16}BrN_3O_2S$: C, 48.74; H, 4.09; N, 10.66. Found: C, 48.53; H, 3.95; N, 10.73.

4.3.4. 2-(4-Bromophenoxy)-1-(4-fluorophenyl)ethan-1-one thiosemicarbazone (**8d**)

Recrystallization in toluene afforded colorless crystals, yield = 69%. M.p. (°C): 160–161. IR (KBr): 3413 and 3339 (NH_2), 3241 (N–H), 1606 (C=N) cm^{-1}. ^1H NMR (300 MHz, DMSO-d_6): δ 5.30 (s, 2H, CH_2), 6.94 (dd, 2H, J = 6.90, 2.10 Hz, Ar–H), 7.17–7.23 (m, 2H, Ar–H), 7.48 (dd, 2H, J = 6.90, 2.10 Hz, Ar–H), 7.95–8.00 (m, 2H, Ar–H), 8.13 (s broad, 1H, NH_2), 8.47 (s broad, 1H, NH_2), 10.84 (s broad, 1H, NH). ^{13}C NMR (75.5 MHz, DMSO-d_6): δ 61.2 (CH_2), 112.8 (Cq Ar), 115.1 (CH Ar), 117.1 (CH Ar), 129.4 (CH Ar), 132.1 (CH Ar), 142.9 (C=N), 156.9 (C–O, Ar), 161.1 (Cq Ar), 164.4 (Cq Ar), 179.2 (C=S). Anal. Calcd. For $C_{15}H_{13}BrFN_3OS$: C, 47.13; H, 3.43; N, 10.99. Found: C, 47.61; H, 2.87; N, 10.80.

4.3.5. 2-(4-Bromophenoxy)-1-(4-chlorophenyl)ethan-1-one thiosemicarbazone (**8e**)

Recrystallization in toluene afforded colorless crystals, yield = 71%. M.p. (°C): 158–160. IR (KBr): 3413 and 3336 (NH_2), 3249 (N–H), 1597 (C=N) cm^{-1}. ^1H NMR (300 MHz, DMSO-d_6): δ 5.30 (s, 2H, CH_2), 6.94 (dd, 2H, J = 8.70, 1.80 Hz, Ar–H), 7.42 (dd, 2H, J = 8.70, 1.80 Hz, Ar–H), 7.48 (dd, 2H, J = 8.40, 1.80 Hz, Ar–H), 7.94 (dd, 2H, J = 8.40, 1.80 Hz, Ar–H), 8.15 (s broad, 1H, NH_2), 8.50 (s broad, 1H, NH_2), 10.88 (s broad, 1H, NH). ^{13}C NMR (75.5 MHz, DMSO-d_6): δ 61.0 (CH_2), 112.8 (Cq Ar), 117.1 (CH Ar), 128.2 (CH Ar), 128.9 (CH Ar), 132.1 (CH Ar), 133.9 (Cq Ar), 134.5 (Cq Ar), 142.6 (C=N), 156.9 (C–O, Ar), 179.3 (C=S). Anal. Calcd. For $C_{15}H_{13}BrClN_3OS$: C, 45.19; H, 3.29; N, 10.54. Found: C, 44.95; H, 2.83; N, 10.54.

4.3.6. 2-(4-Bromophenoxy)-1-(4-bromophenyl)ethan-1-one thiosemicarbazone (**8f**)

Recrystallization in toluene afforded colorless crystals, yield = 82%. M.p. (°C): 149–150. IR (KBr): 3415 and 3333 (NH_2), 3251 (N–H), 1597 (C=N) cm^{-1}. ^1H NMR (300 MHz, DMSO-d_6): δ 5.30 (s, 2H, CH_2), 6.94 (dd, 2H, J = 8.70, 1.50 Hz, Ar–H), 7.49 (dd, 2H, J = 8.70, 1.50 Hz, Ar–H), 7.57 (dd, 2H, J = 9.00, 1.80 Hz, Ar–H), 7.88 (dd, 2H, J = 9.00, 1.80 Hz, Ar–H), 8.16 (s broad, 1H, NH_2), 8.52 (s broad, 1H, NH_2), 10.90 (s broad, 1H, NH). ^{13}C NMR (75.5 MHz, DMSO-d_6): δ 61.0 (CH_2), 112.8 (Cq Ar), 117.1 (CH Ar), 122.8 (Cq Ar), 129.1 (CH Ar), 131.1 (CH Ar), 132.1 (CH Ar), 134.8 (Cq Ar), 142.7 (C=N), 156.9 (C–O, Ar), 179.3 (C=S). Anal. Calcd. For $C_{15}H_{13}Br_2N_3OS$: C, 40.65; H, 2.96; N, 9.48. Found: C, 41.09; H, 3.55; N, 9.11.

4.3.7. 1-([1,1′-Biphenyl]-4-yl)-2-(4-bromophenoxy)ethan-1-one thiosemicarbazone (**8g**)

Recrystallization in toluene afforded yellow crystals, yield = 70%. M.p. (°C): 127–128. IR (KBr): 3424 and 3330 (NH_2), 3236 (N–H), 1597 (C=N) cm^{-1}. ^1H NMR (300 MHz, DMSO-d_6): δ 5.36 (s, 2H, CH_2), 6.99 (d, 2H, J = 9.00 Hz, Ar–H), 7.38–7.51 (m, 5H, Ar–H), 7.67–7.72 (m, 4H, Ar–H), 8.02 (d, 2H, J = 8.70 Hz, Ar–H), 8.16 (s broad, 1H, NH_2), 8.51 (s broad, 1H, NH_2), 10.88 (s broad, 1H, NH). ^{13}C NMR (75.5 MHz, DMSO-d_6): δ 62.0 (CH_2), 112.3 (Cq Ar), 120.3 (CH Ar), 122.8 (CH Ar), 124.5 (CH Ar), 126.7 (CH Ar), 128.4 (CH Ar), 130.3 (CH Ar), 133.1 (CH Ar), 134.6 (Cq Ar), 138.5 (Cq Ar), 139.9 (Cq Ar), 143.9 (C=N), 157.1 (C–O, Ar), 179.6 (C=S). Anal. Calcd. For $C_{21}H_{18}BrN_3O$: C, 57.28; H, 4.12; N, 9.54. Found: C, 57.11; H, 3.75; N, 9.35.

4.3.8. 2-(4-Bromophenoxy)-1-(naphthalen-1-yl)ethan-1-one thiosemicarbazone (**8h**)

Recrystallization in toluene afforded yellow crystals, yield = 78%. M.p. (°C): 77–80. IR (KBr): 3417 and 3332 (NH_2), 3248 (N–H), 1610 (C=N) cm^{-1}. ^1H NMR (400 MHz, DMSO-d_6): δ 5.45 (s, 2H, CH_2), 7.58 (d, 2H, Ar–H), 7.48–7.54 (m, 4H, Ar–H), 7.88–7.96 (m, 3H, Ar–H), 8.24 (d, 2H, Ar–H), 8.40 (s broad, 1H, NH_2), 8.58 (s broad, 1H, NH_2), 10.88 (s broad, 1H, NH). ^{13}C NMR (100 MHz, DMSO-d_6): δ 61.7 (CH_2), 113.3 (Cq Ar), 117.7 (CH Ar), 124.9 (CH Ar), 126.8 (CH Ar), 127.2 (CH Ar), 127.3 (CH Ar), 127.9 (CH Ar), 128.1 (CH Ar), 129.0 (CH Ar), 132.6 (CH Ar), 133.1 (Cq Ar), 133.5 (Cq Ar), 133.7 (Cq Ar), 143.9 (C=N), 157.5 (C–O, Ar), 179.6 (C=S). Anal. Calcd. For $C_{19}H_{16}BrN_3OS$: C, 55.08; H, 3.89; N, 10.14. Found: C, 54.80; H, 4.07; N, 10.01.

4.3.9. 2-(4-Bromophenoxy)-1-(4-methoxyphenyl)ethan-1-one N-methyl thiosemicarbazone (**8i**)

Recrystallization in toluene afforded yellow crystals, yield = 80%. M.p. (°C): 143–146. IR (KBr): 3332 (N–H), 3254 (N–H), 1554 (C=N) cm^{-1}. ^1H NMR (400 MHz, DMSO-d_6): δ 3.05 (d, 3H, J = 4.39 Hz, CH_3), 3.79 (s, 3H, OCH_3), 5.28 (s, 2H, CH_2), 6.94 (d, 2H, J = 8.39 Hz, Ar–H), 6.94 (d, 2H, J = 8.79 Hz, Ar–H), 7.47 (d, 2H, J = 8.79 Hz, Ar–H), 7.87 (d, 2H, J = 8.39 Hz, Ar–H), 8.62 (q, 1H, J = 4.39 Hz, NH), 10.73 (s broad, 1H, NH). ^{13}C NMR (100 MHz, DMSO-d_6): δ 31.1 (CH_3), 55.2 (OCH_3), 61.4 (CH_2), 112.7 (Cq Ar), 113.6 (CH Ar), 117.1 (CH Ar), 128.0 (Cq Ar), 128.6 (CH Ar), 132.1 (CH Ar), 143.4 (C=N), 156.9 (C–O, Ar), 160.2 (Cq Ar), 178.5 (C=S). Anal. Calcd. For $C_{17}H_{18}BrN_3O_2S$: C, 50.01; H, 4.44; N, 10.29. Found: C, 54.80; H, 4.57; N, 10.01.

4.3.10. 2-(4-Bromophenoxy)-1-(4-methoxyphenyl)ethan-1-one N-phenyl thiosemicarbazone (**8j**)

Recrystallization in toluene afforded colorless crystals, yield = 79%. M.p. (°C): 159–162. IR (KBr): 3255 (N–H), 3210 (N–H), 1550 (C=N) cm^{-1}. ^1H NMR (400 MHz, DMSO-d_6): δ 3.79 (s, 3H, CH_3), 5.36 (s, 2H, CH_2), 6.95 (d, 2H, J = 8.79 Hz, Ar–H), 6.99 (d, 2H, J = 8.39 Hz, Ar–H), 7.22 (t, 1H, J = 7.19 Hz, Ar–H), 7.38 (dd, 2H, J = 7.99, 7.19 Hz, Ar–H), 7.50 (d, 2H, J = 8.79 Hz, Ar–H), 7.57 (d, 2H, J = 7.99 Hz, Ar–H), 7.96 (d, 2H, J = 8.39 Hz, Ar–H), 10.14 (s broad, 1H, NH), 11.05 (s broad, 1H, NH–Ar). ^{13}C NMR (100 MHz, DMSO-d_6): δ 55.2 (CH_2), 61.6 (CH_2), 112.8 (Cq Ar), 113.7 (CH Ar), 117.2 (CH Ar), 125.4 (CH Ar), 125.9 (CH Ar), 127.8 (Cq Ar), 128.1 (CH Ar), 128.9 (CH

Ar), 132.1 (CH Ar), 139.0 (C–NH, Ar), 144.6 (C=N), 156.9 (C–O, Ar), 160.4 (Cq Ar), 176.9 (C=S). Anal. Calcd. For $C_{22}H_{20}BrN_3O_2S$: C, 56.18; H, 4.29; N, 8.93. Found: C, 59.88; H, 4.49; N, 9.05.

4.3.11. 2-(4-Bromophenoxy)-1-(4-fluorophenyl)ethan-1-one N-methyl thiosemicarbazone (**8k**)

Recrystallization in toluene afforded colorless crystals, yield = 83%. M.p. (°C): 128–130. IR (KBr): 3345 (N–H), 3249 (N–H), 1561 (C=N) cm^{-1}. ^1H NMR (400 MHz, DMSO-d_6): δ 3.05 (d, 3H, J = 4.39 Hz, CH_3), 5.30 (s, 2H, CH_2), 6.93 (d, 2H, J = 8.79 Hz, Ar–H), 7.22 (dd, 2H, J = 7.99, 5.59 Hz, Ar–H), 7.47 (d, 2H, J = 8.79 Hz, Ar–H), 7.96 (dd, 2H, J = 7.99, 5.59 Hz, Ar–H), 8.62 (q, 1H, J = 4.39 Hz, NH), 10.87 (s broad, 1H, NH). ^{13}C NMR (100 MHz, DMSO-d_6): δ 31.2 (CH_3), 61.3 (CH_2), 112.8 (Cq Ar), 115.1 (CH Ar), 117.1 (CH Ar), 129.3 (CH Ar), 132.1 (CH Ar), 142.7 (C=N), 156.9 (C–O, Ar), 161.5 (Cq Ar), 163.9 (Cq Ar), 178.7 (C=S). Anal. Calcd. For $C_{16}H_{15}BrFN_3OS$: C, 48.50; H, 3.82; N, 10.60. Found: C, 48.78; H, 3.94; N, 10.25.

4.3.12. 2-(4-Bromophenoxy)-1-(4-fluorophenyl)ethan-1-one N-phenyl thiosemicarbazone (**8l**)

Recrystallization in toluene afforded colorless crystals, yield = 82%. M.p. (°C): 174–175. IR (KBr): 3284 (N–H), 3238 (N–H), 1552 (C=N) cm^{-1}. ^1H NMR (400 MHz, DMSO-d_6): δ 5.38 (s, 2H, CH_2), 6.98 (d, 2H, J = 8.39 Hz, Ar–H), 7.23 (dd, 2H, J = 8.79, 6.79 Hz, Ar–H), 7.24 (t, 1H, J = 6.79 Hz, Ar–H), 7.39 (dd, 2H, J = 8.39, 5.19 Hz, Ar–H), 7.50 (d, 2H, J = 8.39 Hz, Ar–H), 7.55 (d, 2H, J = 8.79 Hz, Ar–H), 8.06 (dd, 2H, J = 8.39, 5.19 Hz, Ar–H), 10.21 (s broad, 1H, NH), 11.18 (s broad, 1H, NH–Ar). ^{13}C NMR (100 MHz, DMSO-d_6): δ 61.6 (CH_2), 112.8 (Cq Ar), 115.1 (CH Ar), 117.1 (CH Ar), 125.5 (CH Ar), 126.1 (CH Ar), 128.1 (CH Ar), 129.7 (CH Ar), 132.1 (CH Ar), 139.0 (C–NH, Ar), 143.7 (C=N), 156.9 (C–O, Ar), 161.6 (Cq Ar), 164.1 (Cq Ar), 177.3 (C=S). Anal. Calcd. For $C_{21}H_{17}BrFN_3OS$: C, 55.03; H, 3.74; N, 9.17. Found: C, 55.38; H, 3.49; N, 9.15.

4.3.13. 1-(4-Bromophenyl)-2-phenoxyethan-1-one thiosemicarbazone (**9a**)

Recrystallization in toluene afforded yellow crystals, yield = 87%. M.p. (°C): 173–176. IR (KBr): 3419 and 3371 (NH_2), 3249 (N–H), 1609 (C=N) cm^{-1}. ^1H NMR (400 MHz, DMSO-d_6): δ 5.31 (s, 2H, CH_2), 6.93–6.99 (m, 3H, Ar–H), 7.29–7.34 (m, 2H, Ar–H), 7.56 (d, 2H, J = 8.79 Hz, Ar–H), 7.89 (d, 2H, J = 8.79 Hz, Ar–H), 8.15 (s broad, 1H, NH_2), 8.51 (s broad, 1H, NH_2), 10.87 (s broad, 1H, NH). ^{13}C NMR (100 MHz, DMSO-d_6): δ 60.9 (CH_2), 114.7 (CH Ar), 121.3 (CH Ar), 122.7 (Cq Ar), 129.1 (CH Ar), 129.4 (CH Ar), 131.1 (CH Ar), 134.9 (Cq Ar), 143.2 (C=N), 157.5 (C–O, Ar), 179.2 (C=S). Anal. Calcd. For $C_{15}H_{14}BrN_3OS$: C, 49.46; H, 3.87; N, 11.54. Found: C, 49.36; H, 3.91; N, 11.66.

4.3.14. 1-(4-Bromophenyl)-2-(4-ethylphenoxy)ethan-1-one thiosemicarbazone (**9b**)

Recrystallization in toluene afforded yellow crystals, yield = 72%. M.p. (°C): 142–144. IR (KBr): 3419 and 3369 (NH_2), 3248 (N–H), 1610 (C=N) cm^{-1}. ^1H NMR (400 MHz, DMSO-d_6): δ 1.13 (t, 3H, J = 7.59 Hz, CH_3), 2.53 (q, 2H, J = 7.59 Hz, CH_2), 5.27 (s, 2H, CH_2), 6.87 (d, 2H, J = 8.39 Hz, Ar–H), 7.13 (d, 2H, J = 8.39 Hz, Ar–H), 7.56 (d, 2H, J = 8.79 Hz, Ar–H), 7.89 (d, 2H, J = 8.79 Hz, Ar–H), 8.15 (s broad, 1H, NH_2), 8.51 (s broad, 1H, NH_2), 10.83 (s broad, 1H, NH). ^{13}C NMR (100 MHz, DMSO-d_6): δ 15.9 (CH_3), 33.8 (CH_2), 61.1 (O–CH_2), 114.6 (CH Ar), 122.7 (Cq Ar), 128.6 (CH Ar), 129.1 (CH Ar), 131.1 (CH Ar), 134.9 (Cq Ar), 136.7 (Cq Ar), 143.3 (C=N), 155.5 (C–O, Ar), 179.1 (C=S). Anal. Calcd. For $C_{17}H_{18}BrN_3OS$: C, 52.05; H, 4.62; N, 10.71. Found: C, 51.57; H, 5.00; N, 10.80.

4.3.15. 1-(4-Bromophenyl)-2-(4-isopropylphenoxy)ethan-1-one thiosemicarbazone (**9c**)

Recrystallization in toluene and posteriorly in ethanol (80%) afforded colorless crystals, yield = 77%. M.p. (°C): 175–177. IR (KBr): 3419 and 3337 (NH_2), 3250 (N–H), 1611 (C=N) cm^{-1}. ^1H NMR (400 MHz, DMSO-d_6): δ 1.16 (d, 6H, J = 6.80 Hz, CH_3), 2.83 (m, 1H, J = 6.80 Hz, CH), 5.27 (s, 2H, CH_2), 6.88 (d, 2H, J = 8.39 Hz, Ar–H), 7.16 (d, 2H, J = 8.39 Hz, Ar–H), 7.56 (d, 2H, J = 8.79 Hz, Ar–H), 7.90 (d, 2H, J = 8.79 Hz, Ar–H), 8.17 (s broad, 1H, NH_2), 8.52 (s broad, 1H, NH_2), 10.85 (s broad, 1H, NH). ^{13}C NMR (100 MHz, DMSO-d_6): δ 24.9 (CH_3), 32.6 (CH), 61.0 (CH_2), 114.6 (CH Ar), 122.8 (Cq Ar), 127.1 (CH Ar), 129.2 (CH Ar), 131.1 (CH Ar), 134.9 (Cq Ar), 141.4 (Cq Ar), 143.3 (C=N), 155.6 (C–O, Ar), 179.1 (C=S). Anal. Calcd. For $C_{18}H_{20}BrN_3OS$: C, 53.21; H, 4.96; N, 10.34. Found: C, 52.85; H, 5.07; N, 10.36.

4.3.16. 1-(4-Bromophenyl)-2-(4-(tert-butyl)phenoxy)ethan-1-one thiosemicarbazone (**9d**)

Recrystallization in toluene and posteriorly in ethanol (80%) afforded colorless crystals, yield = 73%. M.p. (°C): 176–177. IR (KBr): 3421 and 3330 (NH_2), 3251 (N–H), 1610 (C=N) cm^{-1}. ^1H NMR (400 MHz, DMSO-d_6): δ 1.24 (s, 9H, CH_3), 5.27 (s, 2H, CH_2), 6.88 (d, 2H, J = 8.39 Hz, Ar–H), 7.31 (d, 2H, J = 8.39 Hz, Ar–H), 7.56 (d, 2H, J = 8.79 Hz, Ar–H), 7.90 (d, 2H, J = 8.79 Hz, Ar–H), 8.17 (s broad, 1H, NH_2), 8.53 (s broad, 1H, NH_2), 10.85 (s broad, 1H, NH). ^{13}C NMR (100 MHz, DMSO-d_6): δ 31.3 (CH_3), 33.8 [$\underline{C}$ (CH_3)], 60.9 (CH_2), 114.2 (CH Ar), 122.8 (Cq Ar), 126.1 (CH Ar), 129.2 (CH Ar), 131.1 (CH Ar), 134.9 (Cq Ar), 143.3 (C=N), 143.6 (Cq Ar), 155.3 (C–O, Ar), 179.2 (C=S). Anal. Calcd. For $C_{19}H_{22}BrN_3OS$: C, 54.29; H, 5.28; N, 10.00. Found: C, 53.98; H, 5.54; N, 9.94.

4.3.17. 1-(4-Bromophenyl)-2-(3-methoxyphenoxy)ethan-1-one thiosemicarbazone (**9e**)

Recrystallization in toluene and posteriorly in ethanol (80%) afforded yellow crystals, yield = 80%. M.p. (°C): 186–187. IR (KBr): 3384 and 3333 (NH_2), 3261 (N–H), 1596 (C=N) cm^{-1}. ^1H NMR (400 MHz, DMSO-d_6): δ 3.71 (s, 3H, CH_3), 5.30 (s, 2H, CH_2), 6.53 (d, 2H, J = 8.39 Hz, Ar–H), 6.56 (s, 1H, Ar–H), 7.19 (t, 1H, J = 8.39 Hz, Ar–H), 7.57 (d, 2H, J = 8.39 Hz, Ar–H), 7.90 (d, 2H, J = 8.39 Hz, Ar–H), 8.17 (s broad, 1H, NH_2), 8.53 (s broad, 1H, NH_2), 10.87 (s broad, 1H, NH). ^{13}C NMR (100 MHz, DMSO-d_6): δ 55.1 (CH_3), 60.9 (CH_2), 100.9 (CH Ar), 107.1 (CH Ar), 122.8 (Cq Ar), 129.2 (CH Ar), 129.9 (CH Ar), 131.1 (CH Ar), 132.7 (CH Ar), 134.8 (Cq Ar), 143.2 (C=N), 158.7 (C–O, Ar), 160.4 ($\underline{C}$ Ar–OCH_3), 179.2 (C=S). Anal. Calcd. For $C_{16}H_{16}BrN_3O_2S$: C, 48.74; H, 4.09; N, 10.66. Found: C, 48.13; H, 4.24; N, 10.88.

4.3.18. 1-(4-Bromophenyl)-2-(4-methoxyphenoxy)ethan-1-one thiosemicarbazone (**9f**)

Recrystallization in toluene and posteriorly in ethanol (80%) afforded colorless crystals, yield = 78%. M.p. (°C): 161. IR (KBr): 3417 and 3327 (NH_2), 3254 (N–H), 1611 (C=N) cm^{-1}. ^1H NMR (400 MHz, DMSO-d_6): δ 3.69 (s, 3H, CH_3), 5.25 (s, 2H, CH_2), 6.86 (d, 2H, J = 9.20 Hz, Ar–H), 6.90 (d, 2H, J = 9.20 Hz, Ar–H), 7.56 (d, 2H, J = 8.39 Hz, Ar–H), 7.89 (d, 2H, J = 8.39 Hz, Ar–H), 8.16 (s broad, 1H, NH_2), 10.81 (s broad, 1H, NH); 8.52 (s broad, 1H, NH_2). ^{13}C NMR (100 MHz, DMSO-d_6): δ 55.4 (CH_3), 61.7 (CH_2), 114.6 (CH Ar), 115.8 (CH Ar), 122.8 (Cq Ar), 129.2 (CH Ar), 131.1 (CH Ar), 134.9 (Cq Ar), 143.4 (C=N), 151.4 ($\underline{C}$ Ar–OCH_3), 154.0 (C–O, Ar), 179.1 (C=S). Anal. Calcd. For $C_{16}H_{16}BrN_3O_2S$: C, 48.74; H, 4.09; N, 10.66. Found: C, 48.42; H, 4.36; N, 10.66.

4.3.19. N-(4-(2-(4-Bromophenyl)-2-oxoethoxy)phenyl)acetamide thiosemicarbazone (**9g**)

Recrystallization in toluene afforded colorless crystals, yield = 69%. M.p. (°C): 187–190. IR (KBr): 3424 and 3368 (NH_2),

3263 (N–H), 1616 (C=N) cm^{-1}. ^1H NMR (400 MHz, DMSO-d_6): δ 2.00 (s, 3H, CH_3), 5.26 (s, 2H, CH_2), 6.89 (d, 2H, J = 8.39 Hz, Ar–H), 7.49 (d, 2H, J = 8.39 Hz, Ar–H), 7.56 (d, 2H, J = 7.99 Hz, Ar–H), 7.88 (d, 2H, J = 7.99 Hz, Ar–H), 8.16 (s largo, 1H, NH_2), 8.52 (s broad, 1H, NH_2), 9.90 (s broad, 1H, NH), 10.84 (s broad, 1H, N–NH). ^{13}C NMR (100 MHz, DMSO-d_6): δ 23.8 (CH_3), 61.2 (CH_2), 114.9 (CH Ar), 120.3 (CH Ar), 122.8 (Cq Ar), 129.2 (CH Ar), 131.1 (CH Ar), 133.4 (Cq Ar), 134.9 (Cq Ar), 143.3 (C=N), 153.1 (C–O, Ar), 167.8 (C=O), 179.2 (C=S). Anal. Calcd. For $C_{17}H_{17}BrN_4O_2S$: C, 48.46; H, 4.07; N, 13.30. Found: C, 48.10; H, 3.84; N, 12.83.

4.3.20. 1-(4-Bromophenyl)-2-(4-fluorophenoxy)ethan-1-one thiosemicarbazone (**9h**)

Recrystallization in toluene and posteriorly in ethanol (80%) afforded yellow crystals, yield = 71%. M.p. (°C): 156–158. IR (KBr): 3431 and 3348 (NH_2), 3254 (N–H), 1607 (C=N) cm^{-1}. ^1H NMR (400 MHz, DMSO-d_6): δ 5.30 (s, 2H, CH_2), 6.98–7.01 (m, 2H, Ar–H), 7.11–7.16 (m, 2H, Ar–H), 7.56 (dd, 2H, J = 8.39, 2.00 Hz, Ar–H), 7.87 (dd, 2H, J = 8.39, 2.00 Hz, Ar–H), 8.05 (s broad, 1H, NH_2), 8.39 (s broad, 1H, NH_2), 10.74 (s broad, 1H, NH). ^{13}C NMR (100 MHz, DMSO-d_6): δ 61.8 (CH_2), 115.6 (CH Ar), 116.2 (CH Ar), 122.5 (Cq Ar), 128.9 (CH Ar), 130.9 (CH Ar), 134.7 (Cq Ar), 142.9 (C=N), 153.7 (Cq Ar), 158.0 (C–O, Ar), 179.2 (C=S). Anal. Calcd. For $C_{15}H_{13}BrFN_3OS$: C, 47.13; H, 3.43; N, 10.99. Found: C, 47.09; H, 3.13; N, 11.20.

4.3.21. 1-(4-Bromophenyl)-2-(3-chloro-4-fluorophenoxy)ethan-1-one thiosemicarbazone (**9i**)

Recrystallization in toluene afforded yellow crystals, yield = 74%. M.p. (°C): 129–130. IR (KBr): 3463 and 3341 (NH_2), 3219 (N–H), 1596 (C=N) cm^{-1}. ^1H NMR (400 MHz, DMSO-d_6): δ 5.31 (s, 2H, CH_2), 6.94–6.98 (m, 1H, Ar–H), 7.23–7.25 (m, 1H, Ar–H), 7.32–7.37 (m, 1H, Ar–H), 7.57 (d, 2H, J = 8.79 Hz, Ar–H), 7.87 (d, 2H, J = 8.79 Hz, Ar–H), 8.06 (s broad, 1H, NH_2), 8.39 (s broad, 1H, NH_2), 10.78 (s broad, 1H, NH). ^{13}C NMR (100 MHz, DMSO-d_6): δ 61.7 (CH_2), 115.5 (CH Ar), 116.4 (CH Ar), 117.0 (CH Ar), 122.6 (Cq Ar), 128.9 (CH Ar), 130.9 (CH Ar), 134.7 (Cq Ar), 142.3 (C=N), 150.9 (Cq Ar), 153.3 (Cq Ar), 154.0 (C–O, Ar), 179.3 (C=S). Anal. Calcd. For $C_{15}H_{12}BrClFN_3OS$: C, 43.24; H, 2.90; N, 10.08. Found: C, 42.94; H, 2.97; N, 9.91.

4.3.22. 1-(4-Bromophenyl)-2-(2-chlorophenoxy)ethan-1-one thiosemicarbazone (**9j**)

Recrystallization in toluene afforded colorless crystals, yield = 75%. M.p. (°C): 159–162. IR (KBr): 3420 and 3350 (NH_2), 3256 (N–H), 1600 (C=N) cm^{-1}. ^1H NMR (400 MHz, DMSO-d_6): δ 5.37 (s, 2H, CH_2), 7.00 (t, 1H, J = 7.99 Hz, Ar–H), 7.24 (d, 1H, 7.59 Hz, Ar–H), 7.35 (t, 1H, J = 7.59 Hz, Ar–H), 7.42 (d, 1H, J = 7.99 Hz, Ar–H), 7.57 (d, 2H, J = 8.79 Hz, Ar–H), 7.91 (d, 2H, J = 8.79 Hz, Ar–H), 8.19 (s broad, 1H, NH_2), 8.54 (s broad, 1H, NH_2), 10.96 (s broad, 1H, NH). ^{13}C NMR (100 MHz, DMSO-d_6): δ 62.1 (CH_2), 114.4 (CH Ar), 121.5 (Cq Ar), 122.2 (CH Ar), 122.6 (Cq Ar), 127.9 (CH Ar), 129.0 (CH Ar), 129.7 (CH Ar), 130.9 (CH Ar), 134.8 (Cq Ar), 142.3 (C=N), 152.8 (C–O, Ar), 179.3 (C=S). Anal. Calcd. For $C_{15}H_{13}BrClN_3OS$: C, 45.19; H, 3.29; N, 10.54. Found: C, 45.24; H, 3.13; N, 10.55.

4.3.23. 1-(4-Bromophenyl)-2-(3-chlorophenoxy)ethan-1-one thiosemicarbazone (**9k**)

Recrystallization in toluene afforded colorless crystals, yield = 83%. M.p. (°C): 171. IR (KBr): 3418 and 3346 (NH_2), 3247 (N–H), 1610 (C=N) cm^{-1}. ^1H NMR (400 MHz, DMSO-d_6): δ 5.32 (s, 2H, CH_2), 6.92 (d, 1H, J = 7.99 Hz, Ar–H), 7.05 (d, 1H, J = 6.79 Hz, Ar–H), 7.09 (s, 1H, Ar–H), 7.33 (dd, 1H, J = 7.99, 6.79 Hz, Ar–H), 7.56 (d, 2H, J = 8.39 Hz, Ar–H), 7.89 (d, 2H, J = 8.39 Hz, Ar–H), 8.16 (s broad, 1H, NH_2), 8.51 (s broad, 1H, NH_2), 10.93 (s broad, 1H, NH). ^{13}C NMR (100 MHz, DMSO-d_6): δ 60.9 (CH_2), 114.1 (CH Ar), 114.7 (CH Ar), 121.1 (CH Ar), 122.8 (Cq Ar), 129.2 (CH Ar), 130.8 (CH Ar), 131.1 (CH Ar), 131.1 (CH Ar), 133.6 (Cq Ar), 134.9 (Cq Ar), 143.5 (C=N), 158.6 (C–O, Ar), 179.3 (C=S). Anal. Calcd. For $C_{15}H_{13}BrClN_3OS$: C, 45.19; H, 3.29; N, 10.54. Found: C, 44.98; H, 3.40; N, 10.89.

4.3.24. 1-(4-Bromophenyl)-2-(4-chlorophenoxy)ethan-1-one thiosemicarbazone (**9l**)

Recrystallization in toluene afforded colorless crystals, yield = 81%. M.p. (°C): 107–110. IR (KBr): 3420 and 3341 (NH_2), 3252 (N–H), 1609 (C=N) cm^{-1}. ^1H NMR (400 MHz, DMSO-d_6): δ 5.30 (s, 2H, CH_2), 6.97 (d, 2H, J = 8.39 Hz, Ar–H), 7.36 (d, 2H, J = 8.39 Hz, Ar–H), 7.56 (d, 2H, J = 8.39 Hz, Ar–H), 7.88 (d, 2H, J = 8.39 Hz, Ar–H), 8.17 (s broad, 1H, NH_2), 8.53 (s broad, 1H, NH_2), 10.91 (s broad, 1H, NH). ^{13}C NMR (100 MHz, DMSO-d_6): δ 61.0 (CH_2), 116.6 (CH Ar), 122.8 (Cq Ar), 125.3 (CH Ar), 129.2 (CH Ar), 131.1 (CH Ar), 134.8 (Cq Ar), 142.7 (C=N), 156.5 (C–O, Ar), 179.2 (C=S). Anal. Calcd. For $C_{15}H_{13}BrClN_3OS$: C, 45.19; H, 3.29; N, 10.54. Found: C, 45.59; H, 3.60; N, 10.17.

4.3.25. 1-(4-Bromophenyl)-2-(2,3-dichlorophenoxy)ethan-1-one thiosemicarbazone (**9m**)

Recrystallization in toluene and posteriorly in ethanol (80%) afforded colorless crystals, yield = 79%. M.p. (°C): 172–173. IR (KBr): 3417 and 3327 (NH_2), 3265 (N–H), 1594 (C=N) cm^{-1}. ^1H NMR (400 MHz, DMSO-d_6): δ 5.40 (s, 2H, CH_2), 7.24 (d, 1H, J = 8.39 Hz, Ar–H), 7.26 (d, 1H, J = 8.39 Hz, Ar–H), 7.38 (t, 1H, J = 8.39 Hz, Ar–H), 7.56 (d, 2H, J = 7.59 Hz, Ar–H), 7.91 (d, 2H, J = 7.59 Hz, Ar–H), 8.19 (s broad, 1H, NH_2), 8.53 (s broad, 1H, NH_2), 11.00 (s broad, 1H, NH). ^{13}C NMR (100 MHz, DMSO-d_6): δ 62.0 (CH_2), 112.8 (CH Ar), 120.1 (Cq Ar), 122.6 (CH Ar), 122.8 (Cq Ar), 128.3 (CH Ar), 129.2 (CH Ar), 131.1 (CH Ar), 132.2 (Cq Ar), 134.7 (Cq Ar), 141.8 (C=N), 154.6 (C–O, Ar), 179.3 (C=S). Anal. Calcd. For $C_{15}H_{12}BrCl_2N_3OS$: C, 41.59; H, 2.79; N, 9.70. Found: C, 41.34; H, 2.28; N, 9.69.

4.3.26. 1-(4-Bromophenyl)-2-(3,4-dichlorophenoxy)ethan-1-one thiosemicarbazone (**9n**)

Recrystallization in toluene and posteriorly in ethanol (80%) afforded colorless crystals, yield = 76%. M.p. (°C): 162–165. IR (KBr): 3474 and 3352 (NH_2), 3167 (N–H), 1590 (C=N) cm^{-1}. ^1H NMR (400 MHz, DMSO-d_6): δ 5.32 (s, 2H, CH_2), 6.97 (dd, 1H, J = 2.80 Hz, J = 8.79 Hz, Ar–H), 7.30 (d, 1H, J = 2.80 Hz, Ar–H), 7.56 (d, 1H, J = 8.79 Hz, Ar–H), 7.57 (d, 2H, J = 8.39 Hz, Ar–H), 7.89 (d, 2H, J = 8.39 Hz, Ar–H), 8.18 (s broad, 1H, NH_2), 8.53 (s broad, 1H, NH_2), 10.96 (s broad, 1H, NH). ^{13}C NMR (100 MHz, DMSO-d_6): δ 61.1 (CH_2), 116.1 (CH Ar), 116.7 (CH Ar), 122.8 (Cq Ar), 123.1 (Cq Ar), 129.2 (CH Ar), 130.9 (CH Ar), 131.2 (CH Ar), 131.5 (Cq Ar), 134.8 (Cq Ar), 142.1 (C=N), 157.2 (C–O, Ar), 179.3 (C=S). Anal. Calcd. For $C_{15}H_{12}BrCl_2N_3OS$: C, 41.59; H, 2.79; N, 9.70. Found: C, 41.62; H, 2.76; N, 9.63.

4.3.27. 2-(3-Bromophenoxy)-1-(4-bromophenyl)ethan-1-one thiosemicarbazone (**9o**)

Recrystallization in toluene afforded colorless crystals, yield = 90%. M.p. (°C): 183. IR (KBr): 3417 and 3319 (NH_2), 3222 (N–H), 1603 (C=N) cm^{-1}. ^1H NMR (400 MHz, DMSO-d_6): δ 5.02 (s, 2H, CH_2), 6.98 (d, 1H, J = 7.99 Hz, Ar–H), 7.12 (d, 1H, J = 7.99 Hz, Ar–H), 7.18 (s, 1H, Ar–H), 7.22 (t, 1H, J = 7.99 Hz, Ar–H), 7.33 (d, 2H, J = 8.39 Hz, Ar–H), 7.70 (d, 2H, J = 8.39 Hz, Ar–H), 8.09 (s broad, 1H, NH_2), 8.48 (s broad, 1H, NH_2), 9.73 (s broad, 1H, NH). ^{13}C NMR (100 MHz, DMSO-d_6): δ 60.8 (CH_2), 114.4 (CH Ar), 117.7 (CH Ar), 122.0 (Cq Ar), 123.2 (Cq Ar), 124.1 (CH Ar), 130.0 (CH Ar), 130.5 (Cq Ar), 131.2 (CH Ar), 132.1 (CH Ar), 134.8 (Cq Ar), 142.4 (C=N), 158.6 (C–O, Ar), 179.2 (C=S). Anal. Calcd. For $C_{15}H_{13}Br_2N_3OS$: C, 40.65; H,

2.96; N, 9.48. Found: C, 40.72; H, 2.86; N, 9.39.

4.3.28. 1-(4-Bromophenyl)-2-(4-iodophenoxy)ethan-1-one thiosemicarbazone (**9p**)

Recrystallization in toluene afforded colorless crystals, yield = 78%. M.p. (°C): 181–183. IR (KBr): 3417 and 3325 (NH_2), 3252 (N–H), 1605 (C=N) cm^{-1}. ^1H NMR (400 MHz, DMSO-d_6): δ 5.28 (s, 2H, CH_2), 6.80 (d, 2H, J = 8.79 Hz, Ar–H), 7.56 (d, 2H, J = 8.39 Hz, Ar–H), 7.62 (d, 2H, J = 8.79 Hz, Ar–H), 7.87 (d, 2H, J = 8.39 Hz, Ar–H), 8.16 (s broad, 1H, NH_2), 8.52 (s broad, 1H, NH_2), 10.90 (s broad, 1H, NH). ^{13}C NMR (100 MHz, DMSO-d_6): δ 60.8 (CH_2), 84.1 (Cq Ar), 117.6 (CH Ar), 122.8 (Cq Ar), 129.2 (CH Ar), 131.1 (CH Ar), 134.8 (Cq Ar), 137.9 (CH Ar), 142.8 (C=N), 157.5 (C–O, Ar), 179.2 (C=S). Anal. Calcd. For $C_{15}H_{13}BrIN_3OS$: C, 36.76; H, 2.67; N, 8.57. Found: C, 36.22; H, 2.26; N, 8.47.

4.3.29. 2-([1,1′-Biphenyl]-3-yloxy)-1-(4-bromophenyl)ethan-1-one thiosemicarbazone (**9q**)

Recrystallization in toluene afforded colorless crystals, yield = 70%. M.p. (°C): 161–163. IR (KBr): 3419 and 3337 (NH_2), 3294 (N–H), 1605 (C=N) cm^{-1}. ^1H NMR (400 MHz, DMSO-d_6): δ 5.02 (s, 2H, CH_2), 6.98 (d, 1H, J = 7.99 Hz, Ar–H), 7.12 (d, 1H, J = 7.99 Hz, Ar–H), 7.18 (s, 1H, Ar–H), 7.58 (d, 2H, J = 8.39 Hz, Ar–H), 7.64 (d, 2H, J = 7.19 Hz, Ar–H), 7.95 (d, 2H, J = 8.39 Hz, Ar–H), 8.20 (s broad, 1H, NH_2), 8.55 (s broad, 1H, NH_2), 10.93 (s broad, 1H, NH). ^{13}C NMR (100 MHz, DMSO-d_6): δ 60.8 (CH_2), 112.7 (CH Ar), 114.3 (CH Ar), 119.7 (CH Ar), 122.8 (Cq Ar), 126.7 (CH Ar), 127.6 (CH Ar), 128.9 (CH Ar), 129.2 (CH Ar), 130.0 (CH Ar), 131.1 (CH Ar), 134.9 (Cq Ar), 139.8 (Cq Ar), 139.8 (Cq Ar), 141.6 (Cq Ar), 143.2 (C=N), 157.9 (C–O, Ar), 179.3 (C=S). Anal. Calcd. For $C_{21}H_{18}BrN_3OS$: C, 57.28; H, 4.12; N, 9.54. Found: C, 56.91; H, 4.27; N, 9.60.

4.3.30. 2-([1,1′-Biphenyl]-4-yloxy)-1-(4-bromophenyl)ethan-1-one thiosemicarbazone (**9r**)

Recrystallization in toluene afforded colorless crystals, yield = 84%. M.p. (°C): 208–210. IR (KBr): 3419 and 3347 (NH_2), 3294 (N–H), 1608 (C=N) cm^{-1}. ^1H NMR (400 MHz, DMSO-d_6): δ 5.36 (s, 2H, CH_2), 7.05 (d, 2H, J = 8.39 Hz, Ar–H), 7.31 (t, 1H, J = 7.19 Hz, Ar–H), 7.42 (dd, 2H, J = 8.39, 7.19 Hz, Ar–H), 7.58 (d, 2H, J = 8.39 Hz, Ar–H), 7.59 (d, 2H, J = 7.99 Hz, Ar–H), 7.62 (d, 2H, J = 8.39 Hz, Ar–H), 7.92 (d, 2H, J = 7.99 Hz, Ar–H), 8.19 (s largo, 1H, NH_2), 8.54 (s broad, 1H, NH_2), 10.93 (s broad, 1H, NH). ^{13}C NMR (100 MHz, DMSO-d_6): δ 61.4 (CH_2), 115.7 (CH Ar), 123.2 (Cq Ar), 126.7 (CH Ar), 127.3 (CH Ar), 128.2 (CH Ar), 129.3 (CH Ar), 129.6 (CH Ar), 131.6 (CH Ar), 133.8 (Cq Ar), 135.3 (Cq Ar), 140.1 (Cq Ar), 143.5 (C=N), 157.6 (C–O, Ar), 179.7 (C=S). Anal. Calcd. For $C_{21}H_{18}BrN_3OS$: C, 57.28; H, 4.12; N, 9.54. Found: C, 57.81; H, 4.28; N, 9.43.

4.3.31. 1-(4-Bromophenyl)-2-(naphthalen-1-yloxy)ethan-1-one thiosemicarbazone (**9s**)

Recrystallization in toluene afforded beige crystals, yield = 85%. M.p. (°C): 208–210. IR (KBr): 3422 and 3334 (NH_2), 3244 (N–H), 1605 (C=N) cm^{-1}. ^1H NMR (400 MHz, DMSO-d_6): δ 5.50 (s, 2H, CH_2), 7.07 (d, 1H, J = 7.59 Hz, Ar–H), 7.41–7.58 (m, 6H, Ar–H), 7.86–7.97 (m, 4H, Ar–H), 8.20 (s broad, 1H, NH_2), 8.53 (s broad, 1H, NH_2), 11.02 (s broad, 1H, NH). ^{13}C NMR (100 MHz, DMSO-d_6): δ 61.2 (CH_2), 105.8 (CH Ar), 120.6 (CH Ar), 121.3 (CH Ar), 122.7 (Cq Ar), 124.7 (Cq Ar), 125.5 (CH Ar), 125.9 (CH Ar), 126.5 (CH Ar), 127.4 (CH Ar), 129.3 (CH Ar), 131.1 (CH Ar), 133.9 (Cq Ar), 134.9 (Cq Ar), 143.4 (C=N), 153.0 (C–O, Ar), 179.3 (C=S). Anal. Calcd. For $C_{19}H_{16}BrN_3OS$: C, 55.08; H, 3.89; N, 10.14. Found: C, 55.50; H, 3.38; N, 10.38.

4.3.32. 1-(4-Bromophenyl)-2-(naphthalen-2-yloxy)ethan-1-one thiosemicarbazone (**9t**)

Recrystallization in toluene afforded colorless crystals, yield = 83%. M.p. (°C): 185. IR (KBr): 3426 and 3335 (NH_2), 3247 (N–H), 1608 (C=N) cm^{-1}. ^1H NMR (400 MHz, DMSO-d_6): δ 5.44 (s, 2H, CH_2), 7.15 (d, 1H, J = 9.19 Hz, Ar–H), 7.37 (t, 1H, J = 7.99 Hz, Ar–H), 7.39 (s, 1H, Ar–H), 7.49 (t, 1H, J = 7.99 Hz, Ar–H), 7.57 (d, 2H, J = 8.39 Hz, Ar–H), 7.78 (d, 1H, J = 7.99 Hz, Ar–H), 7.83 (d, 1H, J = 9.19 Hz, Ar–H), 7.85 (d, 1H, J = 7.99 Hz, Ar–H), 7.93 (d, 2H, J = 8.39 Hz, Ar–H), 8.18 (s broad, 1H, NH_2), 8.53 (s broad, 1H, NH_2), 10.99 (s broad, 1H, NH). ^{13}C NMR (100 MHz, DMSO-d_6): δ 60.8 (CH_2), 107.6 (CH Ar), 118.4 (CH Ar), 122.8 (Cq Ar), 123.9 (CH Ar), 126.6 (CH Ar), 127.6 (CH Ar), 128.7 (Cq Ar), 129.3 (CH Ar), 131.1 (CH Ar), 133.9 (Cq Ar), 134.9 (Cq Ar), 143.1 (C=N), 152.4 (C–O, Ar), 179.3 (C=S). Anal. Calcd. For $C_{19}H_{16}BrN_3OS$: C, 55.08; H, 3.89; N, 10.14. Found: C, 54.97; H, 3.98; N, 10.21.

4.4. X-ray crystallography

X-ray diffraction data collections were performed on an Enraf-Nonius Kappa-CCD diffractometer (95 mm CCD camera on κ-goniostat) using graphite monochromated MoK_radiation (0.71073 Å), at room temperature. Data collections were carried out using the COLLECT software [43] up to 50° in 2θ. Final unit cell parameters were based on 8742 reflections for compound **8e** and 6629 reflections for compound **9h**. Integration and scaling of the reflections, correction for Lorentz and polarization effects were performed with the HKL DENZO-SCALEPACK system of programs [44]. The structures of the compounds were solved by direct methods with SHELXS-97 [45]. The models were refined by full-matrix least squares on F^2 using the SHELXL-97 [45]. The program ORTEP-3 [46] was used for graphic representation and the program WINGX [47] to prepare materials for publication. All H atoms were located by geometric considerations (C–H = 0.93–0.97 Å; N–H = 0.86 Å) and refined as riding with U_{iso} (H) = 1.5 U_{eq} (C-methyl) or 1.2 U_{eq} (other). The main crystallographic data is available in the Supplementary material.

4.5. Cells

BALB/c mouse, housed in the Centro de Pesquisas Aggeu Magalhaes (Recife, Brazil), were used to collect splenocytes accordingly to a previously reported protocol [48]. *T. cruzi* Dm28c epimastigotes, cloned derived from Dm28 strain (TcI) [49], were maintained at 26 °C in Liver Infusion Tryptose (LIT) medium supplemented with 10% fetal bovine serum (FBS) (Life Technologies, Carlsbad, CA, USA), 1% hemin (Sigma–Aldrich), 1% R9 medium (Sigma–Aldrich), and 50 μg/mL gentamycin (Novafarma, Anápolis, Brazil). Y strain (TcII) trypomastigotes were obtained from the supernatant of infected LLC-MK2 cells and were maintained in RPMI-1640 medium (Sigma–Aldrich) supplemented with 10% FBS, and 50 μg/mL gentamycin at 37 °C and 5% CO_2. Experiments were carried out in accordance with the recommendations of ethical issues guidelines and were approved by the local Animal Ethics Committee (number 0266/05).

4.6. Cytotoxicity in mouse splenocytes

BALB/c mouse splenocytes were seeded at 5×10^6 cells/well in 96-well plate. Compounds were dissolved in DMSO and then diluted in RPMI-1640 medium in a serial dilution (1.23, 3.7, 33.33 and 100 μg/mL) and added to respective wells, in triplicate. The final DMSO concentration was 1%. The plate was incubated for 24 h at 37 °C and 5% CO_2. After, 1.0 μCi of ^3H-thymidine (Perkin Elmer, Waltham, MA, USA) was added, incubated and cells were harvested and then transferred to a liquid scintillation counter (WALLAC 1209, Rackbeta Pharmacia, Stockholm, Sweden) and the percent of ^3H-thymidine incorporation was determined. The

highest non-cytotoxic concentration (HNC) was determined for each compound. For determining the CC_{50} values, five different concentrations were used.

4.7. Anti-T. cruzi activity (epimastigotes)

Epimastigotes (Dm28c strain) grown in LIT media were counted in a hemocytometer and then seeded at 10^6 cells/well into a 96-well plate. Compounds were dissolved in DMSO and then diluted in LIT médium in a serial dilution (1.23, 3.70, 11.11, 33.33 and 100 μg/mL) and added to respective wells, in triplicate. The final DMSO concentration in the plate was 1%. Plate was incubated for 5 days at 26 °C, aliquots of each well were collected, and the number of viable parasites were counted in a Neubauer chamber and compared to untreated parasite culture. Inhibitory concentration for 50% (IC_{50}) was calculated using nonlinear regression on Prism 4.0 GraphPad software. Benznidazole and nifurtimox were used as the reference drugs.

4.8. Anti-T. cruzi activity (trypomastigotes)

Metacyclic trypomastigotes were collected from the supernatant of infected LLC-MK2 cells and then seeded at 4×10^5 cells/well in RPMI-1640 medium. All compounds were dissolved in DMSO and then diluted in RPMI-1640 medium in a serial dilution (1.23, 3.70, 11.11, 33.33 and 100 μg/mL) and added to respective wells, in triplicate. The final DMSO concentration was 1%. Plate was incubated for 24 h at 37 °C and 5% of CO_2. Aliquots of each well were collected, and the number of viable parasites was counted in a Neubauer chamber. The percentage of inhibition was calculated in relation to untreated cultures. Cytotoxic concentration for 50% (CC_{50}) was determined using nonlinear regression with Prism 4.0 GraphPad software. Benznidazole and nifurtimox were used as the reference drugs.

4.9. Anti-T. cruzi activity (amastigotes/trypomastigotes)

The *in vitro* anti-trypanosomal activity in amastigote and trypomastigote forms of *T. cruzi* was evaluated by colorimetric beta-galactosidase assay developed by Buckner et al. (1996) [50] and modified by Romanha et al. (2010) [39]. *T. cruzi* (Tulahuen strain) expressing the *Escherichia coli* beta-galactosidase gene were grown on monolayer of mouse L-929 fibroblasts. Cultures assayed for beta-galactosidase activity were grown in RPMI 1640 medium without phenol red plus 10% fetal bovine serum and glutamine. Ninety-six-well tissue culture micro plates were seeded with L-929 fibroblasts at 4.0×10^3 per well in 80 μL and incubated overnight at 37 °C, 5% CO_2. Beta-galactosidase-expressing trypomastigotes were then added at 4.0×10^4 per well in 20 μL. After 2 h, the medium with trypomastigotes that have not penetrated in the cells was discarded and replaced by 200 μL of fresh medium. After 48 h, the medium was discarded again and replaced by 180 μL of fresh medium and 20 μL of test compounds. Each compound was tested in quadruplicate. After 7 days culture development, chlorophenol red beta-D-galactopyranoside at 100 μM and Nonidet P-40 at 0.1% were added to the plates and incubated overnight, at 37 °C. The absorbance was measured at 570 nm in an automated microplate reader. Benznidazole at its IC_{50} (1 μg/mL = 3.81 μM) was used as positive control. The results are expressed as percentage of parasite growth inhibition. Two independent experiments were performed.

4.10. Cytotoxicity in mouse L-929 fibroblasts

The active compounds were tested *in vitro* for determination of cytotoxic over L-929 cells using the alamarBlue® dye. Were used the same cell number, time of the cell development and time of compound exposure used for the beta-galactosidase assay. The cells were exposed to compounds at crescents concentrations starting at IC_{50} value of the *T. cruzi*. The compounds were tested in quadruplicate. After 96 h of exposure, alamarBlue® was added and the absorbance at 570 and 600 nm was measured 6 h later. The cell viability was expressed as the percentage of difference in the reduction between treated and untreated cells [39]. CC_{50} values were calculated by linear interpolation and the selectivity index (SI) was determined based on the ratio between CC_{50} and IC_{50} values.

4.11. Inhibition of catalytic activity of cruzain

The cruzain activity was measured by monitoring the cleavage of the fluorescent substrate Z-Phe-Arg-aminomethylcoumarin (Z-FR-AMC), in a Synergy 2 (Biotek) fluorimeter, of the Centre for Flow Cytometry Fluorimetry at the Department of Biochemistry and Immunology from the Federal University of Minas Gerais (UFMG), Brazil. All assays were performed in a buffer solution of 0.1 M sodium acetate pH 5.5 in the presence of 1 mM betamercaptoethanol, 0.01% Triton X-100, 0.5 nM cruzain and 2.5 μM of substrate ($K_m = 1$ μM). Initially the compounds were pre-incubated in a solution containing the enzyme. After 10 min of incubation the substrate was added. The enzymatic activity was calculated based on comparison with DMSO control, from initial rates of reaction. The screen with 50 μM of inhibitor was performed at least twice, each in triplicate, and was monitored for 5 min. IC_{50} determinations were performed at least twice for each compound, and each curve was constructed based on at least seven compound concentrations, each in triplicate, with the software GraphPad Prism 5.

4.12. PI staining

Y strain trypomastigotes (4×10^5) in RPMI-1640 medium supplemented with 10% FBS were treated with benznidazole (25 μM) or thiosemicarbazones and incubated for 24 h at 37 °C in 5% CO_2. Triton X-100 (Sigma–Aldrich, 10 μL) was used as positive control. Parasites were labeled with 5 μL PI from the BD apoptosis detection kit (BD Pharmingen, New Jersey, USA) according to the manufacturer instructions. Acquisition of at least 10,000 events was performed using a FACSCalibur flow cytometer (BD Biosciences, San Jose, CA, USA), and data were analyzed using CellQuest software (BD Biosciences). Two independent experiments were performed.

Acknowledgments

This work was funded by CNPq, FAPESB and FACEPE. A.C.L.L. (305506/2013-1), R.S.F., C.A.S. and M.B.P.S. are recipients of a CNPq fellowship. M.V.O.C. is the recipient of a FACEPE scholarship (BFP-0107-4.03/12). M.V.O.C. also thanks FACEPE for funding this research (APQ-0289-4.03/13). T.M.B. is recipient of CAPES doctoral study. C.A.S. thanks Conselho Nacional de Desenvolvimento Científico e Tecnológico (CNPq, Proc. 474797/2013-9). We would also like to thank the Physics Institute of USP (São Carlos) for kindly allowing the use of the KappaCCD diffractometer. Authors are thankful to Centro de Citometria e Fluorimetria of UFMG/FAPEMIG for allowing the use of the fluorimeter. The authors thank the Program for Technological Development of Tools for Health-PDTIS-FIOCRUZ for use of its facilities. Our thanks are also due to the Department of Chemistry at the Federal University of Pernambuco (UFPE) for recording the NMR (^1H and ^{13}C), IR spectra and the elemental analysis of all compounds. Crystallographic data for compounds can be obtained free of charge from the Cambridge Crystallographic Data Centre (Deposit numbers CCDC 1061149 (**9h**) and CCDC 1061150 (**8e**), www.ccdc.cam.ac.uk/data_request/cif).

Appendix A. Supplementary data

Supplementary data related to this article can be found at http://dx.doi.org/10.1016/j.ejmech.2015.06.048.

References

[1] J.R. Coura, J.C.P. Dias, Epidemiology, control and surveillance of Chagas disease: 100 years after its discovery, Mem. Inst. Oswaldo Cruz 104 (Suppl. 1) (2009) 31–40, http://dx.doi.org/10.1590/S0074-02762009000900006.

[2] J.A. Urbina, New advances in the management of a long-neglected disease, Clin. Infect. Dis. 49 (2009) 1685–1687, http://dx.doi.org/10.1086/648073.

[3] M.P. Barrett, R.J.S. Burchmore, A. Stich, J.O. Lazzari, A.C. Frasch, J.J. Cazzulo, et al., The trypanosomiases, Lancet 362 (2003) 1469–1480, http://dx.doi.org/10.1016/S0140-6736(03)14694-6.

[4] A. Rassi, J.A. Marin-Neto, Chagas disease, Lancet 375 (2010) 1388–1402, http://dx.doi.org/10.1016/S0140-6736(10)60061-X.

[5] F.S. Machado, L.A. Jelicks, L.V. Kirchhoff, J. Shirani, F. Nagajyothi, S. Mukherjee, et al., Chagas heart disease, Cardiol. Rev. 20 (2012) 1, http://dx.doi.org/10.1097/CRD.0b013e31823efde2.

[6] S. Gupta, X. Wan, M.P. Zago, V.C.M. Sellers, T.S. Silva, D. Assiah, et al., Antigenicity and diagnostic potential of vaccine candidates in human Chagas disease, PLoS Negl. Trop. Dis. 7 (2013) e2018, http://dx.doi.org/10.1371/journal.pntd.0002018.

[7] M.B.P. Soares, R.S. Lima, B.S.F. Souza, J.F. Vasconcelos, L.L. Rocha, R.R. Dos Santos, et al., Reversion of gene expression alterations in hearts of mice with chronic chagasic cardiomyopathy after transplantation of bone marrow cells, Cell Cycle 10 (2011) 1448–1455. http://www.pubmedcentral.nih.gov/articlerender.fcgi?artid=3117044&tool=pmcentrez&rendertype=abstract (accessed 19.03.15).

[8] R.A. Cutrullis, T.J. Poklépovich, M. Postan, H.L. Freilij, P.B. Petray, Immunomodulatory and anti-fibrotic effects of ganglioside therapy on the cardiac chronic form of experimental Trypanosoma cruzi infection, Int. Immunopharmacol. 11 (2011) 1024–1031, http://dx.doi.org/10.1016/j.intimp.2011.02.022.

[9] V.E. Alvarez, G.T. Niemirowicz, J.J. Cazzulo, The peptidases of Trypanosoma cruzi: digestive enzymes, virulence factors, and mediators of autophagy and programmed cell death, Biochim. Biophys. Acta 1824 (2012) 195–206, http://dx.doi.org/10.1016/j.bbapap.2011.05.011.

[10] H.J. Wiggers, J.R. Rocha, W.B. Fernandes, R. Sesti-Costa, Z.A. Carneiro, J. Cheleski, et al., Non-peptidic cruzain inhibitors with trypanocidal activity discovered by virtual screening and in vitro assay, PLoS Negl. Trop. Dis. 7 (2013) e2370, http://dx.doi.org/10.1371/journal.pntd.0002370.

[11] V.G. Duschak, M. Ciaccio, J.R. Nassert, M.A. Basombrio, Enzymatic activity, protein expression, and gene sequence of cruzipain in virulent and attenuated Trypanosoma cruzi strains, J. Parasitol. 87 (2001) 1016–1022 doi:10.1645/0022-3395(2001)087[1016:EAPEAG]2.0.CO;2.

[12] J.H. McKerrow, C. Caffrey, B. Kelly, P. Loke, M. Sajid, Proteases in parasitic diseases, Annu. Rev. Pathol. 1 (2006) 497–536, http://dx.doi.org/10.1146/annurev.pathol.1.110304.100151.

[13] X. Du, E. Hansell, J.C. Engel, C.R. Caffrey, F.E. Cohen, J.H. McKerrow, Aryl ureas represent a new class of anti-trypanosomal agents, Chem. Biol. 7 (2000) 733–742, http://dx.doi.org/10.1016/S1074-5521(00)00018-1.

[14] J.M. dos Santos Filho, A.C.L. Leite, B.G. de Oliveira, D.R.M. Moreira, M.S. Lima, M.B.P. Soares, et al., Design, synthesis and cruzain docking of 3-(4-substituted-aryl)-1,2,4-oxadiazole-N-acylhydrazones as anti-Trypanosoma cruzi agents, Bioorg. Med. Chem. 17 (2009) 6682–6691, http://dx.doi.org/10.1016/j.bmc.2009.07.068.

[15] N.C. Romeiro, G. Aguirre, P. Hernández, M. González, H. Cerecetto, I. Aldana, et al., Synthesis, trypanocidal activity and docking studies of novel quinoxaline-N-acylhydrazones, designed as cruzain inhibitors candidates, Bioorg. Med. Chem. 17 (2009) 641–652, http://dx.doi.org/10.1016/j.bmc.2008.11.065.

[16] J.M. dos Santos Filho, D.R.M. Moreira, C.A. de Simone, R.S. Ferreira, J.H. McKerrow, C.S. Meira, et al., Optimization of anti-Trypanosoma cruzi oxadiazoles leads to identification of compounds with efficacy in infected mice, Bioorg. Med. Chem. 20 (2012) 6423–6433, http://dx.doi.org/10.1016/j.bmc.2012.08.047.

[17] T. Franklim, L. Freire-de-Lima, J. de Nazareth Sá Diniz, J. Previato, R. Castro, L. Mendonça-Previato, et al., Design, synthesis and trypanocidal evaluation of novel 1,2,4-triazoles-3-thiones derived from natural piperine, Molecules 18 (2013) 6366–6382, http://dx.doi.org/10.3390/molecules18066366.

[18] K. Brak, P.S. Doyle, J.H. McKerrow, J.A. Ellman, Identification of a new class of nonpeptidic inhibitors of cruzain, J. Am. Chem. Soc. 130 (2008) 6404–6410, http://dx.doi.org/10.1021/ja710254m.

[19] K. Brak, I.D. Kerr, K.T. Barrett, N. Fuchi, M. Debnath, K. Ang, et al., Nonpeptidic tetrafluorophenoxymethyl ketone cruzain inhibitors as promising new leads for Chagas disease chemotherapy, J. Med. Chem. 53 (2010) 1763–1773, http://dx.doi.org/10.1021/jm901633v.

[20] X. Du, C. Guo, E. Hansell, P.S. Doyle, C.R. Caffrey, T.P. Holler, et al., Synthesis and structure–activity relationship study of potent trypanocidal thio semicarbazone inhibitors of the trypanosomal cysteine protease cruzain, J. Med. Chem. 45 (2002) 2695–2707, http://dx.doi.org/10.1021/jm010459j.

[21] D.C. Greenbaum, Z. Mackey, E. Hansell, P. Doyle, J. Gut, C.R. Caffrey, et al., Synthesis and structure–activity relationships of parasiticidal thiosemicarbazone cysteine protease inhibitors against Plasmodium falciparum, Trypanosoma brucei, and Trypanosoma cruzi, J. Med. Chem. 47 (2004) 3212–3219, http://dx.doi.org/10.1021/jm030549j.

[22] R. Siles, S.-E. Chen, M. Zhou, K.G. Pinney, M.L. Trawick, Design, synthesis, and biochemical evaluation of novel cruzain inhibitors with potential application in the treatment of Chagas' disease, Bioorg. Med. Chem. Lett. 16 (2006) 4405–4409, http://dx.doi.org/10.1016/j.bmcl.2006.05.041.

[23] N. Beatriz Huaman Lozano, V. Goncalves Maltarollo, K. Cacilda Weber, K. Maria Honorio, R. Victorio Carvalho Guido, A. Defini Andricopulo, et al., Molecular features for antitrypanosomal activity of thiosemicarbazones revealed by OPS-PLS QSAR studies, Med. Chem. (Los. Angeles) 8 (2012) 1045–1056, http://dx.doi.org/10.2174/157340612804075043.

[24] W. Porcal, P. Hernández, L. Boiani, M. Boiani, A. Ferreira, A. Chidichimo, et al., New trypanocidal hybrid compounds from the association of hydrazone moieties and benzofuroxan heterocycle, Bioorg. Med. Chem. 16 (2008) 6995–7004, http://dx.doi.org/10.1016/j.bmc.2008.05.038.

[25] M. Vieites, P. Smircich, L. Guggeri, E. Marchán, A. Gómez-Barrio, M. Navarro, et al., Synthesis and characterization of a pyridine-2-thiol N-oxide gold(I) complex with potent antiproliferative effect against Trypanosoma cruzi and Leishmania sp. insight into its mechanism of action, J. Inorg. Biochem. 103 (2009) 1300–1306, http://dx.doi.org/10.1016/j.jinorgbio.2009.02.011.

[26] G.H.G. Trossini, A. Malvezzi, A. T-do Amaral, C.O. Rangel-Yagui, M.A. Izidoro, M.H.S. Cezari, et al., Cruzain inhibition by hydroxymethylnitrofurazone and nitrofurazone: investigation of a new target in Trypanosoma cruzi, J. Enzyme Inhib. Med. Chem. 25 (2010) 62–67, http://dx.doi.org/10.3109/14756360902941058.

[27] M.E. Caputto, L.E. Fabian, D. Benítez, A. Merlino, N. Ríos, H. Cerecetto, et al., Thiosemicarbazones derived from 1-indanones as new anti-Trypanosoma cruzi agents, Bioorg. Med. Chem. 19 (2011) 6818–6826, http://dx.doi.org/10.1016/j.bmc.2011.09.037.

[28] B. Demoro, C. Sarniguet, R. Sánchez-Delgado, M. Rossi, D. Liebowitz, F. Caruso, et al., New organoruthenium complexes with bioactive thiosemicarbazones as co-ligands: potential anti-trypanosomal agents, Dalton Trans. 41 (2012) 1534–1543, http://dx.doi.org/10.1039/C1DT11519G.

[29] L. Blau, R.F. Menegon, G.H.G.G. Trossini, J.V.D. Molino, D.G. Vital, R.M.B. Cicarelli, et al., Design, synthesis and biological evaluation of new aryl thiosemicarbazone as antichagasic candidates, Eur. J. Med. Chem. 67 (2013) 142–151, http://dx.doi.org/10.1016/j.ejmech.2013.04.022.

[30] D.R. Magalhaes Moreira, A.D.T. de Oliveira, P.A. Teixeira de Moraes Gomes, C.A. de Simone, F.S. Villela, R.S. Ferreira, et al., Conformational restriction of aryl thiosemicarbazones produces potent and selective anti-Trypanosoma cruzi compounds which induce apoptotic parasite death, Eur. J. Med. Chem. 75 (2014) 467–478, http://dx.doi.org/10.1016/j.ejmech.2014.02.001.

[31] D.R.M. Moreira, S.P.M. Costa, M.Z. Hernandes, M.M. Rabello, G.B. de Oliveira Filho, C.M.L. de Melo, et al., Structural investigation of anti-Trypanosoma cruzi 2-iminothiazolidin-4-ones allows the identification of agents with efficacy in infected mice, J. Med. Chem. 55 (2012) 10918–10936, http://dx.doi.org/10.1021/jm301518v.

[32] M. Ishikawa, Y. Hashimoto, Improvement in aqueous solubility in small molecule drug discovery programs by disruption of molecular planarity and symmetry, J. Med. Chem. 54 (2011) 1539–1554, http://dx.doi.org/10.1021/jm101356p.

[33] A.E. Kümmerle, M. Schmitt, S.V.S. Cardozo, C. Lugnier, P. Villa, A.B. Lopes, et al., Design, synthesis, and pharmacological evaluation of N-acylhydrazones and novel conformationally constrained compounds as selective and potent orally active phosphodiesterase-4 inhibitors, J. Med. Chem. 55 (2012) 7525–7545, http://dx.doi.org/10.1021/jm300514y.

[34] A.E. Kümmerle, J.M. Raimundo, C.M. Leal, G.S. da Silva, T.L. Balliano, M.A. Pereira, et al., Studies towards the identification of putative bioactive conformation of potent vasodilator arylidene N-acylhydrazone derivatives, Eur. J. Med. Chem. 44 (2009) 4004–4009, http://dx.doi.org/10.1016/j.ejmech.2009.04.044.

[35] M. Aveniente, E.F. Pinto, L.S. Santos, B. Rossi-Bergmann, L.E.S. Barata, Structure-activity relationship of antileishmanials neolignan analogues, Bioorg. Med. Chem. 15 (2007) 7337–7343, http://dx.doi.org/10.1016/j.bmc.2007.08.016.

[36] D.R.M. Moreira, A.C. Lima Leite, M.V.O. Cardoso, R.M. Srivastava, M.Z. Hernandes, M.M. Rabello, et al., Structural design, synthesis and structure-activity relationships of thiazolidinones with enhanced anti-Trypanosoma cruzi activity, ChemMedChem 9 (2014) 177–188, http://dx.doi.org/10.1002/cmdc.201300354.

[37] C.A. Lipinski, F. Lombardo, B.W. Dominy, P.J. Feeney, Experimental and computational approaches to estimate solubility and permeability in drug discovery and development settings, Adv. Drug Deliv. Rev. 23 (1997) 3–25, http://dx.doi.org/10.1016/S0169-409X(96)00423-1.

[38] M.S. Lopes, R.C.C. de Souza Pietra, T.F. Borgati, C.F.D. Romeiro, P.A.S. Júnior, A.J. Romanha, et al., Synthesis and evaluation of the anti parasitic activity of aromatic nitro compounds, Eur. J. Med. Chem. 46 (2011) 5443–5447, http://dx.doi.org/10.1016/j.ejmech.2011.09.002.

[39] A.J. Romanha, S.L. De Castro, M.D.N.C. Soeiro, J. Lannes-Vieira, I. Ribeiro, A. Talvani, et al., In vitro and in vivo experimental models for drug screening and development for Chagas disease, Mem. Inst. Oswaldo Cruz 105 (2010) 233–238, http://dx.doi.org/10.1590/S0074-02762010000200022.

[40] M.S. Lopes, P.A. Sales Júnior, A.G.F. Lopes, M.I. Yoshida, T.H.A. da Silva,

A.J. Romanha, et al., The activity of a metronidazole analogue and its β-cyclodextrin complex against Trypanosoma cruzi, Mem. Inst. Oswaldo Cruz 106 (2011) 1055–1057. http://www.ncbi.nlm.nih.gov/pubmed/22241134 (accessed 06.04.15).

[41] R.S. Ferreira, C. Bryant, K.K.H. Ang, J.H. McKerrow, B.K. Shoichet, A.R. Renslo, Divergent modes of enzyme inhibition in a homologous structure-activity series, J. Med. Chem. 52 (2009) 5005–5008, http://dx.doi.org/10.1021/jm9009229.

[42] C. Bryant, I.D. Kerr, M. Debnath, K.K.H. Ang, J. Ratnam, R.S. Ferreira, et al., Novel non-peptidic vinylsulfones targeting the S2 and S3 subsites of parasite cysteine proteases, Bioorg. Med. Chem. Lett. 19 (2009) 6218–6221, http://dx.doi.org/10.1016/j.bmcl.2009.08.098.

[43] E.-N. Collect, Nonius BV, Delft, The Netherlands, 2000 (1997) 585.

[44] Z. Otwinowski, W. Minor, Methods in enzymology, Macromol. Crystallogr. Part A 276 (1997) 307–326, http://dx.doi.org/10.1016/S0076-6879(97)76066-X.

[45] G. Sheldrick, SHELXL-97 and SHELXS-97, Program for X-ray Crystal Structure Solution and Refinement, Univ. Göttingen, 1997. http://scholar.google.com.br/scholar?q=SHELXS-97. Program for Crystal Structure Resolution#3 (accessed 13.11.12).

[46] L.J. Farrugia, ORTEP-3 for windows – a version of ORTEP-III with a Graphical User Interface (GUI), J. Appl. Crystallogr. 30 (1997), http://dx.doi.org/10.1107/S0021889897003117, 565.

[47] L.J. Farrugia, WinGX suite for small-molecule single-crystal crystallography, J. Appl. Crystallogr. 32 (1999) 837–838, http://dx.doi.org/10.1107/S0021889899006020.

[48] E. de F. Santiago, S.A. de Oliveira, G.B. de Oliveira Filho, D.R.M. Moreira, P.A.T. Gomes, A.L. da Silva, et al., Evaluation of the anti-Schistosoma mansoni activity of thiosemicarbazones and thiazoles, Antimicrob. Agents Chemother. 58 (2014) 352–363, http://dx.doi.org/10.1128/AAC.01900-13.

[49] B. Zingales, S.G. Andrade, M.R.S. Briones, D.A. Campbell, E. Chiari, O. Fernandes, et al., A new consensus for Trypanosoma cruzi intraspecific nomenclature: second revision meeting recommends TcI to TcVI, Mem. Inst. Oswaldo Cruz 104 (2009) 1051–1054, http://dx.doi.org/10.1590/S0074-02762009000700021.

[50] F.S. Buckner, C.L.M.J. Verlinde, A.C. La Flamme, W.C. Van Voorhis, Efficient technique for screening drugs for activity against Trypanosoma cruzi using parasites expressing β-galactosidase, Antimicrob. Agents Chemother. 40 (1996) 2592–2597. http://www.pubmedcentral.nih.gov/articlerender.fcgi?artid=163582&tool=pmcentrez&rendertype=abstract.

European Journal of Medicinal Chemistry 111 (2016) 46–57

Contents lists available at ScienceDirect

European Journal of Medicinal Chemistry

journal homepage: http://www.elsevier.com/locate/ejmech

Research paper

Phthalimido-thiazoles as building blocks and their effects on the growth and morphology of *Trypanosoma cruzi*

Paulo André Teixeira de Moraes Gomes [a], Arsênio Rodrigues Oliveira [a], Marcos Veríssimo de Oliveira Cardoso [a], Edna de Farias Santiago [a], Miria de Oliveira Barbosa [a], Lucianna Rabelo Pessoa de Siqueira [a], Diogo Rodrigo Magalhães Moreira [b], Tanira Matutino Bastos [b], Fábio André Brayner [c], Milena Botelho Pereira Soares [b, d], Andresa Pereira de Oliveira Mendes [e], Maria Carolina Accioly Brelaz de Castro [e], Valéria Rego Alves Pereira [e], Ana Cristina Lima Leite [a, *]

[a] Departamento de Ciências Farmacêuticas, Centro de Ciências da Saúde, Universidade Federal de Pernambuco, 50740-520 Recife, PE, Brazil
[b] Fundação Oswaldo Cruz, Centro de Pesquisas Gonçalo Moniz, CEP 40296-710 Salvador, BA, Brazil
[c] Laboratório de Imunologia Keizo Asami-LIKA/UFPE, CEP, 50670-901 Recife, PE, Brazil
[d] Centro de Biotecnologia e Terapia Celular, Hospital São Rafael, Avenida São Rafael, 2152, São Marcos, CEP 41253-190, Salvador BA, Brazil
[e] Centro de Pesquisas Aggeu Magalhães, Fundação Oswaldo Cruz, CEP, 50670-420 Recife, PE, Brazil

ARTICLE INFO

Article history:
Received 21 September 2015
Received in revised form
21 December 2015
Accepted 9 January 2016
Available online 11 January 2016

Keywords:
Chagas disease
Trypanosoma cruzi
Thiazole
Hydrazone
Phthalimide

ABSTRACT

Chagas disease is a parasitic infection caused by protozoan *Trypanosoma cruzi* that affects approximately 6–7 million people worldwide. Benznidazole is the only drug approved for treatment during the acute and asymptomatic chronic phases; however, its efficacy during the symptomatic chronic phase is controversial. The present work reports the synthesis and anti-*T. cruzi* activities of a novel series of phthalimido-thiazoles. Some of these compounds showed potent inhibition of the trypomastigote form of the parasite at low cytotoxicity concentrations in spleen cells, and the resulting structure-activity relationships are discussed. We also showed that phthalimido-thiazoles induced ultrastructural alterations on morphology, flagellum shortening, chromatin condensation, mitochondria swelling, reservosomes alterations and endoplasmic reticulum dilation. Together, these data revealed, for the first time, a novel series of phthalimido-thiazoles-structure-based compounds with potential effects against *T. cruzi* and lead-like characteristics against Chagas disease.

1. Introduction

Chagas disease, also known as American trypanosomiasis, is a potentially life-threatening illness caused by the protozoan parasite *Trypanosoma cruzi* (*T. cruzi*). Approximately 6–7 million people are estimated to be infected worldwide, mostly in Latin America, where Chagas disease is endemic [1].

Despite the efforts of many investigators to research new anti-Chagas drugs, only one drug is currently used in therapy, benznidazole (Bdz) [2,3]. Current chemotherapy for Chagas disease is unsatisfactory due to the limited efficacy of Bdz, particularly during the chronic phase, with frequent side effects that can lead to discontinuation of treatment [4].

One pragmatic way to improve the quality of both the candidate drugs and screening collections is by improving the quality of the building blocks (reagents) that are used to synthesize them. Our strategic program focused on substructures and properties that are known to have imparted biological activity and good 'drug-like' properties previously. Among the chemical groups explored for anti-Chagas activity, thiazolyl hydrazones are noteworthy because of their wide biological, especially anti-parasitic, activities [5–8]. Caputo et al. have demonstrated trypanocidal activity for a series of 4- arylthiazolylhydrazones [9], which have broad and potent activities for all forms of the parasite.

Our efforts toward new antichagasic drugs since 2006 have led

* Corresponding author.
E-mail address: acllb2003@yahoo.com.br (A.C.L. Leite).

http://dx.doi.org/10.1016/j.ejmech.2016.01.010
0223-5234/

us to develop a variety of thiosemicarbazones and 1,3-thiazolyl hydrazones as trypanocidal agents [4,7,10–14]. In continuation of our search for bioactive molecules, we envisaged that the derivatization of the thiosemicarbazone group into a thiazole moiety would generate novel templates that are likely to exhibit anti-*T. cruzi* activity [4].

However, much effort has been invested to identify the key differences between drugs and other organic compounds. High-quality libraries are expected to exhibit drug-likeness to produce compounds with desirable pharmacokinetic and safety profiles. The phthalimide functional group has been used as an important tool in organic synthesis because it protects against unwanted reactions. Many research teams have used this nucleus as a building block to improve compound quality. In fact, phthalimide derivatives have shown a broad spectrum of pharmacological properties, such as analgesic [15], anticonvulsant [16], antitubercular [17,18], hypolipidaemic [18], anxiolytic [15], anti-inflammatory [15], antimicrobial [17,19,20] and antipsychotic [21].

For this reason, our research group has explored the pharmacological properties of phthalimide derivatives. As a result, bioactive prototypes were identified with potent anti-inflammatory [22], anti-proliferative [23], immunomodulatory [22,24,25], antitumor [23], antiangiogenic [26] and schistosomicidal properties [27], Indeed, Santiago et al. identified phthalimido-thiazole derivatives with potent schistosomicidal activities. The phthalimide **LpQM-45** caused significant ultrastructural changes, including destruction of the integument in both male and female worms [27], however, their antichagasic properties have not been explored.

Considering the promising results achieved by compounds bearing a thiazole ring and phthalimides nuclei, they were chosen as common pharmacophores that exist in diverse drug classes. In this way, we synthesized a set of molecules with phthalimide and thiazole nucleus. In this synthetic design of a substructure-based compound library, substituents around the phenyl ring attached at C4 in the thiazole ring (compounds **2b-n**) were explored. In addition, a spacer group between phthalimide and the thiazole ring was inserted and a phenyl group at N3 of the thiazole ring was also introduced (**6b-l**). To investigate the influence of the phthalimido moiety at the anti-*T. cruzi* activity, 26 new compounds were tested *in vitro* against the *T. cruzi* parasite epimastigote and trypomastigote forms. Ultrastructural studies and flow cytometry analysis were also investigated (Fig. 1).

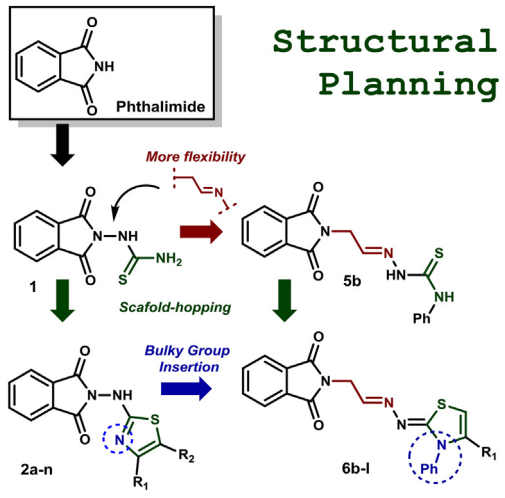

Fig. 1. Structural planning of the proposed compounds.

2. Results and discussion

2.1. Chemistry

Initially, 14 phthalimido-thiazoles (**2a-n**) were synthesized in a two-step reaction, following the procedures reported by Pessoa et al. [25]. Firstly, a reaction of phthalic anhydride with thiosemicarbazide, in DMF under reflux for 4 h, with a catalytic amount of DMAP, led us to compound **1**. The synthesis of the series **2a-n** was performed via Hantsch cyclization between compound **1** and the appropriate α-halogenated ketone (1,3-dichloroacetone for compound **2a**), under ultrasound irradiation, at room temperature (rt) for 1 h. This reaction condition led to average yields from 36 to 65%. To synthesize the series **6a-l**, was followed the reaction protocol reported by Cardoso et al. [23]. The desired compounds **6a-l** were obtained by the reaction of Intermediate **5b** (or **5a**, for compound **6a**) with the appropriate α-halogenated ketone (1,3-dichloroacetone for compound **6a**), via Hantsch cyclization, leading good yields (46–82%) (Scheme 1). All the synthesized compounds were well characterized by infrared (IR), nuclear magnetic resonance (^{1}H, ^{13}C NMR), mass spectroscopy (ESI-TOF) and, in case of compounds **2e**, **2f** and **2g**, by single crystal X-ray diffraction analysis (Fig. 2).

The ^{1}H NMR spectra of some compounds showed that phthalimido-thiazoles **6a-l** are composed by diastereomers. Next, we aimed to define the configuration of the major isomer by crystallographic analysis. However, we did not succeed in crystallizing phthalimido-thiazoles **6a-l** suitable for X-ray analysis. Based on previous crystallized compounds by our group, we suggest that the major isomer formed present the *E-Z* configuration (Fig. 3). Indeed, hydrazine double-bond C2=N2 is commonly assigned as *E* configuration [4,23,28]. Concerning the exocyclic double-bond N3=C3, we suggest that the predominant configuration is in *Z*-configuration [7,29]. Besides, a representative ^{1}H-NMR spectrum of compound **6i** is presented in Supplementary Material.

2.2. Anti-T. cruzi evaluation

Initially, compounds **2a-n** were planned to improve the trypanocidal activity and cytotoxic tolerance with the cyclization of phthalimido-thiosemicarbazone to the phthalimido-thiazole ring. From the results, it was observed in most of the cases that new phthalimido-thiazoles showed high cytotoxic activity in spleen cells. In opposition, only compounds **2i** and **2j** showed low cytotoxicity.

Concerning trypanocidal activity for epimastigotes, it is observed that 16 compounds (of 28) present better potency than Benznidazole (Table 1). Among series **2a-n**, compound **2i** was the most active, among the series and the entire work. The most active compound in series **6** is **6k**, a 3-NO_2 derivative, presenting an IC_{50} of 6.0 μM. Observing compounds with withdrawer substituents (**2e-h**, **2k-n**), compound 2,4-dichloro substituted (**2m**) was the most active. It analogue disubstituted 3,4-dichloro (**2l**) present lower trypanocidal activity and high toxicity for BALB/c mice spleen cells, denoting that the orientation of the substituents is important for the activity. Observing bulk substituted compounds (phenyl, 2-naphthyl and 4-biphenylyl), in series **2a-n**, a relationship of LogP and trypanocidal activity (Fig. 4) is observed, being compound **2i** the most active of this sub-series.

The trend of bulky substituents (LogP) observed for series **2a-n** is not observed for series **6a-l**, being compound **6k** (3-NO_2) the most active of the series **6a-l**.

When comparing the trypanocidal activity against the trypomastigote form of the series **2a-n** of phthalimido-thiazole derivatives, compound **2j** was found to be the most potent of this sub-

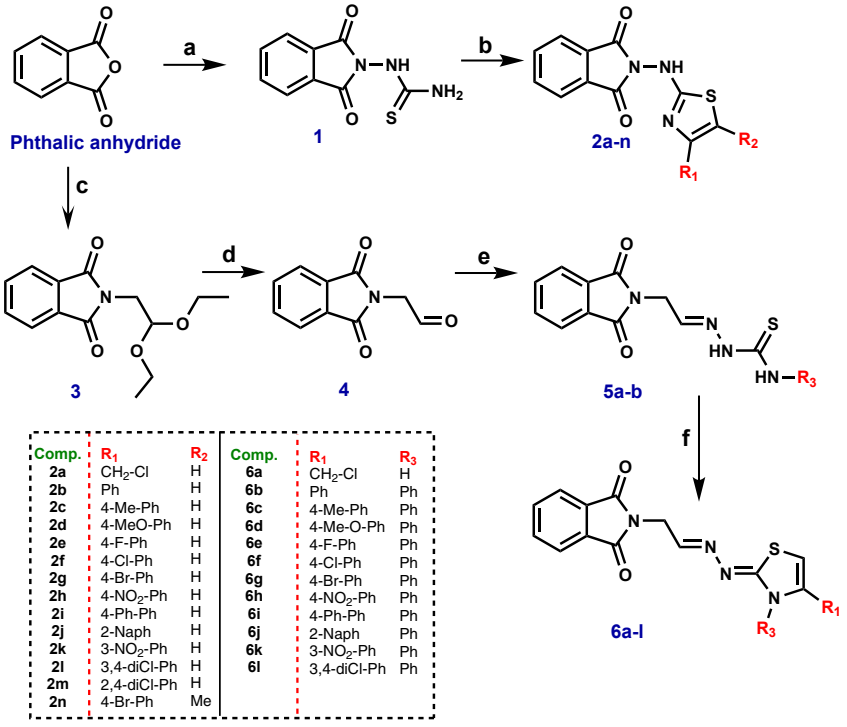

Comp.	R_1	R_2
2a	CH_2-Cl	H
2b	Ph	H
2c	4-Me-Ph	H
2d	4-MeO-Ph	H
2e	4-F-Ph	H
2f	4-Cl-Ph	H
2g	4-Br-Ph	H
2h	4-NO_2-Ph	H
2i	4-Ph-Ph	H
2j	2-Naph	H
2k	3-NO_2-Ph	H
2l	3,4-diCl-Ph	H
2m	2,4-diCl-Ph	H
2n	4-Br-Ph	Me

Comp.	R_1	R_3
6a	CH_2-Cl	H
6b	Ph	Ph
6c	4-Me-Ph	Ph
6d	4-Me-O-Ph	Ph
6e	4-F-Ph	Ph
6f	4-Cl-Ph	Ph
6g	4-Br-Ph	Ph
6h	4-NO_2-Ph	Ph
6i	4-Ph-Ph	Ph
6j	2-Naph	Ph
6k	3-NO_2-Ph	Ph
6l	3,4-diCl-Ph	Ph

Scheme 1. Global synthesis of compounds **2a-n** and **6a-l**. Reagents and conditions: (a) thiosemicarbazide, DMF, DMAP, reflux, 4h; (b) corresponding α-halogenated ketone (1,3-dichloroacetone for compound 2a), 2-propanol, ultrasound, rt, 1 h; (c) 1-aminoacetaldehyde diethyl acetal, toluene, reflux, DMAP, 2 h; (d) H_2SO_4 (70%), reflux, 2 h; (e) thiosemicarbazide (5a) or 4-phenyl-3-thiosemicarbazide (5b), EtOH, HCl, reflux, 4 h; (f) for 6a, 1,3-dichloroacetone, DMF, rt, 1 h; for 6b-l, corresponding α-halogenated ketone, 2-propanol, rt, 1 h.

series, presenting lower cytotoxic levels (269.2 μM) and equipotent trypanocidal activity compared with Bdz (4.7 vs 6.3 μM) (Table 1).

No clear correlation was observed between the substituents at the thiazole C4 and the biological activity. For example, 2-naphthyl is a bulky substituent present in **2j**; however, compound **2i**, which was also substituted with a bulky biphenylyl substituent, did not present good activity. The influence of the phenyl linked at C4 in the thiazole ring was also investigated, but no noticeable improvement in activity was observed. Comparing compound **2a** with the phenyl-unsubstituted compound **2b**, a decrease in trypanocidal activity and higher cytotoxicity were observed, while the phenyl-substituted compounds maintained or increased both activities.

A structural optimization involving addition of a spacer group ($-CH_2-CH=$) between the phthalimide and the thiazole core was performed in order to increase the flexibility of the molecules and to investigate its influence on biological activities (Fig. 5). A substitution of H with phenyl at N3 was also performed to explore the influence of bulky substituents based on the results of compounds **2i** and **2j**, both substituted with 4-biphenylyl and 2-naphthyl at C4, respectively, which displayed lower cytotoxicity.

Compounds that contained a spacer group (**6a-l**) and phenyl at N3 (**6b-l**) in general showed low cytotoxicity profiles and improved trypanocidal activity for trypomastigote form, highlighting compounds **6a** (2.2 μM), **6h** (3.2 μM), **6j** (0.5 μM) and **6k** (0.9 μM). In fact, compound **6j** presented a selective index (SI, for trypomastigote form) of 409.8, which was approximately 27-fold more selective than Bdz (SI: 15.25), the standard drug in clinical use. As observed in the **2a-n** series, the compound substituted at C4 with chloromethyl (**6a**, 2.2 μM) was more active than compounds substituted with phenyl (**6b**, 8.8 μM); indeed, phenyl-substituted compounds **6j** (0.5 μM) and **6k** (0.9 μM) were more active than **6a**. Comparing compound **6a** with **2a**, which were both substituted with chloromethyl at C4 with the unique difference of the presence of the spacer group in **6a**, a 24-fold improvement in trypanocidal activity (2.2 vs 54.4 μM) and a 4-fold increase in cytotoxicity (73.7 vs 17.0 μM) were observed for **6a**. Compounds **6k** and **6h**, both nitro-substituted compounds at the *meta* and *para* positions, respectively, presented high trypanocidal activity with selective indexes of 114.9 and 64.6, respectively (Table 1). Compound **6e** (with the electron withdrawing fluorine substituent) and **6i** (with 4-biphenylyl substituent) did not present good trypanocidal activity. Compound **6j**, which was substituted with the bulky substituent 2-naphthyl, presented the highest trypanocidal activity.

The SAR studies revealed that a series of phthalimido-thiazoles were interesting anti-*T. cruzi* compounds, which five new compounds showed low cytotoxicity in spleen cells of BALB/c mice and anti-trypanocidal activity against the trypomastigote form of the parasite.

Congreve et al. proposed a rule-of-three (RO3) [30] representing a set of guidelines for constructing a fragment library (molecular weight, <300; cLogP, ≤3; number of hydrogen bond donors, ≤3; and the number of hydrogen bond acceptors, ≤3). Recently, RO3 was accredited by most medicinal chemists and could be useful for efficient fragment selection [31]. As seen in Table 2, the phthalimide and thiazole fragments are in agreement with RO3.

The trypanocidal profile of these phthalimido-thiazoles revealed a group of privileged structure-based compounds that can be used as building blocks to obtain new lead-like compounds. They possess some structural features, such as lower molecular weights, decreased complexity and decreased hydrophobicity, which are consistent with lead-like characteristics. These compounds can be used to produce structurally simple leads with modest activity, allowing for further derivatization at a later stage to improve affinity and selectivity while retaining drug-like

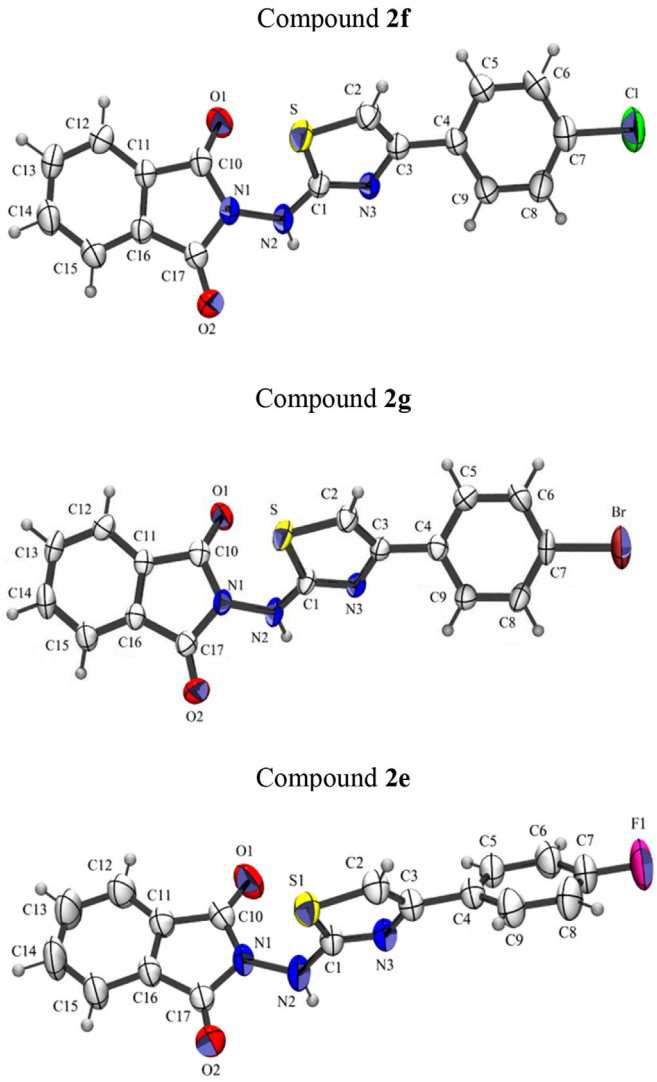

Fig. 2. The molecular structure of the title compounds showing the atom-labelling scheme and displacement ellipsoids at the 50% probability level.

characteristics.

2.3. Ultra structural studies

In view to investigate the effects of phthalimido-thiazoles on parasite morphology, compound **6k**, one of the most active compound of this work, was selected. The ultrastructural effects of **6k** on trypomastigotes after 24 h were analysed by TEM and SEM at the IC_{50} concentration and twice the IC_{50} value (Table 1), and the ultrastructural analysis showed several morphological alterations (Fig. 6).

SEM analysis revealed that treatment with 0.9 μM (1 × IC_{50}) and 1.8 μM (2 × IC_{50}) of **6k** caused blebs in the flagellum and shortening of the flagellum with a drastic decrease in the number of parasites, respectively (Fig. 6B–C), while the control group retained its typical morphology (Fig. 6A).

TEM analysis revealed that untreated parasites showed normal ultrastructural morphologies of organelles, such as kinetoplast, nucleus, nucleolus, flagellum, ribosomes and microtubule membranes (Fig. 6D), whereas parasites treated with 0.9 μM of **6k** showed alterations in the reservosomes, and a large number of cells showed intense cytoplasmic vacuolization. In addition, alterations

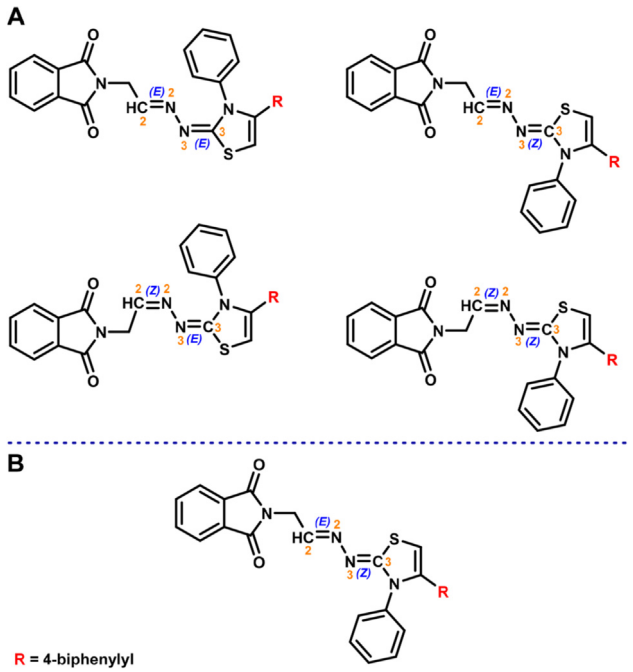

Fig. 3. Isomers representation of compound 6i. A- Possible isomers for compound 6i. B- Suggested isomer for compound 6i.

of the parasite morphology, large nuclear chromatin clumps that resembled the nuclei of apoptotic cells, mitochondria swelling and loss of cytoplasmic material were observed (Fig. 6E–F). The parasites treated with 1.8 μM of **6k** showed alterations of parasite morphology, abnormal chromatin condensation, dilated endoplasmic reticula, intense vacuolization in the cytoplasm, swelling of the kinetoplast and alterations in the reservosomes (Fig. 6G).

Ultrastructural analysis was applied to explore the damages induced by the drugs in trypomastigotes *T. cruzi* parasites and clearly showed severe morphological changes, of which intense cytoplasmic vacuolization, chromatin condensation, alterations in the reservosomes and swelling of the mitochondria were most frequent. These ultrastructural alterations are similar to those previously reported [32–36]. The ultrastructural evaluation indicated a dose-dependent action because a drastic decrease in the number of parasites was observed with increasing drug doses.

2.4. Flow cytometry analysis

After confirming that **6k** was an antiparasitic compound that affected ultrastructural cellular organization, we sought to determine whether **6k** caused parasite cell death. To this end, Y strain trypomastigotes were treated with different concentrations of **6k**. After 24 h incubation, parasite cells were stained with propidium iodide (PI) and annexin-V and analysed by flow cytometry. The results are shown in Fig. 7.

Compared with untreated cells, benznidazole resulted in PI-staining in a concentration-dependent manner, while no significant annexin-V staining was observed (data not shown). At 25 μM, benznidazole induced 56 ± 6% PI-staining in parasite cells. At the same concentration, treatment with compound **6k** induced PI-staining in 11 ± 3% of parasite cells. No PI or annexin-V staining were observed under treatment with **6k** (data not shown). Therefore, these phthalimido-thiazoles do not destroy parasite cells by classical cell death processes. Based on electronic microscopy observations, it is possible that phthalimido-thiazoles decrease

Table 1
Cytotoxicity and trypanocidal activity against epimastigotes and trypomastigotes forms.

CODE	R_1	R_2	R_3	Cytotoxicity μM[a]	IC_{50} epimastigotes (*T. cruzi*) - μM[b]	IC_{50} trypomastigotes (*T. cruzi*) - μM[c]
1	–	H	–	4.5	56.8	52.0
				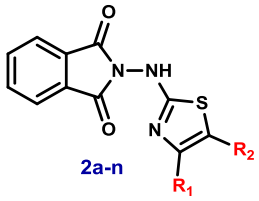		
				2a-n		
2a	Cl–Me	H	–	17.0	225.7	54.4
2b	Ph	H	–	3.1	70.2	107.5
2c	4-Me-Ph	H	–	14.9	70.4	107.0
2d	4-Me-O-Ph	H	–	14.2	6.4	50.3
2e	4-F-Ph	H	–	2.9	26.5	52.1
2f	4-Cl-Ph	H	–	2.8	30.6	86.2
2g	4-Br-Ph	H	–	2.5	14.8	89.8
2h	4-NO_2-Ph	H	–	2.7	13.3	84.9
2i	4-Ph-Ph	H	–	251.6	4.0	27.5
2j	2-Naph	H	–	269.2	8.0	4.7
2k	3-NO_2-Ph	H	–	2.7	43.2	91.1
2l	3,4-diCl-Ph	H	–	2.6	69.3	88.8
2m	2,4-diCl-Ph	H	–	12.8	10.1	22.7
2n	4-Br-Ph	Me	–	2.4	13.9	38.2
5b	–	–	Ph	50	36.9	ND
				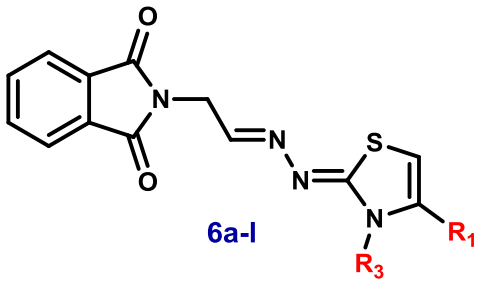		
				6a-l		
6a	Cl–Me	–	H	73.7	85.7	2.2
6b	Ph	–	Ph	228.1	ND	8.8
6c	4-Me-Ph	–	Ph	221.2	57.8	33.3
6d	4-Me-O-Ph	–	Ph	213.4	ND	10.0
6e	4-F-Ph	–	Ph	219.1	ND	73.8
6f	4-Cl-Ph	–	Ph	211.4	10.6	18.4
6g	4-Br-Ph	–	Ph	96.6	ND	9.7
6h	4-NO_2-Ph	–	Ph	206.8	12.2	3.2
6i	4-Ph-Ph	–	Ph	194.3	44.2	98.0
6j	2-Naph	–	Ph	204.9	11.9	0.5
6k	3-NO_2-Ph	–	Ph	103.4	6.0	0.9
6l	3,4-diCl-Ph	–	Ph	197.1	ND	ND
Bdz	–	–	–	96.1	48.8	6.3

[a] Highest non-toxic concentration (>90% incorporation of tritiated thymidine) in spleen cells of BALB/c mice.
[b] Determined 24 h after incubation of Y strain trypomastigotes with the compounds.
[c] Determined 11 days after incubation of epimastigotes with the compounds.[a,b] Only values with a standard deviation < 10% were included.[a,b] IC_{50} was calculated from at least five concentrations, in triplicate (SD < 10%). Bdz = Benznidazole; ND = Not Determined.

parasite viability by altering cytosol organization, mainly by causing intense cytoplasmic vacuolization.

3. Conclusion

Twenty-six phthalimido-thiazoles were obtained in reasonable yields using a simple methodology. Compounds with important trypanocidal activity, especially compounds **2j**, **6a**, **6h**, **6j** and **6k**, were identified. Flow cytometry and ultrastructural studies showed that compound **6k** did not kill the parasite via necrosis or apoptosis; however, it promoted several morphological changes in the parasite. Compound **6j**, the most potent trypanocidal agent identified in this work, presented a selective index of 409, which was approximately 26-fold more selective than Bdz, the standard drug in clinical use. Our results indicated that phthalimido-thiazoles can be used as building blocks to design promising candidates to treat Chagas disease.

4. Experimental section

4.1. Chemistry

4.1.1. Equipment and reagents

All reagents were used as purchased from commercial sources (Sigma–Aldrich, Acros Organics, Vetec or Fluka). Reaction progress was followed by thin-layer chromatography (TLC) analysis (Merck, silica gel 60 F_{254} in aluminium foil). The purities of the target compounds were confirmed by combustion analysis (for C, H, N,

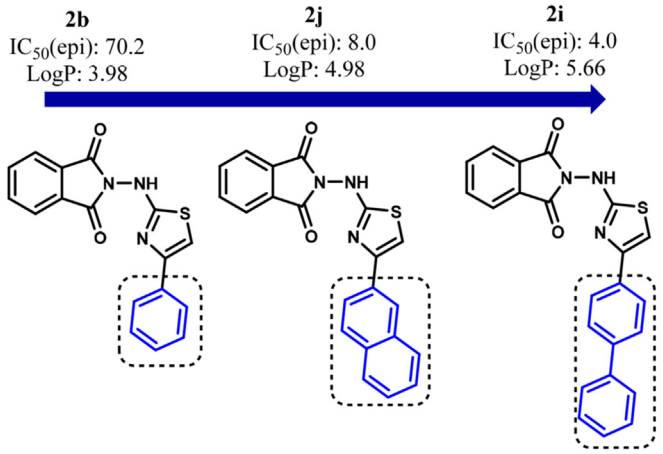

Fig. 4. Trend in trypanocidal activity for epimastigote form.

cyclization between **1** and respective α-halogenated ketone (1,3-dichloroacetone for compound **2a**), via ultrasound irradiation for 1 h, as previously related [4]. These reactions proceeded well under ultrasound conditions at room temperature using 2-propanol as solvent, resulting in satisfactory yields (36–65%) and shorter reaction times (60 min in most cases).

*4.1.2.1. 2-[4-(chloromethyl)thiazol-2-ylamino]isoindoline-1,3-dione (**2a**).* White crystals; Yield: 50%; m.p. (°C) 207–208; Rf: 0.53 (hexane/ethyl acetate 1:1). IR (KBr, cm^{-1}): 3119.15 (NH), 1743.24 (C=O). ^{1}H NMR (300 MHz, DMSO-d_6), δ $_{ppm}$: 4.54 (s, 2H, CH_2), 7.03 (s, 1H, thiazole), 7.93–7.99 (m, 4H, Ar), 10.54 (s, 1H, NH). ^{13}C NMR (75.5 MHz, DMSO-d_6), δ $_{ppm}$: 41.1 (CH_2), 109.8 (CH, thiazole), 123.9 (CH, Ar), 129.4 (C, Ar), 135.4 (CH, Ar), 147.1 (C, thiazole), 165.6 (C=O), 168.3 (S–C=N, thiazole). Anal. Calcd for $C_{12}H_8ClN_3O_2S$: C, 49.07; H, 2.75; N, 14.31; S, 10.92. found: C, 48.50; H, 2.81; N, 14.34; S 10.43. HRMS: 294.0097 $[M+H]^+$.

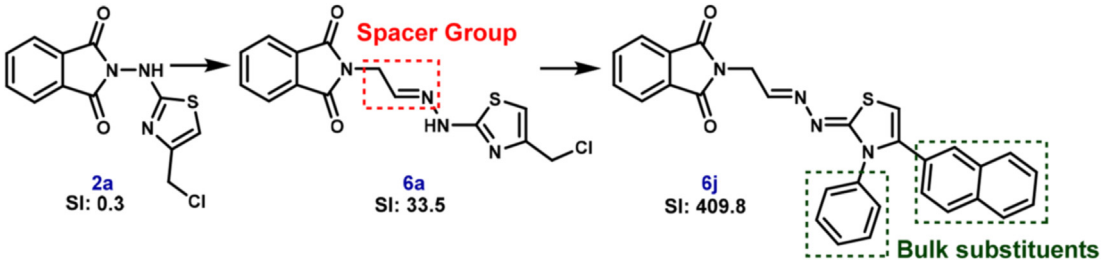

Fig. 5. Structural optimization of proposed compounds. Selective index (SI) = highest non-toxic concentration in spleen cells of BALB/c mice/IC_{50} trypomastigotes.

Table 2
Rule-of-three (RO3) calculations of the fragments phthalimide and thiazole.

Rule	Phthalimide	Thiazole	Criteria met
Molecular weight (<300)	147.13	85.12	Yes
cLogP (<3)	1.148	0.486	Yes
Number of hydrogen bond donors (<3)	1	0	Yes
Number of hydrogen bond acceptors (<3)	2	1	Yes

and S) performed using a Carlo-Erba instrument (model EA 1110). Melting points were determined on a Fisatom 430D electrothermal capillary melting point apparatus and were uncorrected. NMR spectra were measured on either a Varian UnityPlus 400 MHz (400 MHz for ^{1}H and 100 MHz for ^{13}C) or a Bruker AMX-300 MHz (300 MHz for ^{1}H and 75.5 MHz for ^{13}C) instrument. DMSO-d_6 and D_2O were purchased from CIL or Sigma–Aldrich. Chemical shifts were reported in ppm, and multiplicities were given as s (singlet), d (doublet), t (triplet), m (multiplet), dd (double doublet), and coupling constants (J) in hertz. Mass spectrometry experiments were performed on a LC-IT-TOF (Shimadzu). Unless otherwise specified, ESI was conducted in positive ion mode. Typical conditions were as follows: capillary voltage of 3 kV, cone voltage of 30 V, and peak scan between 50 and 1000 m/z. IR spectra were recorded with a Bruker model IFS66 FT-IR spectrophotometer using KBr pellets.

4.1.2. General procedure for the syntheses of 2a-n

The compound **1** was prepared by reacting commercially available thiosemicarbazide with the phthalic anhydride (1:1 mol ratio) using DMF under reflux in the presence of a catalytic amount of DMAP, for 4 h. This reaction condition led to satisfactory yield (58%). The phthalimido-thiazoles (**2a-n**) were prepared via

*4.1.2.2. 2-(4-Phenylthiazol-2-ylamino)isoindoline-1,3-dione (**2b**).* Light yellow crystals; Yield: 65%; m.p. (°C) 194–196; Rf: 0.60 (hexane/ethyl acetate 1:1). IR (KBr, cm^{-1}): 3123.66 (NH), 1742.23 (C=O). ^{1}H NMR (400 MHz, DMSO-d_6), δ $_{ppm}$: 7.25 (t, J = 7.4 Hz, 1H, Ar), 7.33 (t, J = 7.4 Hz, 2H, Ar), 7.38 (s, 1H, thiazole), 7.70 (d, J = 7.6 Hz, 2H, Ar), 7.95–8.02 (m, 4H, Ar), 10.65 (s, 1H, NH). ^{13}C NMR (100 MHz, DMSO-d_6), δ $_{ppm}$: 104.8 (CH, thiazole), 123.8 (CH, Ar), 125.5 (CH, Ar), 127.7 (CH, Ar), 128.6 (CH, Ar) 129.3 (C, Ar), 133.9 (C, Ar), 135.4 (CH, Ar), 149.9 (C, thiazole), 165.5 (C=O), 167.6 (S–C=N, thiazole). Anal. Calcd for $C_{17}H_{11}N_3O_2S$: C, 62.08; H, 3.41; N, 12.98; S, 9.71. found: C, 63.54; H, 3.45; N, 12.53; S, 9.98. HRMS: 322.0619 $[M+H]^+$.

*4.1.2.3. 2-(4-p-Tolylthiazol-2-ylamino)isoindoline-1,3-dione (**2c**).* Light yellow crystals; Yield: 37%; m.p. (°C) 214–216; Rf: 0.65 (hexane/ethyl acetate 1:1). IR (KBr, cm^{-1}): 3117.64 (NH), 1738.51 (C=O). ^{1}H NMR (400 MHz, DMSO-d_6), δ $_{ppm}$: 2.26 (s, 3H, CH_3), 7.14 (d, J = 6.8 Hz, 2H, Ar), 7.30 (s, 1H, thiazole), 7.59 (d, J = 6.8 Hz, 2H, Ar), 7.99 (m, 4H, Ar), 10.41 (s, 1H, NH). ^{13}C NMR (100 MHz, DMSO-d_6), δ $_{ppm}$: 20.8 (CH_3), 103.9 (CH, thiazole), 123.9 (CH, Ar), 125.5 (CH, Ar), 129.17 (CH, Ar), 129.3 (C, Ar), 131.4 (C, Ar), 135.4 (C, Ar), 137.1 (C, Ar), 150.2 (C, thiazole), 165.6 (C=O), 167.5 (S–C=N, thiazole). Anal. Calcd for $C_{18}H_{13}N_3O_2S$: C, 63.17; H, 3.81; N, 18.12; S, 9.17. found: C,

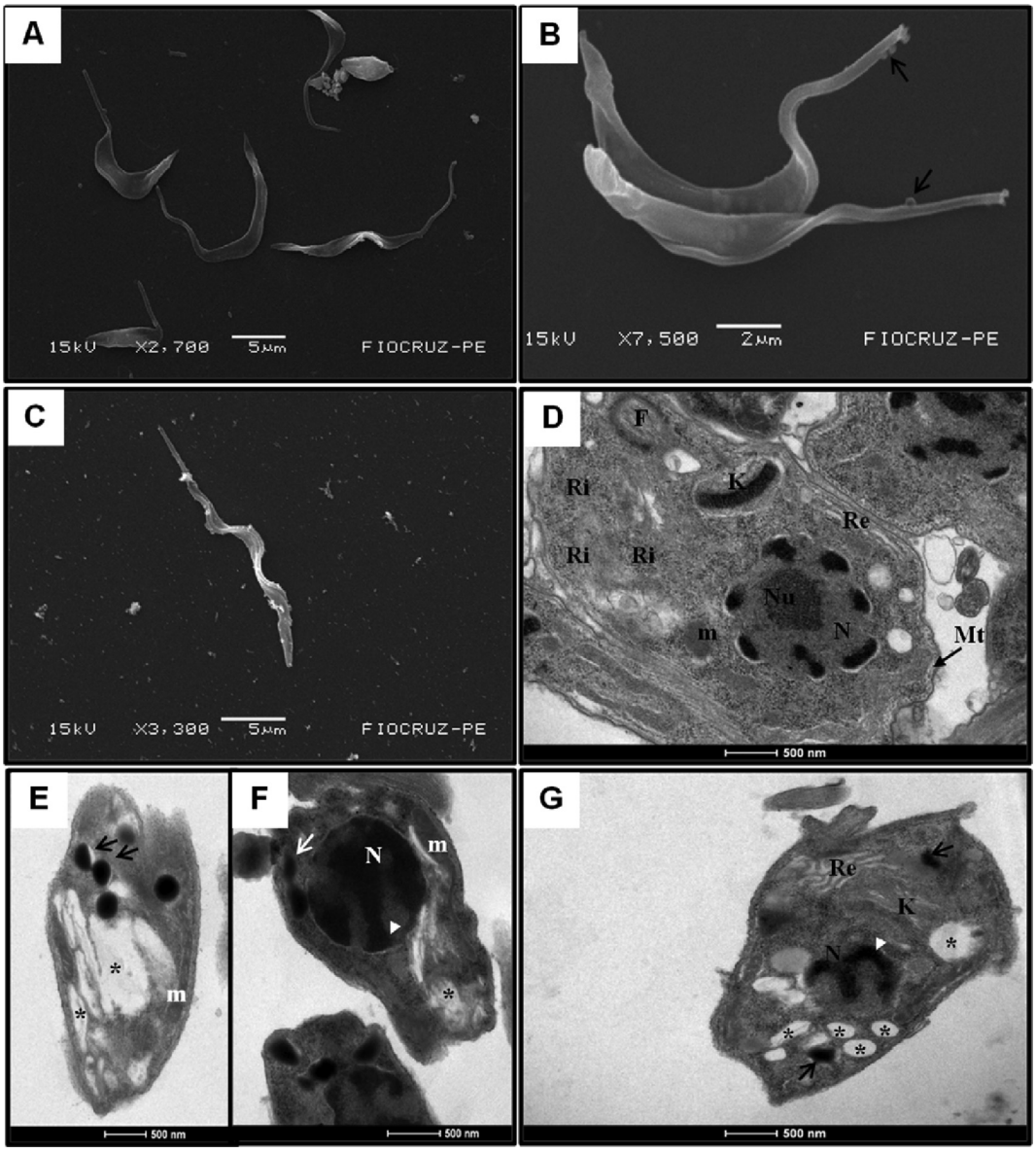

Fig. 6. Ultrastructural alterations in trypomastigotes forms of T. cruzi treated with 6k as observed by SEM and TEM. A- SEM of control untreated trypomastigotes showing the typical elongated body. B- SEM of parasite treated with 0.9 μM of 6k showing blebs in the flagellum. C- SEM of parasite treated with 1.8 μM of 6k showing drastic reduction in the number of parasites and shortening of the flagellum. D- TEM of untreated trypomastigotes showing the normal morphology with kinetoplast (K), nucleus (N), nucleolus (Nu), flagellum (F), ribosomes (Ri), mitochondria (m) and Microtubules Mt). E and F- TEM of parasite treated with 0.9 μM of 6k showing alterations of the parasite morphology, abnormal chromatin condensation (arrowhead) no nucleus (N), swelling of the mitochondrion (m), alterations in the reservosomes (arrows) and loss of cytoplasmic material (asterisks). G- TEM of parasite treated with 1.8 μM of 6k showing alterations of the parasite morphology, abnormal chromatin condensation (arrowhead), endoplasmic reticulum dilated (Re), intense vacuolization in the cytoplasm (asterisk), swelling of the kinetoplast (K) and alterations in the reservosomes (arrows).

64.46; H, 3.91; N, 18.53; S, 9.56. HRMS: 336.0812 $[M+H]^+$.

*4.1.2.4. 2-[4-(4-methoxyphenyl) thiazol-2-ylamino]isoindoline-1,3-dione (**2d**).* Light yellow crystals; Yield: 72%; m.p. (°C) 215–218; Rf: 0.53 (hexane/ethyl acetate 3:2). IR (KBr, cm^{-1}): 3232.68 (NH), 1748.64 (C=O). ^1H NMR (300 MHz, DMSO-d_6), δ $_{ppm}$: 1.025 (s, 3H, CH_3), 6.90 (d, J = 11.6 Hz, 2H, Ar), 7.20 (s, 1H, thiazole), 7.62 (d, J = 11.6 Hz, 2H, Ar), 7.98 (m, 4H, Ar), 10.72 (s, 1H, NH). ^{13}C NMR (75.5 MHz, DMSO-d_6), δ $_{ppm}$: 25.5 (CH_3), 102.7 (CH, thiazole), 114.0 (CH, Ar), 123.9 (CH, Ar), 126.7 (C, Ar), 127.0 (CH, Ar), 129.4 (C, Ar), 135.4 (CH, Ar), 149.5 (C, thiazole), 158.6 (CO, Ar), 165.6 (C=O), 167.6 (S–C=N, thiazole). Anal. Calcd for $C_{18}H_{13}N_3O_3S$: C, 58.88; H, 3.87; N, 11.38; S, 8.77. found: C, 61.53; H, 3.73; N, 11.96; S, 9.13. HRMS: 352.0825 $[M+H]^+$.

*4.1.2.5. 2-[4-(4-fluorophenyl)thiazol-2-ylamino]isoindoline-1,3-dione (**2e**).* Yellow crystals; Yield: 51%; m.p. (°C) 208–210; Rf: 0.53 (hexane/ethyl acetate 3:2). IR (KBr, cm^{-1}): 3130.14 (NH), 1743.63 (C=O). ^1H NMR (400 MHz, DMSO-d_6), δ $_{ppm}$: 7.17 (d, J = 17.6 Hz, 2H, Ar), 7.37 (s, 1H, thiazole), 7.73 (d, J = 14.0 Hz, 2H, Ar), 7.99 (m, 4H, Ar), 10.42 (s, 1H, NH). ^{13}C NMR (100 MHz, DMSO-d_6), δ $_{ppm}$: 104.6 (CH, thiazole), 115.4 (CH, Ar), 115.6 (CH, Ar), 123.9 (CH, Ar), 127.5 (CH, Ar), 129.3 (C, Ar), 135.4 (CH, Ar), 160.4 (C, thiazole), 162.9 (CF, Ar), 165.5 (C=O), 167.6 (S–C=N, thiazole). Anal. Calcd for $C_{17}H_{10}FN_3O_2S$: C, 60.32; H, 3.02; N, 12.32; S, 9.58. found: C, 60.17; H, 2.97; N, 12.38; S, 9.45. HRMS: 340.0566 $[M+H]^+$.

*4.1.2.6. 2-[4-(4-chlorophenyl)thiazol-2-ylamino]isoindoline-1,3-dione (**2f**).* Light yellow crystals; Yield: 62%; m.p. (°C) 217–218; Rf:

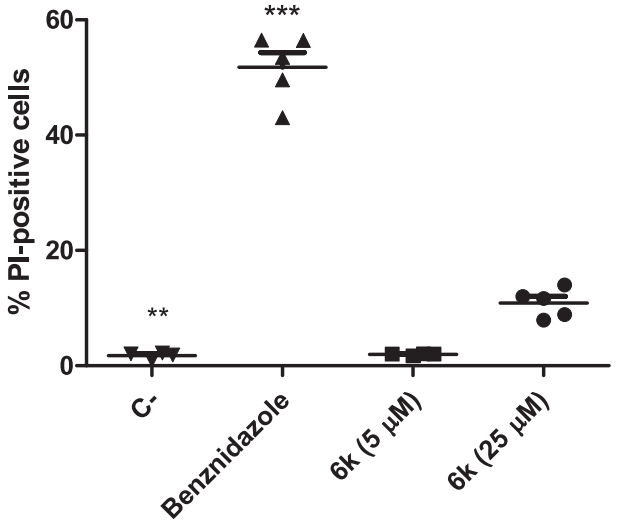

Fig. 7. % of PI-positive cells analysis under 6k treatment. Trypomastigotes were treated with complex for 24 h and examined by flow cytometry with PI staining. (C-) Untreated; Drug concentration is given in parenthesis. Two independent experiments, each concentration in duplicate. ***$p < 0.0001$ in comparison to (C-).

0.53 (hexane/ethyl acetate 1:1). IR (KBr, cm^{-1}): 3119.79 (NH), 1739.00 (C=O). ^1H NMR (400 MHz, DMSO-d_6), δ ppm: 7.39 (d, $J = 8.0$ Hz, 2H, Ar), 7.46 (s, 1H, thiazole), 7.72 (d, $J = 8$ Hz, 2H, Ar). 7.99 (m, 4H, Ar), 10.46 (s, 1H, NH). ^{13}C NMR (100 MHz, DMSO-d_6), δ ppm: 105.7 (CH, thiazole), 123.9 (CH, Ar), 127.3 (CH, Ar), 128.7 (CH, Ar), 129.3 (C, Ar) 132.2 (C, Ar), 132.9 (C, Ar), 135.4 (CCl, Ar), 148.9 (C, thiazole), 165.5 (C=O), 167.7 (S–C=N, thiazole). Anal. Calcd for $C_{17}H_{10}ClN_3O_2S$: C, 57.55; H, 2.96; N, 11.62; S, 9.03. found: C, 57.39; H, 2.83; N, 11.81; S, 9.01. HRMS: 356.0260 $[M+H]^+$.

*4.1.2.7. 2-[4-(4-bromophenyl)thiazol-2-ylamino]isoindoline-1,3-dione (**2g**).* Light yellow crystals; Yield: 55%; m.p. (°C) 220–221; Rf: 0.68 (hexane/ethyl acetate 1:1). IR (KBr, cm^{-1}): 3117.68 (NH), 1739.19 (C=O). ^1H NMR (400 MHz, DMSO-d_6), δ ppm: 7.47 (s, 1H, thiazole), 7.53 (d, $J = 8.4$ Hz, 2H, Ar), 7.65 (d, $J = 8.0$ Hz, 2H, Ar), 7.96 (m, 4H, Ar), 10.46 (s, 1H, NH). ^{13}C NMR (100 MHz, DMSO-d_6), δ ppm: 105.8 (CH, thiazole), 120.8 (CH, Ar), 123.9 (CH, Ar), 127.6 (CH, Ar), 129.3 (C, Ar) 131.6 (C, Ar), 135.4 (CBr, Ar), 148.9 (C, thiazole), 165.5 (C=O), 167.7 (S–C=N, thiazole). Anal. Calcd for $C_{17}H_{10}BrN_3O_2S$: C, 51.15; H, 2.58; N, 11.62; S, 9.03. found: C, 51.01; H, 2.52; N, 11.50; S, 8.91. HRMS: 401.9764 $[M+H]^+$.

*4.1.2.8. 2-[4-(4-nitrophenyl)thiazol-2-ylamino]isoindoline-1,3-dione (**2h**).* Yellow crystals; Yield: 41%; m.p. (°C) 239–240; Rf: 0.45 (hexane/ethyl acetate 3:2). IR (KBr, cm^{-1}): 3309.85 (NH), 1724.82 (C=O). ^1H NMR (400 MHz, DMSO-d_6), δ ppm: 7.77 (s, 1H, thiazole), 7.97 (m, 4H, Ar), 8.02 (d, $J = 8.8$ Hz, 2H, Ar), 8.21 (d, $J = 8.8$ Hz, 2H, Ar), 10.54 (s, 1H, NH). ^{13}C NMR (100 MHz, DMSO-d_6), δ ppm: 109.6 (CH, thiazole), 123.9 (CH, Ar), 124.1 (CH, Ar), 126.4 (CH, Ar), 129.3 (CN Ar), 135.4 (CH, Ar), 139.9 (C, Ar), 146.3 (C, Ar), 147.9 (C, thiazole), 165.382 (C=O), 168,0 (S–C=N, thiazole). Anal. Calcd for $C_{17}H_{10}N_4O_4S$: C, 54.40; H, 2.87; N, 15.23; S, 9.11. found: C, 55.73; H, 2.75; N, 15.29; S, 8.75. HRMS: 367.0517 $[M+H]^+$.

*4.1.2.9. 2-[4-(biphenyl-4-yl)thiazol-2-ylamino]isoindoline-1,3-dione (**2i**).* Light yellow crystals; Yield: 46%; m.p. (°C) 240–241; Rf: 0.65 (hexane/ethyl acetate 3:2). IR (KBr, cm^{-1}): 3324.67 (NH), 1660.10 (C=O). ^1H NMR (300 MHz, DMSO-d_6), δ ppm: 7.35 (s, 1H, thiazole), 7.48 (t, $J = 10.0$ Hz, 1H, Ar), 7.63 (m, 4H, Ar), 7.72 (d, $J = 11.6$ Hz, 2H, Ar), 7.82 (m, 4H, Ar) 7.96 (d, $J = 11.6$ Hz, 2H, Ar), 10.65 (s, 1H, NH). ^{13}C NMR (75.5 MHz, DMSO-d_6), δ ppm: 103.4 (CH, thiazole), 126.5 (CH, Ar), 126.9 (CH, Ar), 127.5 (CH, Ar), 128.0 (CH, Ar) 129.0 (CH, Ar), 130.1 (CH, Ar), 131.5 (CH, Ar), 133.9 (C, Ar), 136.1 (CH, Ar), 139.0 (C, Ar), 139.7 (C Ar), 150.2 (C, thiazole), 167.6 (C=O), 168.3 (S–C=N, thiazole). Anal. Calcd for $C_{23}H_{15}N_3O_2S$: C, 66.81; H, 3.98; N, 10.48; S, 7.95. found: C, 66.50; H, 3.80; N, 10.57; S, 8.07. HRMS: 398.0958 $[M+H]^+$.

*4.1.2.10. 2-[4-(naphthalen-2-yl)thiazol-2-ylamino]isoindoline-1,3-dione (**2j**).* Light yellow crystals; Yield: 47%; m.p. (°C) 225–227; Rf: 0.50 (hexane/ethyl acetate 3:2). IR (KBr, cm^{-1}): 3169.87 (NH), 1743.89 (C=O). ^1H NMR (400 MHz, DMSO-d_6), δ ppm: 7.47 (t, 2H, Ar), 7.53 (s, 1H, thiazole), 7.87 (d, $J = 11.6$ Hz, 4H, Ar), 8.03 (m, 4H, Ar), 8.23 (s, 1H, Ar), 10.48 (s, 1H, NH). ^{13}C NMR (100 MHz, DMSO-d_6) δ ppm: 105.5 (CH, thiazole), 123.9 (CH, Ar), 124.2 (CH, Ar), 126.1 (CH, Ar), 126.4 (CH, Ar) 127.1 (CH, Ar), 127.6 (CH, Ar), 128.1 (CH, Ar), 128.2 (CH, Ar), 129.3 (C, Ar), 131.5 (C, Ar), 132.4 (C, Ar), 133.0 (C, Ar), 135.4 (CH, Ar), 150.1 (C, thiazole), 165.6 (C=O), 168.0 (S–C=N, thiazole). Anal. Calcd for $C_{21}H_{13}N_3O_2S$: C, 64.89; H, 3.48; N, 11.45; S, 8.26. found: C, 67.91; H, 3.53; N, 11.11; S, 8.63. HRMS: 367.0517 $[M+H]^+$.

*4.1.2.11. 2-[4-(3-nitrophenyl)thiazol-2-ylamino]isoindoline-1,3-dione (**2k**).* Light yellow crystals; Yield: 44%; m.p. (°C) 206–207; Rf: 0.55 (hexane/ethyl acetate 3:2). IR (KBr, cm^{-1}): 3287.35 (NH), 1732.47 (C=O). ^1H NMR (300 MHz, DMSO-d_6) δ ppm: 7.65 (t, $J = 7.2$ Hz, 1H, Ar), 7.73 (s, 1H, thiazole), 8.00 (m, 4H, Ar), 8.13 (m, 2H, Ar), 8.48 (s, 1H, Ar) 10.36 (s, 1H, NH). ^{13}C NMR (75.5 MHz, DMSO-d_6), δ ppm: 107.7 (CH, thiazole), 119.9 (CH, Ar), 122.3 (CH, Ar), 123.9 (CH, Ar), 129.3 (CN, Ar) 130.3 (CH, Ar), 131.7 (CH, Ar), 135.5 (CH, Ar), 147.7 (C, Ar), 148.2 (C, thiazole), 165.5 (C=O), 168.2 (S–C=N, thiazole). Anal. Calcd for $C_{17}H_{10}N_4O_4S$: C, 53.04; H, 2.88; N, 15.49; S, 8.90. found: C, 54.73; H, 2.75; N, 15.29; S, 8.75. HRMS: 367.0517 $[M+H]^+$.

*4.1.2.12. 2-[4-(3,4-dichlorophenyl)thiazol-2-ylamino]isoindoline-1,3-dione (**2l**).* Light yellow crystals; Yield: 57%; m.p. (°C) 217–218; Rf: 0.53 (hexane/ethyl acetate 3:2). IR (KBr, cm^{-1}): 3337.03 (NH), 1742.53 (C=O). ^1H NMR (300 MHz, DMSO-d_6), δ ppm: 7.52 (s, 1H, thiazole), 7.62 (s, 1H, Ar), 7.68 (d, $J = 2.1$ Hz, 1H, Ar), 7.94 (d, $J = 1.8$ Hz, 1H, Ar), 8.00 (m, 4H, Ar), 10.51 (s, 1H, NH). ^{13}C NMR (75.5 MHz, DMSO-d_6), δ ppm: 107.1 (CH, thiazole), 123.9 (CH, Ar), 127.1 (CH, Ar), 129.3 (CCl, Ar), 129.5 (CH, Ar), 130.9 (CCl, Ar), 131.4 (C, Ar), 134.5 (CH, Ar), 135.4 (C, Ar), 136.0 (CH, Ar), 147.9 (C, thiazole), 165.4 (C=O), 167.9 (S–C=N, thiazole). Anal. Calcd for $C_{17}H_9Cl_2N_3O_2S$: C, 51.19; H, 2.43; N, 11.04; S, 8.58. found: C, 52.32; H, 2.32; N, 10.77; S, 8.22. HRMS: 356.0260 $[M+H]^+$.

*4.1.2.13. 2-[4-(2,4-dichlorophenyl)thiazol-2-ylamino]isoindoline-1,3-dione (**2m**).* Colourless crystals; Yield: 46%; m.p. (°C) 217–218; Rf: 0.55 (hexane/ethyl acetate 3:2). IR (KBr, cm^{-1}): 3130.90 (NH), 1741.75 (C=O). ^1H NMR (400 MHz, DMSO-d_6), δ ppm: 7.41 (d, $J = 7.2$ Hz, 1H, Ar), 7.45 (s, 1H, thiazole), 7.63 (s, 1H, Ar), 7.65 (d, $J = 8.4$ Hz, 1H, Ar). 7.97 (m, 4H, Ar), 10.46 (s, 1H, NH). ^{13}C NMR (100 MHz, DMSO-d_6), δ ppm: 110.45 (CH, thiazole), 123.8 (CH, Ar), 127.5 (CH, Ar), 129.3 (CCl, Ar), 129.7 (CH, Ar), 131.5 (CCl, Ar), 131.5 (C, Ar), 132.1 (CH, Ar), 132.7 (C, Ar), 135.4 (CH, Ar), 145.4 (C, thiazole), 165.4 (C=O), 166.7 (S–C=N, thiazole). Anal. Calcd for $C_{17}H_9Cl_2N_3O_2S$: C, 52.25; H, 2.26; N, 10.50; S, 7.91. found: C, 52.32; H, 2.32; N, 10.77; S, 8.22. HRMS: 356.0260 $[M+H]^+$.

*4.1.2.14. 2-[4-(4-bromophenyl)-5-methylthiazol-2-ylamino]isoindoline-1,3-dione (**2n**).* Yellow crystals; Yield: 36%; m.p. (°C) 235–236; Rf: 0.60 (hexane/ethyl acetate 3:2). IR (KBr, cm^{-1}): 3188.90 (NH), 1745.97 (C=O). ^1H NMR (400 MHz, DMSO-d_6), δ ppm: 2.36 (s, 3H, CH_3), 7.41 (d, $J = 8.4$ Hz, 2H, Ar), 7.55 (d, $J = 8.4$ Hz, 2H, Ar), 7.96 (m, 4H, Ar), 10.23 (s, 1H, NH); ^{13}C NMR (100 MHz, DMSO-d_6), δ ppm: 12.1

(CH_3), 119.3 (C, thiazole), 120.4 (C, Ar), 123.8 (CH, Ar), 129.3 (C, Ar), 129.8 (CH, Ar), 131.2 (CH, Ar), 133.7 (CBr, Ar), 135.3 (CH, Ar), 144.0 (C, thiazole), 163.5 (C=O), 165.5 (S–C=N, thiazole). Anal. Calcd for $C_{17}H_{12}BrN_3O_2S$: C, 51.75; H, 3.00; N, 9.93; S, 7.58. found: C, 52.19; H, 2.92; N, 10.10; S, 7.74. HRMS: 401.9764 $[M+H]^+$.

4.1.3. Procedure for the syntheses of intermediate compounds 5a-b

Compound **3** was prepared by the condensation of commercially available aminoacetaldehyde diethyl acetal with the phthalic anhydride (1:1 mol ratio), using toluene under reflux, in the presence of a catalytic amount of DMAP (yield 52%) for 2 h. In the next step, 2-(2,2-diethoxyethyl)isoindoline-1,3-dione (**3**) underwent acid hydrolysis (sulphuric acid at 70%) in reflux for 2 h. After the reaction was completed, it was allowed to reach at room temperature and was then cooled to induce precipitation. The formed precipitate was filtered on a sintered funnel with distilled water, yielding 55% of the pure product. For the synthesis of **5a** and **5b**, 2-(1,3-dioxoisoindol-2-yl) acetaldehyde (**4**) reacted with thiosemicarbazide (in the ratio 1:1) (for **5a**) or 4-phenyl-3-thiosemicarbazide (for **5b**), in ethanol, under reflux with catalytic amount of HCl (4 drops) for 4 h. The reactions were followed by thin layer chromatographic plate analysis. The formed precipitate was filtered on a sintered funnel with ethanol to yield the pure product (yield 76% for **5a** and 70% for **5b**).

*4.1.3.1. (E)-2-[2-(1,3-dioxoisoindolin-2-yl)ethylidene]hydrazinecarbothioamide (**5a**).* White crystals; Yield: 76%; m.p. (°C) 223–224; Rf 0.45 (hexane/ethyl acetate 3:2); IR (KBr, cm^{-1}): 3423 and 3308 (N–H), 1769 and 1713 (C=O), 1602 (C=N); ^1H NMR (300 MHz, DMSO-d_6), δ_{ppm}: 4.36 (d, $J = 3.6$ Hz, 2H, CH_2), 7.36 (s, 1H, NH), 7.42 (t, $J = 3.6$ Hz, 1H, CH=N), 7.83–7.90 (m, 4H, Ar), 8.03 and 11.27 (s, 1H, NH_2); ^{13}C NMR (75.5 MHz, DMSO-d_6), δ_{ppm}: 40.1 (CH_2), 123.1 (Ar), 131.7 (Ar), 134.4 (Ar), 140.4 (C=N), 167.5 (C=O), 177.9 (C=S). Anal. Calcd for $C_{11}H_{10}N_4O_2S$: C, 50.37; H, 3.84; N, 21.36; S, 12.22. found: C, 50.03; H, 3.45; N, 20.98; S, 12.30. HRMS: 262.3388 $[M+H]^+$.

*4.1.3.2. (E)-2-[2-(1,3-dioxoisoindolin-2-yl)ethylidene]-N-phenylhydrazinecarbothioamide (**5b**).* White crystals; Yield: 70%; m.p. (°C) 174–176; Rf 0.52 (hexane/ethyl acetate 3:2); ^1H NMR (300 MHz, DMSO-d_6), δ_{ppm}: 4.46 (d, $J = 4.2$ Hz, 2H, CH_3), 7.14 (t, $J = 7.8$ Hz, 1H, Ar), 7.29 (t, $J = 7.8$ Hz, 2H, Ar), 7.42 (d, $J = 7.8$ Hz, 2H), 7.52 (t, $J = 4.2$ Hz, 1H, Ar), 7.85–7.99 (m, 4H, Ar), 9.66 (s, 1H, NH), 11.72 (s, 1H, NH); ^{13}C NMR (75.5 MHz, DMSO-d_6), δ_{ppm}: 40 (CH_2), 123.2 (Ar), 124.7 (Ar), 125.1 (Ar), 128.1 (Ar), 131.7 (Ar), 134.5 (Ar), 138.7 (Ar), 140.9 (C=N), 167.6 (C=O), 175.8 (C=S). Anal. Calcd for $C_{17}H_{14}N_4O_2S$: C, 60.34; H, 4.17; N, 16.56; S, 9.48. found: C, 60.03; H, 4.45; N, 16.35; S, 11.30. HRMS: 339.0845 $[M+H]^+$.

4.1.4. Procedure for the synthesis of 6a

In a round bottom flask was added 2-(2-(1,3-dioxoisoindolin-2-yl) ethylidene)hydrazinecarbothioamide (**5a**), 1,3-dichloroacetone and DMF. The reaction mixture was stirred at room temperature for about 1 h. The reaction was followed by thin layer chromatographic plate. After addition of distilled water, the pure product precipitates.

*4.1.4.1. (E)-2-(2-{2-[4-(chloromethyl)thiazol-2-yl]hydrazono}ethyl) isoindoline-1,3-dione (**6a**).* White crystals; Yield: 82%; m.p. (°C) 191–193; Rf 0.23 (hexane/ethyl acetate 3:2); IR (KBr, cm^{-1}): 3159.36 and 3113.44 (N–H), 1771.01 and 1717.67 (C=O), 1565.77 (C=N). ^1H NMR (400 MHz, DMSO-d_6), δ_{ppm}: 4.41 (d, $J = 3.2$ Hz, 2H, CH_2), 4.53 (s, 2H, CH_2), 6.76 (s, 1H, CH, thiazole), 7.32 (s, 1H, CH), 7.86–7.89 (m, 4H, CH Ar), 11.75 (s, 1H, NH); ^{13}C NMR (75.5 MHz, DMSO-d_6), δ_{ppm}: 38 (CH_2), 41.7 (CH_2), 107.9 (CH, thiazole), 123.1 (Ar), 131.7 (Ar), 134.5 (Ar), 138.4 (C, thiazole), 147.8 (C=N), 167.5 (C=O), 168.6 (S–C=N, thiazole). Anal. Calcd for $C_{14}H_{11}ClN_4O_2S$: C, 50.23; H, 3.31; N, 16.74; S, 9.58. found: C, 49.91; H, 3.30; N, 16.82; S, 10.03. HRMS: 335.0463 $[M+H]^+$.

4.1.5. General procedure for the synthesis of 6b-l

In round bottom flask was added 2-(2-(1,3-dioxoisoindolin-2-yl)ethylidene)-*N*-phenyl-hydrazine-carbothioamide (**5b**), the respective α-halogenated ketone and 2-propanol. The reaction mixture was kept under magnetic stirring, at room temperature, for 1 h. The reactions were followed by thin layer chromatographic plate. The formed precipitate was filtered on sintered funnel with distilled water, yielding the pure product.

*4.1.5.1. 2-((E)-2-{(Z)-[3,4-diphenylthiazol-2(3H)-ylidene]hydrazono} ethyl)isoindoline-1,3-dione (**6b**).* Orange crystals; Yield: 56%; m.p. (°C) 196–198; Rf 0.46 (hexane/ethyl acetate 3:2); IR (KBr, cm^{-1}): 1712.40 (C=O). ^1H NMR (300 MHz, DMSO-d_6), δ_{ppm}: 4.42 (d, $J = 3$ Hz 2H, CH_2), 6.45 (s, 1H, CH, thiazole), 7.09–7.32 (m, 10H, CH Ar), 7.44 (t, $J = 3$ Hz, 1H, HC=N), 7.91–7.88 (m, 4H, CH Ar, phthalimide); ^{13}C NMR (75.5 MHz, DMSO-d_6), δ_{ppm}: 40.3 (CH_2), 104.2 (CH, thiazole), 123.0 (Ar), 125.2 (Ar), 128.0 (Ar), 128.1 (Ar), 128.3 (Ar), 128.6 (Ar), 128.8 (Ar), 130.6 (Ar), 131.8 (Ar), 134.4 (Ar), 137.3 (Ar), 139.3 (C, thiazole), 148.2 (C=N), 167.5 (C=O), 169.9 (S–C–N, thiazole). Anal. Calcd for $C_{25}H_{18}N_4O_2S$: C, 68.48; H, 4.14; N, 12.78; S, 7.31. found: C, 66.88; H, 4.30; N, 12.48; S, 7.12. HRMS: 439.1028 $[M+H]^+$.

*4.1.5.2. 2-((E)-2-{(Z)-[3-phenyl-4-p-tolylthiazol-2(3H)-ylidene] hydrazono}ethyl)isoindoline-1,3-dione (**6c**).* Yellow crystals; Yield: 52%; m.p. (°C) 156–158; Rf: 0.7 (hexane/ethyl acetate 3:2). IR (KBr, cm^{-1}): 1712.39 (C=O). ^1H NMR (300 MHz, DMSO-d_6), δ_{ppm}: 2.19 (s, 3H,CH_3), 4.42 (d, $J = 3$ Hz, 2H, CH_2), 6.41 (s, 1H, CH thiazole), 6.95–6.99 (m, 4H, CH Ar), 7.17–7.45 (m, 6H, CH Ar), 7.88–7.95 (m, 4H, CH Ar phthalimide); ^{13}C NMR (75.5 MHz, DMSO-d_6), δ_{ppm}: 20.7 (CH_3), 38.9 (CH_2), 100.7 (CH, thiazole), 123.1 (Ar), 127.7 (Ar), 128.1 (Ar), 128.7 (Ar), 128.8 (Ar), 128.9 (Ar), 129.8 (Ar), 131.8 (Ar), 134.5 (Ar), 137.4 (Ar), 137.9 (Ar), 139.456 (C, thiazole), 148.2 (C=N), 167.6 (C=O), 170.1 (S–C–N, thiazole). Anal. Calcd for $C_{26}H_{20}N_4O_2S$: C, 69.01; H, 4.45; N, 12.38; S, 7.09. found: C, 68.66; H, 4.36; N, 12.12; S, 6.96. HRMS: 453.1138 $[M+H]^+$.

*4.1.5.3. 2-((E)-2-{(Z)-[4-(4-methoxyphenyl)-3-phenylthiazol-2(3H)-ylidene]hydrazono}ethyl)isoindoline-1,3-dione (**6d**).* Yellow crystals; Yield: 54%; m.p. (°C) 173–175; Rf 0.49 (hexane/ethyl acetate 3:2); IR (KBr, cm^{-1}): 1713.83 (C=O). ^1H NMR (300 MHz, DMSO-d_6), δ_{ppm}: 4.18 (s, 3H, CH_3), 4.44 (d, $J = 3$ Hz, 2H, CH_2), 6.83–8.10 (m, 14H, Ar); ^{13}C NMR (75.5 MHz, DMSO-d_6), δ_{ppm}: 40.1 (CH_2), 56.4 (CH_3), 104.3 (CH, thiazole), 123.1 (Ar), 123.3 (Ar), 127.9 (Ar), 128.4 (Ar), 128.8 (Ar), 129.2 (Ar), 131.7 (Ar), 134.5 (Ar), 136.6 (Ar), 136.7 (Ar), 137.6 (Ar), 139.0 (C, thiazole), 146.8 (C=N), 167.5 (C=O), 169.6 (S–C–N, thiazole). Anal. Calcd for $C_{26}H_{20}N_4O_3S$: C, 66.65; H, 4.30; N, 11.96; S, 6.84. found: C, 65.60; H, 4.08; N, 11.85; S, 6.68. HRMS: 469.1276 $[M+H]^+$.

*4.1.5.4. 2-((E)-2-{(Z)-[4-(4-fluorophenyl)-3-phenylthiazol-2(3H)-ylidene]hydrazono}ethyl)isoindoline-1,3-dione (**6e**).* Yellow crystals; Yield: 50%; m.p. (°C)176–179; Rf: 0.63 (hexane/ethyl acetate 3:2); IR (KBr, cm^{-1}): 1714.47 (C=O); ^1H NMR (300 MHz, DMSO-d_6), δ_{ppm}: 4.43 (d, $J = 3$ Hz, 2H, CH_2), 6.47 (s, 1H, CH thiazole), 7.02–7.36 (m, 9H, CH Ar), 7.45 (t, $J = 3$ Hz, 1H, CH), 7.86–7.95 (m, 4H, CH Ar phthalimide); ^{13}C NMR (75.5 MHz, DMSO-d_6), δ_{ppm}: 38.9 (CH_2), 101.3 (CH, thiazole), 115.1 (Ar), 115.3 (Ar), 123.1 (Ar), 127.1 (Ar), 128.0 (Ar), 128.7 (Ar), 128.9 (Ar), 130.6 (Ar), 131.8 (Ar), 134.5 (Ar), 137.2 (Ar),138.3 (C, thiazole), 148.3 (C=N), 160.2 and 163.4 (C–F), 167.6

(C=O), 169.9 (S–C–N, thiazole). Anal. Calcd for $C_{25}H_{17}FN_4O_2S$: C, 65.78; H, 3.75; N, 12.27; S, 7.02. found: C, 63.91; H, 3.79; N, 12.01; S, 6.94. HRMS: 457.1083 $[M+H]^+$.

*4.1.5.5. 2-(2-{(Z)-[4-(4-chlorophenyl)-3-phenylthiazol-2(3H)-ylidene]hydrazono}ethyl)isoindoline-1,3-dione (**6f**).* Yellow crystals; Yield: 58%; m.p. (°C) 176–179; Rf: 0.84 (hexane/ethyl acetate 3:2); IR (KBr, cm^{-1}): 1717.30 (C=O). ^1H NMR (300 MHz, DMSO-d_6), δ ppm: 4.41 (d, $J = 3$ Hz, 2H, CH_2), 6.50 (s, 1H, thiazole), 7.07–7.37 (m, 9H, Ar), 7.44 (t, $J = 3$ Hz, 1H) 7.85–7.94 (m, 5H, Ar); ^{13}C NMR (75.5 MHz, DMSO-d_6), δ ppm: 56.0 (CH_2), 101.8 (CH, thiazole), 123.1 (Ar), 127.9 (Ar), 128.1 (Ar), 128.6 (Ar), 128.9 (Ar), 129.5 (Ar), 129.9 (Ar), 131.8 (Ar), 133.1 (Ar), 134.5 (Ar), 137.2 (Ar), 138.7 (C, thiazole), 148.3 (C=N), 167.6 (C=O), 169.9 (S–C–N, thiazole). Anal. Calcd for $C_{25}H_{17}ClN_4O_2S$: C, 63.49; H, 3.62; N, 11.85; S, 6.78. found: C, 61.17; H, 3.43; N, 11.47; S, 6.79. HRMS: 473.0793 $[M+H]^+$.

*4.1.5.6. 2-((E)-2-{(Z)-[4-(4-bromophenyl)-3-phenylthiazol-2(3H)-ylidene]hydrazono}ethyl)isoindoline-1,3-dione (**6g**).* White crystals; Yield: 55%; m.p. (°C) 189–193; Rf: 0.73 (hexane/ethyl acetate 3:2); IR (KBr, cm^{-1}): 1717.05 (C=O). ^1H NMR (300 MHz, DMSO-d_6), δ ppm: 4.42 (d, $J = 3$ Hz, 2H, CH_2), 6.51 (s, 1H, thiazole), 7.01–7.94 (m, 14H, Ar); ^{13}C NMR (75.5 MHz, DMSO-d_6), δ ppm: 39.3 (CH_2), 101.87 (CH, thiazole), 121.7 (Ar), 123.1 (Ar), 127.9 (Ar), 128.6 (Ar), 128.9 (Ar), 129.8 (Ar), 130.1 (Ar), 131.2 (Ar), 131.8 (Ar), 134.5 (Ar), 137.2 (Ar), 138.1 (C, thiazole), 148.5 (C=N), 167.6 (C=O), 169.9 (S–C–N, thiazole). Anal. Calcd for $C_{25}H_{17}BrN_4O_2S$: C, 58.03; H, 3.31; N, 10.83; S, 6.20. found: C, 57.27; H, 3.28; N, 10.68; S, 6.06. HRMS: 517.0005 $[M+H]^+$.

*4.1.5.7. 2-((E)-2-{(Z)-[4-(4-nitrophenyl)-3-phenylthiazol-2(3H)-ylidene]hydrazono}ethyl)isoindoline-1,3-dione (**6h**).* Orange crystals; Yield: 46%; m.p. (°C) 186–189; Rf: 0.75 (hexane/ethyl acetate 3:2). IR (KBr, cm^{-1}): 1713.38 (C=O). ^1H NMR (300 MHz, DMSO-d_6), δ ppm: 4.45 (d, $J = 3$ Hz, 2H, CH_2), 6.78–8.10 (m, 15H, Ar); ^{13}C NMR (75.5 MHz, DMSO-d_6), δ ppm: 40.1 (CH_2), 102.0 (CH, thiazole), 123.2 (Ar), 123.3 (Ar), 124.5 (Ar), 128.0 (Ar), 128.4 (Ar), 129.0 (Ar), 131.7 (Ar), 131.7 (Ar), 134.5 (Ar), 136.7 (Ar), 137.4 (Ar), 138.7 (C, thiazole), 146.7 (C=N), 167.5 (C=O), 169.6 (S–C–N, thiazole). Anal. Calcd for $C_{25}H_{17}N_5O_4S$: C, 62.10; H, 3.54; N, 14.48; S, 6.63. found: C, 59.19; H, 3.65; N, 13.76; S, 6.93. HRMS: 484.0975 $[M+H]^+$.

*4.1.5.8. 2-((E)-2-{(Z)-[4-(biphenyl-4-yl)-3-phenylthiazol-2(3H)-ylidene]hydrazono}ethyl)isoindoline-1,3-dione (**6i**).* Yellow crystals; Yield: 73%; m.p. (°C) 157–159; Rf 0.43 (hexane/ethyl acetate 3:2); IR (KBr, cm^{-1}): 1716.38 (C=O). ^1H NMR (400 MHz, DMSO-d_6), δ ppm: 4.48 (d, $J = 3.6$ Hz, 2H, CH_2), 6.05 (s, 1H, thiazole), 7.00–7.82 (m, 19H, Ar); ^{13}C NMR (75.5 MHz, DMSO-d_6), δ ppm: 39.2 (CH_2), 101.2 (CH, thiazole), 123.3 (Ar), 126.8 (Ar), 126.9 (Ar), 127.7 (Ar), 128.3 (Ar), 128.4 (Ar), 128.5 (Ar), 128.6 (Ar), 128.7 (Ar), 128.8 (Ar), 129.2 (Ar), 129.6 (Ar), 132.3 (Ar), 133.9 (Ar), 133.9 (Ar), 139.9 (C, thiazole), 141.2 (C=N), 167.8 (C=O), 169.0 (S–C–N, thiazole). Anal. Calcd for $C_{31}H_{22}N_4O_2S$: C, 72.35; H, 4.31; N, 10.89; S, 6.23. found: C, 70.19; H, 4.32; N, 10.35; S, 6.53. HRMS: 515.1416 $[M+H]^+$.

*4.1.5.9. 2-((E)-2-{(Z)-[4-(naphthalen-2-yl)-3-phenylthiazol-2(3H)-ylidene]hydrazono}ethyl)isoindoline-1,3-dione (**6j**).* Yellow crystals; Yield: 68%; m.p. (°C) 159–161; Rf 0.43 (hexane/ethyl acetate 3:2); IR (KBr, cm^{-1}): 1713.93 (C=O). ^1H NMR (400 MHz, DMSO-d_6), δ ppm: 4.56 (d, $J = 4$ Hz, 2H, CH_2), 6.18 (s, 1H, thiazole), 6.99–7.91 (m, 17H, Ar); ^{13}C NMR (75.5 MHz, DMSO-d_6), δ ppm: 39.2 (CH_2), 101.6 (CH, thiazole), 123.3 (Ar), 125.4 (Ar), 126.5 (Ar), 126.7 (Ar), 127.6 (Ar), 127.7 (Ar) 127.8 (Ar), 128.0 (Ar), 128.1 (Ar), 128.3 (Ar), 128.4 (Ar), 128.7 (Ar), 129.2 (Ar), 132.3 (Ar), 132.8 (Ar), 133.9 (Ar), 137.5 (Ar), 140.3 (C, thiazole), 149.5 (C=N), 167.8 (C=O), 171.0 (S–C–N, thiazole). Anal. Calcd for $C_{29}H_{20}N_4O_2S$: C, 71.29; H, 4.13; N, 11.47; S, 6.56. found: C, 70.09; H, 4.21; N, 11.41; S, 6.70. HRMS: 489.1296 $[M+H]^+$.

*4.1.5.10. 2-((E)-2-{(Z)-[4-(3-nitrophenyl)-3-phenylthiazol-2(3H)-ylidene]hydrazono}ethyl)isoindoline-1,3-dione (**6k**).* Yellow crystals; Yield: 63%; m.p. (°C) 154-154; Rf 0.34 (hexane/ethyl acetate 3:2); IR (KBr, cm^{-1}): 1712.80 (C=O). ^1H NMR (300 MHz, DMSO-d_6), δ ppm: 4.43 (d, $J = 2.7$ Hz, 2H, CH_2), 6.76 (s, 1H, CH thiazole), 7.25–7.38 (m, 5H, CH Ar), 7.48–7.51 (m, 3H, CH Ar), 7.86–7.95 (m, 6H, CH Ar), 8.07 (t, $J = 2.4$ Hz, 1H, HC=N); ^{13}C NMR (75.5 MHz, DMSO-d_6), δ ppm: 39.3 (CH_2), 104.3 (CH, thiazole), 123.2 (Ar), 123.4 (Ar), 123.6 (Ar), 128.8 (Ar), 128.9 (Ar), 129.1 (Ar), 129.3 (Ar), 129.5 (Ar), 129.6 (Ar), 130.0 (Ar), 130.3 (Ar), 135.0 (Ar), 135.6 (Ar), 138.8 (C, thiazole), 149.3 (C=N), 167.5 (C=O), 169.6 (S–C–N, thiazole). Anal. Calcd for $C_{25}H_{17}N_5O_4S$: C, 62.10; H, 3.54; N, 14.48; S, 6.63. found: C, 60.45; H, 3.70; N, 14.10; S, 6.48. HRMS: 484.0976 $[M+H]^+$.

*4.1.5.11. 2-((E)-2-{(Z)-[4-(3,4-dichlorophenyl)-3-phenylthiazol-2(3H)-ylidene]hydrazono}ethyl)isoindoline-1,3-dione (**6l**).* Yellow crystals; Yield: 48%; m.p. (°C) 155–157; Rf: 0.89 (hexane/ethyl acetate 3:2); IR (KBr, cm^{-1}): 1714.45 (C=O). ^1H NMR (300 MHz, DMSO-d_6), δ ppm: 4.45 (d, $J = 3$ Hz, 2H, CH_2), 6.81–7.92 (m, 14H, Ar); ^{13}C NMR (75.5 MHz, DMSO-d_6), δ ppm: 40.1 (CH_2), 104.6 (CH, thiazole), 123.1 (Ar), 128.3 (Ar), 128.6 (Ar), 128.9 (Ar), 129.3 (Ar), 130.3 (Ar), 130.5 (Ar), 130.9 (Ar), 131.4 (Ar), 131.7 (Ar), 134.3 (Ar), 134.6 (Ar), 136.1 (Ar), 137.3 (C, thiazole), 149.2 (C=N), 167.5 (C=O), 169.6 (S–C–N, thiazole); Anal. Calcd for $C_{25}H_{16}Cl_2N_4O_2S$: C, 59.18; H, 3.18; N, 11.04; S, 6.32. found: C, 56.85; H, 3.30; N, 10.58; S, 6.02. HRMS: 507.0432 $[M+H]^+$.

4.2. X-ray analysis

X-ray diffraction data collections were performed on an Enraf-Nonius Kappa-CCD diffractometer (95 mm CCD camera on κ-goniostat) using graphite monochromated MoKα radiation (0.71073 Å) at room temperature. Data were collected using the COLLECT software [37] up to 50° (2θ). The final unit cell parameters were based on 15666, 9327, and 12333 reflections to **2e**, **2f** and **2g**, respectively. Integration and scaling of the reflections as well as the corrections for Lorentz and polarization effects were performed with the HKL DENZO-SCALEPACK system of programs [38]. The compound structures were solved by direct methods with SHELXS-97 [39]. The model was refined by full-matrix least squares on F2 using SHELXL-97 [39]. The program ORTEP-3 [40] was used for graphic representations, and the program WinGX [41] was used to prepare the material for publication. All H atoms were located by geometric considerations placed (C–H = 0.93 Å; N–H = 0.86 Å) and refined using a riding model with Uiso(H) = 1.5Ueq(C-methyl) or 1.2Ueq(other). An Ortep-3 diagram of the molecules is shown in Fig. 2, and Table S1 shows the main crystallographic data. Crystallographic data (excluding structure factors) for the structures reported in this paper have been deposited with the Cambridge Crystallographic Data Centre as supplementary material (No. CCDC 1411254, 1411262 and 1411263).

4.3. Biological assays of toxicity to splenocytes

Splenocytes from BALB/c mice were divided into a 96 well plate at a density of 5×10^6 cells per well in RPMI-1640 medium containing 10% inactivated Foetal Bovine Serum (FBS). Each chemical inhibitor was dissolved in DMSO at a concentration of 10 mg/mL, and then the sample was serially diluted in RPMI-1640 medium supplemented with 10% FBS at concentrations of 1.0, 5.0, 10, 25, 50 and 100 μg/mL, in triplicate. As a positive control, saponin was used

at a concentration of 0.1 μg/mL, while RPMI-1640 medium supplemented with 10% FBS and DMSO was used as a negative control. A total of 1.0 μCi of 3H-thymidine was added to each well, and the plate was incubated for 24 h at 37 °C and 5% CO2.

The plate was then read in the counter beta irradiation reader (Multilabel Reader, Finland), and the percent incorporation of tritiated thymidine was determined. Cells that were not treated with drugs (negative controls) were calculated as 100% of tritiated thymidine incorporation (100% viable cells). For cells treated with saponin, cell viability was 5%. When the percentage of incorporation was higher than 90%, the concentration of the drug was regarded as nontoxic to splenocytes.

4.4. Antiproliferative activity for the epimastigote form

Epimastigotes of Dm28c strain were distributed into a 96 well plate to a final density of 10^6 cells per well. Each chemical inhibitor was dissolved in the respective wells, in triplicate. Benznidazole was used as positive controls in this assay. The plate was then cultivated for 4 days at 27 °C. After this time, aliquots from each well were collected, and the number of parasites was calculated in a Neubauer chamber. Epimastigotes not treated with the chemical inhibitors (negative control) were assumed as 100% the number of parasites. The dose–response curves were determined, and the IC_{50} values were calculated using at least five concentrations (data points) and a nonlinear equation (Prism, version 4.0).

4.5. Toxicity to trypomastigotes

Strain Y trypomastigotes were collected from Vero cell supernatants and distributed in a 96 well plate to a final density of 4×10^5 cells per well. Each chemical inhibitor was added to the wells, in triplicate. Benznidazole was used as positive controls in this assay. The plate was then cultivated for 24 h at 37 °C and 5% CO2. After this time, aliquots from each well were collected, and the number of viable parasites (i.e., with apparent motility) was counted in a Neubauer chamber. The wells that did not receive the chemical inhibitors were assumed as 100% the number of viable parasites. The dose–response curves were determined, and the IC_{50} values were calculated by nonlinear regression (Prism, version 4.0) using at least seven concentrations (data points).

4.6. Ultrastructural studies

The parasites were cultured for 24 h in RPMI 1640 medium (Sigma–Aldrich, St. Louis, MO, USA) buffered to pH 7.5 and supplemented with HEPES (20 mM), 10% foetal bovine serum, penicillin (100 U/mL), and streptomycin (100 μg/mL) containing the compound **6k** at the IC_{50} concentration and twice the value of IC_{50}. The parasites were collected, washed in PBS and fixed with 2.5% glutaraldehyde, 4% formaldehyde, and 0.1 M cacodylate buffer at pH 6.8. They were then postfixed in 2% osmium tetroxide (OsO_4) in a 0.1 M cacodylate buffer at pH 6.8 and processed for routine transmission electron microscopy (TEM) and scanning electron microscopy (SEM).

For SEM analysis, the parasites were dehydrated in graded ethanol and dried by the critical point method with CO_2. The samples were mounted on aluminium stubs, coated with gold and examined under a JEOL-5600LV microscope.

For TEM analysis, the parasites were dehydrated in a graded series of acetone and finally embedded in epon. Sections were stained with uranyl acetate and lead citrate and observed with Tecnai spirit G2 Biotwin microscope.

4.7. Propidium iodide and annexin V staining

Trypomastigotes (1×10^7) were incubated for 24 h at 37 °C in the absence or presence of compound **6k**. After incubation, the parasites were labelled with propidium iodide (PI) and annexin V using the annexin V-FITC apoptosis detection kit (Sigma–Aldrich), according to the manufacturer's instructions. Acquisition and analyses were performed using a FACS Calibur flow cytometer (Becton Dickinson, CA, USA) with FlowJo software (Tree Star, CA, USA). A total of 30,000 events were acquired in the region previously established as trypomastigote forms of *T. cruzi*. Two independent experiments were performed.

Acknowledgements

This work was funded by Conselho Nacional de Desenvolvimento Científico e Tecnológico (CNPq), Fundação de Amparo à Ciência e Tecnologia de Pernambuco (FACEPE, APQ-0549-2.11/14, APQ-0289-4.03/13). P.A.T.M.G. holds a FACEPE doctoral scholarship. Authors are thankful to the Departamento de Química Fundamental (DQF-UFPE) for recording the ^1H NMR, ^{13}C NMR, LCMS and IR spectra of compounds. We are also thankful to Julia Campos of Centro de Tecnologias Estratégicas do Nordeste (CETENE) for recording the MS spectra of compounds **6a-l**. All authors declare no competing financial interest.

Appendix A. Supplementary data

Supplementary data related to this article can be found at http://dx.doi.org/10.1016/j.ejmech.2016.01.010.

References

[1] WHO, Chagas Disease (American Trypanosomiasis), 2015. http://www.who.int/mediacentre/factsheets/fs340/en/index.html.
[2] J. Urbina, Chemotherapy of chagas disease, Curr. Pharm. Des. 8 (2002) 287–295, http://dx.doi.org/10.2174/1381612023396177.
[3] J.a Pérez-Molina, J. Sojo-Dorado, F. Norman, B. Monge-Maillo, M. Díaz-Menéndez, P. Albajar-Viñas, et al., Nifurtimox therapy for chagas disease does not cause hypersensitivity reactions in patients with such previous adverse reactions during benznidazole treatment, Acta Trop. 127 (2013) 101–104, http://dx.doi.org/10.1016/j.actatropica.2013.04.003.
[4] M.V. de O. Cardoso, L.R.P. de Siqueira, E.B. da Silva, L.B. Costa, M.Z. Hernandes, M.M. Rabello, et al., 2-pyridyl thiazoles as novel anti- Trypanosoma cruzi agents : structural design, synthesis and pharmacological evaluation, Eur. J. Med. Chem. 86 (2014) 48–59, http://dx.doi.org/10.1016/j.ejmech.2014.08.012.
[5] S.S. Gawande, S.C. Warangkar, B.P. Bandgar, C.N. Khobragade, Synthesis of new heterocyclic hybrids based on pyrazole and thiazolidinone scaffolds as potent inhibitors of tyrosinase, Bioorg. Med. Chem. 21 (2013) 2772–2777, http://dx.doi.org/10.1016/j.bmc.2012.12.053.
[6] G.N. Masoud, A.M. Youssef, M.M. Abdel Khalek, A.E. Abdel Wahab, I.M. Labouta, A.a.B. Hazzaa, Design, synthesis, and biological evaluation of new 4-thiazolidinone derivatives substituted with benzimidazole ring as potential chemotherapeutic agents, Med. Chem. Res. 22 (2012) 707–725, http://dx.doi.org/10.1007/s00044-012-0057-3.
[7] D.R.M. Moreira, S.P.M. Costa, M.Z. Hernandes, M.M. Rabello, G.B. de Oliveira Filho, C.M.L. de Melo, et al., Structural investigation of anti-Trypanosoma cruzi 2-iminothiazolidin-4-ones allows the identification of agents with efficacy in infected mice, J. Med. Chem. 55 (2012) 10918–10936, http://dx.doi.org/10.1021/jm301518v.
[8] C. Pizzo, C. Saiz, A. Talevi, L. Gavernet, P. Palestro, C. Bellera, et al., Synthesis of 2-hydrazolyl-4-thiazolidinones based on multicomponent reactions and biological evaluation against Trypanosoma Cruzi, Chem. Biol. Drug Des. 77 (2011) 166–172, http://dx.doi.org/10.1111/j.1747-0285.2010.01071.x.
[9] M.E. Caputto, A. Ciccarelli, F. Frank, A.G. Moglioni, G.Y. Moltrasio, D. Vega, et al., Synthesis and biological evaluation of some novel 1-indanone thiazolylhydrazone derivatives as anti-Trypanosoma cruzi agents, Eur. J. Med. Chem. 55 (2012) 155–163, http://dx.doi.org/10.1016/j.ejmech.2012.07.013.
[10] M.Z. Hernandes, M.M. Rabello, A.C.L. Leite, M.V.O. Cardoso, D.R.M. Moreira, D.J. Brondani, et al., Studies toward the structural optimization of novel thiazolylhydrazone-based potent antitrypanosomal agents, Bioorg. Med. Chem. 18 (2010) 7826–7835, http://dx.doi.org/10.1016/j.bmc.2010.09.056.
[11] A.C.L. Leite, R.S. de Lima, D.R.D.M. Moreira, M.V.D.O. Cardoso, A.C. Gouveia de Brito, L.M. Farias Dos Santos, et al., Synthesis, docking, and in vitro activity of

thiosemicarbazones, aminoacyl-thiosemicarbazides and acyl-thiazolidones against Trypanosoma cruzi, Bioorg. Med. Chem. 14 (2006) 3749–3757, http://dx.doi.org/10.1016/j.bmc.2006.01.034.
[12] A.C.L. Leite, D.R. de M. Moreira, M.V. de O. Cardoso, M.Z. Hernandes, V.R. Alves Pereira, R.O. Silva, et al., Synthesis, Cruzain docking, and in vitro studies of aryl-4-oxothiazolylhydrazones against Trypanosoma cruzi, Chem. Med. Chem. 2 (2007) 1339–1345, http://dx.doi.org/10.1002/cmdc.200700022.
[13] J.W.P. Espíndola, M.V. de O. Cardoso, G.B. de O. Filho, D.A. Oliveira e Silva, D.R.M. Moreira, T.M. Bastos, et al., Synthesis and structure–activity relationship study of a new series of antiparasitic aryloxyl thiosemicarbazones inhibiting Trypanosoma cruzi cruzain, Eur. J. Med. Chem. 101 (2015) 818–835, http://dx.doi.org/10.1016/j.ejmech.2015.06.048.
[14] G.B. de Oliveira Filho, M.V. de Oliveira Cardoso, J.W.P. Espíndola, L.F.G.R. Ferreira, C.A. de Simone, R.S. Ferreira, et al., Structural design, synthesis and pharmacological evaluation of 4-thiazolidinones against Trypanosoma cruzi, Bioorg. Med. Chem. 23 (2015) 7478–7486, http://dx.doi.org/10.1016/j.bmc.2015.10.048.
[15] A.M. Alanazi, A.S. El-Azab, I.A. Al-Suwaidan, K.E.H. ElTahir, Y.A. Asiri, N.I. Abdel-Aziz, et al., Structure-based design of phthalimide derivatives as potential cyclooxygenase-2 (COX-2) inhibitors: anti-inflammatory and analgesic activities, Eur. J. Med. Chem. 92 (2015) 115–123, http://dx.doi.org/10.1016/j.ejmech.2014.12.039.
[16] K. Kamiński, J. Obniska, B. Wiklik, D. Atamanyuk, Synthesis and anticonvulsant properties of new acetamide derivatives of phthalimide, and its saturated cyclohexane and norbornene analogs, Eur. J. Med. Chem. 46 (2011) 4634–4641, http://dx.doi.org/10.1016/j.ejmech.2011.07.043.
[17] H. Akgün, İ. Karamelekoğlu, B. Berk, I. Kurnaz, G. Sarıbıyık, S. Öktem, et al., Synthesis and antimycobacterial activity of some phthalimide derivatives, Bioorg. Med. Chem. 20 (2012) 4149–4154, http://dx.doi.org/10.1016/j.bmc.2012.04.060.
[18] A.A.-M. Abdel-Aziz, A.S. El-Azab, S.M. Attia, A.M. Al-Obaid, M.A. Al-Omar, H.I. El-Subbagh, Synthesis and biological evaluation of some novel cyclicimides as hypoglycaemic, anti-hyperlipidemic agents, Eur. J. Med. Chem. 46 (2011) 4324–4329, http://dx.doi.org/10.1016/j.ejmech.2011.07.002.
[19] G. Singh, A. Saroa, S. Girdhar, S. Rani, S. Sahoo, D. Choquesillo-Lazarte, Synthesis, characterization, electronic absorption and antimicrobial studies of N-(silatranylpropyl)phthalimide derived from phthalic anhydride, Inorganica Chim. Acta 427 (2015) 232–239, http://dx.doi.org/10.1016/j.ica.2015.01.011.
[20] K. Elumalai, M.A. Ali, M. Elumalai, K. Eluri, S. Srinivasan, S. Sivannan, et al., Synthesis, characterization and biological evaluation of acetazolamide, cycloserine and isoniazid condensed some novel phthalimide derivatives, Int. J. Chem. Anal. Sci. 4 (2013) 57–61, http://dx.doi.org/10.1016/j.ijcas.2013.04.004.
[21] R. Williams, J.T. Manka, A.L. Rodriguez, P.N. Vinson, C.M. Niswender, C.D. Weaver, et al., Synthesis and SAR of centrally active mGlu5 positive allosteric modulators based on an aryl acetylenic bicyclic lactam scaffold, Bioorg. Med. Chem. Lett. 21 (2011) 1350–1353, http://dx.doi.org/10.1016/j.bmcl.2011.01.044.
[22] A.C.L. Leite, F.F. Barbosa, M.V.D.O. Cardoso, D.R.M. Moreira, L.C.D. Coêlho, E.B. Silva, et al., Phthaloyl amino acids as anti-inflammatory and immunomodulatory prototypes, Med. Chem. Res. (2013), http://dx.doi.org/10.1007/s00044-013-0730-1.
[23] M.V.D.O. Cardoso, D.R.M. Moreira, G.B.O. Filho, S.M.T. Cavalcanti, L.C.D. Coelho, J.W.P. Espíndola, et al., Design, synthesis and structure–activity relationship of phthalimides endowed with dual antiproliferative and immunomodulatory activities, Eur. J. Med. Chem. 96 (2015) 491–503, http://dx.doi.org/10.1016/j.ejmech.2015.04.041.
[24] L.C.D. Coêlho, M.V. de O. Cardoso, D.R.M. Moreira, P.A.T. de M. Gomes, S.M.T. Cavalcanti, A.R. Oliveira, et al., Novel phthalimide derivatives with TNF-α and IL-1β expression inhibitory and apoptotic inducing properties, Medchemcomm 5 (2014) 758, http://dx.doi.org/10.1039/c4md00070f.
[25] C. Pessoa, P.M.P. Ferreira, L.V.C. Lotufo, M.O. de Moraes, S.M.T. Cavalcanti, L.C.D. Coêlho, et al., Discovery of phthalimides as immunomodulatory and antitumor drug prototypes, Chem. Med. Chem. 5 (2010) 523–528, http://dx.doi.org/10.1002/cmdc.200900525.
[26] P.M. da Costa, M.P. da Costa, A.A. Carvalho, S.M.T. Cavalcanti, M.V. de Oliveira Cardoso, G.B. de Oliveira Filho, et al., Improvement of in vivo anticancer and antiangiogenic potential of thalidomide derivatives, Chem. Biol. Interact. 239 (2015) 174–183, http://dx.doi.org/10.1016/j.cbi.2015.06.037.
[27] E. de F. Santiago, S.A. de Oliveira, G.B. de Oliveira Filho, D.R.M. Moreira, P.A.T. Gomes, A.C.L.A.C.L. da Silva, et al., Evaluation of the anti-schistosoma mansoni activity of Thiosemicarbazones and Thiazoles, Antimicrob. Agents Chemother. 58 (2014) 352–363, http://dx.doi.org/10.1128/AAC.01900-13.
[28] M. Cardosoa, M. Hernandes, D. Moreira, F. Pontes, C. Simone, A. Leite, Structural insights into bioactive Thiazolidin-4-one: experimental and theoretical data, Lett. Org. Chem. 12 (2015) 262–270, http://dx.doi.org/10.2174/1570178612666150203005612.
[29] D.R.M. Moreira, A.C. Lima Leite, M.V.O. Cardoso, R.M. Srivastava, M.Z. Hernandes, M.M. Rabello, et al., Structural design, synthesis and structure-activity relationships of thiazolidinones with enhanced anti-trypanosoma cruzi activity, Chem. Med. Chem. 9 (2014) 177–188, http://dx.doi.org/10.1002/cmdc.201300354.
[30] M. Congreve, R. Carr, C. Murray, H. Jhoti, A "Rule of Three" for fragment-based lead discovery? Drug Discov. Today 8 (2003) 876–877, http://dx.doi.org/10.1016/S1359-6446(03)02831-9.
[31] H. Chen, X. Zhou, A. Wang, Y. Zheng, Y. Gao, J. Zhou, Evolutions in fragment-based drug design: the deconstruction–reconstruction approach, Drug Discov. Today 20 (2015) 105–113, http://dx.doi.org/10.1016/j.drudis.2014.09.015.
[32] M. Gonzales-Perdomo, S.L. de Castro, M.N. Meirelles, S. Goldenberg, Trypanosoma cruzi proliferation and differentiation are blocked by topoisomerase II inhibitors, Antimicrob. Agents Chemother. 34 (1990) 1707–1714, http://dx.doi.org/10.1128/AAC.34.9.1707.
[33] E.M. De Souza, A. Lansiaux, C. Bailly, W.D. Wilson, Q. Hu, D.W. Boykin, et al., Phenyl substitution of furamidine markedly potentiates its anti-parasitic activity against trypanosoma cruzi and Leishmania amazonensis, Biochem. Pharmacol. 68 (2004) 593–600, http://dx.doi.org/10.1016/j.bcp.2004.04.019.
[34] L.R. Garzoni, A. Caldera, M. de N.L. Meirelles, S.L.d. Castro, R. Docampo, G.A. Meints, et al., Selective in vitro effects of the farnesyl pyrophosphate synthase inhibitor risedronate on trypanosoma cruzi, Int. J. Antimicrob. Agents 23 (2004) 273–285, http://dx.doi.org/10.1016/j.ijantimicag.2003.07.020.
[35] M.V. Braga, J.A. Urbina, W. de Souza, Effects of squalene synthase inhibitors on the growth and ultrastructure of trypanosoma cruzi, Int. J. Antimicrob. Agents 24 (2004) 72–78, http://dx.doi.org/10.1016/j.ijantimicag.2003.12.009.
[36] A.P. Dantas, K. Salomão, H.S. Barbosa, S.L. De Castro, The effect of Bulgarian propolis against trypanosoma cruzi and during its interaction with host cells, Mem. Inst. Oswaldo Cruz 101 (2006) 207–211, http://dx.doi.org/10.1590/S0074-02762006000200013.
[37] E.-N. Collect, Nonius BV, Delft, The Netherlands. 2000 (1997) 585.
[38] Z. Otwinowski, W. Minor, Methods in enzymology, Macromol. Crystallogr. Part A 276 (1997) 307–326, http://dx.doi.org/10.1016/S0076-6879(97)76066-X.
[39] G. Sheldrick, SHELXL-97 and SHELXS-97, Program for X-ray Crystal Structure Solution and Refinement, Univ. Göttingen, 1997. http://scholar.google.com.br/scholar?q=SHELXS-97:Program for Crystal Structure Resolution#3.
[40] L.J. Farrugia, ORTEP -3 for Windows - a version of ORTEP -III with a Graphical User interface (GUI), J. Appl. Crystallogr. 30 (1997) 565, http://dx.doi.org/10.1107/S0021889897003117.
[41] L.J. Farrugia, WinGX suite for small-molecule single-crystal crystallography, J. Appl. Crystallogr. 32 (1999) 837–838, http://dx.doi.org/10.1107/S0021889899006020.

NJC

PAPER

View Article Online
View Journal | View Issue

Cite this: *New J. Chem.*, 2017, **41**, 4468

Structural isomerism of Ru(II)-carbonyl complexes: synthesis, characterization and their antitrypanosomal activities†

M. I. F. Barbosa,[a] R. S. Correa,[b] T. M. Bastos,[c] L. V. Pozzi,[d] D. R. M. Moreira,[c] J. Ellena,[e] A. C. Doriguetto,[a] R. G. Silveira,[df] C. R. Oliveira,[d] A. E. Kuznetsov,[d] V. S. Malta,[g] M. B. P. Soares[ch] and A. A. Batista*[d]

New complexes with the general formula [RuCl(CO)(dppb)(diimine)]PF_6, [dppb = 1,4-bis(diphenylphosphino)butane; diimine = 2,2′-bipyridine (bipy) or 1,10-phenanthroline (phen)], were prepared. Thus, the complexes *ct*-[RuCl(CO)(dppb)(bipy)]PF_6 (**1**), *ct*-[RuCl(CO)(dppb)(phen)]PF_6 (**2**), *tc*-[RuCl(CO)(dppb)(bipy)]PF_6 (**3**), *tc*-[RuCl(CO)(dppb)(phen)]PF_6 (**4**), *cc*-[RuCl(CO)(dppb)(bipy)]PF_6 (**5**) and *cc*-[RuCl(CO)(dppb)(phen)]PF_6 (**6**) were obtained and characterized. In this case, the first letter in the prefixes indicates the position of CO with respect to the chlorido ligand and the second one is related to the phosphorus atoms. The compositions of the complexes were confirmed by analytical techniques and an octahedral environment around the ruthenium was confirmed by single-crystal X-ray diffraction of the complexes *ct*-[RuCl(CO)(dppb)(bipy)]PF_6 and *cc*-[RuCl(CO)(dppb)(phen)]PF_6. The oxidation potentials of the complexes were determined by cyclic voltammetry and it was found that they vary according to the CO position in the complexes. In order to obtain information on the stability of the *ct*, *tc* and *cc*-[RuCl(CO)(dppb)(bipy)]PF_6 (**1**), (**3**) and (**5**) isomers, computational studies were carried out, and they showed large differences between the HOMO/LUMO energies. As monitored by ^{13}C NMR, the stability of the complexes with respect to CO displacement, for at least 72 h, in DMSO-d_6 solution, is independent of the CO position in the complexes. Pharmacological evaluation of the complexes against the *Trypanosoma cruzi* parasite revealed the structure–activity relationships, showing that the presence and position of the CO ligand in the complexes are relevant for the antiparasitic activity of the compounds. The most active compound, the *tc*-[RuCl(CO)(dppb)(bipy)]PF_6 isomer, presented potent antiparasitic activity, which was achieved by causing oxidative stress followed by parasite cell death through necrosis. Thus, the findings presented here demonstrate that the use of a carbonyl ligand provides stability and pharmacological properties to ruthenium/diphosphine/diimine complexes.

Received 11th January 2017,
Accepted 20th April 2017

DOI: 10.1039/c7nj00125h

rsc.li/njc

[a] *Instituto de Química, Universidade Federal de Alfenas, CEP 37130-000, Alfenas, MG, Brazil. E-mail: mariliaifrazab@yahoo.com.br*
[b] *ICEB, Departamento de Química, Universidade Federal de Ouro Preto, CEP 35400-000, Ouro Preto, MG, Brazil*
[c] *FIOCRUZ, Instituto Gonçalo Moniz, CEP 40296-710, Salvador, BA, Brazil*
[d] *Departamento de Química, Universidade Federal de São Carlos, CP 676, CEP 13565-905, São Carlos, SP, Brazil. E-mail: daab@ufscar.br*
[e] *Instituto de Física de São Carlos, Universidade de São Paulo, CP 369, CEP 13560-970, São Carlos, SP, Brazil*
[f] *Instituto Federal Goiano, Campus Ceres, CEP 76300-000, Ceres, GO, Brazil*
[g] *Instituto de Química e Biotecnologia, Universidade Federal de Alagoas, CEP 57072-970, Maceió, Brazil*
[h] *Centro de Biotecnologia e Terapia Celular, Hospital São Rafael, 41253-190, Salvador, BA, Brazil*

† Electronic supplementary information (ESI) available: Crystal data and structure refinement for *ct*-[RuCl(CO)(dppb)(bipy)]PF_6 and *cc*-[RuCl(CO)(dppb)(phen)]PF_6; the $^{13}C\{^1H\}$ NMR spectrum of isomers at different times; computational studies; and the $^{31}P\{^1H\}$ NMR spectrum after electrolysis and stability available $^{13}C\{^1H\}$ NMR. CCDC 1472477 (*ct*-[RuCl(CO)(dppb)(bipy)]PF_6) and 1453145 (*cc*-[RuCl(CO)(dppb)(phen)]PF_6). For ESI and crystallographic data in CIF or other electronic format see DOI: 10.1039/c7nj00125h

Introduction

Chagas disease (American trypanosomiasis) is a neglected tropical disease caused by the protozoan *Trypanosoma cruzi*. It is estimated that up to 10 million people are infected worldwide, mostly in Latin American countries, where the disease is endemic.[1] Chronic cardiomyopathy is the most important and severe manifestation of human chronic Chagas disease and it is characterized by heart failure, ventricular arrhythmias, heart blocks, thromboembolic phenomena and sudden death.[2] This disease was classically associated with rural areas, because the main triatominae vector grows in low income areas.[3] The antiparasitic drug treatment for Chagas disease lacks efficacy and causes serious side effects, highlighting that drug development is necessary.[4–6]

For many years, carbon monoxide (CO) was known only as a colorless, odorless, tasteless and toxic gas produced upon

oxidation of organic compounds.[7,8] The discovery that CO is capable of interacting with specific biomacromolecules, such as mitochondrial enzymes, cellular membranes and ion channels, has changed the view on CO from an environmental toxicant to a valuable molecule for drug design.[9–11] To study the functional properties of CO, a good model is complexes containing carbonyl bonded to metals. Thus, by using metal-carbonyl complexes, the interaction of CO with molecular targets can be understood, as well as its controlled release under photodynamic conditions.[12] Moreover, it has been shown that the metal-carbonyl complexes, in which the CO does not dissociate easily in a solution, can be pharmacologically active as anticancer and antimicrobial agents, indicating that stable metal-carbonyl complexes can be attractive candidates for drug development.[13–15]

Metal complexes can be antiparasitic agents against *T. cruzi*;[16–20] however, to our knowledge there are only a few reports on the study of metal-carbonyl complexes with antiparasitic properties. In 2011, Arancibia *et al.* observed that the $Re(CO)_3$ complexes show stronger activity against *Mycobacterium tuberculosis* than their ferrocene analogs,[18,19] and in 2013, Patra *et al.* demonstrated that $Cr(CO)_3$ complexes containing the antiparasitic drug praziquantel are more potent against *Schistosoma mansoni* than the metal-free praziquantel.[20] More recently, Gambino *et al.* demonstrated that $Re(CO)_3$ complexes presented superior activity against *T. cruzi* than their thiosemicarbazone metal-free ligands.[21] Given this promising outlook, it is clear how important it is to investigate ruthenium-carbonyl complexes against *T. cruzi.* Thus, here we synthesized and characterized six new ruthenium carbonyl complexes using a general formula $[RuCl(CO)(dppb)(diimine)]PF_6$ and analyzed their chemistry and biological properties. The influence of the position of the CO in the complexes for their reactivity was determined, as well as for their biological activity against *T. cruzi*.

Materials and methods

Materials for synthesis

Solvents were purified by standard methods. All chemicals used were of reagent grade or comparable purity. $RuCl_3{\cdot}3H_2O$ and ligands 1,4-bis(diphenylphosphino)butane (dppb), 2,2′-bipyridine (bipy) and 1,10-phenanthroline (phen) were used as received from Sigma-Aldrich. Reactants *cis*-$[RuCl_2(dppb)(bipy)]$ and *cis*-$[RuCl_2(dppb)(phen)]$ were prepared following the protocol described by Queiroz and coworkers,[22] while $[Ru_2Cl_4(CO)_2(dppb)_3]$ was prepared as described by Bressan and Rigo.[23] $CO_{(g)}$ was generated by dehydration of formic acid in concentrated sulfuric acid.

Instrumentation

Elemental analyses were performed in a Fisons EA 1108 model (Thermo Scientific, Waltham, Massachusetts). The FTIR spectra of the powder complexes were recorded using CsI pellets in the 4000–200 cm^{-1} region, in a FT MB-102 instrument (Bomen–Michelson). The UV-Vis spectra of the complex were recorded in CH_2Cl_2 solution, in a Hewlett Packard diode array – 8452A. Cyclic voltammetry (CV) measurements of the complexes in the solution were performed in an electrochemical analyzer BAS model 100B (Bioanalytical Systems, West Lafayette, Indiana). These experiments were carried out at room temperature in previously degassed CH_2Cl_2 containing 0.1 mol L^{-1} $Bu_4N^+ClO_4^-$ (TBAP) (FlukaPurum, St. Louis, MO) as a support electrolyte, and using a one-compartment cell, with both working and auxiliary electrodes, which were stationary Pt foils, while the reference electrode was Ag/AgCl, 0.1 mol L^{-1} TBAP in CH_2Cl_2. Under these conditions, ferrocene is oxidized at 0.43 V (Fc^+/Fc). All the NMR spectra were recorded at 298 K and measured using a 9.4 T Bruker Avance III spectrometer. To check the stability of the complexes, NMR spectra were immediately obtained after preparing the solution, and 24, 48 and 72 h after the first spectrum was obtained. The molar conductivity measurements (Λ_m) were taken in acetone at 298 K, using concentrations of 1.0×10^{-3} M for the complexes.

X-Ray crystallography

Yellow crystals of *ct*-$[RuCl(CO)(dppb)(bipy)]PF_6$ (**1**) and *cc*-$[RuCl(CO)(dppb)(phen)]PF_6$ (**6**) were obtained by slow evaporation of a dichloromethane/diethyl ether solution (2 : 1), at 298 K. Diffraction data were collected on an Enraf-Nonius Kappa-CCD diffractometer with graphite-monochromated Mo Ka radiation (λ = 0.71073 Å). The final unit cell parameters were based on all reflections. Data collections were performed using the COLLECT program, and integration and scaling of the reflections were performed using the HKL Denzo–Scalepack system of programs.[24,25] Absorption corrections were carried out using the Gaussian method.[26] The structures were solved by direct methods with SHELXS-97.[27] The models were refined by full-matrix least-squares on F^2 by means of SHELXL-97.[28] The projection views of the structures were prepared using ORTEP-3 for Windows.[29] Hydrogen atoms were stereochemically positioned and refined with the riding model. Data collections and experimental details are summarized in Table S1 (ESI†). The hydrogen atoms were calculated at idealized positions using the riding model option of SHELXL-97.[32] Table S2 (ESI†) summarizes the main crystallographic data for complexes **1** and **6**.

Synthesis of complexes *ct*-$[RuCl(CO)(dppb)(bipy)]PF_6$ (1) and *ct*-$[RuCl(CO)(dppb)(phen)]PF_6$ (2)

In a Schlenk flask (0.066 mmol; 50.0 mg) of the precursor *cis*-$[RuCl_2(dppb)(bipy)]$, or (0.128 mmol; 100.0 mg) of *cis*-$[RuCl_2(dppb)(phen)]$, was dissolved in 10 mL of dichloromethane previously degassed. Thus, the Schlenk flask was subjected to vacuum, and $CO_{(g)}$ was introduced into it. The red solution, under pressurization, was stirred until it became yellowish, then NH_4PF_6 (1 : 1), previously dissolved in methanol, was added. After 15 min of reaction, the volume was reduced to *ca.* 2 mL, and 10 mL of diethyl ether was added to yield a pale yellowish solid, which was filtered off, washed with water (2 × 5 mL) and diethyl ether (2 × 5 mL), and dried under vacuum.

***ct*-$[RuCl(CO)(dppb)(bipy)]PF_6$ (1).** Yield: 93%. Elemental analysis (%) calc. for $C_{39}H_{36}ClF_6N_2OP_3Ru$: C 52.50, H 4.07, N 3.14. Found: C 52.70, H 4.04 and N 3.39. IR (CsI): ν(CO) 1987 cm^{-1}.

UV-Vis [CH_2Cl_2, λ/nm (ε/M^{-1} cm^{-1})]: 273 (1.52 × 10^3), 298 (1.06 × 10^3), 320 (6.22 × 10^3). $^{31}P\{^1H\}$ NMR (161.98 MHz, DMSO-d_6): 36.6 ppm (d) and 8.4 ppm (d) MHz ($^2J_{P-P}$ = 34.3 Hz). ^1H NMR (400.21 MHz, $CDCl_3$): δ(ppm) (aromatic hydrogens of bipy): 9.18 (d, 1H); 8.36 (d, 1H); 8.10 (d, 1H); 7.25 (d, 1H); 7.74 (t, 1H); 6.93 (t, 1H); 6.32 (t, 1H); (overlapped signals, 21H aromatic hydrogens of dppb and bipy); 7.71–7.00; (8H, CH_2 of dppb) 3.00–1.5. $^{13}C\{^1H\}$ NMR (100 MHz, $CDCl_3$): δ (ppm) (CH_2 of dppb): 20.8 (s, CH_2), 22.0 (d, CH_2), 23.6 (s, CH_2), 25.3 (d, CH_2), (CH of dppb and bipy): 123.9 (d), 124.5 (d), 127.8–132.9 (m, C-Ph), 136.7 (d), 139.4 (d), 149.8, 155.0, 156.7, 157.3, 196.1 (d, $^1J_{C-P}$ = 27.3 Hz, CO). Conductivity (acetone): 129.7 ohm^{-1} cm^2 mol^{-1}, T = 298 K (1 : 1 electrolyte rate is 59 a 188 ohm^{-1} cm^2 mol^{-1}, in acetone).

***ct*-[RuCl(CO)(dppb)(phen)]PF_6 (2).** Yield: 89%. Elemental analysis (%) calc. for $C_{41}H_{36}ClF_6N_2OP_3Ru$: C 53.75, H 3.96, N 3.06. Found: C 53.91, H 4.01, N 3.17. IR (CsI): ν(CO) 1987 cm^{-1}. UV-Vis [CH_2Cl_2, λ/nm (ε/M^{-1} cm^{-1})]: 270 (6.71 × 10^3), 372 (1.30 × 10^3). $^{31}P\{^1H\}$ NMR (161.98 MHz, DMSO-d_6): 37.3 ppm (d) and 9.4 ppm (d) MHz ($^2J_{P-P}$ = 30.8 Hz). ^1H NMR (400.21 MHz, $CDCl_3$ K): δ (ppm) (aromatic hydrogens of phen): 9.61 (d, 1H); 8.72 (t, 1H); 8.20 (d, 1H); 8.10 (s, 1H); 8.00 (t, 1H); 7.81 (t, 1H); 6.60 (t, 1H); 6.05 (t, 1H); (overlapped signals, 20H aromatic hydrogens of dppb): 6.90–7.70; (8H, CH_2 of dppb): 3.0–1.5. $^{13}C\{^1H\}$ NMR (100 MHz, $CDCl_3$): δ (ppm) (CH_2 of dppb): 20.7 (s, CH_2), 23.5 (d, CH_2), 24.1 (s, CH_2), 26.7 (d, CH_2), (CH of dppb and phen) 125.3, 125.7, 136.3, 136.8, 138.29, 139.09, 145.7, 147.7, 150.8, 157.3, 134.0–120.0 (m, C-Ph), 195.7 (d, $^1J_{CP}$ 29.2, CO). Conductivity (acetone): 147.3 ohm^{-1} cm^2 mol^{-1} (1 : 1 electrolyte).

Synthesis of complexes *tc*-[RuCl(CO)(dppb)(bipy)]PF_6 (3) and *tc*-[RuCl(CO)(dppb)(phen)]PF_6 (4)

In a Schlenk flask (0.30 mmol; 500.0 mg) of $[Ru_2Cl_4(CO)_2(dppb)_3]$ was dissolved in methanol and (0.90 mmol; 144.0 mg) of bipy (**3**) or (0.92 mmol; 167.0 mg) of phen (**4**) and NH_4PF_6 (0.90 mmol; 150 mg) were added and the solution was refluxed for 6 h for **3** and 24 h for complex **4**. The solution volume was reduced to *ca.* 2 mL and 10 mL of diethyl ether was added to precipitate a pale yellow powder, which was filtered off, washed with water (2 × 5 mL) and diethyl ether (2 × 5 mL), and dried under vacuum.

***tc*-[RuCl(CO)(dppb)(bipy)]PF_6 (3).** Yield: 80%. Elemental analysis (%) calc. for $C_{39}H_{36}ClF_6N_2OP_3Ru$: C 52.50, H 4.07, N 3.14. Found: C 52.17, H 4.22, N 3.21. IR (CsI): ν(CO) 1970 cm^{-1}. UV-Vis [CH_2Cl_2, λ/nm (ε/M^{-1} cm^{-1})]: 274 (1.06 × 10^5), 321 (3.82 × 10^4), 428 (9.20 × 10^3). $^{31}P\{^1H\}$ NMR (161.98 MHz, DMSO-d_6): 27.6 ppm (s). ^1H NMR (400.21 MHz, $CDCl_3$): δ (ppm) (aromatic hydrogens for bipy) 8.73 (d, 1H); 8.22 (s, 1H); 7.17 (t, 1H) (overlapped signals, 25H aromatic hydrogens of dppb and bipy): 7.80–7.30; (8H CH_2 of dppb): 2.8–1.75. $^{13}C\{^1H\}$ NMR (100 MHz, $CDCl_3$): δ (ppm) (CH_2 of dppb): 22.5 (s, CH_2), 30.1 (t, CH_2); (CH and C-Ph of dppb and bipy): 124.4, 125.2, 128.9, 130.4, 133.8, 140.46, 154.3, 157.0, 197.6 (CO). Conductivity (acetone): 163.0 ohm^{-1} cm^2 mol^{-1} (1 : 1 electrolyte).

***tc*-[RuCl(CO)(dppb)(phen)]PF_6 (4).** Yield: 74%. Elemental analysis (%) calc. for $C_{40}H_{34}ClF_6N_2OP_3Ru{\cdot}CH_2Cl_2$: C 50.39, H 3.83 and N 2.80. Found: C 50.72, H 4.01 and N 3.06. IR (CsI): ν(CO) 1965 cm^{-1}. UV-Vis [CH_2Cl_2, λ/nm (ε/M^{-1} cm^{-1})]: 276 (2.26 × 10^4), 306 (9.94 × 10^3), 363 (2.82 × 10^3). $^{31}P\{^1H\}$ NMR (161.98 MHz, DMSO-d_6): 28.4 ppm (s). ^1H NMR (400.21 MHz, $CDCl_3$): δ (ppm) (aromatic hydrogens for phen): 8.86 (d, 1H); 8.50 (s, 1H); 8.29 (s, 1H); (overlapped signals, 25H aromatic hydrogens of dppb and phen): 8.00–7.50; (8H, CH_2 of dppb): 2.90–1.70. $^{13}C\{^1H\}$ NMR (100 MHz, $CDCl_3$): δ (ppm) (CH_2 of dppb): 22.9 (s, CH_2), 30.5 (t, CH_2), (CH and C-Ph of dppb and phen): 124.8, 127.9, 129.4, 131.8, 131.9, 132.5, 134.6, 140.2, 147.3, 154.9, 198.1 (CO). Conductivity (acetone): 155.0 ohm^{-1} cm^2 mol^{-1} (1 : 1 electrolyte).

Synthesis of complexes *cc*-[RuCl(CO)(dppb)(bipy)]PF_6 (5) and *cc*-[RuCl(CO)(dppb)(phen)]PF_6 (6)

Complexes *cc*-[RuCl(CO)(dppb)(diimine)]PF_6 were obtained by refluxing their respective *tc*-[RuCl(CO)(dppb)(diimine)]PF_6 isomers in 20 mL, CH_2Cl_2/MeOH (50/50 v/v), for 24 h. The solution volume was reduced to 2 mL, approximately, followed by the addition of 10 mL of diethyl ether to precipitate a yellow solid, which was washed with diethyl ether (2 × 5 mL), filtered off, and dried under vacuum.

***cc*-[RuCl(CO)(dppb)(bipy)]PF_6 (5).** Yield: 73%. Elemental analysis (%) calc. for $C_{39}H_{36}ClF_6N_2OP_3Ru$: C 52.50, H 4.07, N 3.14. Found: C 52.26, H 3.86, N 3.22. IR (CsI): ν(CO) 1976 cm^{-1}. UV-Vis [CH_2Cl_2, λ/nm (ε/M^{-1} cm^{-1})]: 275 (6.30 × 10^4), 323 (1.68 × 10^4), 432, sh (3.10 × 10^3). $^{31}P\{^1H\}$ NMR (161.98 MHz, $CDCl_3$, at 300 K): 32.8 ppm (d) and 26.7 ppm (d), MHz ($^2J_{P-P}$ = 28.5 Hz). ^1H NMR (400.21 MHz, $CDCl_3$, 298 K): δ (ppm) (aromatic hydrogens of bipy): 9.65 (d, 1H); 8.99 (d, 1H); 8.69 (d, 1H); 8.35 (d, 1H); 8.22 (t, 1H); 8.11 (t, 1H); 8.01 (t, 1H,) (overlapped signals, 21H aromatic hydrogens of dppb and bipy): 7.80–7.30, (8H, CH_2 of dppb): 3.3–1.7. $^{13}C\{^1H\}$ NMR (100 MHz, $CDCl_3$, 298 K): δ (ppm) (CH_2 of dppb): 21.8 (s, CH_2), 24.5 (s, CH_2), 25.8 (d, CH_2), 27.14 (d, CH_2), (CH and C-Ph of dppb and bipy): 124.4, 124.8, 126.7, 133.9, 134.7, 139.5, 141.2, 153.6, 154.8, 155.2, 156.0; (m, C-Ph): 127.0–133.0 and 203.4 (CO). Conductivity (acetone): 155.0 ohm^{-1} cm^2 mol^{-1} (1 : 1 electrolyte).

***cc*-[RuCl(CO)(dppb)(phen)]PF_6 (6).** Yield: 86%. Elemental analysis (%) calc. for $C_{41}H_{36}ClF_6N_2OP_3Ru$: C 53.75, H 3.96, N 3.06. Found: C 53.91, H 3.95, N 3.09. IR (CsI): ν(CO) 1975 cm^{-1}. UV-Vis [CH_2Cl_2, λ/nm (ε/M^{-1} cm^{-1})]: 274 (1.63 × 10^4), 307 (4.74 × 10^3), 364 (1.20 × 10^3). $^{31}P\{^1H\}$ NMR (161.98 MHz, DMSO-d_6): 35.0 ppm (d) and 27.0 ppm (d) MHz ($^2J_{P-P}$ = 29.6 Hz). ^1H NMR (400.21 MHz, $CDCl_3$): δ (ppm) (aromatic hydrogens of phen): 9.45 (d, 1H); 8.89 (d, 1H); 8.40 (d, 1H); 8.22 (d, 1H); 8.04 (t, 1H); 7.91 (t, 1H); 7.70 (t, 1H) (overlapped signals, 21H aromatic hydrogens of dppb and phen): 7.68–6.73, (8H, CH_2 of dppb): 3.5–1.7. $^{13}C\{^1H\}$ NMR (100 MHz, $CDCl_3$): δ (ppm) (CH_2 of dppb): 21.8 (s, CH_2), 24.5 (s, CH_2), 25.8 (d, CH_2), 27.14 (d, CH_2), (CH and C-Ph of dppb and phen): 124.4, 124.8, 126.7, 133.9, 134.7, 135.01, 139.5, 141.2, 142.4, 153.6, 154.8, 155.2, 156.0; (m, C-Ph), 127.0–133.0 and 205.1 (CO). Conductivity (acetone): 148.0 ohm^{-1} cm^2 mol^{-1} (1 : 1 electrolyte).

Computational details

Geometry optimization of isomers *ct*-[RuCl(CO)(dppb)(bipy)]PF_6 (**1**), *tc*-[RuCl(CO)(dppb)(bipy)]PF_6 (**3**) and *cc*-[RuCl(CO)(dppb)(bipy)]PF_6

(**5**) was performed using the Gaussian 09 software package[30] by using the B3LYP hybrid density function.[31] For ruthenium atoms, the Stevens/Basch/Krauss effective core potential (ECP) triple-split basis set[32] was used, while for light atoms, a full-electron polarized double-zeta basis set 6-31G*[33] was executed. The geometry optimizations were followed by the vibrational frequency calculations using the same approach. All structures were shown to be the real minima by the vibrational frequency analysis (no imaginary frequencies). The geometry optimizations were done in the gas phase and with implicit effects from water taken into account (dielectric constant ε = 78.3553). With implicit solvent effects the geometries and vibrational frequencies were calculated using the self-consistent reaction field IEF-PCM method[34] (the UFF default model used in the GAUSSIAN 09 package, with the electrostatic scaling factor (α[35] set to 1.0)). In addition, using the B3LYP/[Ru:CEP-121G; C,N,O,Cl,P,H:6-31G*] approach we assessed the Natural Bonding Orbital (NBO)[36,37] charge distributions in the complexes along with atomic contributions (%) in the HOMO and LUMO of the three complexes.

Pharmacological evaluation

Animals. Female BALB/c mice (18–20 g) were maintained in sterilized cages under a controlled environment, receiving a rodent balanced diet and water *ad libitum* at the Instituto Gonçalo Moniz (Fundação Oswaldo Cruz, Bahia, Brazil). All experiments were carried out in accordance with the recommendations from the Ethical Issues Guidelines and were approved by the local Animal Ethics Committee (protocol number 06/2013).

Parasites. All experiments were performed using the Y strain of *T. cruzi*. The trypomastigote form of *T. cruzi* was obtained from the supernatant of infected LLC-MK2 cells and maintained in RPMI-1640 medium (Sigma-Aldrich) supplemented with 10% FBS (Cultilab, Campinas, Brazil) and 50 μg mL^{-1} of gentamicin (Novafarma, Anápolis, Brazil) at 37 °C, with 5% CO_2.

Drug dilution. All complexes as well as the reference drugs were dissolved in DMSO (Sigma-Aldrich) and then diluted in RPMI-1640. The final concentration of DMSO was less than 1% in all *in vitro* experiments.

Activity against trypomastigotes. Trypomastigotes were cultured in 96-well plates (2×10^6 cells per mL) in RPMI-1640 in the presence or absence of the complexes at different concentrations for 24 h. Viable parasites were counted in a hemocytometer and the complex activity was expressed as EC_{50}, corresponding to the effective concentration at 50% in comparison to untreated parasites. Each drug concentration was carried out in triplicate and three independent experiments were performed. The reference drug, benznidazole, was used as the positive control.

Host cell toxicity. BALB/c splenocytes in RPMI-1640 medium supplemented with 10% FBS were seeded on 96-well plates at 5×10^5 cells per mL, treated with the complexes for 48 h. Gentian Violet was used as a positive control. Following this, the cells were washed with PBS twice and the cell viability was pulsed with 1 μCi of ^{3}H-thymidine incorporation assay (Perkin Elmer, Carlsbad, CA); the cells were harvested and thymidine incorporation was measured in a beta-plate counter (Packard, Meriden, Connecticut). CC_{50} values were calculated using data-points gathered from three independent experiments.

Cytotoxicity in cancer cells. HepG2 cells were seeded in 100 μL of RPMI at 1 × 104 cells per mL in 96-well plates. Drugs were added 24 h later in a volume of 100 μL suspended in medium and the plates were incubated for 72 h at 37 oC and 5% CO_2. Drugs were tested in eight concentrations (50–0.78 μM), each one in triplicate. Oxaliplatin (Sigma-Aldrich) diluted in methanol was used as a positive control, while untreated cells were employed as negative controls. Then, 20 μL of AlamarBlue (Life) were added and incubated for 4 h. Colorimetric readings were performed at 570 and 600 nm using a SpectraMA× 190 instrument (Molecular Devices, Sunnyvale, CA). CC50 values were calculated using data-points gathered from two independent experiments.

Parasite cell death. Trypomastigotes (1×10^7 cells per mL) were resuspended in RPMI-1640 medium and treated with a complex (*tc*-[RuCl(CO)(dppb)(phen)]PF_6 at 0.45, 0.9 and 1.8 μM) for 36 h at 37 °C, with 5% CO_2. Parasites were labeled with propidium iodide (PI) and annexin V using the annexin V-FITC apoptosis detection kit (Sigma-Aldrich), according to the manufacturer's instructions. The experiment was performed using a FACSCalibur flow cytometer (BD Biosciences, San Jose, CA) by acquiring at least 10 000 events, and data were analyzed using the CellQuest software (BD Biosciences). Three independent experiments were performed.

MitoSOX staining. Trypomastigotes at 1×10^7 cells per mL were resuspended in RPMI-1640 medium and incubated in the absence or presence of *cis*-[Ru(bipy)Cl_2(dppb)] and *tc*-[RuCl(CO)(dppb)(bipy)]PF_6 (**3**) for 3 and 24 h at 37 °C with 5% CO_2. H_2O_2 (30 wt% in H_2O) plus anti-Mouse IgG–peroxidase antibody diluted 1 : 1000 (Sigma-Aldrich) was used as a positive control and incubated for 30 min prior to adding MitoSox Red. Then, 5 μM of MitoSOX Red (Molecular Probes, Invitrogen, Carlsbad, CA) diluted in HBSS/Ca/Mg buffer was added according to the manufacturer's recommendations, and incubated in the dark for 10 min at 37 °C with 5% CO_2. Parasites were washed three times with HBSS/Ca/Mg buffer and analyzed in a FACSCalibur flow cytometer (BD Biosciences, San Jose, CA) by acquiring at least 10 000 events in the PE/cy7 channel. Three independent experiments were performed.

Results and discussion

In this work, six new mononuclear complexes *ct*-[RuCl(CO)(dppb)(bipy)]PF_6 (**1**), *ct*-[RuCl(CO)(dppb)(phen)]PF_6 (**2**), *tc*-[RuCl(CO)(dppb)(bipy)]PF_6 (**3**), *tc*-[RuCl(CO)(dppb)(phen)]PF_6 (**4**), *cc*-[RuCl(CO)(dppb)(bipy)]PF_6 (**5**) and *cc*-[RuCl(CO)(dppb)(phen)]PF_6 (**6**) (Fig. 1) were obtained, in good purity and good yield (73–93%), by varying the ruthenium precursor containing the desired diimine ligand. The complexes were characterized by elemental analysis, $^{31}P\{^1H\}$, $^{13}C\{^1H\}$ and ^1H NMR spectroscopy, UV-Vis and IR spectra, molar conductance, and cyclic voltammetry and compounds **1** and **6** had their structures determined by X-ray crystallography. All the complexes were stable in air and DMSO-d_6 solutions for at least 72 h.

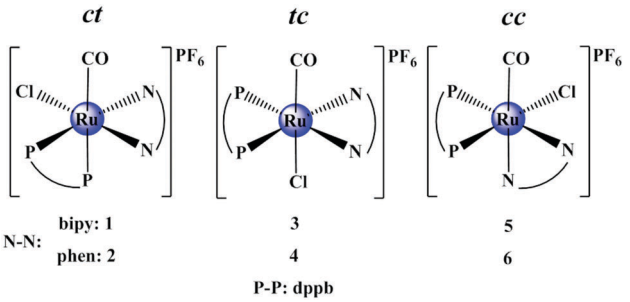

Fig. 1 Structures suggested for the new [RuCl(CO)(dppb)(diimine)]PF_6 complexes.

ct-[RuCl(CO)(dppb)(bipy)]PF_6 (**1**), *tc*-[RuCl(CO)(dppb)(bipy)]PF_6 (**3**) and *cc*-[RuCl(CO)(dppb)(bipy)]PF_6 (**5**) are structural isomers and despite having the same empirical formula and color, their physical and biological properties are different. These three isomers can be easily differentiated by $^{31}P\{^1H\}$ NMR experiments, where their $^{31}P\{^1H\}$ NMR spectra, in DMSO-d_6 (Fig. 2), revealed doublets for compound *ct*-[RuCl(CO)(dppb)(bipy)]PF_6 (36.6 and 8.4 ppm, $^2J_{P-P}$ = 34.3 Hz) (Fig. 2A), due to the magnetically different phosphorus atoms and a singlet for isomer *tc*-[RuCl(CO)(dppb)(bipy)]PF_6 (27.6 ppm) (Fig. 2B), due to the magnetic similarity of the phosphorus atoms of the dppb ligand.

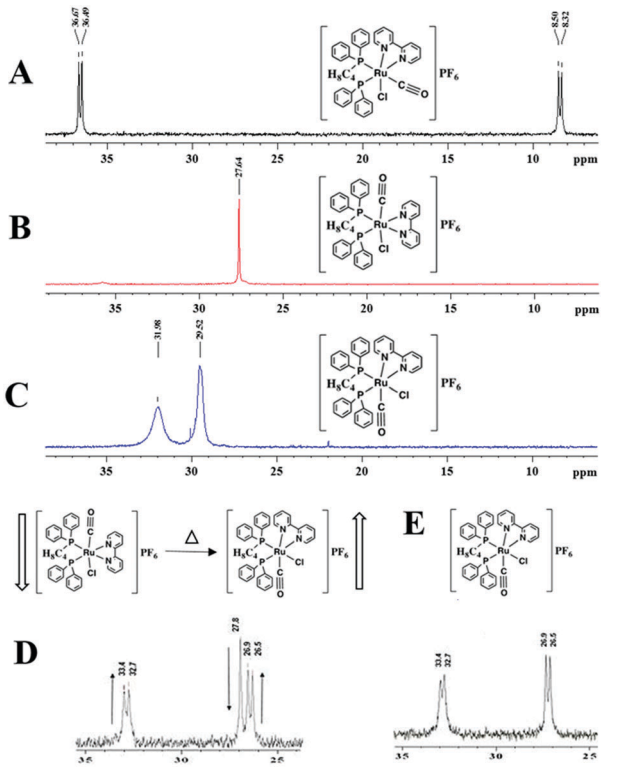

Fig. 2 $^{31}P\{^1H\}$ NMR spectrum of (A) *ct*-[RuCl(CO)(dppb)(bipy)]PF_6 (**1**), (B) *tc*-[RuCl(CO)(dppb)(bipy)]PF_6 (**3**), and (C) *cc*-[RuCl(CO)(dppb)(bipy)]PF_6 (**5**) complexes in DMSO-d_6 at 300 K. (D) Scheme of the isomerization process of (**3**) into (**5**) species and $^{31}P\{^1H\}$ NMR spectrum of reaction mixture after 8 h of reaction under reflux. (E) the $^{31}P\{^1H\}$ NMR spectrum of complex (**5**) in $CDCl_3$ at 300 K.

For complex *cc*-[RuCl(CO)(dppb)(bipy)]PF_6, two signals were observed (31.9 and 29.5 ppm), in DMSO-d_6 (Fig. 2C), as broad "singlets". *cc*-[RuCl(CO)(dppb)(bipy)]PF_6 was isolated by isomerization of *tc*-[RuCl(CO)(dppb)(bipy)]PF_6 in CH_2Cl_2/CH_3OH (1 : 1) under heating for 24 h. By carrying out the $^{31}P\{^1H\}$ NMR experiment, in $CDCl_3$, the isomerization process was followed (Fig. 2D) and then, after 24 h of reaction, pure isomer *cc*-[RuCl(CO)(dppb)(bipy)]PF_6 (Fig. 2E) was isolated. $^{31}P\{^1H\}$ NMR of the *cc*-[RuCl(CO)(dppb)(bipy)]PF_6 spectra was obtained from $CDCl_3$ as it is known that the spin relaxation time of phosphorus compounds varies significantly and can be highly dependent on the solvent and temperature.[38] In this case, the spectrum of this complex is better defined in $CDCl_3$ than in DMSO-d_6.

In order to check the possible release of CO from the carbonyl complexes $^{13}C\{^1H\}$ NMR experiments were carried out. Thus, the complexes were diluted in DMSO-d_6 and analyzed using the ^{13}C NMR technique in the range of 0 to 72 h (see Fig. 3A–C and Fig. S1–S3, ESI†), for isomers *ct*-, *tc*- and *cc*-[RuCl(CO)(dppb)(bipy)]PF_6, respectively. The ^{13}C NMR spectrum reveals that the carbon monoxide ligand of the complexes, in the range of time investigated, is not released from the metal center, as is shown in Fig. 2, by the presence of the signal corresponding to (C≡O), at 196.1, 197.6 and 203.4 ppm for complexes **1**, **3** and **5**, respectively, in all spectra obtained (0, 24, 48 and 72 h). Only for the *ct* isomers, doublets were observed in the $^{13}C\{^1H\}$ NMR spectrum of the CO species, which refers to P–C coupling (Fig. 3A), where CO is *trans* positioned to the phosphorous atoms from the dppb ligand. All complexes dissolved in DMSO-d_6 presented the same $^{31}P\{^1H\}$ NMR spectra after 48 h, compared with the one run immediately after dissolution of the sample.

The redox behavior of the complexes was studied by cyclic voltammetry. Although the coordination spheres of the three isomers *ct*, *cc* and *tc*-[RuCl(CO)(dppb)(bipy)]PF_6 are the same, their oxidation potentials are different. As can be seen in Fig. 4, after oxidation of the *ct*-[RuCl(CO)(dppb)(bipy)]PF_6 complex (**1**), in an acetonitrile solution, from Ru(II) to Ru(III), a quasi-reversible process at 1.15 V was observed, which can be attributed to the Ru^{II}/Ru^{III} process in complex *ct*-[RuCl(CH_3CN)(dppb)(bipy)]PF_6.

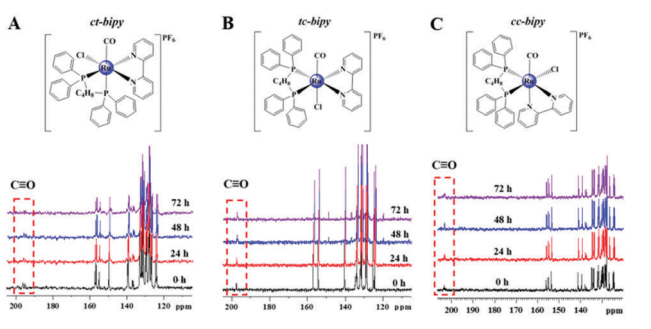

Fig. 3 Expanded regions of the $^{13}C\{^1H\}$ NMR spectra at 100–210 ppm for *ct*-[RuCl(CO)(dppb)(bipy)]PF_6 (A), *tc*-[RuCl(CO)(dppb)(bipy)]PF_6 (B) and *cc*-[RuCl(CO)(dppb)(bipy)]PF_6. Spectra recorded in DMSO-d_6 at different incubation times.

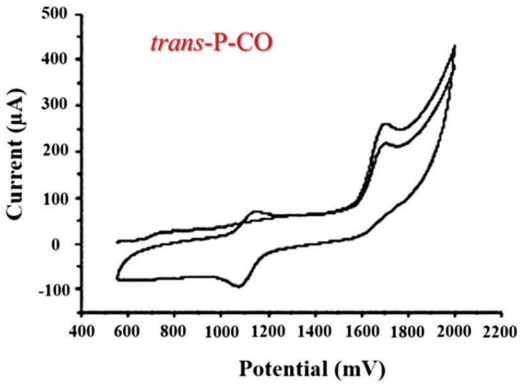

Fig. 4 Cyclic voltammetry of the isomer *ct*-[RuCl(CO)(dppb)(bipy)]PF_6 (**1**) (Pt working electrode *vs.* Ag/AgCl, TBAP 0.1 mol L^{-1}, in CH_3CN).

This complex was formed by the dissociation of the CO ligand from complex (**1**), after the oxidation of the metal center, forming a d^5 configuration, which decreases its ability to make back donation, destabilizing the Ru–CO bond, and allowing the displacement of the carbonyl group, which is replaced by the CH_3CN molecule.

The *ct*-[RuCl(CH_3CN)(dppb)(bipy)]PF_6 complex was obtained, in the solid state, after the exhaustive electrolysis of the *ct*-[RuCl(CO)(dppb)(bipy)]PF_6 isomer (oxidation and reduction at 1.70 V and 1.05 V, respectively) in CH_3CN. Afterwards, the solution was dried and washed with water (3 × 5 mL) and diethyl ether (3 × 5 mL). The complex was characterized by elemental analysis (C, N, H), $^{31}P\{^1H\}$ NMR and the cyclic voltammogram of the *ct*-[RuCl(CH_3CN)(dppb)(bipy)]PF_6 complex (Fig. S4, ESI†). Moreover, the *tc*-[RuCl(CO)(dppb)(bipy)]PF_6 and the *cc*-[RuCl(CO)(dppb)(bipy)]PF_6 isomers showed a displacement of the carbonyl group, under electrolysis, leading to the formation of the respective solvate complexes, with a process at 1.26 V for *tc*-[RuCl(CH_3CN)(dppb)(bipy)]PF_6 and at 1.06 V for *cc*-[RuCl(CH_3CN)(dppb)(bipy)]PF_6. These complexes were characterized based on their $^{31}P\{^1H\}$ NMR spectra, where the *tc*-isomer presented a singlet at δ 35.9 ppm, which is characteristic of phosphorous *trans* positioned to equivalent nitrogen atoms of 2,2′-bipyridine, and for isomer *cc*-[RuCl(MeCN)(dppb)(bipy)]PF_6 two doublets were obtained, at δ 39.2 and 32.6 ppm, which refer to the phosphorous atoms *trans* positioned to chlorido and to nitrogen from the 2,2′-bipyridine ligand [Fig. S5A and B, ESI†]. Additionally the $^{13}C\{^1H\}$ NMR spectrum showed the displacement of CO after electrolysis in the three isomers (see Fig. S6, ESI†).

Considering the fact that both the CO and the phosphorus atoms from the dppb ligand are suitable for back donation, when the CO is *trans* to the P_{dppb}, a strong competition for the ruthenium electrons is expected. In contrast, when the CO is in *trans* position to N_{bipy}, the competition for the ruthenium electrons is weakened. Thus, the position of the CO ligand in the complex plays an important role in the oxidation potential of the metal center, and the properties of the complexes. In agreement with this, the CO stretching in the IR spectra of the complexes revealed that the $\nu_{C\equiv O}$ signal decreases in the order

Table 1 Summary of spectroscopic and electrochemical data of Ru–CO complexes

Compound	CO stretching (cm^{-1})	Oxidation potential (V)	UV-Vis absorption[a] (nm)	CO bond lengths (Å)
1	1987	1.69	(273, 1520)	1.148(4)
2	1987	1.65	(270, 6710)	—
3	1970	2.11	(274, 106 000)	—
4	1965	2.10	(276, 22 600)	—
5	1976	1.92	(275, 63 000)	—
6	1975	1.94	(274, 16 300)	1.154(5)

[a] M^{-1} cm^{-1}.

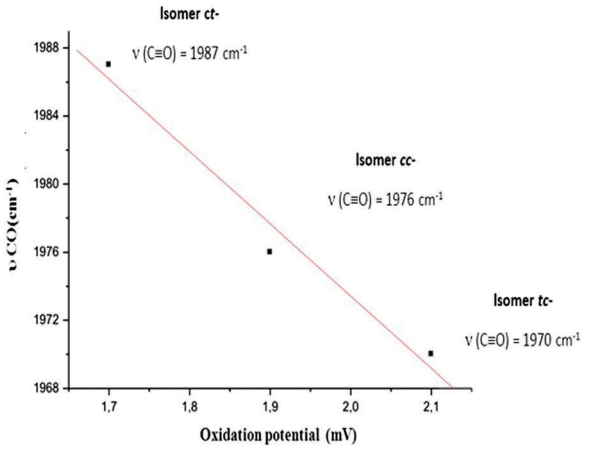

Fig. 5 Oxidation potentials *versus* νCO-stretching for the isomers *ct*-, *cc*- and *tc*-[RuCl(CO)(dppb)(bipy)]PF_6.

ct-[RuCl(CO)(dppb)(bipy)]PF_6 > *cc*-[RuCl(CO)(dppb)(bipy)]PF_6 > *tc*-[RuCl(CO)(dppb)(bipy)]PF_6 (Table 1 and Fig. 5).

The UV-Vis spectra of isomers *ct*-[RuCl(CO)(dppb)(bipy)]PF_6, *tc*-[RuCl(CO)(dppb)(bipy)]PF_6 and *cc*-[RuCl(CO)(dppb)(bipy)]PF_6, in dichloromethane, show bands and shoulders, from 270 to 320 nm, which are typically of intra-ligand type, $\pi \rightarrow \pi^*$ transitions. The bands above 320 nm were attributed to metal-to-ligand charge transfer, probably from the ruthenium to the diimine and to the dppb ligands.[22,23]

An analysis of the spectroscopic data for the complexes (Table 1) showed that the isomer "*ct*" with higher density in the metal center (lower oxidation potentials) provides higher

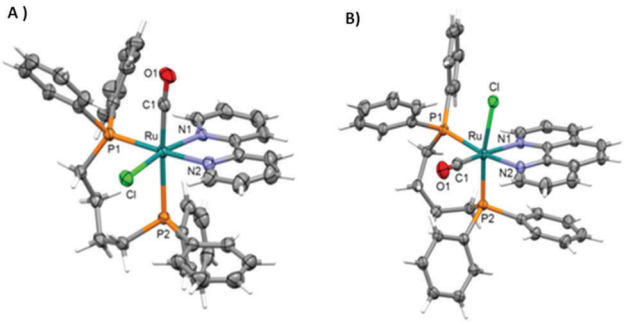

Fig. 6 ORTEP view of (A) *ct*-[RuCl(CO)(dppb)(bipy)]PF_6 and (B) *cc*-[RuCl(CO)(dppb)(phen)]PF_6. The PF_6^- was omitted for clarity.

Table 2 Selected bond lengths [Å] for *ct*-[RuCl(CO)(dppb)(bipy)]PF_6 (**1**) and *cc*-[RuCl(CO)(dppb)(phen)]PF_6 (**6**)

Bond fragment	(**1**)	(**6**)
Ru–C(1)	1.861(3)	1.845(4)
Ru–N(1)	2.116(3)	2.159(3)
Ru–N(2)	2.128(3)	2.119(3)
Ru–P(1)	2.361(9)	2.3863(9)
Ru–P(2)	2.529(8)	2.3652(9)
Ru–Cl	2.403(9)	2.4410(9)
C(1)–O(1)	1.148(4)	1.154(5)

electron density to CO (higher frequency values in IR absorption).

The crystal structures of *ct*-[RuCl(CO)(dppb)(bipy)]PF_6 and *cc*-[RuCl(CO)(dppb)(phen)]PF_6 complexes were examined by single-crystal X-ray diffraction. ORTEP representations with atom numbering are given in Fig. 6. Selected bond lengths and angles for these compounds are shown in Table 2.

These complexes exhibit six-coordinated structures, where the ruthenium is bonded to phosphorous atoms P(1) and P(2) from the dppb; to nitrogen atoms N(1) and N(2) from the respective diimine, one monoanionic chlorido ligand and, finally to the carbon atom C(1) from the CO. The position of the CO group is determined in each complex. Thus, for the *ct*-[RuCl(CO)(dppb)(bipy)]PF_6 complex, the chlorido is *cis* positioned in relation to CO, and *trans* positioned to diimine, while for *cc*-[RuCl(CO)(dppb)(phen)]PF_6 the chlorido is *cis* positioned to CO and to diimine. Interestingly, the bond length of Ru–P(**2**) in the *ct*-[RuCl(CO)(dppb)(bipy)]PF_6 complex is 2.529 Å, while Ru–P(**1**) is 2.361 Å. This can be attributed to the strong *trans* competition between the phosphorus atom and the CO group by the electron density of the metal center.[38]

Furthermore, the theoretical calculations were carried out in order to find the relative energies of the isomers in the gas phase and with effects of implicit water. As a model for the initial calculations, three isomers were selected: *ct*-[RuCl(CO)(dppb)(bipy)]PF_6 (**1**), *tc*-[RuCl(CO)(dppb)(bipy)]PF_6 (**3**) and *cc*-[RuCl(CO)(dppb)(bipy)]PF_6 (**5**) (Table 3). The calculations of energy for the optimized structures revealed that complex **1** has the lowest value among them, both under gas and implicit water effect conditions.

The geometry optimization of the three isomers revealed that complex **5**, a *cc*-isomer, has the lowest energy among the three isomers with the implicit effects from water taken into account, whereas complex **3**, a *tc*-isomer, was calculated to be the most stable isomer in the gas phase. However, as can be seen from Table 3, all the isomers studied were found to be very close in energy, with isomers **3** and **5** being essentially degenerate in energy in both phases.

Table 3 Relative energies of the optimized isomers *ct*-[RuCl(CO)(dppb)(bipy)]PF_6 (**1**), *tc*-[RuCl(CO)(dppb)(bipy)]PF_6 (**3**) and *cc*-[RuCl(CO)(dppb)(bipy)]PF_6 (**5**), calculated using the B3LYP/[Ru:CEP-121G; C,H,O,N,P,Cl:6-31G*] approach

	E, a.u.			
Species	Gas phase	ΔE, kcal mol^{-1}	H_2O	ΔE, kcal mol^{-1}
1 opt	−2930.875803	0.0	−2930.935346	0.0
3 opt.	−2930.270491	379.8	−2930.325242	382.8
5 opt.	−2930.152633	453.8	−2930.212445	453.6
1 X-ray*	−2930.198244	425.2	−2930.258673	424.6

Table 4 Energies of the frontier orbitals (a.u.) and HOMO/LUMO gaps and optical gaps (eV) of the Ru-isomers *ct*-[RuCl(CO)(dppb)(bipy)]PF_6 (**1**), *tc*-[RuCl(CO)(dppb)(bipy)]PF_6 (**3**) and *cc*-[RuCl(CO)(dppb)(bipy)]PF_6 (**5**)

		E, a.u.		*E*, eV
Species		HOMO	LUMO	ΔH/L
1 Opt.	Gas-phase	−0.32078	−0.19786	3.34
	H_2O	−0.24342	−0.10407	3.79
3 Opt.	Gas-phase	−0.31262	−0.25607	1.54
	H_2O	−0.22963	−0.17198	1.57
5 Opt.	Gas-phase	−0.30636	−0.21821	2.40
	H_2O	−0.22166	−0.13591	2.33
1 X-ray[a]	Gas-phase	−0.31648	−0.1980	3.22
	H_2O	−0.23752	−0.10172	3.70

[a] First optical gap value has low oscillator strength value, $f < 0.01$.

The contributions of frontier orbitals to the stability and reactivity of these complexes were investigated as well. Complex *ct*-[RuCl(CO)(dppb)(bipy)]PF_6 (**1**) showed the smallest HOMO/LUMO gaps both under gas and implicit water conditions (Table 4). It also showed the smallest optical gap value calculated in the gas phase but an intermediate optical gap value calculated in implicit water. Complex *cc*-[RuCl(CO)(dppb)(bipy)]PF_6 (**5**) showed the intermediate HOMO/LUMO gap values both in the gas phase and in the implicit water but has the largest computed optical gap value in the gas phase and the smallest computed optical gap value in the implicit water (Table 4). An in-depth analysis revealed for all the three complexes that ruthenium and chlorine contribute roughly 90% of HOMO composition, while atomic contributions to LUMO are mostly due to light atoms (N, C, and H) of the ligands (Table S4, ESI†). For both optimized and non-optimized complexes, large contributions of ruthenium to the HOMO composition were observed (see Tables S3 and S4, ESI†), which makes the complex more prone to oxidation.

After chemical characterization, the complexes were evaluated in pharmacological assays. The antiparasitic activity against trypomastigotes of Y strain of *T. cruzi* was determined by calculating the effective concentration to 50% (EC_{50}) 24 h after incubation. The EC_{50} values were compared with an antiparasitic reference drug, benznidazole. The host cell cytotoxicity was evaluated in splenocytes isolated from BALB/c mice by calculating the cytotoxic concentration to 50% (CC_{50}) 48 h after incubation and the CC_{50} values were compared with a cytotoxic compound, gentian violet. Finally, the cytotoxicity in hepatocellular carcinoma cell line HepG2 was evaluated by calculating the CC_{50} 72 h after incubation and the CC_{50} values were compared with an anticancer compound, oxaliplatin. The results are shown in Table 5.

In comparison to benznidazole, ruthenium complexes were more active antiparasitic agents. Regarding the structure–activity relationship among complexes containing bipy, it was observed that the *ct*-bipy (**1**) and *tc*-bipy (**3**) isomers were equipotent

Table 5 Anti-*T. cruzi* activity and cytotoxicity for the [RuCl(CO)(dppb)(N-N)]PF_6 complexes

Compounds	*T. cruzi* EC_{50} ± S.E.M.[a] (μM)	CC_{50} ± S.E.M. (μM)	
		Host cells[b]	HepG2[c]
1	0.95 ± 0.1	1.2 ± 0.2	12.4 ± 0.5
2	0.09 ± 0.2	0.54 ± 0.5	6.3 ± 0.3
3	0.93 ± 0.1	3.1 ± 0.10	14.9 ± 1.0
4	1.8 ± 0.1	0.53 ± 0.10	11.1 ± 0.9
5	2.0 ± 0.4	0.66 ± 0.50	23.5 ± 1.6
6	3.3 ± 0.5	0.42 ± 0.10	17.7 ± 1.1
Benznidazole	10.6 ± 2.3	>100	>100
Gentian violet	0.09 ± 0.001	11.2 ± 2.1	—

[a] Determined against Y strain *T. cruzi* trypomastigotes 24 h after incubation with drugs. [b] Determined in BALB/c splenocytes 48 h after treatment. [c] Determined in HepG2 cancer cells 72 h after treatment. S.E.M. = standard error of the mean.

antiparasitic agents, while they were twice more potent than *cc*-bipy (**5**) isomer. Regarding the complexes containing 1,10-phenanthroline, *ct*-phen (**2**) was 20-fold more potent than *tc*-phen (**4**), while the latter was only twice more active than *cc*-phen (**6**). When the complexes containing bipy and phen are compared, in general the presence of a bipy leads to more active complexes than the presence of a phen ligand.

The cytotoxicity was analyzed in both host and cancer cells. In comparison to gentian violet, all ruthenium complexes were shown to be more cytotoxic in host cells. In contrast, none of the ruthenium complexes were more cytotoxic in cancer cells than oxaliplatin (CC_{50} = 2.61 ± 0.42 μM). The *ct*-phen (**2**) and *tc*-bipy (**3**) complexes were three and six times more cytotoxic for parasites than host cells, respectively. However, since *ct*-phen (**2**) presented the highest CC_{50} value against host and cancer cells among complexes, we decided to proceed with *tc*-bipy (**3**) due to its lowest cytotoxicity.

The mechanism of action by which *tc*-bipy (**3**) causes parasite death was studied. By flow cytometry using propidium iodide (PI) and annexin-V staining, it was observed that this complex increases the number of parasite cells positive for PI staining, while no significant parasite cells were stained for annexin-V (Fig. 7). Importantly, treatment with *tc*-bipy (**3**) increased PI-staining in a concentration-dependent manner,

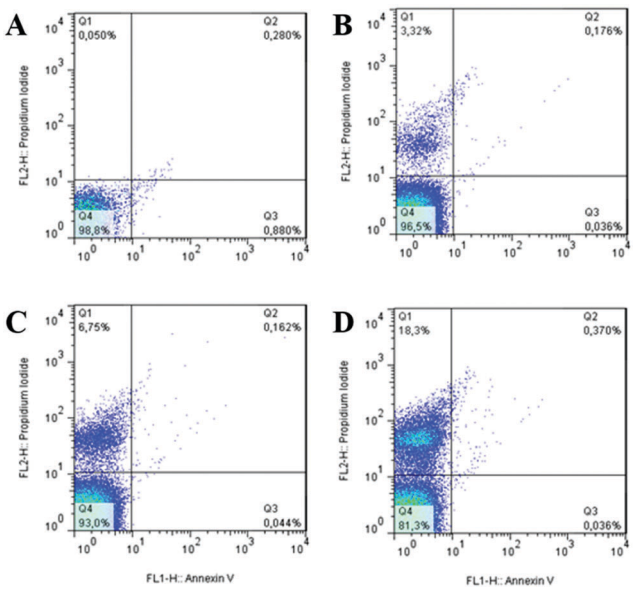

Fig. 7 Trypomastigotes treated with complex *tc*-[RuCl(CO)(dppb)(bipy)]PF_6 for 36 h. Parasites were examined by flow cytometry with annexin-V and PI. Cells plotted in each quadrant represent the following: lower left, double negative; upper left, PI single positive; lower right, annexin-V single positive; upper right, PI and annexin V double positive. (A) Untreated; (B) complex *tc*-[RuCl(CO)(dppb)(bipy)]PF_6 at 0.45 μM; (C) complex *tc*-[RuCl-(CO)(dppb)(bipy)]PF_6 at 0.9 M; (D) complex *tc*-[RuCl(CO)(dppb)(bipy)]PF_6 at 1.8 μM. Data shown are from three representative experiments that were carried out.

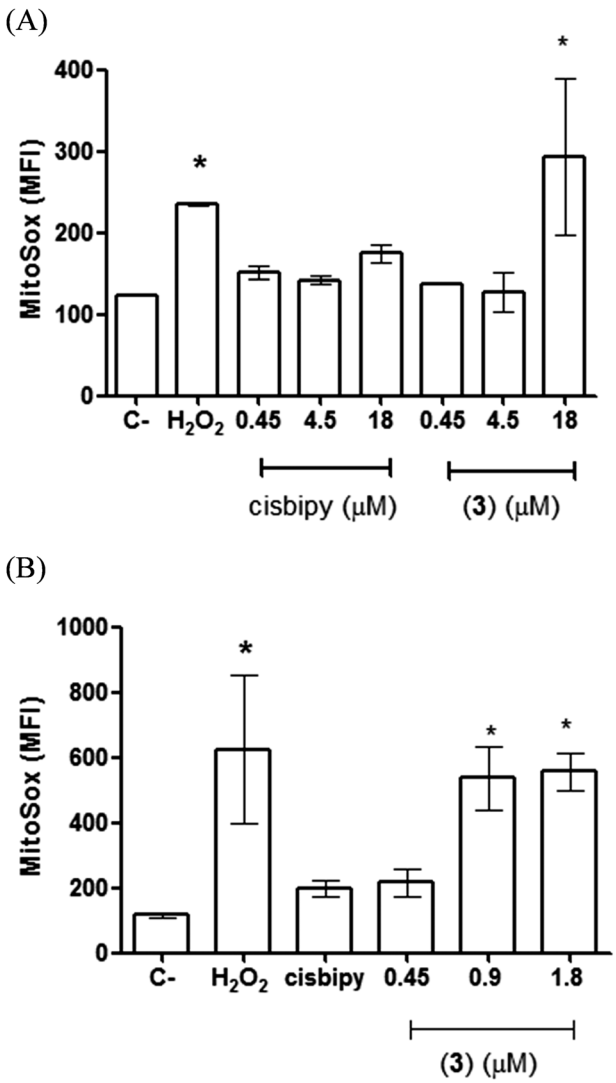

Fig. 8 Treatment with *tc*-[RuCl(CO)(dppb)(bipy)]PF_6 (**3**) complex induces oxidative stress in trypomastigotes. Parasites were examined by flow cytometry with MitoSox Red after incubation for 3 h (panel A) and 24 h (panel B). C- = untreated is parasite plus MitoSox Red. H_2O_2 is positive control. cisbipy = *cis*-[Ru(bipy)Cl_2(dppb)]. Concentration of complexes is indicated in the *x* axis. In panel B, cisbipy was tested at 1.8 μM. MFI = median fluorescence intensity. Data shown are from one representative experiment of three that were carried out. Error bars represent the standard errors of the means. One-way ANOVA: *, $p < 0.05$ compared to C-.

leading to a 3.3 and 18.2% of parasites stained for PI at concentrations of 0.45 and 1.8 μM, respectively.

Next, we investigated the ability of complexes in producing reactive oxygen species. This was assayed in trypomastigotes and determined 3 and 24 h after drug exposure by flow cytometry using the mitochondrial superoxide probe MitoSox Red. For comparison purposes, a ruthenium complex lacking CO ligand, the *cis*-[Ru(bipy)Cl_2(dppb)] complex[39] and denoted here as *cis*bipy was evaluated in this assay. When incubated for 3 h, the *tc*-bipy (**3**) complex increased MitoSox Red fluorescence at a concentration of 18 μM in comparison to untreated parasite (C-), while the *cis*bipy complex did not increase the MitoSox Red fluorescence (Fig. 8, panel A). In the assay incubated for 24 h, complexes were tested at lower concentrations to warrant viable parasites. In comparison to untreated parasite (C-), *tc*-bipy (**3**) increased the MitoSox Red fluorescence and this effect was concentration-dependent. In contrast, the *cis*bipy complex at 1.8 μM did not increase the MitoSox Red fluorescence (Fig. 8, panel B).

In fact, compounds that induce oxidative stress can be lethal for parasites, since such a property can cause irreversible cytosolic alterations, followed by blockage of mitochondrial activity and ultimately leading to parasite cell death. While for other parasites this has been documented,[40,41] this is the first time that a ruthenium carbonyl complex is shown to achieve antiparasitic activity against *T. cruzi* by triggering oxidative stress.

Conclusions

By synthesizing and testing mononuclear ruthenium diimine/phosphine complexes, a key role of carbonyl ligands in complex reactivity was observed, as well as in pharmacological properties. As noted by cyclic voltammetry, the potential of oxidation of the metal center is affected by the position of CO. As a result, the complex *ct*-[RuCl(CO)(dppb)(bipy)]PF_6 is more easily oxidized than the *cc*-[RuCl(CO)(dppb)(bipy)]PF_6, while complex *tc*-[RuCl(CO)(dppb)(bipy)]PF_6 is more difficult to be oxidized. In addition, the computational studies revealed that the energies and frontier orbitals gaps are different when the CO position is changed.

Regarding antiparasitic activity, both the position of CO as well as the nature of the diimine used had effects on the activity. Phenanthroline compounds did not show selectivity for the parasite, while bipyridine compounds resulted in selective compounds, such as the *tc*-[RuCl(CO)(dppb)(bipy)]PF_6, the most potent among them, which showed antiparasitic activity against *T. cruzi*, better than the reference drug, benznidazole.

An important aspect is the liability of CO in these complexes. NMR experiments, in DMSO-d_6, showed that this ligand does not change in a period of up to 48 h. Based on this, it is likely that CO achieves pharmacological activity when bonded to ruthenium. Another possibility is that CO is only released under biological metabolism. The isomer *tc*-[RuCl(CO)(dppb)(bipy)]PF_6 is harder to be oxidized than *ct*-[RuCl(CO)(dppb)(bipy)]PF_6, but both were equally potent antiparasitic agents. However, *tc*-[RuCl(CO)(dppb)(bipy)]PF_6 showed higher selectivity towards the parasite *versus* host cells than *ct*-[RuCl(CO)(dppb)(bipy)]PF_6. Therefore, it is suggested that, in addition to redox behavior, which allows labilization of the CO molecule, other factors such as the geometry and the interactions between the molecular target and complexes are involved in the pharmacological activity of this bind of complexes.

An in-depth investigation of ruthenium phosphines/diimines complexes containing a carbonyl ligand was carried out for the first time. It revealed important chemical and pharmacological aspects, having significant implications for drug discovery and development of ruthenium complexes. The carbonyl ligand plays a key role in the redox behavior and stability by governing ruthenium electrons with phosphines/diimines ligands. The pharmacological findings demonstrate that attaching a carbonyl coligand to ruthenium phosphine/diimine complexes provides antiparasitic activity against *T. cruzi*, which is mechanistically achieved by triggering oxidative stress and culminating to an irreversible necrotic death.

Acknowledgements

This work was supported by Fundação de Amparo à Pesquisa do Estado de São Paulo (FAPESP, Processo 2014/10516-7) and Fundação de Amparo à Pesquisa do Estado da Bahia (FAPESB, grant PET0042/2013 and PRONEX PNX0002/2014). The authors acknowledge the Centro Nacional de Processamento de Alto Desempenho/UFC for the computational facility and the flow cytometry facility of IGM (Fiocruz/Bahia). M. I. F. B. is currently receiving a CAPES post-doctoral scholarship, T. M. B is currently receiving a CAPES doctoral scholarship. D. R. M. M, J. E., A. C. D., M. B. P. S. and A. A. B. are recipients of CNPq fellowships.

Notes and references

1 A. Rassi, Jr., A. Rassi and J. M. De Rezende, *Infect. Dis. Clin. North Am.*, 2012, **26**, 275–291.
2 A. L. Ribeiro, M. P. Nunes, M. M. Teixeira and M. O. Rocha, *Nat. Rev. Cardiol.*, 2012, **2**, 576–589.
3 P. Nouvellet, Z. M. Cucunubá and S. Gourbière, *Adv. Parasitol.*, 2015, **87**, 135–191.
4 M. J. Pinazo, L. Guerrero, E. Posada, E. Rodríguez, D. Soy and J. Gascon, *Antimicrob. Agents Chemother.*, 2013, **57**, 390–395.
5 D. Soy, E. Aldasoro, L. Guerrero, E. Posada, N. Serret, T. Mejía, J. A. Urbina and J. Gascón, *Antimicrob. Agents Chemother.*, 2015, **59**, 3342–3349.
6 A. F. Francisco, M. D. Lewis, S. Jayawardhana, M. C. Taylor, E. Chatelain and J. M. Kelly, *Antimicrob. Agents Chemother.*, 2015, **59**, 4653–4661.
7 S. H. Heinemann, T. Hoshi, M. Westerhausend and A. Schiller, *Chem. Commun.*, 2014, **50**, 3644–3660.
8 R. Motterlini and L. E. Otterbein, *Nat. Rev. Drug Discovery*, 2010, **9**, 728–743.

9 L. S. Nobre, H. Jeremias, C. C. Romão and L. M. Saraiva, *Dalton Trans.*, 2016, **45**, 1455–1466.
10 E. O. Owens, *Clin. Biochem.*, 2010, **43**, 1183–1188.
11 R. Ramachandran and P. Viswanathamurthi, *Spectrochim. Acta, Part A*, 2013, **103**, 53–61.
12 A. A. Petruk, A. Vergara, D. Marasco, D. Bikiel, F. Doctorovich, D. A. Estrin and A. Merlino, *Inorg. Chem.*, 2014, **53**, 10456.
13 L. Côrte-Real, M. P. Robalo, F. Marques, G. Nogueira, F. Avecilla, T. Silva, F. Santos, A. I. Tomaz, M. H. Garcia and A. Valente, *J. Inorg. Biochem.*, 2015, **150**, 148–159.
14 C. Rodrigues, A. A. Batista, R. Aucelio, L. Teixeira, L. Visentin and H. Beraldo, *Polyhedron*, 2008, **25**, 3061–3066.
15 C. Rodrigues, A. A. Batista, J. Ellena, E. E. Castellano, D. Benitéz, H. Cerecetto, M. González, L. R. Teixeira and H. Beraldo, *Eur. J. Med. Chem.*, 2010, **45**, 2847–2853.
16 J. J. Nogueira Silva, W. R. Pavanelli, F. R. Gutierrez, F. C. Alves Lima, A. B. Ferreira da Silva, J. S. Silva and D. W. Franco, *J. Med. Chem.*, 2008, **51**, 4104–4114.
17 B. Demoro, M. Rossi, F. Caruso, D. Liebowitz, C. Olea-Azar, U. Kemmerling, J. D. Maya, H. Guiset, V. Moreno, C. Pizzo, G. Mahler and L. Otero, *Biol. Trace Elem. Res.*, 2013, **153**, 371–381.
18 R. Sesti-Costa, Z. A. Carneiro, M. C. Silva, M. Santos, G. K. Silva, C. Milanezi, R. S. da Silva and J. S. Silva, *PLoS Neglected Trop. Dis.*, 2014, **10**, 3207.
19 C. Quintana, A. H. Klahn, V. Artigas, M. Fuentealba, C. Biot, I. Halloum, L. Kremer and R. Arancibia, *Inorg. Chem. Commun.*, 2015, **55**, 48–50.
20 M. Patra, K. Ingram, V. Pierroz, S. Ferrari, B. Spingler, R. B. Gasser, J. Keiser and G. Gasser, *Chemistry*, 2013, **19**, 2232–2235.
21 E. R. Arce, I. Machado, B. Rodríguez, M. Lapier, M. C. Zúñiga, J. D. Maya, C. O. Azar, L. Otero and D. Gambino, *J. Inorg. Biochem.*, 2017, **170**, 125–133.
22 S. L. Queiroz, A. A. Batista, G. Oliva, M. T. P. Gambardella, R. H. A. Santos, K. S. Macfarlane, S. J. Rettig and B. R. James, *Inorg. Chim. Acta*, 1998, **267**, 09–221.
23 M. Bressan and P. Rigo, *Inorg. Chem.*, 1975, **14**, 2286–2288.
24 R. H. Blessing, *Acta Crystallogr.*, 1995, **51**, 33–38.
25 Enraf-Nonius (1997–2000), COLLECT Nonius BV, Delft, The Netherlands.
26 Z. Otwinowski and W. Minor, *Processing of X-ray diffraction data collected in, Oscillation Mode*, Academic Press, New York, 1997.
27 G. M. Sheldrick, *SHELXS-97. Program for Crystal Structure Resolution*, Univ. of Göttingen, Göttingen, Germany, 1997.
28 G. M. Sheldrick, *SHELXL-97, Programs of Refinement for Crystal Structure*, University of Göttingen, Germany, 1997.
29 L. J. Farrugia, *J. Appl. Crystallogr.*, 1197, **30**, 565–566.
30 M. J. Frisch, G. W. Trucks, H. B. Schlegel, G. E. Scuseria, M. A. Robb, J. R. Cheeseman, G. Scalmani, V. Barone, B. Mennucci, G. A. Petersson, H. Nakatsuji, M. Caricato, X. Li, H. P. Hratchian, A. F. Izmaylov, J. Bloino, G. Zheng, J. L. Sonnenberg, M. Hada, M. Ehara, K. Toyota, R. Fukuda, J. Hasegawa, M. Ishida, T. Nakajima, Y. Honda, O. Kitao, H. Nakai, T. Vreven, J. A. Montgomery, Jr., J. E. Peralta, F. Ogliaro, M. Bearpark, J. J. Heyd, E. Brothers, K. N. Kudin, V. N. Staroverov, R. Kobayashi, J. Normand, K. Raghavachari, A. Rendell, J. C. Burant, S. S. Iyengar, J. Tomasi, M. Cossi, N. Rega, J. M. Millam, M. Klene, J. E. Knox, J. B. Cross, V. Bakken, C. Adamo, J. Jaramillo, R. Gomperts, R. E. Stratmann, O. Yazyev, A. J. Austin, R. Cammi, C. Pomelli, J. W. Ochterski, R. L. Martin, K. Morokuma, V. G. Zakrzewski, G. A. Voth, P. Salvador, J. J. Dannenberg, S. Dapprich, A. D. Daniels, Ö. Farkas, J. B. Foresman, J. V. Ortiz, J. Cioslowski and D. J. Fox, *Density-functional theory of atoms and molecules*, Oxford University Press, Oxford, 1st edn, 1989.
31 M. J. Frisch, G. W. Trucks, H. B. Schlegel, G. E. Scuseria, M. A. Robb, J. R. Cheeseman, G. Scalmani, V. O. Farkas, J. B. Foresman, J. V. Ortiz, J. Cioslowski and D. J. Fox, *Gaussian 09, Revision A.02*, Gaussian, Inc., Wallingford, CT, 2009.
32 W. J. Stevens, H. Basch and M. Krauss, *J. Chem. Phys.*, 1984, **81**, 6026–6033.
33 E. Cancès, B. Mennucci and J. Tomasi, *J. Chem. Phys.*, 1997, **107**, 3032–3041.
34 V. Barone, M. Cossi and J. Tomasi, *J. Chem. Phys.*, 1997, **107**, 3210–3221.
35 A. E. Reed, L. A. Curtiss and F. Weinhold, *Chem. Rev.*, 1988, **88**, 899–926.
36 A. E. Reed, R. B. Weinstock and F. Weinhold, *J. Chem. Phys.*, 1985, **83**, 735–746.
37 A. E. Reed, L. A. Curtiss and F. Weinhold, *Chem. Rev.*, 1988, **88**, 899–926.
38 M. I. F. Barbosa, E. M. A. Valle, S. L. Queiroz, J. Ellena, E. E. Castellano, V. R. S. Malta, J. R. de Sousa, O. Piro, M. P. de Araújo and A. A. Batista, *Polyhedron*, 2010, **29**, 2297.
39 T. M. Bastos, M. I. Barbosa, M. M. da Silva, J. W. Júnior, C. S. Meira, E. T. Guimaraes, J. Ellena, D. R. Moreira, A. A. Batista and M. B. P. Soares, *Antimicrob. Agents Chemother.*, 2014, **58**, 6044–6055.
40 F. Dubar, C. Slomianny, J. Khalife, D. Dive, H. Kalamou, Y. Guérardel, P. Grellier and C. Biot, *Angew. Chem.*, 2013, **52**, 7690–7693.
41 Y. Toledano-Magaña, J. C. García-Ramos, C. Torres-Gutiérrez, C. Vázquez-Gasser, J. M. Esquivel-Sánchez, M. Flores-Alamo, L. Ortiz-Frade, R. Galindo-Murillo, M. Nequiz, M. Gudiño-Zayas, J. P. Laclette, J. C. Carrero and L. Ruiz-Azuara, *J. Med. Chem.*, 2017, **60**, 899–912.